NUREG/CR-6728

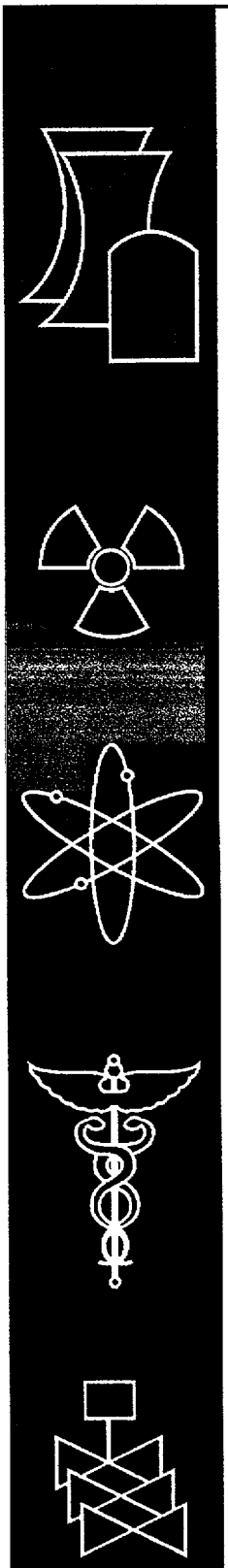

Technical Basis for Revision of Regulatory Guidance on Design Ground Motions: Hazard- and Risk-consistent Ground Motion Spectra Guidelines

Risk Engineering, Inc.

U.S. Nuclear Regulatory Commission
Office of Nuclear Regulatory Research
Washington, DC 20555-0001

AVAILABILITY OF REFERENCE MATERIALS IN NRC PUBLICATIONS

NRC Reference Material

As of November 1999, you may electronically access NUREG-series publications and other NRC records at NRC's Public Electronic Reading Room at www.nrc.gov/NRC/ADAMS/index.html.
Publicly released records include, to name a few, NUREG-series publications; *Federal Register* notices; applicant, licensee, and vendor documents and correspondence; NRC correspondence and internal memoranda; bulletins and information notices; inspection and investigative reports; licensee event reports; and Commission papers and their attachments.

NRC publications in the NUREG series, NRC regulations, and *Title 10, Energy*, in the Code of *Federal Regulations* may also be purchased from one of these two sources.

1. The Superintendent of Documents
   U.S. Government Printing Office
   Mail Stop SSOP
   Washington, DC 20402–0001
   Internet: bookstore.gpo.gov
   Telephone: 202-512-1800
   Fax: 202-512-2250
2. The National Technical Information Service
   Springfield, VA 22161–0002
   www.ntis.gov
   1–800–553–6847 or, locally, 703–605–6000

A single copy of each NRC draft report for comment is available free, to the extent of supply, upon written request as follows:

Address: Office of the Chief Information Officer,
Reproduction and Distribution
Services Section
U.S. Nuclear Regulatory Commission
Washington, DC 20555-0001
E-mail: DISTRIBUTION@nrc.gov
Facsimile: 301–415–2289

Some publications in the NUREG series that are posted at NRC's Web site address www.nrc.gov/NRC/NUREGS/indexnum.html are updated periodically and may differ from the last printed version. Although references to material found on a Web site bear the date the material was accessed, the material available on the date cited may subsequently be removed from the site.

Non-NRC Reference Material

Documents available from public and special technical libraries include all open literature items, such as books, journal articles, and transactions, *Federal Register* notices, Federal and State legislation, and congressional reports. Such documents as theses, dissertations, foreign reports and translations, and non-NRC conference proceedings may be purchased from their sponsoring organization.

Copies of industry codes and standards used in a substantive manner in the NRC regulatory process are maintained at—

The NRC Technical Library
Two White Flint North
11545 Rockville Pike
Rockville, MD 20852–2738

These standards are available in the library for reference use by the public. Codes and standards are usually copyrighted and may be purchased from the originating organization or, if they are American National Standards, from—

American National Standards Institute
11 West 42nd Street
New York, NY 10036–8002
www.ansi.org
212–642–4900

Legally binding regulatory requirements are stated only in laws; NRC regulations; licenses, including technical specifications; or orders, not in NUREG-series publications. The views expressed in contractor-prepared publications in this series are not necessarily those of the NRC.

The NUREG series comprises (1) technical and administrative reports and books prepared by the staff (NUREG–XXXX) or agency contractors (NUREG/CR–XXXX), (2) proceedings of conferences (NUREG/CP–XXXX), (3) reports resulting from international agreements (NUREG/IA–XXXX), (4) brochures (NUREG/BR–XXXX), and (5) compilations of legal decisions and orders of the Commission and Atomic and Safety Licensing Boards and of Directors' decisions under Section 2.206 of NRC's regulations (NUREG–0750).

NUREG/CR-6728

Technical Basis for Revision of Regulatory Guidance on Design Ground Motions: Hazard- and Risk-consistent Ground Motion Spectra Guidelines

Manuscript Completed: May 2001
Date Published: October 2001

Prepared by
R. K. McGuire[1]
W. J. Silva[2]
C. J. Costantino[3]

[1]Risk Engineering, Inc., Principal Contractor
4155 Darley Avenue, Suite A
Boulder, CO 80305

Subcontractor:
[2]Pacific Engineering & Analysis
311 Pomona Avenue
El Cerrito, CA 94530

[3]Carl J. Costantino, Consultant
4 Rockingham Road
Spring Valley, NY 10977

R. M. Kenneally, NRC Project Manager

Prepared for
Division of Engineering Technology
Office of Nuclear Regulatory Research
U.S. Nuclear Regulatory Commission
Washington, DC 20555-0001
NRC Job Code W6248

Abstract

Recommendations for seismic design ground motions for nuclear facilities require a consistency with both observed strong motion data and with seismological theory on the characteristics of strong shaking. Different recommendations are appropriate for various regions of the US, because both earthquake source characteristics differ and the earth's crustal properties vary with region.

A database of recorded time histories forms the foundation of empirical recommendations for spectral shapes. This database includes motions recorded as recently as the 1999 Turkey and Taiwan earthquakes. Empirical attenuation equations derived primarily from California strong motion data form the basis for spectral shape recommendations for western US (WUS) sites on rock, and these spectral shape recommendations are confirmed and supported by the empirical database.

For the central and eastern US (CEUS), a well-validated, simple model of strong motion allows quantification of the difference between WUS and CEUS motions, accounting for differences in both the seismic source and in path and site attenuation. This model adjusts the WUS empirical soft-rock spectral shapes to CEUS hard-rock conditions. These spectral shape recommendations are made for both the 1-corner and 2-corner seismic source model for the CEUS, which are competing models that imply different spectral shapes for design.

Selecting the appropriate design spectrum or spectra requires a probabilistic seismic hazard analysis (PSHA) at the site for rock conditions. The seismic hazard is deaggregated at 10 and 1 Hz to determine the dominant magnitudes and distances at those frequencies. Two sets of spectral shapes are developed for those magnitudes and distances: one from the recommended functions, and a second from the attenuation equations used in the PSHA. In the CEUS, the designer will use both the 1- and 2-corner earthquake source models to develop weighted spectral shapes, both from the recommended functions and from the PSHA attenuation equations. The spectral shapes are scaled to match the uniform hazard spectrum (UHS) amplitudes at 10 and 1 Hz, typically at the 10^{-4} annual frequency of exceedence level. The two sets of spectral shapes provide a consistency check with the UHS.

For design recommendations, the UHS is modified by a scale factor to a Uniform Reliability Spectrum (URS). This scale factor achieves a relatively consistent annual frequency of plant component failure across the range of plant locations and structural frequencies. It does this by accounting for the slope of the seismic hazard curve, which changes with structural frequency and site location. For some sites and natural frequencies the URS exceeds the UHS, and at other sites and frequencies it lies below the UHS.

For design purposes the spectral shapes determined from the attenuation equations are scaled to the 10 Hz and 1 Hz URS amplitudes. The URS must be matched within certain tolerances by the scaled spectral shapes, but the use of two (or more) design shapes allows a more accurate representation of the seismic threat, for example when a broad-banded spectrum is unlikely.

The database of recorded time histories on rock is divided into magnitude and distance bins, and three component records (two horizontals and one vertical) are archived on a CD-ROM for both the WUS and CEUS. We augmented available recorded rock motions for the CEUS by modifying WUS rock records to account for differences in seismic source and crustal properties between the two regions. This database allows designers to select one or a set of records from the appropriate magnitude and distance range and to adjust those records to match a rock design spectrum, for the derivation of detailed input motions.

For these artificial motions, we recommend criteria for matching their spectra to the target (scaled) spectra. The matching criteria lead to mean-based fits, with half of the spectral values above the target and half below, within specified limits. The matching is done with the response spectrum at 5% of critical damping, obviating the need to meet a minimum power spectral density requirement or to match at multiple dampings. However, checks are required of peak motion parameters, duration of shaking, and directional correlation.

For soil sites, a PSHA is conducted for rock conditions to determine spectra scaled to the 10 Hz and 1 Hz UHS amplitudes, as discussed above. These spectra represent control motions input to a soil model that calculates soil response and that accounts for uncertainties in soil properties. The soil analysis gives the mean soil amplification, its uncertainty, and its slope with increasing rock amplitude. These factors allow the engineer to estimate the soil UHS at 10^{-4} and 10^{-5} annual frequencies of exceedence, from which the 10^{-4} URS can be determined for that soil. Generic soil spectral shapes are not derived here because the soil spectra should be obtained from a site-specific analysis. The site-specific soil amplification studies yield spectral shapes that are scaled to the UHS (for a consistency check) and to the URS (for design purposes).

The database of recorded time histories includes motions at WUS and CEUS soil sites, divided into magnitude and distance bins, and these three-component motions are archived on a CD-ROM. The CEUS soil site motions were derived from WUS soil motions by modeling differences in seismic sources and crustal properties between the two regions. These archived records allow designers to select one or a set of records from the appropriate magnitude and distance range and to adjust those records to match a soil design spectrum, for the derivation of detailed input motions.

We demonstrate the procedures for developing design spectra for rock conditions and for four soil profiles in the WUS and in the CEUS, using as example sites a location in the Mojave desert, California, and Columbia, South Carolina. To demonstrate that the URS gives reliability-consistent design amplitudes, we examine eleven sites across the US and use three ground motion parameters at each. These results indicate that the URS, as calculated here, provides reliability-consistent designs over a range of site locations and structural frequencies.

REVISION OF REGULATORY GUIDANCE ON DESIGN GROUND MOTION

TABLE OF CONTENTS

List of Figures

List of Tables

Acknowledgments

This study was sponsored by the US Nuclear Regulatory Commission under Contract NRC-04-96-037. The technical team was assisted by Gabriel Toro of Risk Engineering, Inc., by Robert Darragh, Nick Gregor and Ky Lang of Pacific Engineering and Analysis, by Norman Abrahamson, Consultant (during early planning phases of the work), by Yoshi Moriwaki and Paul Somerville of URS Greiner Woodward-Clyde, and by Robert Youngs of Geomatrix Consultants. The work was reviewed continuously during its development by a Peer Review Panel consisting of Carl Stepp (Chair), David M. Boore, C. Allin Cornell, I.M. Idriss, and Robert P. Kennedy. The insight and direction provided by this Panel were invaluable.

Roger Kenneally of the Nuclear Regulatory Commission was the Contract Monitor for this work, and his support, guidance and reviews of draft reports are gratefully acknowledged. We also acknowledge reviews of draft reports provided by Nilesh C. Chokshi, Andrew J. Murphy, Robert L. Rothman, Clifford G. Munson, and Abou-Bakr K. Ibraham, of the Nuclear Regulatory Commission. Finally, Katherine Morgan of Risk Engineering, Inc. shepherded the project reports through their many drafts with editorial accuracy and grace, for which we are grateful.

List of Terms

a_1	spectral amplitude on rock at 1 Hz
a_{10}	spectral amplitude on rock at 10 Hz
A(f)	crustal amplification
AF	amplification factor, soil amplitude/rock amplitude
A^R, a	ground motion amplitude on rock
A_R	slope parameters on hazard curve
A^S	ground motion amplitude on soil
b_1, b_2	coefficients for magnitude dependence of stress drop
c	constant in stochastic ground motion model
c_1, c_2, ... c_9	coefficients used to define spectral shapes for the WUS (eq. 4-8) and the CEUS (eq. 4-9)
C_1	seismic capacity curve 1
C_2	seismic capacity curve 2
CAP_{10}	ground motion or seismic demand with 10% frequency of failure
CAP_{50}	ground motion or seismic demand with 50% frequency of failure
CAV	cumulative absolute velocity
d_1, d_2, d_3	coefficients for distance-dependent duration
D	strong motion duration
DES1	deaggregated spectrum scaled to 1 Hz
DES10	deaggregated spectrum scaled to 10 Hz
DF	frequency window
DRS	design response spectrum
DT	time increment in artificial records
f	frequency in Hz
f_c	interface frequency
f_O	source corner frequency
F_R	factor of safety
FA(f)	Fourier amplitude of acceleration
FAS	Fourier amplitude spectrum
FT	scaling factor for Fourier spectra
G/G_{max}	shear modulus behavior of non-linear soils
G_O	elastic shear modulus at low strain levels
$G_Z(z)$	complementary cumulative function
h	width of smoothing operator for attenuation equation weights
H	horizontal component of motion
H(•)	seismic hazard
H1	one horizontal component of motion
H2	second horizontal component of motion
HCLPF	high confidence of low probability of failure point on fragility curve
I(t)	normalized Arias intensity
K_H	slope parameters of hazard curve

List of Terms (continued)

M, m	earthquake magnitude (moment magnitude scale)
m_L, m_M, m_H	low, medium, and high magnitudes used to discretize a magnitude distribution
m_{Lg}	earthquake magnitude (Lg magnitude scale)
M_{min}	minimum magnitude
M_O	seismic moment
M_X	maximum magnitude
P	compressional waves
P_F	probability of component failure
P(f)	high-frequency truncation filter
PGA	peak ground acceleration
PGD	peak ground displacement
PGV	peak ground velocity
PI	plasticity index
PSD	power spectral density
PSHA	probabilistic seismic hazard analysis
Q_o	frequency-independent component of Q model
Q(f)	deep crustal damping quality factor
R, r	source-to-site distance
r_c	cutoff distance for distance-dependent duration
S	site term coefficient for duration
$S_a^s(f)$	spectral acceleration on soil
$S_a^r(f)$	spectral acceleration on rock
SA	spectral acceleration
SF	scale factor for converting UHS to URS
Syz	effective shear strain
SV	vertical component of shear waves
t	statistic of T distribution
T_{95}	time to reach 95% of total Arias intensity
$T_{5\text{-}75}$	time from 5% to 75% of total Arias intensity
$T_{5\text{-}95}$	time from 5% to 95% of total Arias intensity
t_1	duration distance dependence on rock
t_2	duration distance dependence on site conditions
T_{max}	maximum duration of artificial records
TBA	average duration of records in bin
TT	strong motion duration of artificial record
T/T_{max}	fraction of total record duration
UHS	uniform hazard spectrum
URS	uniform reliability spectrum
V	vertical component of motion
v(f)	block diagonal matrix of residuals
V_s	shear-wave velocity
V_p	compressional-wave velocity

List of Terms (continued)

$w(f)_k^T$	weight given to k'th attenuation equation using τ statistics
$w(f)_k^L$	weight given to k'th attenuation equation using likelihood function
$w(f)_k^*$	smoothed weight given to k'th attenuation equation
x_p	number of standard deviates for HCLPF
$z(x)$	normal density function
α	deterministic acceptance criterion
β_C	logarithmic uncertainty in capacity OR logarithmic standard duration of capacity ??
β_O	shear-wave velocity at the source
β_R	logarithmic uncertainty in response
$\gamma_{64\%}$	shear strain at 64% of G_{max}
Δt, dt	time interval for strong motion records
$\Delta\sigma$	earthquake stress drop
$\varepsilon(f)$	residual of logarithmic deviation of observed SA from predicted value
$\varepsilon_1(f)$, $\varepsilon_2(f)$	residuals in random effects model
ζ	accuracy desired for regression analysis
η	frequency exponent of Q model
κ	shallow crustal damping
κ_O	coefficient of lateral earth pressure
ξ	damping (fraction or percent of critical)
ξ_c	compressional-wave viscous damping
ξ_s	shear-wave damping
σ	standard deviation
σ_m^2	modeling variance
σ_p^2	parametric variance
σ_T^2	total variance
π_O	coefficient of permeability
ρ_O	crustal density at the source
$\tau_1(f)$, $\tau_2(f)$	standard deviations of $\varepsilon_1(f)$, $\varepsilon_2(f)$
$\upsilon(\ )$	frequency of exceedence
υ_i	frequency of earthquake occurrence on fault i
Φ_O	friction angle

1. INTRODUCTION

1.1 Historical Perspective

The regulatory guidance for determination of seismic design basis ground motion at nuclear plant sites emphasizes the essential need for the design ground response spectrum to be a broad-band, smooth spectrum that has adequate energy in all frequencies represented by a plant's structures, systems and components. For this and economic considerations nuclear plants generally have been designed for a site-independent standard broad-band spectrum such as the Regulatory Guide 1.60 spectrum (NRC, 1973), scaled to a site-specific peak ground acceleration value. Regulatory guidance for the determination of Safe Shutdown Earthquake (SSE) ground motion (NRC, 1997a) provides a hazard-consistent approach for determining the seismic design basis ground motion spectrum at a site. The procedure emphasizes site-specific determination of the SSE ground motion. Although a standard site-independent spectrum may still be used as the design basis ground motion spectrum, the procedure requires that this spectrum be scaled to the site-specific average ground motion levels for 5 and 10 Hz, and 1 and 2.5 Hz, representing the controlling earthquake as determined from deaggregation of a probabilistic seismic hazard analysis. These guidelines substantially advance the state of practice for determination of seismic design basis ground motion by including the effects of specific, dominant earthquakes on the frequency content of ground motion. However, it is recognized that additional improvements could be provided with respect to site-specific spectral shape estimation.

Revision 3 of the Standard Review Plan (SRP) 2.5.2 (NRC, 1997b) provides a hierarchy of acceptable approaches for the estimation of seismic ground motion at a site. In descending order of preference these are:

1. The direct use of a sufficiently large number of both horizontal and vertical component strong motion recordings selected to model the site-specific conditions for the controlling earthquakes, including: magnitude, type of faulting, tectonic environment, distance, source depth, regional attenuation and local site wave propagation characteristics;

2. For sites where a large enough ensemble of strong motion recordings is not available representing the site-specific controlling earthquake conditions, the guidance permits scaling strong motion recordings to represent the best estimate of the earthquake source, propagation path and site properties and doing sensitivity studies to evaluate the effects of scaling;

3. For a combination of site and controlling earthquake conditions where representative strong motion recordings are not available, peak motion parameters (peak acceleration, spectral acceleration, velocity and displacement) estimated using state-of-the-art attenuation relationships appropriate for the region of the site and the site geology, may be used to scale site-independent, standard spectral shapes; and

4. The use of theoretical-empirical estimation procedures may be used in a supplemental role when the appropriateness of the model is thoroughly documented.

The development of the SRP ground motion estimation hierarchy attempts to reflect the current state of the profession's uncertainty in ground motion estimation methods together with limitations of available data and to provide reasonable assurance that the ground motion at any site would be conservatively estimated. Recent studies (EPRI, 1993a) have shown however that the uncertainty in ground motion estimates results from the complex interaction of the large number of parameters of the ground motion estimation model. It is difficult to capture the total uncertainty even with the large number of strong motion recordings now available in California. This fact is confirmed by each successive large earthquake, which seems to require modification of the empirically-based ground motion estimation models.

The hierarchy also assumes that ground motion data are transferable from one region to another by matching important source properties such as magnitude, fault type, and tectonic environment; path properties such as distance, hypocenter depth, and attenuation; and site properties such as shear wave velocity. The EPRI (1993a) work has shown that these parameters contain significant random variability and uncertainty and interact in complex ways that are not likely to be adequately captured even by a reasonably large data set, and almost certainly would not be captured by a limited data set that would pass the site-controlling earthquake combination screening. In addition it is now recognized that strong motion recordings at sites in California and other active tectonic regions can not be transferred to continental interior regions. That is, it is not appropriate to use (without proper modification) empirical data from California to represent ground motions in the central and eastern United States (CEUS), and the available data set in the CEUS is too limited to use a direct empirical approach.

For the above reasons it is necessary to use the theoretical-empirical modeling method to estimate ground motions in the eastern United States. The method, described in EPRI (1993a), uses a theoretical model to estimate ground motion amplitudes in the frequency band of interest to engineering analysis and design. The power of the method is that it can be validated using large California data sets that span a wide range of magnitudes. The method develops a *theoretical* estimate of the ground motion spectrum based on parameters of the fault rupture (magnitude, stress drop) and travel path (distance, crustal and surficial rock properties). In regions of few recordings of strong shaking, the parameters can be estimated with *empirical* data from seismograph records. This gives a means to reliably estimate strong ground shaking when records of only weak shaking are available. In addition, site-specific geology and soil information can be quantitatively incorporated directly into the ground motion estimation at any particular site. Thus the method can be applied to any site-controlling earthquake combination to estimate site-specific ground motion and its uncertainty. The method may be applied equally well to develop standardized response spectra for combinations of well-defined site categories, controlling earthquakes and tectonic or regional seismic wave propagation environments.

The Regulatory Guide 1.60 spectrum was derived from a limited set of strong motion recordings primarily at deep alluvial sites in California, beyond 20 km from moderate to large magnitude earthquakes. The data set resulted in relatively high spectral amplification (Sa/A) in the frequency range of primary interest, but spectral amplification for frequencies above 10 Hz was too low even for California sites on rock conditions. Scaling this spectrum at 33 Hz to typical peak acceleration values derived from seismological considerations normally resulted in excessively conservative seismic

demands on plant structures, systems and components (SSCs), particularly for sites located in the eastern United States. This reality stimulated extensive research to develop an "effective acceleration" parameter to scale the standard spectrum so that it would represent the appropriate level of regulatory conservatism (Kennedy et al., 1984; Kennedy et al., 1985; Luco et al., 1986; Power et al., 1986). More recently this work has been extended, taking the somewhat different direction of focusing on the role of inelastic energy absorption in the damaging effectiveness of ground motions (EPRI, 1993b). The results of the EPRI work indicate that high frequency motions above about 20 Hz are not likely damaging, except to brittle components such as relays and ceramic insulators. The work provides the basis for establishing a displacement criterion for conditioning the high frequency amplitudes and developing a damage-consistent ground motion spectrum. This displacement criterion would rely on structural response to condition the ground motion spectral shape and should adequately consider the response of secondary systems. Spatial coherency also has been shown to be an important consideration for establishing ground motion design spectra (Abrahamson et al., 1991). Incoherency increases with increasing frequency. Thus we need a criterion coupling the high frequency amplitude reduction based on inelastic energy absorption with the reduction caused by spatial incoherency is needed. These considerations will be very important in the development of standard response spectra for future application. It would be desirable to develop generic criteria for deriving a damage consistent response spectrum that is fully compatible and easily implemented with ground motion spectral estimates based on geotechnical considerations, either in a site-specific mode or for standardized spectra for different classes of site and regional attenuation conditions.

The limitations in the use of the R.G. 1.60 spectrum involve both the shape of the spectrum and the consequences to structural design and liquefaction analyses. The limitations of the R.G. 1.60 shape fundamentally stem from its early development during the late 1960's and reflect both the limited data available and knowledge base at that time. Approximately 15 earthquakes were available with recordings at about 15 sites. The strong motion data set was comprised of earthquakes of varying magnitudes (M about 5.2 to over 7.5), mixed mechanisms, a large distance range, and poorly known site conditions (mostly deep soil; Newmark et al., 1973).

To develop design spectra two teams (Blume et al., 1972 and Mohraz et al., 1972) separately analyzed almost identical data sets. To develop shapes, different normalization schemes were used by each team. In both studies, amplification or scale factors on peak ground motion parameters were derived from statistical analyses on normalized shapes to construct smooth design spectra for varying fractile and damping levels. In the Blume study, a single normalization parameter, peak ground acceleration ("A"), forms the basis for the shapes with scaling factors specified at fixed anchor points. Although data were partitioned, no clear trends in the shapes based on A level, site condition, or distance were discerned.

In the Newmark study (Mohraz et al., 1972) spectral amplification factors on A, peak ground velocity ("V"), and peak ground displacement ("D") were developed to construct the design spectrum. The Newmark study led to the scaling of A, V, and D over regions of reasonably constant spectral acceleration, velocity and displacement. Because the variability in strong ground motion data increases with increasing period, normalizing to high, medium, and low frequency parameters over high, medium, and low frequency ranges in the spectra results in scaling factors that reflect more

uniform statistics. Because of this multiparameter scaling based on peak ground motion values and variable anchor points, the shape based on A, V, and D does, to some extent, accommodate site and magnitude dependencies in V/A and AD/V^2 ratios. (These ratios are often labeled "V/A" and AD/V^2," respectively.)

Based on the two studies, the NRC adopted and formalized a slightly modified form of the single parameter shape (Newmark et al., 1973) as a recommendation in R.G. 1.60.

The single parameter scaling resulted in a shape that was source, path, and site independent. That is, the relative spectral content did not vary and only the absolute levels changed with A (Coats, 1980; Gupta, 1990). A limitation that resulted from the small size of the data set available was that both the fractiles and damping scaling were not well constrained. In addition, due to the normalization to A, the fractiles were not uniform over frequency. The R.G. 1.60 horizontal component shape was generally representative of an 84^{th} percentile for **M** of about 6.75 at a deep soil site and at a distance of about 20-30 km, the 84^{th} percentile representing variability in spectra scaled to the same values of A, V, and D. The scale factors for the vertical component, 1 at high frequency (>3 Hz) and 2/3 at low frequency were reasonable for distances in the 20-40 km range for soil and about the 10-20 km range for rock. The appropriateness of these factors at other distance ranges was questionable, based on recent empirical data.

Later analyses of spectral shapes (Sa/A) with an emphasis on site conditions (Seed et al., 1976; Mohraz, 1976) attempted to resolve strong differences in shapes as well as V/A and AD/V^2 ratios based primarily on site stiffness. Depending on site conditions, site specific smooth response spectral shapes may significantly depart from these standard spectral shapes.

Recent work shows that the dependence of spectral shapes on source, path, and site conditions is well constrained by both recorded motions and the results of well validated modeling (Silva, 1991; Silva et al., 1997). In general, shapes broaden and show a shifting of the peak spectral amplification to lower frequencies with increasing magnitude due to a decrease in the earthquake source corner frequency (Silva, 1991; Silva and Darragh, 1995). Site dependencies are reflected in an increase in spectral levels at low frequencies and a decrease in levels at high frequencies as site stiffness decreases due to a combination of site amplification and material damping. This site effect also results in a shifting of the peak spectral amplification to lower frequencies, presumably as a result of an increase in material damping with decreasing site stiffness. This is especially evident at very stiff (rock) sites (Silva and Darragh, 1995). An additional observation of site effects is the reduction in maximum spectral amplification with decreasing site stiffness. For rock sites, the maximum spectral amplification is approximately 2.1 to 2.3 and decreases for soil sites. This reduction in peak spectral amplification is directly related to the shear-wave velocity gradient in the relatively shallow (<200 ft) portion of the rock/soil column, and to nonlinear, amplitude-dependent response of the soil itself.

In addition to these far-field dependencies, near-fault effects such as pulse-like motions can dramatically influence spectral content in large earthquakes ($M \geq 6$). Some of these effects are most pronounced within about 10 km: the fault normal component is about 30% larger than the fault parallel component in the frequency range 0.2 to 0.5 sec due primarily to rupture directivity, and the vertical motions can exceed the horizontal at frequencies above about 5 Hz. Directivity effects are

strongest for strike slip motion on vertical faults but can also be significant for cases of updip directivity for sites located near dipping faults. Other factors, perhaps strongest at close distances, include hanging wall/foot wall site location as well as thrust verses strike slip or normal slip mechanisms. These additional factors can have significant impacts on spectral composition.

In summary, the R.G. 1.60 spectral shape given A is very conservative for hard rock sites, at frequencies below 10 Hz and for distances exceeding about 10 km (Reed et al., 1993). For frequencies above 10 Hz the spectral shape is unconservative for these conditions. For soil sites, the degree of conservatism or underconservatism depends upon the particular site soil profile and whether the controlling magnitude differs significantly from about 6.75. The results of systematic SSI analyses (Power et al., 1986) for varying input motions and foundation conditions supported the desirability of site-specific ground motion characterization. The analyses also indicated that the R.G. 1.60 spectral shape provides a generally conservative design basis due to its broad-band nature. Another issue associated with using the R.G. 1.60 spectral shape as the design motion at the ground surface is that it leads to problems when applied at softer soil sites. When using typical deconvolution methodology incorporating strain dependent soil degradation properties, numerical problems are often encountered when generating foundation level motions (EPRI, 1993a). These problems indicate that the broad-band nature of the R.G. 1.60 spectral shape is generally incompatible with the softer soils.

R.G. 1.165, released in March, 1997, looks at the safe shutdown earthquake ground motion as a composite design motion resulting from many possible earthquakes. Two frequency ranges are defined: 5-10 Hz, for a high-frequency controlling earthquake, and 1-2 Hz for a low-frequency controlling earthquake. Deaggregation of seismic hazard is recommended for both frequency ranges, and the dominant magnitudes and distances from a seismic hazard perspective are identified. Spectra from these dominant events are then developed and scaled to probabilistic seismic hazard results for the high- and low-frequency controlling earthquakes. These spectra are smoothed and enveloped to obtain a safe shutdown ground motion.

Several issues are not addressed by R.G. 1.165. Specifically, the spectral shapes to be used for dominant events are not documented, the ground motion time histories for use in dynamic analysis are not described, and the issue of soil response is not addressed in detail in terms of an acceptable procedure. Also, methods for modifying hazard-consistent spectra (with constant annual frequency of exceedence) to achieve *risk*-consistent spectra (with constant annual frequency of component or plant failure) is not addressed. The overall purpose of the current project is to facilitate the R.G. 1.165 methodology by addressing these issues and documenting ground motion records and spectra. The following subsection describes details of the objectives of the current study.

1.2 Objectives and Scope

The overall objectives of this project are to (1) update the standardized design spectra used in the evaluation of nuclear facilities to accommodate the effects of magnitude, site condition, distance, and tectonic environment, (2) assemble a database of strong motion records appropriate for use in design analyses, (3) recommend procedures and requirements for the scaling of ground motion records to be consistent with design spectra, (4) develop recommendations for conducting site response analyses to produce soil motions consistent with rock outcrop hazard results (hazard consistency), and (5)

develop recommendations on how to derive seismic design spectra that provide risk consistency (uniform conservatism) across structural frequency. These objectives support the goal of developing uniform hazard spectra and design spectra that take into account the seismic threat at a site and the response of surficial rock and soil to that threat. Figures 1-1 and 1-2 present flowcharts of the recommended procedure for developing design ground motions on rock and soil, respectively, with references to Sections of this report.

The procedure for rock sites (Figure 1-1) starts with a probabilistic seismic hazard analysis (PSHA) at a site using rock conditions. The hazard results at 10 and 1 Hz are then deaggregated following the method of RG 1.165 described in the previous section, and are scaled to achieve approximate risk-consistency over all sites and frequencies to calculate a Uniform Reliability Spectrum (URS). This deaggregation and scaling is described in Section 7 of this report.

The scaled spectral values at 10 and 1 Hz are then used to scale rock spectral shapes for the appropriate magnitude **M** and distance R. This procedure is described in Section 4. With the scaled rock spectral shapes, time histories are selected from the appropriate **M**-R bin, as described in Section 3. The time histories are then scaled to the URS at 10 and 1 Hz, are compared to the scaled spectral shapes, and are adjusted (using procedures described in Section 5) to match the target. For rock sites these adjusted time histories are used to conduct building dynamic analysis.

For soil sites (Figure 1-2) the first five steps are the same as for rock sites, except that the uniform hazard spectrum (UHS) is not scaled to a URS but is used as calculated to define the target spectra. The reason is that the scaling of UHS to URS depends on the slope of the hazard curve, and for soil sites, the slope must be determined by several soil analyses at different amplitudes. Following the adjustment of time histories to match the target spectra, dynamic soil analysis is performed with parameter uncertainty, using the scaled rock time histories as input. Recommendations for this soil analysis are presented in Section 6. The relevant soil spectrum or spectra (depending on the number of dominant earthquakes) are calculated as the average spectrum (or spectra) over earthquake and soil uncertainties. These average spectra themselves become target spectra and are adjusted to a URS to account for the slope of the soil hazard curves, as described in Section 7. Then time histories from soil sites are chosen based on the dominant **M** and R values (in a similar manner to rock time histories, as described in Section 3). The soil time histories are then spectral matched to the target spectra (as described in Section 5) and are used as input to building dynamic analysis.

Figures 1-1 and 1-2 indicate that one or several time histories may be picked and adjusted to spectral shapes. While it may be possible to conduct a structural analysis with one time history that meets a target spectrum, it is preferable to conduct multiple analyses (perhaps up to 10 or 20) whose spectra on average, meet a target spectrum, so that the natural variability and phasing are peak-to-valley included in the analysis. For these records, a "weak matching" to the target spectrum may be appropriate. Details of these recommendations will be presented in an applications report to be issued at a later date.

This project defines the recommended procedure for developing design ground motions in terms of databases (spectral shapes and time histories) and recommended methods of analysis (deaggregation and scaling of hazard results to achieve risk-consistency, scaling of spectral shapes, spectral matching,

and soil dynamic analysis). Overviews of these databases and procedures are described in the following sections. Using these procedures, design ground motions can be calculated at sites that reflect up-to-date spectral shapes, both for the western US (WUS) and central and eastern US (CEUS). The motions will be approximately risk-consistent across frequency and for different seismic threats. Time histories of motion can be derived consistent with the spectral shapes for dynamic analysis. Finally, motions on soil sites can be derived by a procedure consistent with that for rock sites. None of these features are available in current methods of developing design ground motions.

1.3 Development of Recommended Spectral Shapes

The recommended spectral shapes accommodate continuous **M** and R scaling as well as potential differences in WUS and CEUS earthquake source processes. They are normalized by peak acceleration, since it is the spectral ordinate with lowest variability (Youngs et al., 1995), and are provided for both soft and hard rock site conditions (defined in Section 4) occurring in either western United States (WUS) or central and eastern United States (CEUS). Shapes for soil categories are not developed since soil response can depend heavily on the characteristics of control motions due to nonlinear dynamic material properties.

The intended use of the revised motions is to provide more realistic spectral shapes for applications of the Regulatory Guide 1.165 (NRC, 1997a) procedure to develop an overall design spectrum. In this procedure, spectral shapes are scaled to the rock outcrop UHS at frequencies near 10 and 1 Hz. For both frequency ranges, shapes are used which reflect the dominant contributions in both magnitude and distance to the UHS. The advantage of this approach, combined with realistic spectral shapes, is that the scaled shapes will represent seismic events that dominate the hazard for different structural frequency ranges as well as distance ranges. The use of rock outcrop control motions avoids the ambiguities in going from soil surface motions to foundation levels and provides for the direct development of site specific motions that accommodate variability in dynamic material properties.

Since the appropriate hazard level is provided by the UHS, which accommodates both epistemic and aleatory variability conditional on **M** and R, the revised shapes reflect median fractile estimates. Increased broadening of the shapes resulting from applying higher fractile levels is neither warranted nor desired as it can lead to potentially unconservative soil motions due to nonlinearity.

The frequency range of the recommended shapes extends from the lowest frequency that can be reliably obtained from the current strong-motion data set from the WUS (principally California), 0.2 Hz, to 100 Hz. The high frequency limit of 100 Hz permits the ratio of spectral acceleration/ peak ground acceleration to reach nearly 1 for hard rock site conditions. For soft rock conditions, this ratio will reach 1 at about 40-50 Hz. Criteria for spectrum compatible time histories extend to 25 Hz, which captures the range of primary importance to nuclear power plant structures and equipment (0.2 Hz to 25 Hz) for both CEUS and WUS motions.

The development of the spectral shapes for WUS conditions involves the use of empirical attenuation relations. Since these attenuation relations are generally defined over applicable magnitude and

distance ranges, these considerations must also apply to the shapes. In general the shapes are considered valid in the **M** (moment magnitude) range of about 4.75 to 8.0 for both WUS and CEUS conditions. Regarding applicable distances, we consider WUS (soft rock) shapes valid from 0 to about 200 km for crustal earthquakes, with appropriate consideration for near fault effects (Section 4), and out to about 400 km for CEUS conditions. The WUS shapes are considered appropriate for Cascadia subduction zone earthquakes for **M** up to about 9 and closest rupture distances out to about 300 km (Section 4).

1.4 Time History Database For Analysis

An important aspect of this project is the development of a time history database for analyses. The database is parsed into **M** and R bins (Table 1-1) which were selected to preserve significant differences in spectral composition and time domain characteristics (e.g. duration). The bins are also appropriate for potential high and low frequency controlling earthquakes in both the WUS and CEUS. The WUS time history bins are the same ones used in developing the WUS spectral shapes, preserving consistency between an average bin shape (Appendix C) and the revised shapes (Section 4) computed for bin average **M** and R values.

The bin database is to provide appropriate records for spectral matching as well as scaling. Since each bin contains records reflecting ranges in **M** and R, guidelines are given for within bin **M** and R adjustments for either constant or narrow band scaling.

For applications to the WUS, the bins are populated largely with recorded motions. Sparse bins have been supplemented with scaled empirical records (from adjoining bins) as well as a few direct finite-fault simulations. For the CEUS, since few recordings exist, the recommendation is to generate motions by scaling WUS records. The scaling procedure is the same as that used to correct the WUS rock shapes to CEUS conditions. While not as desirable as recorded motions, these time histories will be suitable for analyses. They should be replaced as appropriate data become available and as simulation methods improve and become better validated for CEUS conditions.

1.5 Site Specific Soil Motions

The most desirable form of site ground motion design requirements are based on hazard curves appropriate for the soil surface, embedment depth, and any other site conditions upon which category 1 structures are founded. The site-specific hazard curves, from which the required sets of UHS may be obtained, should also accommodate uncertainty in site-specific dynamic material properties as well as local and regional seismicity and attenuation characteristics. This ideal situation of exact consistency among hazard curves for different elevations and soils at a site would then permit the seismic risk to all structures, systems, and components to be evaluated on a consistent basis. One calculation-intensive way to accomplish this is to perform seismic hazard analyses separately for all elevations and site conditions at a site. While this approach has been used on several occasions (for a single rock/soil column), it is not a particularly straightforward task, and involves many assumptions and several limitations. For one thing, a rock PSHA can be performed with regional, not site-specific data, and so can be completed prior to site-specific soil parameters being collected. Also, if multiple distinct soil columns exist at a plant site, or if some critical structures are founded on soil and some

on rock, the same rock PSHA should be used for all. Finally, if new soil data are collected, the effects on design spectra can be determined quickly, without redoing the PSHA. For all of these reasons, it is recommended to perform the PSHA for appropriate rock (rock like) conditions, then modify the rock UHS to reflect the effects of local soils.

There are several approaches to estimate soil UHS given rock outcrop UHS and these are demonstrated in Section 6. These methods are compared to directly computed soil UHS using site specific attenuation relations. Applying these methods at two hazard levels one can then approximate the slope of the soil hazard curve. Also discussed are approximate methods to compute the soil hazard curve given rock UHS and a set of numerical convolutions. The method selected for a particular application will likely depend upon desired accuracy (minimize overconservatism), degree of currently available site information, and computational rigor required.

1.6 Development of Uniform Reliability Spectra (URS)

One of the objectives in developing seismic design spectra is to achieve approximate uniformity of seismic risk for structures, equipment, and components designed to those spectra, across a range of seismic environments, annual probabilities, and structural frequencies. By "seismic risk" we mean the annual frequency of failure of a plant system or of its components, as opposed to "seismic hazard" which is the annual frequency of exceedence of a level of ground motion. By "uniformity," we mean that the procedures should not result in relatively high seismic risk for certain conditions, and relatively low seismic risk for others.

The procedures for developing risk-consistent spectra are illustrated by examining nine existing nuclear plant sites in the central and eastern US, and two hypothetical sites in the western US (California and Washington). Existing seismic hazard curves are used to convolve seismic hazard with component fragility curves to calculate probabilities of failure for a range of structural frequencies. The characteristics of seismic hazard span the range of amplitudes and slopes that can be expected in the US.

A simple modification to the uniform hazard spectrum (UHS) is recommended to achieve a uniform reliability spectrum (URS) consistent across structural frequencies. This modification accounts for the varying slopes of the hazard curves; the UHS is increased where the slope is shallow (e.g., at low frequencies), and is decreased where the slope is steep, so that approximate uniform reliability risks result from choosing a modified UHS with a target annual probability of exceedence.

1.7 Contents of Report

Section 2 of this report presents a background on the differences between WUS and CEUS strong ground motions on rock sites. These are important differences, and they influence many of the procedures used in this project. We do not, for example, develop recommended spectral shapes empirically in the WUS, and apply those to CEUS earthquakes.

One of the fundamental results of this project is a library of strong motion records. For the WUS these are largely empirical records, for the CEUS these are largely synthetic time histories. These databases are described in Section 3.

The design spectral shapes are documented in Section 4. These shapes are presented for the same **M** and *R* bins used for the strong motion library but are continuous functions of magnitude and distance, and Section 4 describes the scaling used to obtain the CEUS spectral shapes.

Synthetic motions are often used for time history analysis of structures, and we make recommendations on the spectral characteristics required of such synthetic motions to achieve an acceptable match with target design spectra. Guidelines are also presented for appropriate durations as well as V/A and AD/V^2 ratios for scaled time histories. These recommendations are documented in Section 5.

Section 6 examines several methods for deriving UHS for soil conditions given the rock UHS at the same site. As discussed above, several methods are available, and each is explored and demonstrated in this section.

Finally, recommendations on achieving risk consistency across sites and structural periods are contained in Section 7. These recommendations take into account the absolute level of hazard and the slope of the hazard curve at different sites.

References

Abrahamson, N.A., J.F. Schneider and J.C. Stepp (1991). "Empirical Spatial Coherency Functions for Application to Soil-Structure Interaction," *Earthquake Spectra*, Vol. 7, Earthquake Engineering Research Institute, Oakland, CA.

Blume, J.A., R.L. Sharpe and J.S. Dalal (1972). "Recommendations for Shape of Earthquake Response Spectra." John A. Blume and Associates, San Francisco, CA. *AEC* Report No. 1254.

Coats, D.W. (1980). "Recommended Revisions to Nuclear Regulatory Commission Seismic Design Criteria." U.S. Nuclear Regulatory Commission Washington, D.C. NRC FIN No. A-0140, NUREG/CR-1161.

EPRI (1993a). "Guidelines for Determining Design Basis Ground Motions, Volume 1: Method and Guidelines for Estimating Earthquake Ground Motion in Eastern North America," TR-102293, Electric Power Research Institute, Palo Alto, CA.

EPRI (1993b). "Analysis of High-Frequency Seismic Effects," TR-102470, Electric Power Research Institute, Palo Alto, CA.

Gupta, A.K. (1990). *"Response Spectrum Method in Seismic Analysis and Design of Structures."* Foreword by W.J. Hall, Blackwell Scientific Publications, Boston Oxford, London Edinburgh Melbourne.

Kennedy, R.P., Short, S.A., Merz, K.L., Tokarz, F.J., Idriss, I.M., Power, M.S, and Sadigh, K. (1984). "Engineering characterization of ground motion, Task I: Effects of characteristics of free-field motion on structural response." Prepared for U.S. Nuclear Regulatory Commission. NUREG/CR-3805, vol. 1., Washington, DC.

Kennedy, R.P., R.H. Kincaid, and S.A. Short. (1985). "Engineering Characterization of Ground Motion, Task II: Effects of Ground Motion Characteristics on Structural Response Considering Localized Structural Nonlinearities and Soil-Structure Interaction Effects," NUREG-3805, Vol. 2, USNRC, Washington, DC.

Luco, J.E. et al. (1986). "Engineering Characterization of Ground Motion, Task II: Soil-Structure Interaction Effects on Structural Response," NUREG-3805, Vol. 4, USNRC, Washington, DC.

Mohraz, B. (1976). "A Study of Earthquake Response Spectra for Different Geological Conditions." *Bull. Seism. Soc. Am.*, 66(3) 915-935.

Mohraz, B., Hall, W.J. and Newmark, N.M. (1972). "A Study of Vertical and Horizontal Earthquake Spectra." Nathan M. Newmark Consulting Engineering Services, Urbana, IL: *AEC Report* No. WASH-1255.

Newmark, N.M., J.A. Blume and K.K. Kapur (1973). "Seismic Design Criteria for Nuclear Power Plants." *Journal of the Power Division,* ASCE 99, 287-303.

NRC (1973). "Design Response Spectra for Seismic Design of Nuclear Power Plants," Regulatory Guide 1.60, Revision 1, USNRC, Washington, DC.

NRC (1997a). "Identification and Characterization of Seismic Sources and Determination of Safe Shutdown Earthquake Ground Motion," Regulatory Guide 1.165, USNRC, Washington, DC.

NRC (1997b). "Standard Review Plan, 2.5.2 Vibratory Ground Motion," USNRC, Washington, DC, NUREG-0800, Rev. 3, March.

Power, M.S., C.Y. Chang, I.M. Idriss and R.P. Kennedy (1986). "Engineering Characterization of Ground Motion." U.S. Nuclear Regulatory Commission, Summary R vol. 5, NUREG/CR-3805.

Reed, J.W., Kennedy, R.P. and Lashkari, B. (1993). "Analysis of High-frequency Seismic Effects." Palo Alto, CA: Electric Power Research Institute, vol. 1-5, EPRI TR-102470.

Seed, H.B., C. Ugas and J. Lysmer (1976). "Site-dependent Spectra for Earthquake Resistant Design." *Bull. Seism. Soc. Am.*, 66(1), 221-243.

Silva, W.J., N. Abrahamson, G. Toro, C. Costantino (1997). "Description and validation of the stochastic ground motion model." Report to Brookhaven National Laboratory, Associated Universities, Inc. Upton, New York, Contract 770573.

Silva, W.J. and R. Darragh (1995). "Engineering Characterization of Earthquake Strong Ground Motion Recorded at Rock Sites." Palo Alto, CA: Electric Power Research Institute, TR-102261.

Silva, W.J. (1991). "Global Characteristics and Site Geometry." Chapter 6 in *Proc.: NSF/EPRI Workshop on Dynamic Soil Properties and Site Characterization.* Palo Alto, CA: Electric Power Research Institute, NP-7337.

Youngs, R.R., N.A. Abrahamson, F. Makdisi, and K. Sadigh (1995). "Magnitude dependent dispersion in peak ground acceleration." *Bull. Seism. Soc. Am.*, 85(1), 1161-1176.

Table 1-1

WUS, CEUS M AND *D* BINS

	Distance (km)				
M	0 - 10	10 - 50	50 - 100	100 - 200	200 - 400
5 - 6	B	B	B	B	-----
6 - 7	B	B	B	B	-----
7+	B	B	B	B	C

B = both WUS and CEUS
C = CEUS only

Overview of Design Ground Motion Procedure and Application to Rock Sites

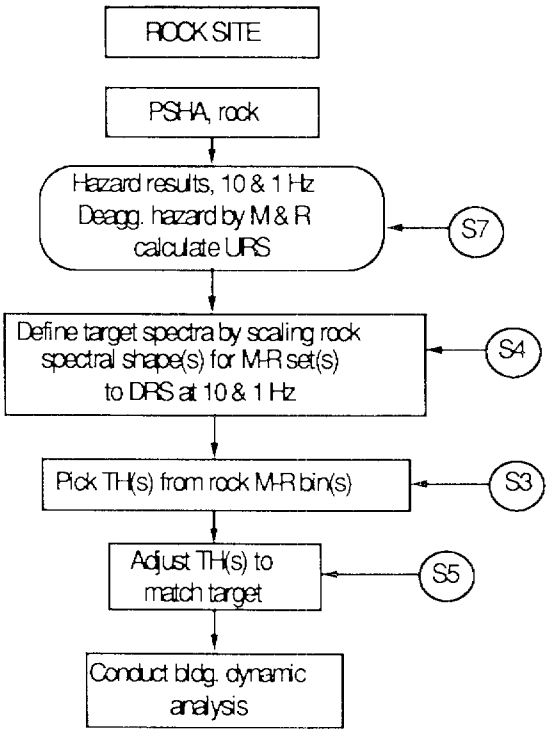

Figure 1-1: Flowchart of design ground motion procedure and application to rock sites. S3, S4, etc. refer to Sections of this report, TH = time history.

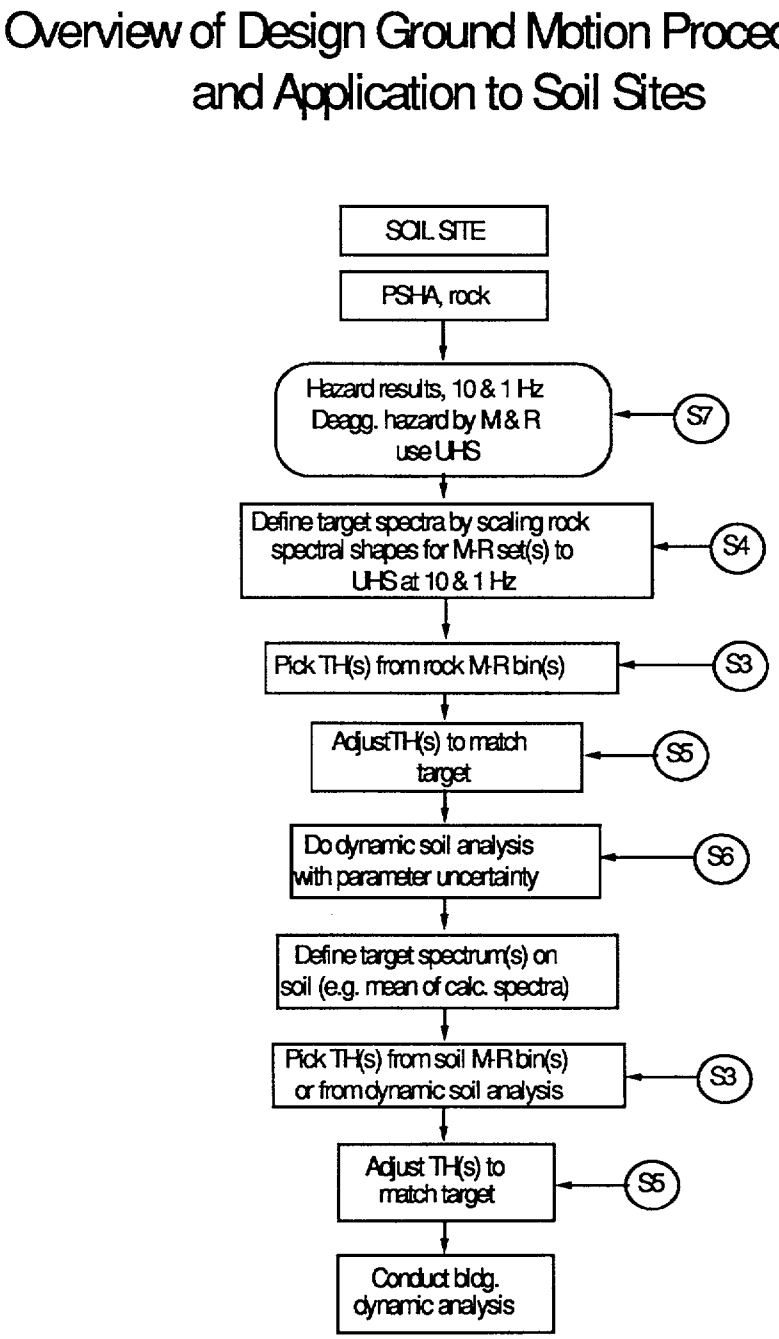

Figure 1-2: Flowchart of design ground motion procedure and application to soil sites. S3, S4, etc. refer to Sections of this report, TH = time history.

2 CHARACTERISTICS OF WUS AND CEUS STRONG GROUND MOTIONS AT ROCK SITES

Ground motion observations of both small and intermediate magnitude earthquakes that have occurred in eastern North America show larger peak ground accelerations as well as higher spectral amplitudes for frequencies > 5 Hz than would be expected based on recordings in western North America, principally California (Brady et al., 1981; Chang, 1983; Borcherdt, 1986; Wesson and Nicholson, 1986; Weichert et al., 1982; 1986; Munro and Weichert, 1989; Silva and Darragh, 1995). In addition to these observations at high frequencies, intermediate magnitude (**M** ≈ 6.2) earthquakes have shown an opposite trend for frequencies below about 2 Hz, having lower motions than comparable (**M**, distance, and site condition) WUS recordings would suggest (Boore and Atkinson, 1992; Atkinson, 1993; Silva and Darragh, 1995). This latter observation, in terms of strong ground motions, is principally limited to the 1988 **M** 5.8 Saguenay, Canada earthquake but is supported by inferences from intensity data (Atkinson, 1993), regional seismograms ($R \approx 1{,}000$ km) of early instrumental recordings in eastern North America (Atkinson and Chen, 1997), and teleseismic data of worldwide intraplate earthquakes (Boatwright and Choy, 1992).

The differences in high frequency spectral content between WUS and CEUS strong ground motions is pervasive and reasonably well understood (Boore and Atkinson, 1987; Boore et al., 1992; EPRI, 1993; Silva and Darragh, 1995; Atkinson, 1996) especially for very stiff (rock) site conditions. As a result, there is little doubt that future earthquakes occurring in the CEUS will have high frequency spectral characteristics at rock sites distinctly different than the WUS (California) experience. Conversely, the differences in low frequency spectral content between WUS and CEUS strong ground motions is neither well constrained through direct observations nor understood physically. The following discussion illustrates the differences between WUS and CEUS rock site motions and suggests the physical bases for the differences.

2.1 Differences Between CEUS And WUS Rock Site Strong Ground Motions

Observations of strong ground motion due to small magnitude earthquakes occurring in eastern North America, although not causing damage to engineered structures, have shown considerably higher peak accelerations than would have been expected based upon WUS experience (Brady et al., 1981; Chang, 1983; Wesson and Nicholson, 1986; Weichert et al., 1982; 1986; Munro and Weichert, 1989). In addition to the relatively higher peak accelerations associated with these CEUS events, response spectral ordinates appear richer in energy for frequencies exceeding about 5 Hz (Brady et al., 1981; Borcherdt, 1986).

It has been known for some time that ground motion for the CEUS attenuates less rapidly with distance than ground motion in the WUS for events of similar moment magnitudes and source depths (Nuttli, 1981; EPRI, 1993; Atkinson and Boore, 1995). The difference in attenuation rate has been attributed to the higher absorptive characteristics generally present in the crust and upper mantle beneath the WUS as compared to the CEUS (Nuttli, 1981; Herrmann and Nuttli, 1982; Singh and Herrmann, 1983; Boore and Atkinson, 1987; Toro and McGuire, 1987; Frankel et al., 1990; Hanks and Johnston, 1992; EPRI, 1993; Frankel, 1994; Benz et al., 1997). This difference is probably a

consequence of active plate margin tectonics in the WUS as opposed to conditions representative of a stable continental interior in the CEUS.

For close-in recordings, where the propagation path is short (< 20 to 30 km), the difference in crustal attenuation between the WUS and CEUS was thought to have a minimal effect, and strong ground motion was expected to be comparable in the two tectonic environments (Campbell, 1981, 1986; Kimball, 1983). However, close-in (< 20 km) strong motion recordings of the 1978 Monticello, South Carolina earthquakes with moment magnitudes of approximately 3 produced a maximum peak-horizontal acceleration of 0.25g (Brady et al., 1981; Mork and Brady, 1981) and the 1986 Painesville, Ohio earthquake with a magnitude of 5.0 ($m_{l,g}$) produced a peak acceleration of nearly 0.20g at an 18 km epicentral distance (Wesson and Nicholson, 1986). Both values are significantly higher than would be expected for earthquakes of similar magnitude and distance in the WUS. Recordings from both of these earthquakes also show unexpected high-frequency energy content in the response spectra compared to similar magnitude WUS recordings (Silva and Darragh, 1995).

Other sources of data also indicate that CEUS ground motions, recorded at rock or very shallow soil sites, are richer in high-frequency energy relative to analogous WUS ground motions. These include aftershocks of the 1982 Miramichi, New Brunswick earthquake (Cranswick et al., 1985), the 1982 Enola, Arkansas swarm (Haar et al., 1984), aftershocks of the 1986 Painesville, Ohio event (Borcherdt, 1986), the 1985 Nahanni earthquakes (Weichert et al., 1986), the 1982 New Hampshire earthquake (Chang, 1983), and the **M** 5.8 1988 Saguenay earthquakes (Boore and Atkinson, 1992). The trends shown in these CEUS data indicate significantly more spectral content at high frequencies compared to WUS rock motion of comparable magnitudes and distances (Fletcher, 1995; Silva and Darragh, 1995).

2.1.1 Effects of Shallow Crustal Damping

The difference in spectral content can perhaps be most easily seen in spectral amplification (spectral acceleration SA/PGA) computed from recordings typical of WUS and CEUS tectonic environments. Figure 2-1 shows average spectral shapes (SA/PGA) computed from recordings made on rock at close distances ($\leq$ 25 km) for **M** $\approx$ 6 and 5 earthquakes in CEUS and WUS tectonic environments, using records archived for this project. The differences are significant and indicate that CEUS spectral content is higher than that in the WUS for frequencies greater than approximately 10 Hz.

The controlling mechanism for the differences in high frequency spectral content (at close distances) between WUS and CEUS ground motions is thought to be due to differences in damping in the shallow (1 to 2 km) part of the crust (Boore and Atkinson, 1987; Silva et al., 1989a, 1989b; Silva, 1991; Silva and Darragh, 1995). The effects of shallow crustal damping were first pointed out and quantified by Hanks (1982) and Anderson and Hough (1984). The parameter that controls the shallow damping is termed kappa and is defined as the thickness of the zone over which the damping is taking place times the damping and divided by the average velocity over the zone of damping (Appendix D).

In a recent study, kappa values have been estimated by fitting spectral shapes computed from the stochastic ground motion model (Appendix D) to shapes computed from motions recorded at rock sites in eastern North America, WUS, Mexico, Italy (Friuli), USSR (Gazli), and Taiwan (SMART1) (Silva and Darragh, 1995). The kappa values are listed in Table 2-1; they reflect properties in the top 1-2 km of the crust. Results of these analyses indicate that kappa depends strongly on the material properties of the site. Rock sites characterized as soft, such as sedimentary, showed significantly higher kappa values than those characterized as hard, e.g. crystalline basement. Hard and soft rock sites may exist in either the WUS or CEUS; however, on the average, sites in stable cratonic regions such as the CEUS are more likely to be classified as hard in the top 1-2 km (low κ) while those associated with active tectonic regions such as the WUS are more likely to be soft in the top 1-2 km (high κ).

2.1.2 Effects of Crustal Amplification

An example of generic crustal models reflecting typical WUS soft rock and CEUS hard rock crustal conditions is shown in Figure 2-2 for both compression- and shear-wave velocities. The CEUS model is the midcontinent structure from EPRI (1993) and is considered appropriate for strong ground motion propagation in the CEUS except for the Gulf Coast region (Toro et al., 1997). The Gulf Coast region is typified by a crustal structure somewhat intermediate between those of the CEUS and WUS and is predicted to have correspondingly different wave propagation characteristics and strong ground motions (EPRI, 1993; Toro et al., 1997). The WUS model reflects an average of several California crustal models (Silva et al., 1997) representing the most seismically active regions, the north coast and peninsular range areas.

The differences in the shallow crustal velocities between the WUS and CEUS models is striking, particularly over the top 2 to 3 km, and the effects on strong ground motions are profound. In terms of amplification from source regions below about 5 km to the surface, the difference between hard (CEUS) and soft (WUS) crustal conditions is a factor of about 3 in amplification for frequencies exceeding about 5 Hz (Figure 2-3). All else being equal, WUS ground motions above ~5 Hz would then be expected to be nearly three times larger than corresponding CEUS motions. As suggested earlier however, pervasive observations reflect the opposite: high frequency CEUS motions generally exceed comparable WUS motions. Damping in the shallow crust, parameterized through kappa, is much greater in soft crustal rocks resulting in a dramatic loss in high frequency energy content compared to hard rock conditions. The differences in shallow crustal damping, or kappa, between soft and hard crustal conditions is a combined effect of lower velocities (Figure 2-2) as well as larger intrinsic damping. Kappa is defined as:

$$\kappa = \frac{H}{\overline{V_S}\,\overline{Q_s}}, \qquad \overline{Q_S} = \frac{1}{2\,\overline{\eta_s}} \tag{2-1}$$

where H is the thickness of the shallow crustal damping zone (1 to 2 km, Anderson and Hough, 1984; Silva and Darragh, 1995), $\overline{V_S}$ and $\overline{Q_S}$ are the average shear-wave velocities and quality factors over depth H, and $\overline{\eta_S}$ is the corresponding critical damping ratio (decimal). For soft rock conditions both the velocities and Q values are lower than hard rock conditions resulting in very large differences in

kappa values and corresponding energy absorption at high frequency. Table 2-1 lists kappa values determined at both WUS and CEUS rock sites (Silva and Darragh, 1995) and shows the strong dependence upon surficial geology in terms of rock quality. Hard and soft conditions can exist in both WUS and CEUS and are reflected in distinct kappa values, increasing as the rock quality degrades. On average, kappa values for the WUS are about 5 times larger than for the CEUS (0.037 sec and 0.008 sec, Table 2-1).

To illustrate the effects of kappa on strong ground motions, Figures 2-4 and 2-5 show response spectral shapes (5% damping) and absolute spectra computed for an **M** 6.5 earthquake occurring at a distance of 25 km for WUS parameters (see Table 2-2, parameter values from Silva et al., 1997) using a range of kappa values from 0.005 sec to 0.160 sec. For the shapes, Figure 2-4, increasing kappa results in a shift in shapes to lower frequencies as the PGA and high frequency spectral amplitudes decrease. For fixed magnitude, the frequency range of maximum spectral amplification is a good estimator of shallow crustal damping (Silva and Darragh, 1995).

The absolute spectra shown in Figure 2-5 further illustrate the effects of kappa on high frequency strong ground motions. A factor-of-two change in kappa results in about a 50% change in peak acceleration. The average difference in WUS and CEUS rock site kappa values of about 5 (Table 2-1) results in a difference of about a factor of four in high frequency ground motions, exceeding the factor of about three in the difference in high frequency (5 Hz) crustal amplification (Figure 2-3). Close-in strong ground motions (that is, at $\leq$ 50 km; "near-source" is reserved for distances $\leq$ 10-15 km), would be expected to be lower at CEUS rock sites than WUS rock sites at low frequencies, because differences in deep crustal properties such as frequency dependent damping (Q(f)) and depth to the Moho and Conrad discontinuities do not have large effects (EPRI, 1993). At high frequencies the converse would be expected, providing source processes are similar in both regions. Several lines of evidence suggest that this is not the case however, with CEUS sources generating more high-frequency energy, than WUS sources for the same **M**.

2.1.3 Effects of Source Processes

Another factor regarding the differences in spectral composition between WUS and CEUS strong ground motions at rock sites is the probable differences in earthquake source processes. Prior to the occurrence of the 1988 **M** 5.8 Saguenay earthquake, there was thought to be a difference of about a factor of two in stress drop (the difference in average stress across the rupture surface before and after an earthquake) between WUS and CEUS sources with the CEUS having larger stress drop values, about 100 bars compared to about 50 bars for the WUS (Atkinson, 1984; Boore, 1986). These measures of stress drop, termed Brune stress drops (Brune, 1970; Appendix D), are primarily based on high frequency ground motion levels assuming that in the frequency domain the source can be represented by a single-corner-frequency source model.

An alternative measure of stress drop is based on the ratio of the seismic moment (M_o) to the rupture area and is termed the static stress drop. The stress drop equation for a circular rupture surface is given by

$$\Delta\sigma = \frac{7}{16}\,\pi\,\frac{M_o}{(Area/\pi)^{\frac{4}{3}}} \qquad (2\text{-}2)$$

where *Area* is the area over which rupture occurs. This measure of stress drop was also thought to be higher (by about a factor of two) for earthquakes occurring in the CEUS compared to the WUS (Kanamori and Anderson, 1975; Kanamori and Allen, 1986). For static stress drops, the scaling of strong ground motions is not at all clear. However, since the average slip (fault displacement) is proportional to moment, and strong ground motions increase with slip (for fixed rupture area), strong ground motions must increase with static stress drop, at least at low frequency.

Apart from the differences in stress drops (Brune and static), overall source processes were thought to be similar in both tectonic regimes. The stochastic single-corner-frequency point-source model (Appendix D), originally developed by Hanks and McGuire (1981), provides accurate predictions of WUS strong ground motions using a stress drop of about 50 bars (Boore, 1986; Boore et al., 1992; Silva and Darragh, 1995) although with a tendency to overpredict low frequency ($\leq$ 1 Hz) motions for large magnitude earthquakes (Atkinson and Silva, 1997).

For the CEUS, the simple point-source model with a stress drop of about 100 bars, about double that of the WUS, provided good agreement with existing data (Atkinson, 1984; Boore and Atkinson, 1987; Toro and McGuire, 1987) until the occurrence of the 1988 M 5.8 Saguenay earthquake. Strong ground motions from this earthquake, the largest to have occurred in the CEUS in over 50 years, depart significantly from predictions of the simple 100 bar stress drop model (Boore and Atkinson, 1992). The stress drop required to match high frequency strong ground motions for this earthquake exceed 500 bars, while the intermediate frequency spectral levels are overestimated by a factor of two or more, requiring a significantly lower stress drop (Boore and Atkinson, 1992). Concurrently, Boatwright and Choy (1992) using teleseismic (low frequency, $\leq$ 2 Hz) data, showed that the source spectra of large intraplate earthquakes differ in general from the simple single-corner-frequency omega-square model, suggesting the presence of a second corner frequency. Based on the limited ground motion data in the CEUS as well as inferences from intensity observations, Atkinson (1993) developed an empirical two-corner source model for CEUS earthquakes. In this model, the high frequency spectral levels are consistent with Brune stress drop of about 150 bars while the equivalent stress drop for the low frequency spectral levels is about 40 to 50 bars (Atkinson, 1993), assuming the crustal model shown in Figure 2-2. This two-corner model currently provides reasonable estimates of recorded CEUS ground motions over the frequency range of the majority of the data, about 10.0 to 0.1 Hz, while the single-corner-frequency model, with stress drops ranging from about 120 to 150 bars, overpredicts ground motions in the frequency range of about 1 Hz to 0.1 Hz but gives a better fit in the 2 to 10 Hz frequency range (Atkinson and Boore, 1998). Both the double and single-corner source models, with stress drops below 200 bars, underpredict ground motions $\geq$ 2 Hz for the Saguenay earthquake by factors of 2 to 3 suggesting anomalous high frequency levels for this event. While it currently appears that the two-corner source model may be the more appropriate model for CEUS strong ground motions, it is evident that in predicting strong ground motions for engineering design, significantly more variability should be accommodated in applications to the CEUS than to the WUS. This increased variability should accommodate both randomness (aleatory variability) in stress drop above that for the WUS as well as uncertainty

(epistemic variability) in the source model. The larger variability in the CEUS should be represented in the PSHA for a site, and will be reflected in the mean hazard for the site.

For the WUS, recent work has shown some interesting results regarding earthquake source spectra. In the context of the single-corner-frequency model, stress drop appears to be magnitude dependent (Silva and Darragh, 1995; Atkinson and Silva, 1997; Silva et al., 1997), decreasing from about 100 bars for **M** 5.5 to about 50 bars for **M** 7.5 with an average value of about 70 bars. Since inferences on stress drop for CEUS sources are based predominantly on small magnitude earthquakes, **M** ≈ 5.2 (Atkinson, 1993), scaling of stress drop with magnitude similar to WUS would imply significantly lower stress drops for large magnitude earthquakes. The 150 bar stress drop for CEUS may reflect a value appropriate for **M** near 5.5. Assuming WUS stress drop scaling with **M** would result in an average stress drop of about 120 bars for **M** ranging from 5.5 to 7.5.

A model that appears to be more consistent with WUS source spectra inferred from the strong motion data is similar to the CEUS two corner model but with a less pronounced spectral sag at intermediate frequencies. The two-corner nature of WUS source spectra is filled-in by crustal amplification (Figure 2-3) resulting in a comparatively subtle feature in strong ground motions compared to CEUS data (Atkinson and Silva, 1997). This observation may provide some comforting linkage to CEUS source processes suggesting an appealing underlying similarity. However, CEUS sources, for the same magnitude, do appear to be considerably more energetic at high frequency, and this is reflected in larger Brune stress drops by a factor of about two on average.

To illustrate the effects of stress drop on ground motions, Figures 2-6 and 2-7 show response spectral shapes and absolute spectra (both for 5% of critical damping) computed for **M** 6.5 at a distance of 25 km using WUS parameters (Table 2-2). For the shapes, Figure 2-6, the effect of stress drop is small, with differences occurring at low frequency below about 1 Hz. Spectral shapes are largely independent of stress drop for ranges of 2 to 3 over most of the frequency band of interest.

The absolute spectra shown in Figure 2-7 illustrate the large effect Brune stress drops have on strong ground motions. The effect is strongest for frequencies exceeding the source corner frequency (Silva, 1993), about 0.2 Hz for a stress drop of 65 bars, and results in about a 70% change in peak acceleration for a factor-of-two change in stress drop. For the single-corner-frequency Brune source model, stress drop is a controlling parameter in absolute levels of strong ground motions.

Comparisons of WUS to CEUS response spectra are shown in Figures 2-8 and 2-9 for shapes and absolute spectra respectively. Also illustrated in the figures are the differences between the single- and double-corner source spectral models. In Figure 2-8, the difference in spectral shapes between the WUS and CEUS at single-corner models (solid and long dash lines) is clearly illustrated in the maximum spectral amplifications at about 5 Hz for the WUS and at about 40 Hz for the CEUS.

The difference between the single- and double-corner source models is also clearly illustrated. For the WUS, the difference is mainly at low frequency and is not large, about 20% near 0.3 Hz. For the CEUS, the single corner source model significantly exceeds the double corner below about 2 Hz. The largest difference occurs near 0.4 Hz and is a factor of over 3 in 5% damped spectral acceleration.

Choices between the two source models for the CEUS, single or double corner, clearly have major impacts on design motions.

The corresponding absolute spectra (not scaled) are shown in Figure 2-9. The WUS and CEUS single-corner spectral estimates are nearly the same for frequencies up to about 5 Hz. This is the result of compensating effects previously discussed, higher stress drop for CEUS (Table 2-2) and larger amplification factors for WUS (Figure 2-3). Beyond about 5 Hz, the differences in kappa values (0.04 sec compared to 0.006 sec, Table 2-2) result in the difference in high frequency spectral estimates.

To see how well the simple point-source models (single and double corner frequency) capture the differences in shapes between the WUS and CEUS rock motions that were illustrated in Figure 2-1, Figures 2-10 and 2-11 compare model predictions to **M** 6 statistical shapes. Figure 2-10 for the WUS compares both the single- and double-corner model predictions to the statistical shape. Both models capture the overall shape reasonably well but overpredict at low frequency (below 1 to 2 Hz). The double-corner model provides a better fit but still shows overprediction in this frequency range.

The comparison to CEUS **M** ≈6 is shown in Figure 2-11. There is only one earthquake, 1985 Nahanni, with hard rock site recordings (3 stations) in this magnitude and distance range. Both spectral models capture the difference in shape between WUS and CEUS equally well with the single-corner model showing an overprediction at low frequency (≤ 1 Hz) similar to the WUS. Interestingly, the double-corner model shows an underprediction for frequencies below about 2 Hz. Since this is only a single earthquake and variability is large in CEUS strong ground motions, these results should not be interpreted as a potential bias in the model for spectral shapes, but they do emphasize the current state of uncertainty regarding CEUS strong ground motions. Although the data have been processed, the overprediction beyond about 20 Hz may be an artifact of the instruments, which had a cutoff frequency of about 25 Hz.

For a comparison at **M** 5 , Figures 2-12 and 2-13 show results for the WUS and CEUS respectively. For the WUS, Figure 2-12 shows reasonable model predictions down to about 1 Hz, below which the number of spectra is greatly reduced because of increasing noise levels. Figure 2-13 shows the corresponding plot for CEUS **M** 5 comparisons. The models capture the shift in shape to higher frequency but overpredict for frequencies above about 20 Hz. As with the **M** 6 comparison, the low frequencies are enveloped by the two models. Since the **M** 5 statistical shape reflects the same Nahanni earthquake sequence with two aftershocks, model departures from observations are not considered particularly significant.

These comparisons to CEUS statistical shapes point out the quandary in estimating strong ground motions in the CEUS. Sufficient recordings at close distances (≤ 50 km) for earthquakes of engineering significance (**M** ≥ 5) are not available to unequivocally distinguish between plausible models.

References

Anderson, J. G. and S. E. Hough (1984). "A Model for the Shape of the Fourier Amplitude Spectrum of Acceleration at High Frequencies." *Bull. Seism. Soc. Am.* 74(5), 1969-1993.

Atkinson, G.M. (1984). "Attenuation of strong ground motion in Canada from a random vibrations approach." *Bull. Seism. Soc. Am.*, 74(5), 2629-2653.

Atkinson, G.M. (1993). "Source spectra for earthquakes in eastern North America." *Bull. Seism. Soc. Am.*, 83(6), 1778-1798.

Atkinson, G.M. (1996). "The high-frequency shape of the source spectrum for earthquakes in eastern and western Canada." *Bull. Seism. Soc. Am.* 86(1A), 106-112.

Atkinson, G.M. and D.M. Boore (1995). "Ground motion relations for eastern North America." *Bull. Seism. Soc. Am.*, 85(1), 17-30.

Atkinson, G.M. and D.M. Boore (1998). "Evaluation of models for earthquake source spectra in Eastern North America." *Bull. Seism. Soc. Am.* 88(4), 917-934.

Atkinson, G.M. and S.Z. Chen (1997). "Regional seismograms from historical earthquakes in southeastern Canada." *Seism. Res. Lett.* 68(5), 797-807.

Atkinson, G.M and W.J. Silva (1997). "An empirical study of earthquake source spectra for California earthquakes." *Bull. Seism. Soc. Am.* 87(1), 97-113.

Benz, H.M., A. Frankel, and D.M. Boore (1997). "Regional *Lg* attenuation for the continental United States." *Bull. Seism. Soc. of Am.*, 87(3), 606-619.

Boatwright, J. and G. Choy (1992). "Acceleration source spectra anticipated for large earthquakes in Northeastern North America." *Bull. Seism. Soc. Am.*, 82, 660-682.

Boore, D.M. (1986). "Short-period P- and S-wave radiation from large earthquakes: implications for spectral scaling relations." *Bull. Seism. Soc. Am.*, 76(1) 43-64.

Boore, D.M. and G.M. Atkinson (1987). "Stochastic prediction of ground motion and spectral response parameters at hard-rock sites in eastern North America." *Bull. Seism. Soc. Am.*, 77(2), 440-467.

Boore, D.M. and G.M. Atkinson (1992). "Source spectra for the 1988 Saguenay, Quebec, earthquakes." *Bull. Seism. Soc. Am.*, 82(2), 683-719.

Boore, D.M., W.B. Joyner, and L. Wennerberg (1992). "Fitting the stochastic ω^{-2} source model to observed response spectra in western North America: Trade-offs between $\Delta\sigma$ and κ" *Bull. Seism. Soc. Am.*, 82(4), 1956-1963.

Borcherdt, R. D. (1986). "Preliminary Report on Aftershock Sequence for Earthquake of January 31, 1986 near Painesville, Ohio." U.S. Geological Survey Open File Report 86-181.

Brady, A.G., P.N. Mork, and J.P. Fletcher (1981). "Processed accelerograms from Monticello Dam, Jenkinsville, South Carolina, August 27, 1978, and two later shocks." *USGS* Open-File Rept. 81-448.

Brune, J.N. (1970). "Tectonic stress and the spectra of seismic shear waves from earthquakes." *J. Geophys. Res.* 75, 4997-5009.

Campbell, K. W. (1981). "A Ground Motion Model for the Central United States Based or Near-Source Acceleration Data." In *Proc. of Conf. on Earthquakes and Earthquake Engineerng: the Eastern United States.*, edited by J. E. Beavers, Knoxville, Tennessee, September 14-16, Ann Arbor Science Publishers, 1, 213-222.

Chang, F.K. (1983). "Analysis of strong motion data from the New Hampshire earthquake of 18 January 1982,." US Nuclear Regulatory Commission Rept. NUREG/CR-3327.

Cranswick, E., R. Wetmiller, and J. Boatwright (1985). "High-frequency observations and source parameters of microearthquakes recorded at hard-rock sites." *Bull. Seism. Soc. Am.*, 75(6), 1535-1567.

Electric Power Research Institute (1993). "Guidelines for determining design basis ground motions." Palo Alto, Calif: Electric Power Research Institute, vol. 1-5, EPRI TR-102293.
vol. 1: Methodology and guidelines for estimating earthquake ground motion in eastern North America.
vol. 2: Appendices for ground motion estimation.
vol. 3: Appendices for field investigations.
vol. 4: Appendices for laboratory investigations.
vol. 5: Quantification of seismic source effects.

Frankel, A. (1994). "Implications of felt area-magnitude relations for earthquake scaling and the average frequency of perceptible ground motion." *Bull. Seism. Soc. Am.*, 84(2), 462-465.

Frankel, A., A. McGarr, J. Bicknell, J. Mori, L. Seeber, and E. Cranswick (1990). "Attenuation of high-frequency shear waves in the crust: Measurements from New York State, South Africa, and southern California." *J. Geo. Research*, 95(B11), 17,441-17,457.

Fletcher, J.B., (1995). "Source parameters and crustal Q for four earthquakes in South Carolina." *Seismol. Research Lett.*, 66(4), 44-58.

Haar, L. C., J. B. Fletcher, and C. S. Mueller (1984). "The 1982 Enola, Arkansas Swarm and Scaling of Ground Motion in the Eastern United States." *Bull. Seism. Soc. Am.*, 74(6), 2463-2482.

Hanks, T.C., and A.C. Johnston (1992). "Common features of the excitation and propagation of strong ground motion for north American earthquakes" *Bull. Seism. Soc. Am.*, 82(1), 1-23

Hanks, T.C. (1982). "f_{max}." *Bull. Seism. Soc. Am.*, 72(6), 1867-1879.

Hanks, T.C., and R.K. McGuire (1981). "The character of high-frequency strong ground motion." *Bull. Seism. Soc. Am.*, 71(6), 2071-2095.

Herrmann, R.B. and O.W. Nuttli (1982). "Magnitude: the relation of M_L to m_{bLg}." *Bull. Seism. Soc. Am.*, 72(2), 389-397.

Kanamori, H., and C.R. Allen (1986). "Earthquake repeat time and average stress drop." *Earthquake Source Mech., Am. Geophys. Union Geophys. Monogr.*, S. Das, J. Boatwright, C.H. Scholz, ed., 37, 227-235.

Kanamori, H., and D.L. Anderson (1975). "Theoretical basis of some empirical relations in seismology." *Bull. Seismol. Soc. Am.*, 65, 1073-1095.

Kimball, J.K. (1983). "The use of site dependent spectra." *Proc. Workshop on Site-Specific Effects of Soil and Rock on Ground Motion and the Importance for Earthquake-Resistant Design,* Santa Fe, New Mexico, USGS Open-File Rept. 83-845, 410-422.

Mork, P. and A. G. Brady (1981). "Processed Accelerograms from Monticello Dam, Jenkinsville, South Carolina, October 16, 1979, 0706 UTC." *U.S. Geological Survey* Open-File Report 81-1214.

Munro, P. S. and D. Weichert. (1989). "The Saguenay earthquake of November 25, 1988: Processed strong motion records." Geological Survey of Canada Open File/Dossier Public 1996.

Nuttli, O. W. (1981). "Similarities and Differences between Western and Eastern United States Earthquakes, and their Consequences for Earthquake Engineering." In *Proceedings of the Conference on Earthquakes and Earthquake Engineering: the Eastern United States,* ed. J. E. Beavers, vol. 1, Ann Arbor Science Publishers, Inc., Ann Arbor, MI, 25-27.

Silva, W.J., N.A. Abrahamson, G.R. Toro, and C.J. Costantino (1997). "Description and validation of the stochastic ground motion model." Report to Brookhaven National Laboratory, Associated Universities, Inc. Upton, New York, Contract 770573.

Silva, W.J. (1991). "Global characteristics and site geometry." Chapter 6 in *Proceedings: NSF/EPRI Workshop on Dynamic Soil Properties and Site Characterization.* Palo Alto, Calif.: Electric Power Research Institute, Rept. NP-7337.

Silva, W.J. (1993). "Factors controlling strong ground motions and their associated uncertainties." *Seismic and Dynamic Analysis and Design Considerations for High Level Nuclear Waste Repositories, ASCE* 132-161.

Silva, W.J. and R. Darragh (1995). "Engineering characterization of earthquake strong ground motion recorded at rock sites." Palo Alto, Calif:Electric Power Research Institute, Rept. TR-102261.

Silva, W.J., R. Darragh, R. Green, and F. Turcotte (1989a). "Spectral characteristics of small magnitude earthquakes with application to western and eastern North American tectonic environments: Surface motions and depth effects." U.S. Army Engineers Waterways Experiment Station Miscellaneous Paper Gl-89-16.

Silva, W.J., R. Darragh, R. Green, and F. Turcotte (1989b). *"Estimated ground motions for a New Madrid event."* U.S. Army Engineers Waterways Experiment Station Miscellaneous Paper GL-89-17.

Singh, S. and R.B. Hermann (1983). "Regionalization of crustal coda Q in the continental United States." *J. Geophys. Res.*, 88, 527-538.

Toro, G.R., N.A. Abrahamson, and J.F. Schneider (1997). "Model of strong ground motions from earthquakes in Central and Eastern North America: Best estimates and uncertainties." *Seismological Research Let.*, 68(1), 41-57.

Toro, G.R. and R.K. McGuire (1987). "An investigation into earthquake ground motion characteristics in eastern North America." *Bull. Seism. Soc. Am.*, 77(2), 468-489.

Weichert, D. H., R. J. Wetmiller, R. B. Horner, P. S. Munro, and P. N. Mork (1986). "Strong Motion Records from the 23 December 1985, M_s 6.9 Nahanni, NWT, and Some Associated Earthquakes." *Geological Survey of Canada,* Open-File Report 1330.

Weichert, D. H., P. W. Pomeroy, P. S. Munro, and P. N. Mork (1982). "Strong motion records from Miramichi, New Brunswick, 1982 aftershocks." *Earth Physics Branch,* Ottawa, Canada, Open File Report 82-31.

Wesson, R. L. and C. Nicholson (1986). *Studies of the January 31, 1986 Northeastern Ohio Earthquake.* Report submitted to the U.S. NRC, USGS Open-File Report 86-331.

Table 2-1

KAPPA VALUES FOR "AVERAGE" SITE CONDITIONS IN WUS AND CEUS*

Tectonic	"Average" Site Condition	N+	Median Kappa (sec)	σ_{ln}	Range of Kappa for This Site Condition (sec)
WUS	Hard rock	11	0.026	0.58	0.010 - 0.060
	Weathered hard rock	9	0.035	0.52	0.015 - 0.100
	Soft rock	15	0.045	0.51	0.015 - 0.080
	Sheared rock	4	0.062	0.41	0.040 - 0.120
	Combined	39	0.037	0.59	0.010 - 0.120
CEUS	Hard rock	16	0.007	0.42	0.004 - 0.016
	Soft rock	3	0.017	0.09	0.015 - 0.018
	Sheared rock	1	0.025		0.025
	Combined	20	0.008	0.55	0.004 - 0.025

* Based on template fits using spectral shapes (Silva and Darragh, 1995)
+ Number of records

"Average" Site Condition is defined as:

Hard Rock: WNA as granite, schist, carbonate, slate
ENA as granitic pluton, carbonate, sites in Canadian Shield region (Saguenay, New Hampshire).

Weathered hard rock: WNA as weathered granitic rock and tonalite

Soft rock: WNA as sandstone and breccias
ENA as sandstone and claystone

Sheared rock: WNA as site near fault zone (Gilroy #6) or greenstone site in Franciscan (Redwood City, Hayward).
ENA as site near fault zone (Nahanni River Site #1)

Table 2-2 POINT-SOURCE PARAMETERS		
	WUS	CEUS
$\Delta\sigma$ (bars)	65	120
kappa (sec)	0.040	0.006
Q_o	220	351
η	0.60	0.84
β (km/sec)	3.50	3.52
ρ (g/cc)	2.70	2.60
Amplification	soft rock (Figure 2-3)	hard rock (Figure 2-3)
Double Corner	Atkinson and Silva (1997)	Atkinson (1993)

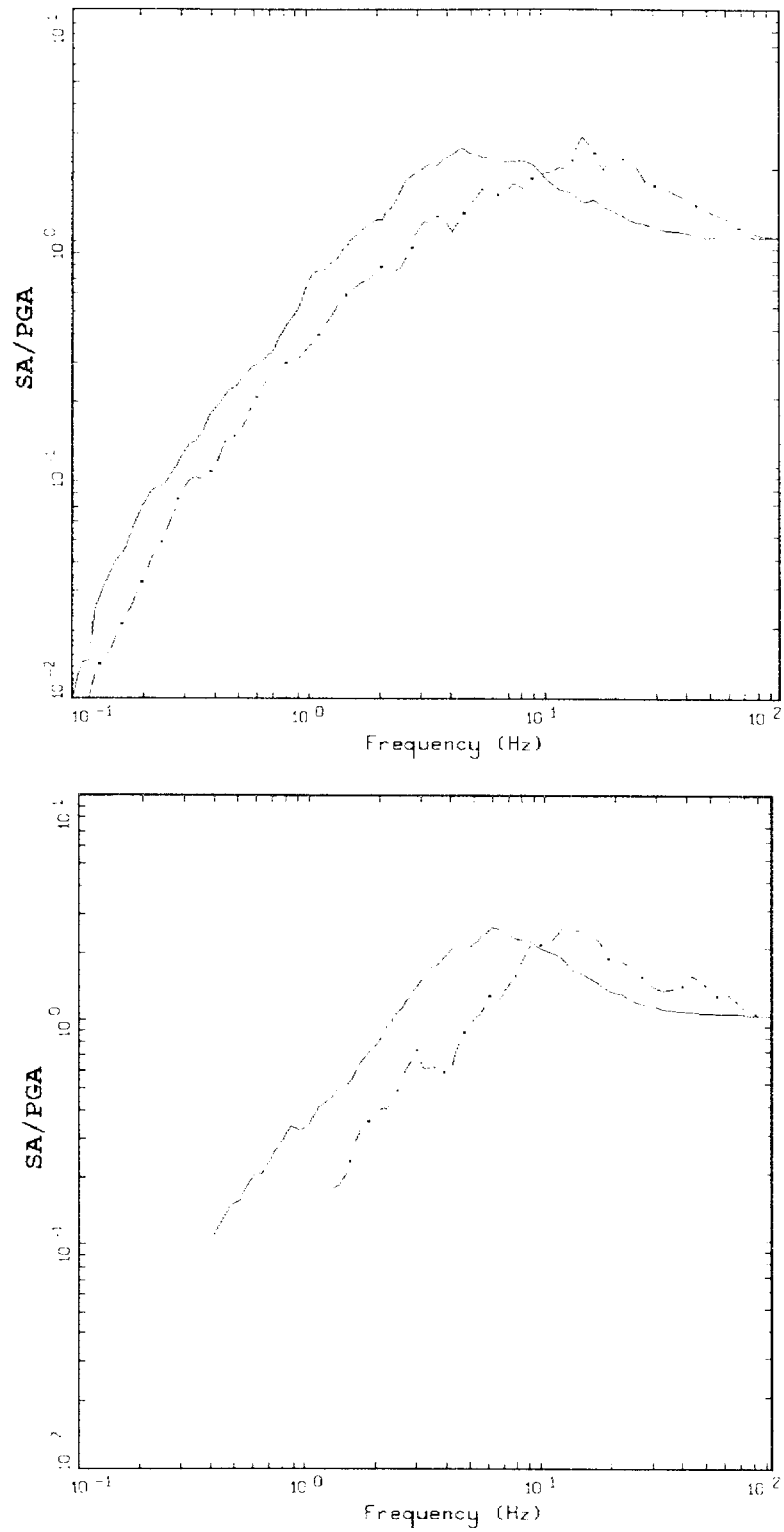

Figure 2-1. Comparison of response spectral shapes (SA/PGA, 5% damping) between CEUS (dashed line), and WUS (solid line) crustal conditions for earthquakes recorded at rock sites: **M** 6¾ (upper) and **M** 5¾ (lower).

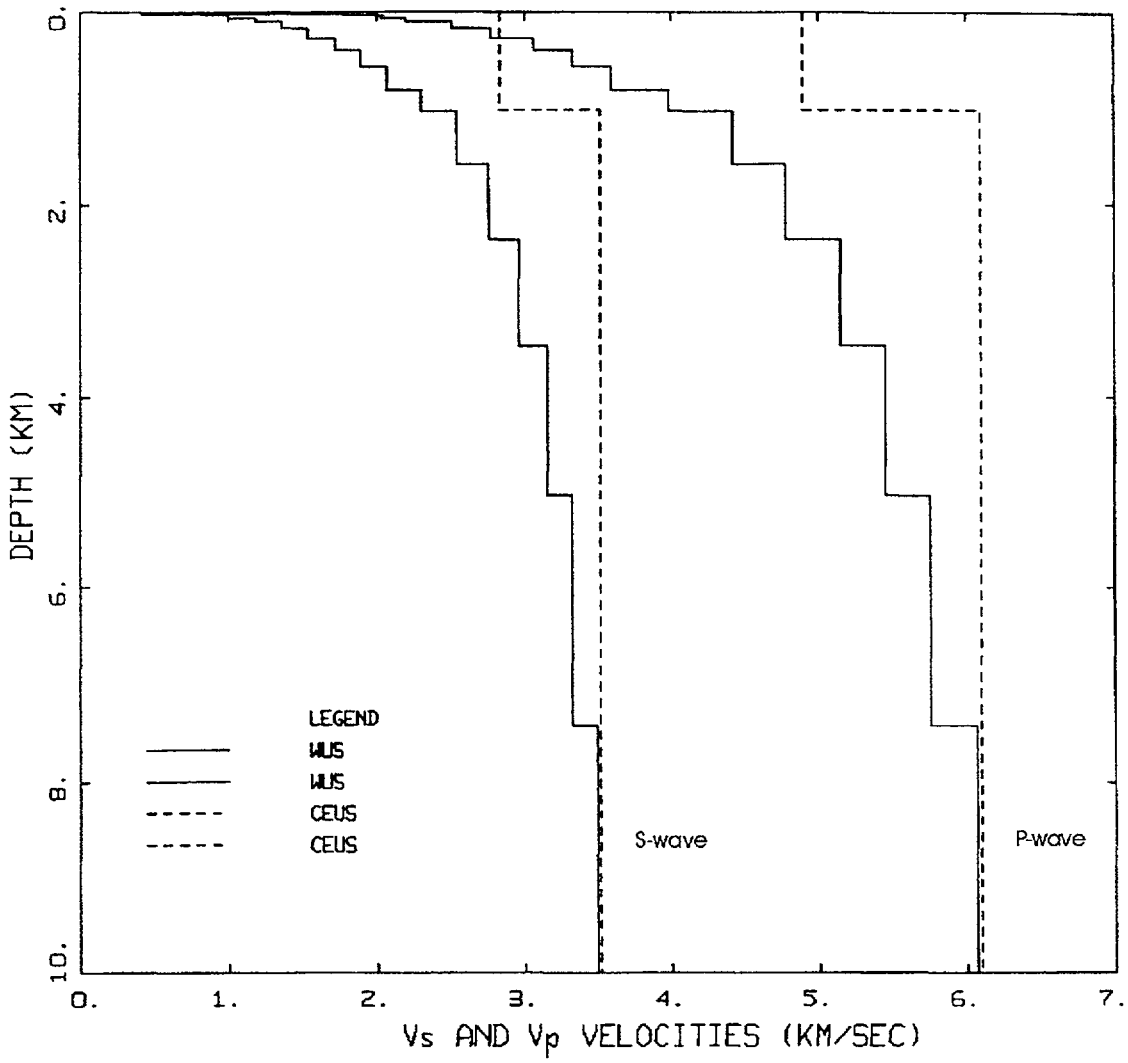

Figure 2-2. Comparison of generic compression (P) and shear (S) wave velocity profiles for WUS and CEUS crustal conditions.

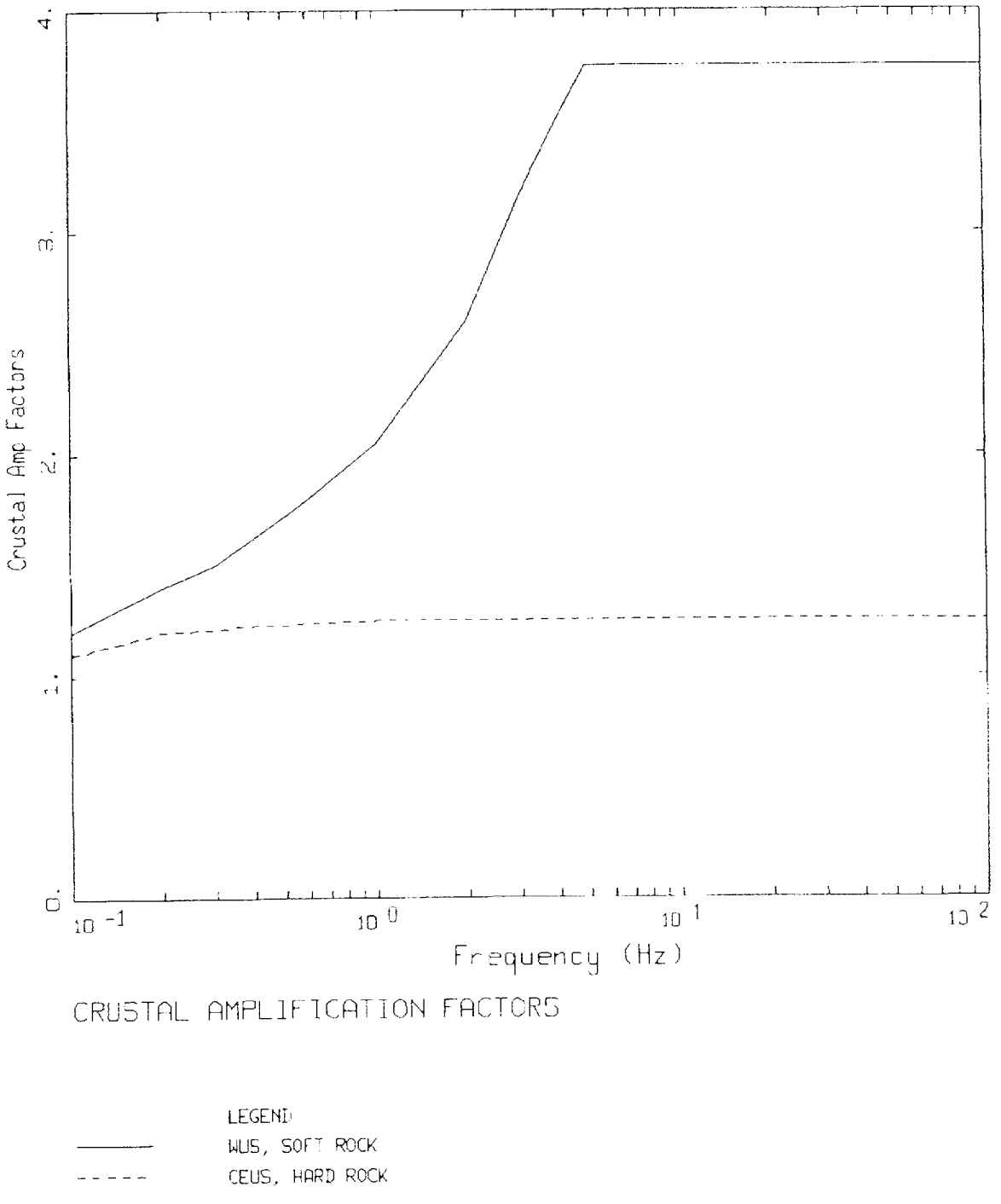

Figure 2-3. Crustal amplification factors (smoothed) for Fourier amplitude spectra computed for the crustal models shown in Figure 2-2 (10 km to the surface).

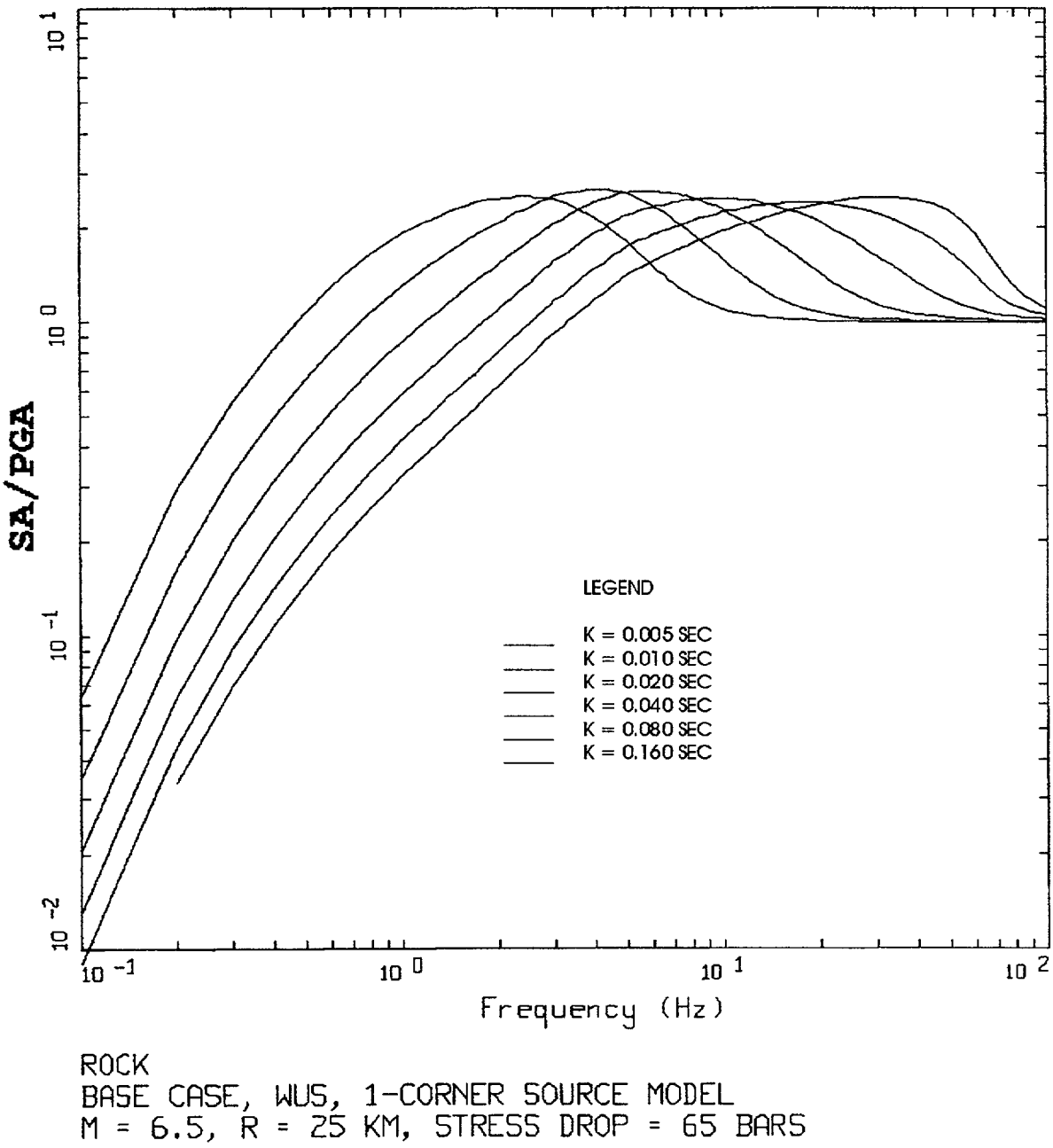

Figure 2-4. Response spectral shapes (SA/PGA, 5% damping) computed for **M** 6.5 at a distance of 25 km for a suite of kappa values using WUS parameters (Table 2-2). The lowest kappa value shows the highest high-frequency amplification, the highest kappa value shows the highest low-frequency amplification.

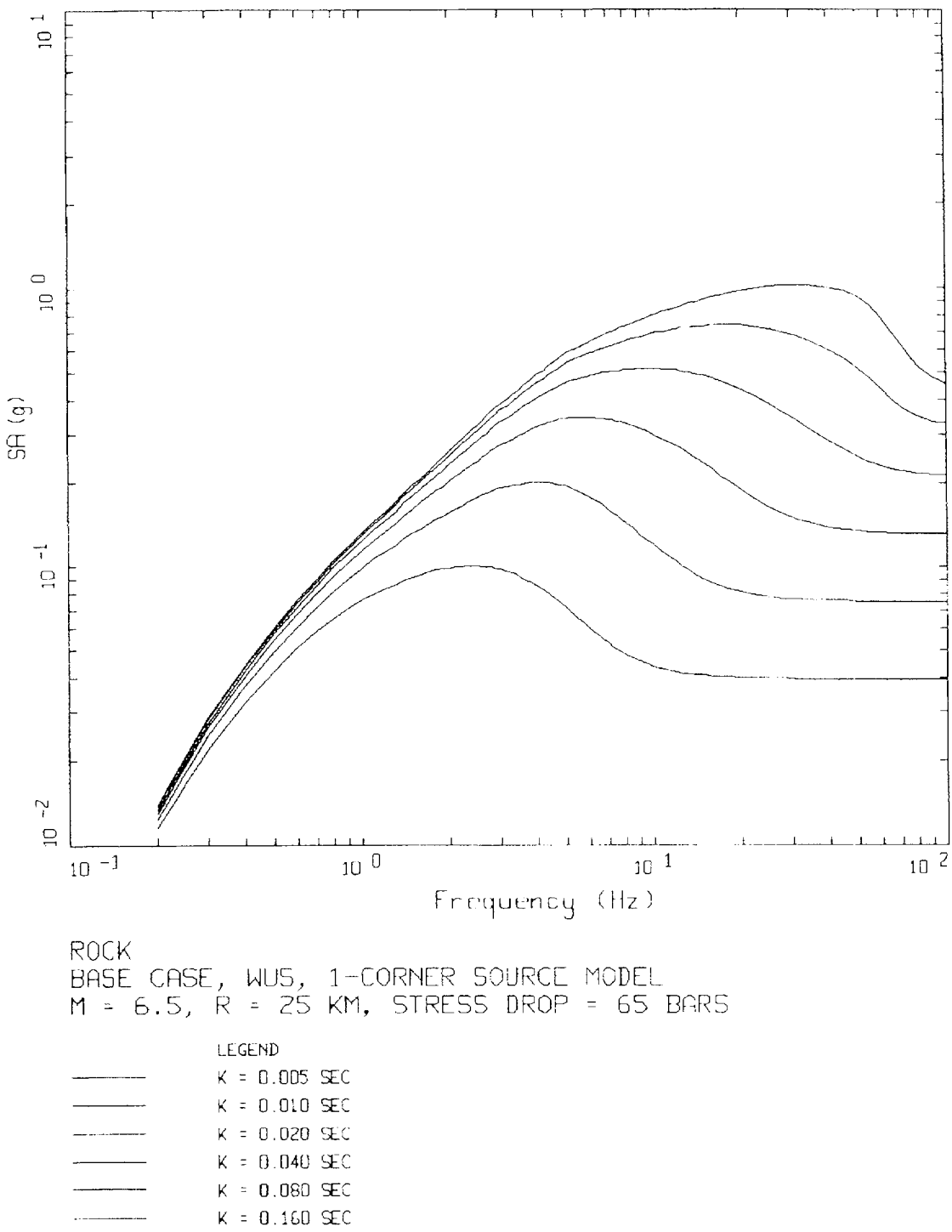

Figure 2-5. Response spectra (5% damping) computed for an **M** 6.5 earthquake at a distance of 25 km for a suite of kappa values using WUS parameters (Table 2-2). The lowest K value shows the highest spectral amplitudes and the highest K value shows the lowest spectral amplitudes.

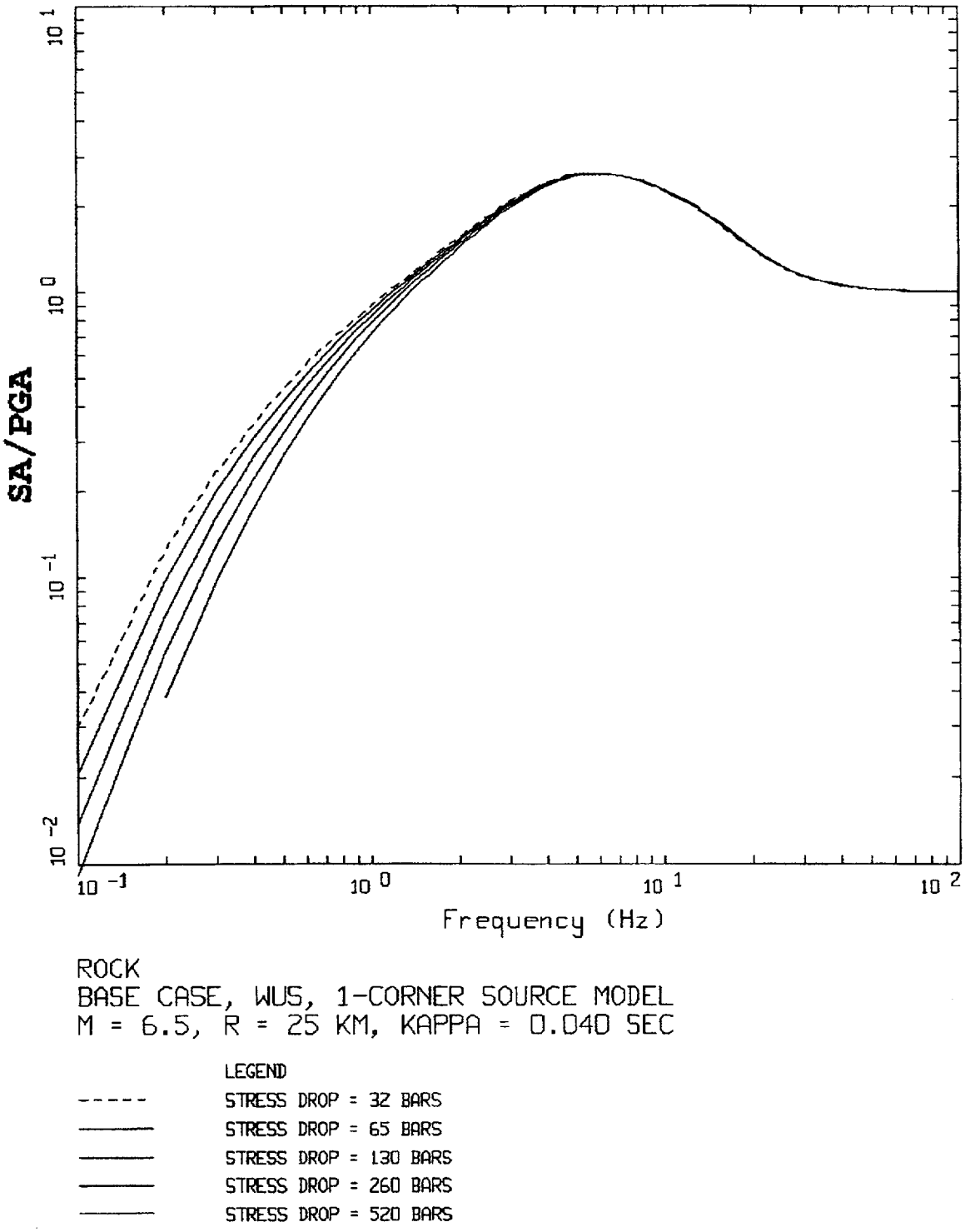

Figure 2-6. Response spectral shapes (SA/PGA, 5% of critical damping) computed for M 6.5 at a distance of 25 km for a suite of stress drop values using WUS parameters (Table 2-2). Spectral shapes reduce with increasing stress drop, beginning with 32 bars.

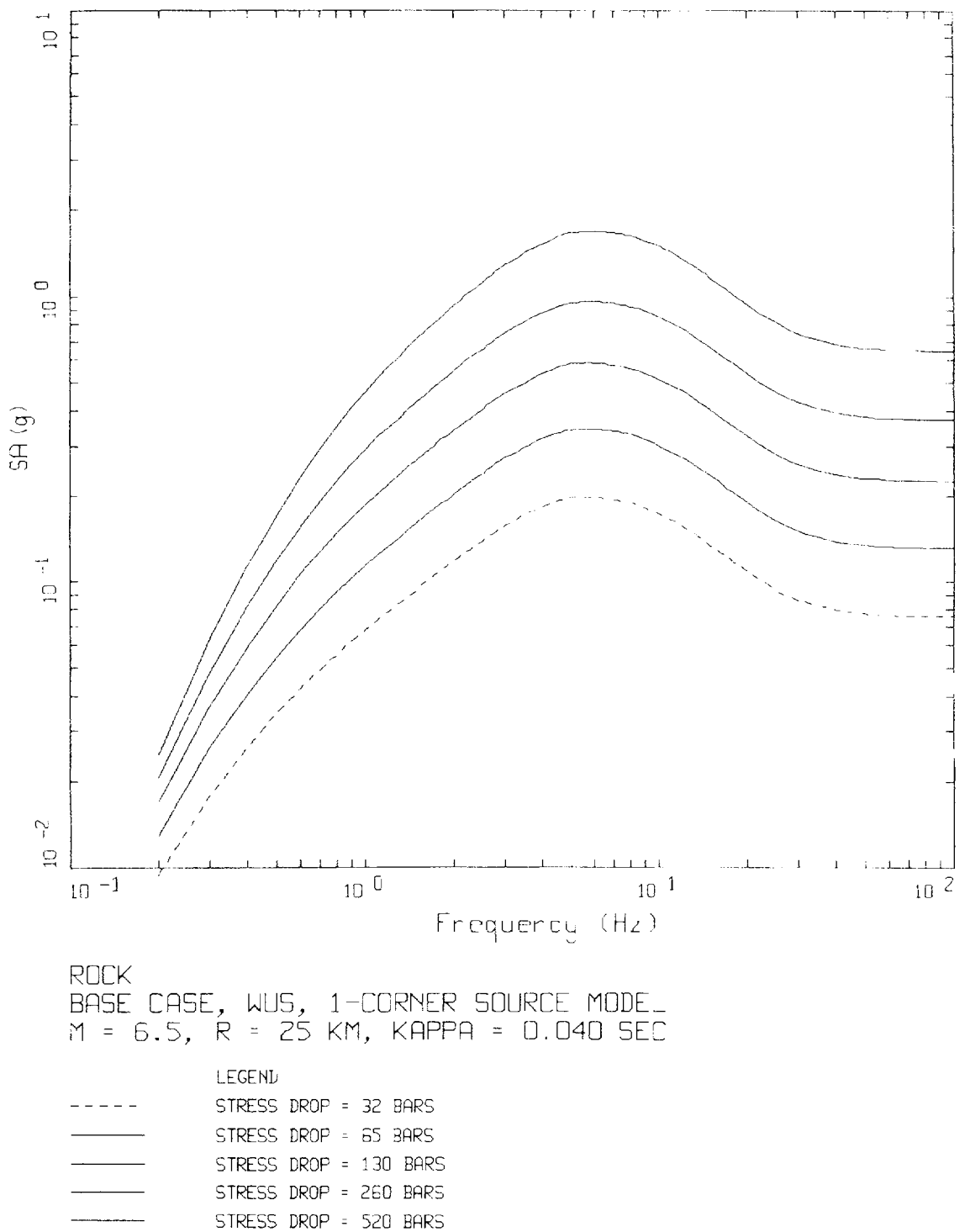

Figure 2-7. Response spectra (5% of critical damping) computed for **M** 6.5 at a distance of 25 km for a suite of stress drop values using WUS parameters (Table 2-2). Spectral shapes increase with increasing stress drop, beginning with 32 bars.

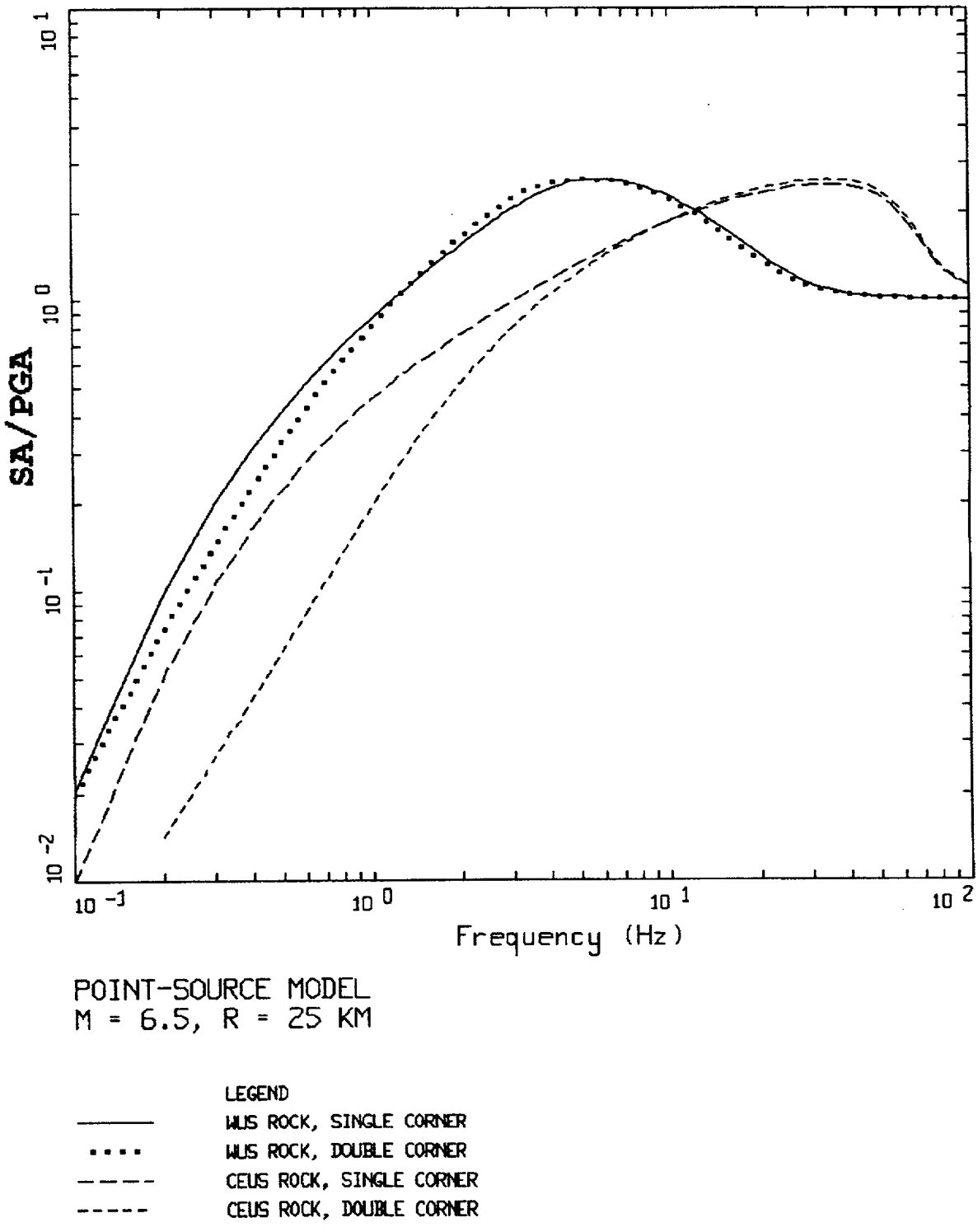

Figure 2-8. Response spectral shapes (5% of critical damping) computed for **M** = 6.5 at *R* = 25 km using both single- and double-corner frequency source spectra for WUS and CEUS conditions (Table 2-2).

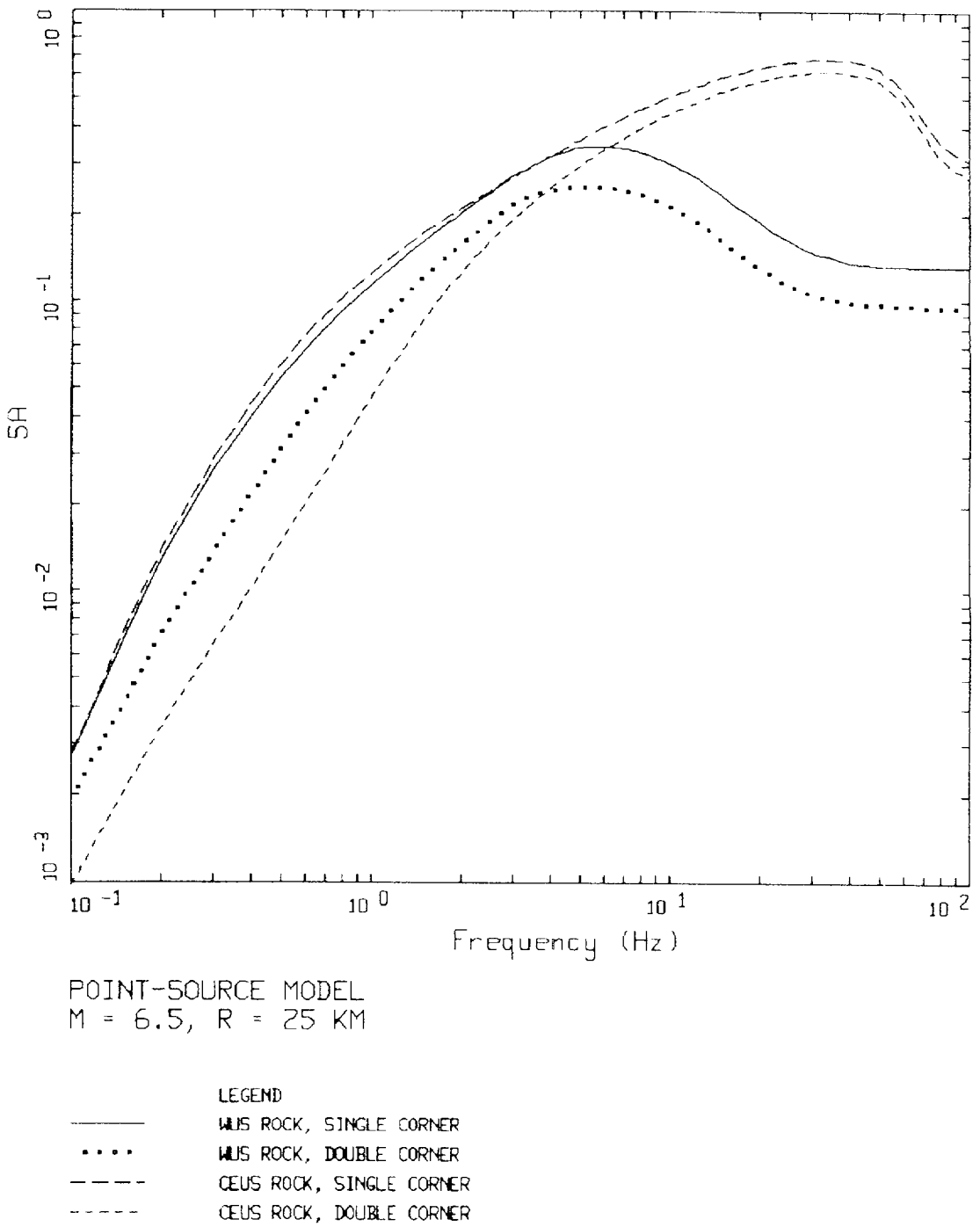

Figure 2-9. Absolute response spectra (5% of critical damping) computed for **M** = 6.5 at R = 25 km using both single- and double-corner frequency source spectra for WUS and CEUS conditions (Table 2-2).

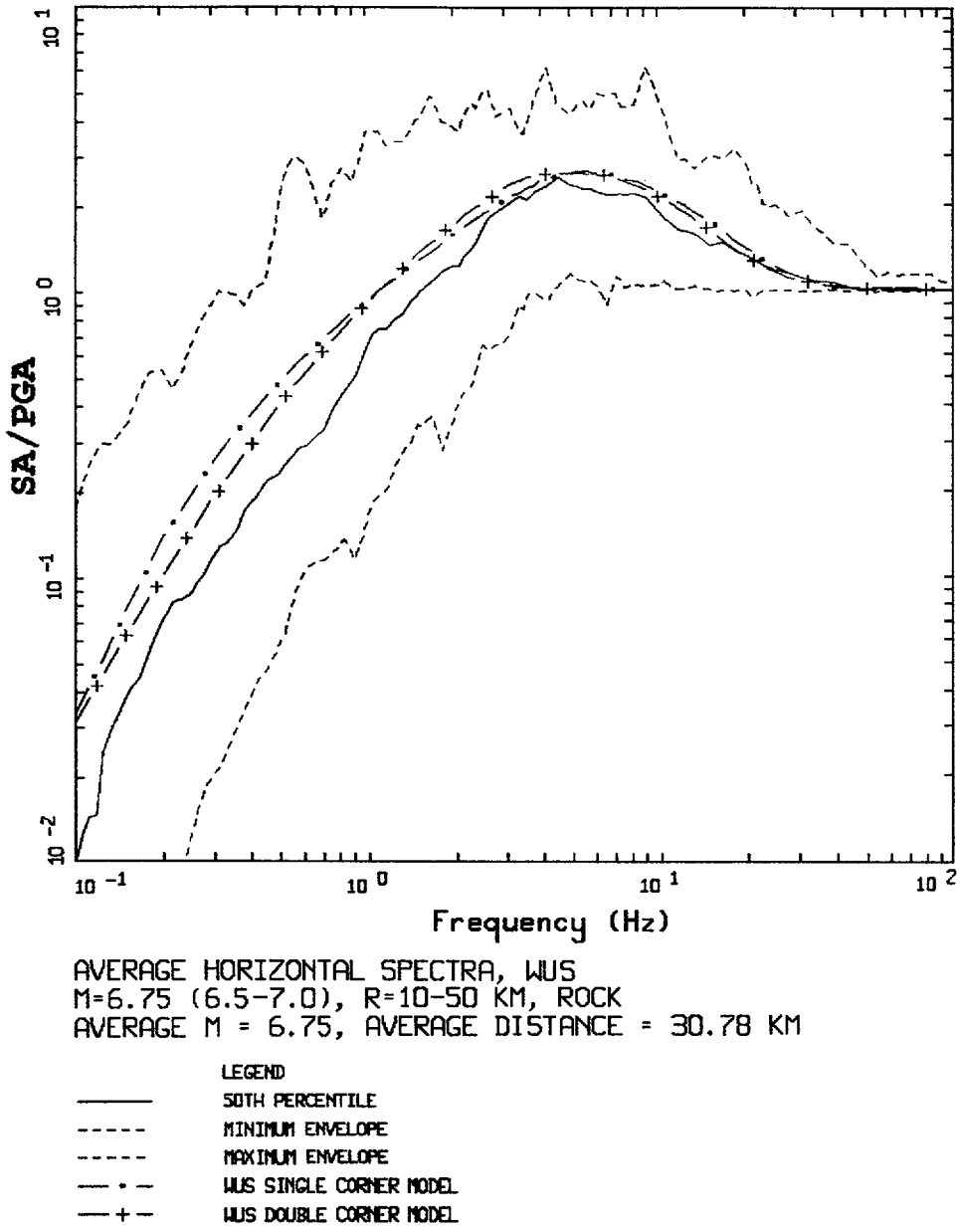

Figure 2-10. Comparison of 5% damped statistical shapes computed for WUS recordings. (**M** 6¾) to single- and double-corner model predictions using the parameters listed in Table 2-2.

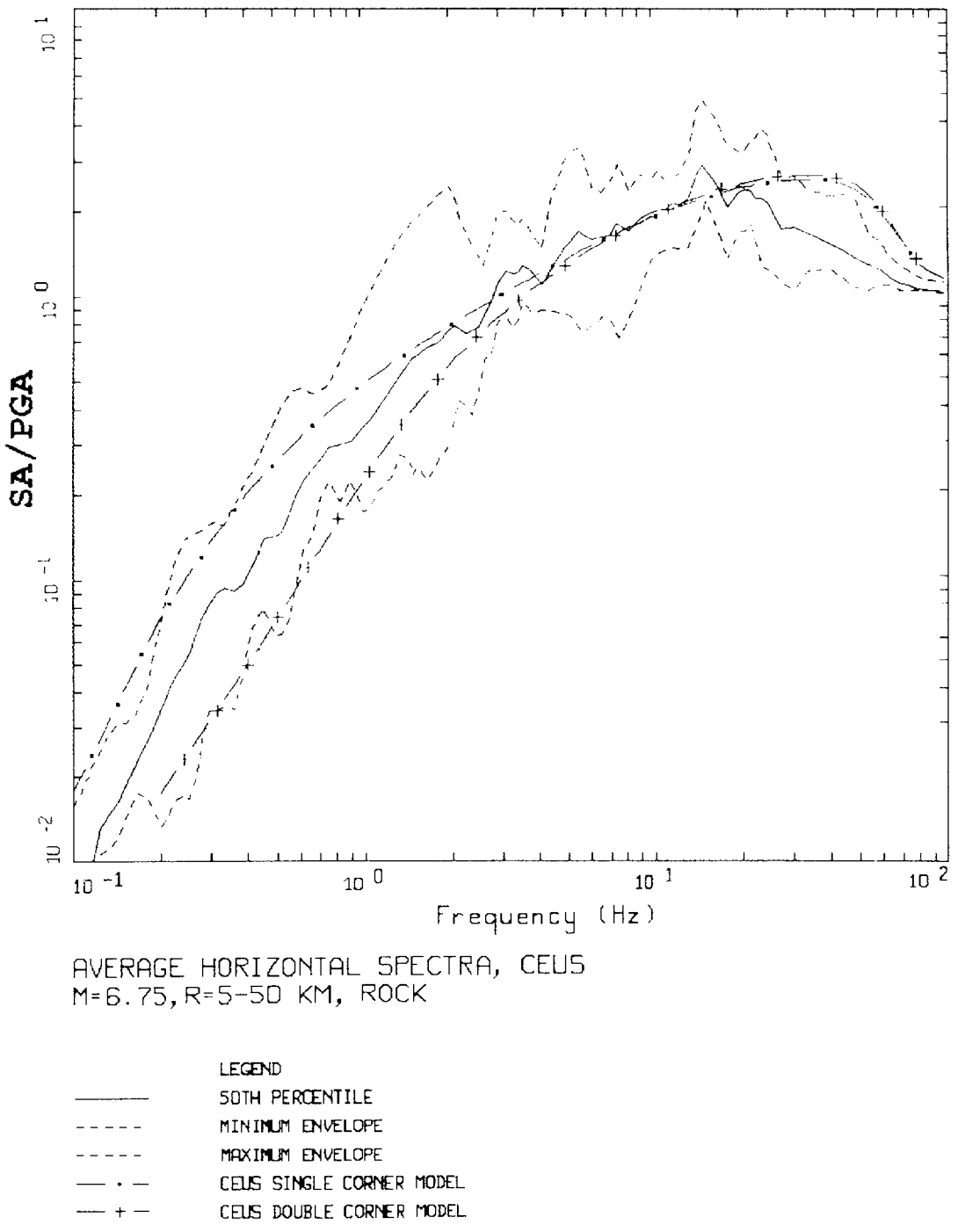

Figure 2-11. Comparison of 5% damped statistical shapes computed for CEUS recordings (**M** 6¾) to single- and double-corner model predictions using the parameters listed in Table 2-2.

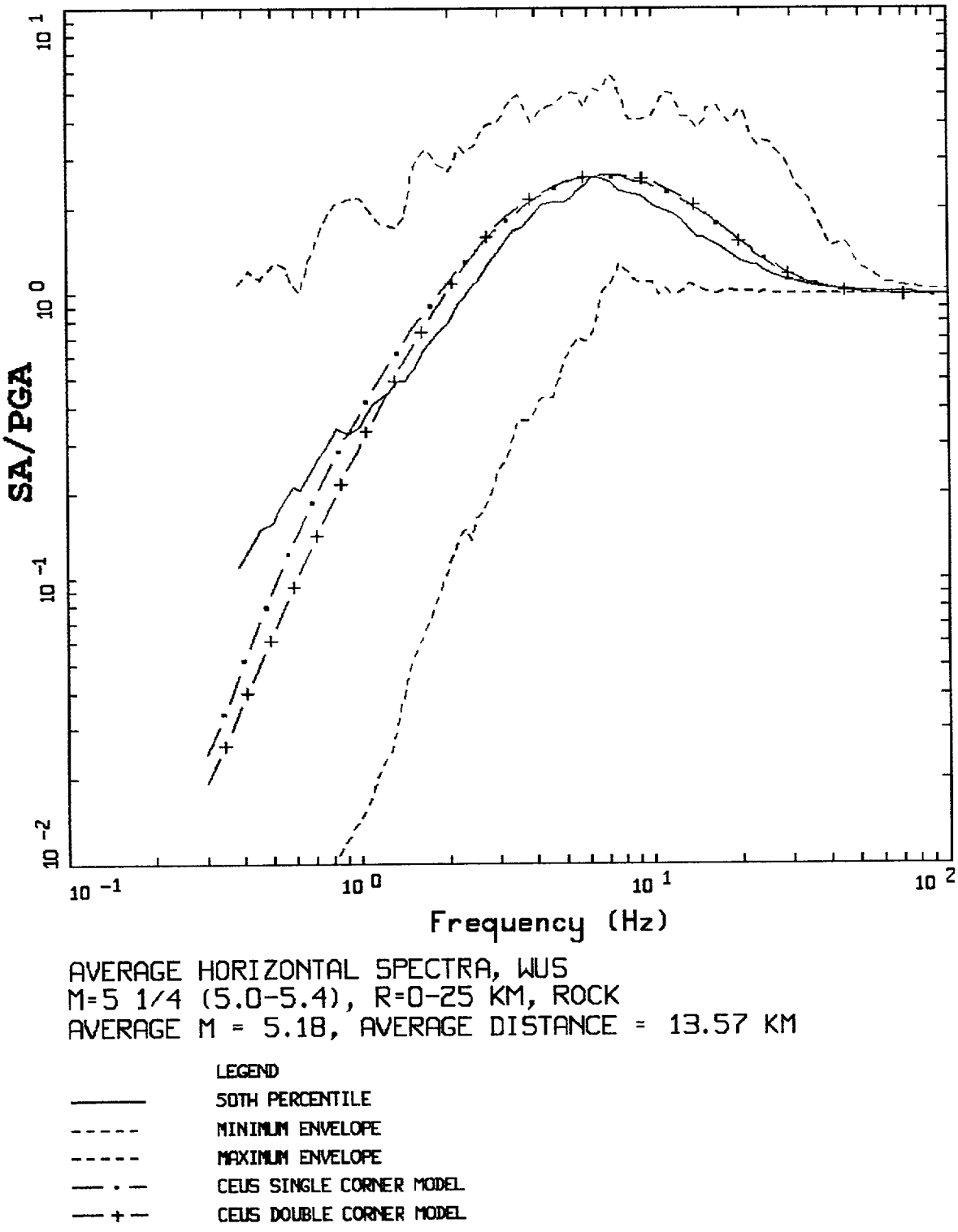

Figure 2-12. Comparison of 5% damped statistical shapes computed for WUS recordings (M 5¼) to single- and double-corner model predictions using the parameters listed in Table 2-2.

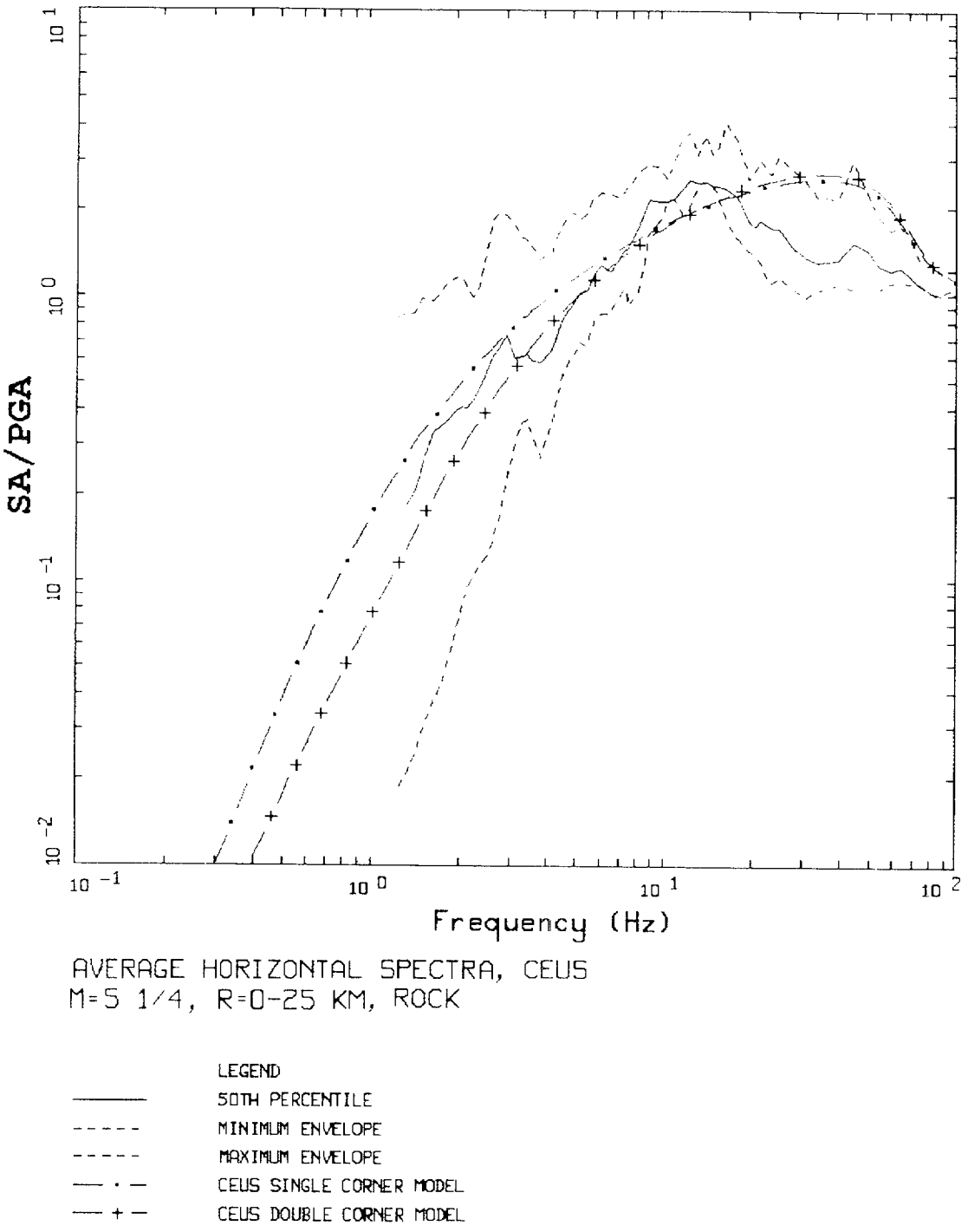

Figure 2-13. Comparison of 5% damped statistical shapes computed for CEUS recordings (M 5¼) to single- and double-corner model predictions using the parameters listed in Table 2-2.

3 TIME HISTORY DATABASE FOR ANALYSES

The time history database provides a suite of motions for structural and soil column analyses. For this intended use, it is assumed the motions will undergo a scaling or matching process to the desired hazard levels (Section 5). The parceling of time histories into magnitude and distance bins provides implicit guidelines on the amount of recommended scaling.

In addition to the magnitude and distance bins, an additional screening is done on duration for WUS records. This duration screening results in time histories that are expected to be unbiased in time domain characteristics that affect nonlinear structural or soil column analyses. Since a robust measure of duration that is significant to nonlinear structural analysis eludes quantification, the duration criteria are not imposed in a strict manner. The magnitude and distance bins and the duration criteria are discussed in Section 3-1.

The library of time histories for analysis is intended to rely on recorded motions for WUS conditions. While the field of modeling has progressed significantly in the last few years as a direct result of the increase in the number of recordings and an emphasis on thorough validations (Appendix D), uncertainties remain as to whether purely synthetic records reflect appropriate phasing between components, frequency-to-frequency variations, and effects of rupture directivity. This is a significant issue for the CEUS because that region has not produced many records, particularly for magnitude-distance combinations of relevance to engineering design. To preserve as much of the natural attributes of recorded motions as possible, we recommend using the WUS bin records as inputs to CEUS spectral matching analyses. To assist this process, the CEUS analysis time history bins have been supplemented with scaled WUS recordings taken from the WUS bins. The scaling process involves computing response spectral transfer functions for WUS rock to CEUS rock and for WUS deep soil to CEUS deep soil. The scaling process uses the single-corner-frequency point-source model (Appendices D and K). The transfer functions for horizontal and vertical motions are then applied to the WUS empirical rock and soil bin spectra. This process results in scaled CEUS target spectra, and the WUS bin records are then used as input to a weak spectral matching process (Silva and Lee, 1987). This process results in fully populated CEUS rock and soil bins, supplemented with hybrid empirical records that maintain realistic phase and amplitude relationships between components and realistic frequency-to-frequency variability. The supplemental bin records should be used only as inputs to additional scaling or matching procedures and are not intended to be used to develop CEUS spectral shapes or spectral levels.

For CEUS single-corner-frequency source models, the main difference between WUS and CEUS rock motions is at high frequency ($\geq$ 5 Hz, Figure 4-10) and the issue in fitting CEUS spectra is the ability of the matching process to sufficiently scale up the high frequencies. The double-corner CEUS shapes are similar to the single-corner but incorporate a broad spectral sag. At very low frequency the two shapes are the same because they reflect similar **M** (or seismic moments). Spectral matching or scaling empirical WUS motions to double-corner CEUS spectra thus presents issues similar to matching CEUS single-corner spectra. Examples of this process are presented in Section 3.2.

An aspect of the resulting CEUS time histories that is largely lost in the scaling approach is the observed general increase in durations over corresponding WUS rock time histories (Atkinson, 1995). Since too few records exist of sufficiently large magnitudes and distances to be of engineering significance, an assessment of differences in durations between WUS and CEUS conditions and their corresponding effects on engineering analyses is currently not available. Users of this time history database in applications to CEUS conditions may wish to select the longer duration records from the bins as a sensitivity analysis. This is the type of test that was envisaged in populating one bin (Table 3-3) with 30 three component sets of time histories. Appendix B contains the WUS and CEUS analysis time history catalog, and separate CD ROMs contain the analysis time histories (acceleration, velocity, and displacement time histories) and the 5% damped response spectra and durations (Section 3.2).

3.1 Site Conditions For Time Histories

Site conditions for the time history database consist of soft rock and firm soil for WUS motions. A convenient site categorization scheme that has been applied to most of the strong motion sites in the US and many abroad is shown in (Table 3-1). Categories A and B are considered appropriate for soft rock and categories C and D for deep firm soil site conditions. The soft rock site conditions for the time histories are consistent with the corresponding site conditions for the response spectral shapes (Section 4).

For CEUS deep (> 300m) soil conditions, the use of corresponding WUS deep soil motions is appropriate because the time histories are intended as inputs to scaling or matching processes. Additionally, deep firm soils (both cohesive and cohesionless) located in the CEUS are not considered to be fundamentally different in dynamic material properties from similar soils located in the WUS. Therefore the CEUS soil motions will be more similar to WUS deep soil motions than corresponding rock motions (Section 6). While the input motions (base of soil and rock outcrop) may be very different between WUS and CEUS conditions, the filtering properties of deep soils significantly reduce the differences. This expectation is strengthened by the observation of possibly similar double corner source spectra in both WUS and CEUS motions that is manifested much more subtly in the WUS due to larger crustal amplification (Section 2).

3.2 Magnitude and Distance Bins for Time Histories

Magnitude and distance bins reflect expected differences in spectral shapes and in time domain characteristics (e.g. duration) that may be of potential significance to engineering analyses. Bin centers and widths control the maximum scaling of records within a bin by a constant factor to adjust for magnitude and distance differences without compensating for changes in spectral shapes. The bin widths also minimize the use of motions with inappropriate time domain characteristics. Continuous scaling approaches would accommodate potential changes in response spectral shapes (Section 3.3; Carballo and Cornell, 1998), particularly for differences in magnitudes (record-to-target) larger than about 1/2 unit in magnitude.

The distance and magnitude bins are listed in Table 3-2. The distance bins are broadly separated into near-source (0 to 10 km fault rupture distance) and beyond (> 10 km). Near-source conditions may

be strongly magnitude (source size) and mechanism dependent and may extend beyond 10 km, particularly for large (**M** > 7) sources. However, the objective here is to capture the overall shorter durations displayed by close-in records and the potential pulse-like low-frequency characteristics of rupture toward a site, both of which are strongly prominent at very small fault distances.

Because duration of shaking may play a significant role in many structural and soil analyses, we apply duration criteria to the magnitude and distance bins. Duration of shaking, expressed as a number of uniform stress cycles, has an influence in the generation of excess pore pressure in soils. This excess pore pressure affects the soil's capacity for failure. The duration definition selected here, which is the time for the cumulative energy (Arias, 1969; Husid, 1969; Dobry et al., 1978) to grow from 5% to 75% of its total value, has been shown to correlate with inelastic structural response for stiff systems (Kennedy et al., 1984). While not being strictly applicable to a duration measure controlling soil deformation, the selected criteria will restrict ranges in time domain characteristics to those that are representative of bin averages.

We use a recently developed empirical relation for WUS strong ground motions to represent the bin average of the 5% to 75% cumulative Arias intensity. The empirical relation is described in Appendix I and is plotted in Figures 3.1 to 3.3 for **M** 5.5, 6.5, and 7.5, respectively. In the figures, the vertical bars represent $\pm$ 1 sigma ranges, with the distance bins (0 to 10 km, 10 to 50 km, 50 to 100 km, 100 to 200 km) spanned by the horizontal dashed lines. Duration ranges for the **M** and *R* bins are taken as $\pm$ 50% (log additions) of the expected median values (solid lines) evaluated at the average (log) bin distance interval (Table 3-2). Liberal duration ranges are considered appropriate because a definitive, causative relationship between strong motion duration and structure and soil response has not yet been quantitatively established. The selected duration criteria for the magnitude and distance bins are represented by the areas enclosed by the dashed lines in Figures 3-1 to 3-3.

To allow a reasonable statistical interpretation of structural and soils analyses, a target number of three-component sets of time histories was set at 15. This number represents a reasonable compromise, allowing the bins to be fully populated with recorded motions (WUS) but not making the bins overly wide in magnitude or distance range. For each of the bins, the numbers of three component recordings are listed in Tables 3-3 and 3-4 for WUS and CEUS respectively, along with bin average magnitudes and distances. The WUS records were selected from the WUS strong motion catalog (Appendix A) by applying the bin criteria and then randomly selecting subsets of 15 (for bins that exceeded 15 three component sets). The duration criteria were applied to the log average duration of the two horizontal components. Since the **M** 5.5, 0 to 10 km bin was sparsely populated and near-source effects are not considered significant for **M** 5 to **M** 6 earthquakes, the 0 to 10 km and 10 to 50 km distance bins were combined into a single 0 to 50 km bin. Also, to provide a bin for assessing the effects of the number of records on the statistical stability of analysis results, the number of three-component sets in the **M** 6.5, 10 to 50 km rock bin was increased from 15 to 30. For the large-magnitude (**M** > 7+), close distance (0 to 10 km) bin, an effort was made to include sites that recorded both forward and backward directivity. For the soil records, sufficient data are available and the number of sets was increased to 18. Because the magnitude of the 1995 Kobe earthquake is near **M** 7 (**M** 6.9), the soil site Takarazuka, at the end of the rupture (maximum directivity), is included in two magnitude bins (**M** 6 to 7 and **M** 7+). The large magnitude (**M** 7+) close distance (0 to 10 km) rock records are dominated by motions obtained during the 1999 Chi Chi earthquake.

To reduce the number of Chi Chi records in this bin and because uncertainty exists regarding site classification, several **M** 6.9 rock site records were added. These include the sites BRN, CLS, and LGPC for the 1989 **M** 6.9 Loma Prieta earthquake, site GAZ for the 1976 **M** 6.8 Gazli earthquake, and sites KBU and KJM for the **M** 6.9 1995 Kobe earthquake. Also, the **M** 6.8 Gazli earthquake is included as both WUS and CEUS. The earthquake was recorded at only one rock site and its horizontal component spectra peak near 10 Hz, so it is considered intermediate between WUS and CEUS rock (Figure 2-8) (Silva and Darragh, 1995).

3.3 WUS to CEUS Scaling

To illustrate the process of scaling the WUS analysis time histories to CEUS conditions, an example is presented for the **M** 6.5, R = 0 to 10 km, rock site bin (Table 3-5).

3.3.1 WUS to CEUS Transfer Functions

The WUS to CEUS transfer functions were computed for rock conditions (going from soft rock in the WUS to hard rock in the CEUS, see Figure 2-2) and for deep soil conditions (Silva, 1997), for both horizontal and vertical components of motion. Because of nonlinear site response, the horizontal-component transfer functions are magnitude and distance dependent. A linear site response model (Silva, 1997; EPRI, 1993) was used for vertical components, but the transfer functions still vary with magnitude and distance because of incidence angle variation with both source depth and distance (Tables 2-1 and 2-2 show WUS and CEUS point-source parameters, respectively). For **M** 6.5, an example suite of median transfer functions is shown in Figure 3-4. The transfer functions for rock (both horizontal and vertical) show peaks at high frequency, which are consistent with the expected high frequency peak in CEUS hard rock spectral acceleration. For the horizontal component transfer functions for deep (> 300m) soil sites, Figure 3-4 suggests similar WUS and CEUS response spectra at high loading levels (amplification near unity). Soil nonlinearity evidently masks the differences in frequency content between WUS soft rock and CEUS hard rock control motions (Silva and Darragh, 1995; Silva, 1991). Similar trends are seen in the **M** 5.5 and **M** 7.5 transfer functions, where magnitudes were selected to be equal to the analysis time history bin center magnitudes (Table 3-5). Distances at which the transfer functions were computed (1, 5, 30, 75, and 130 km) span the range of bin mean distances. The transfer function closest to the actual site-to-earthquake rupture distance was used to transform a WUS record to a CEUS record.

3.3.2 Example Case: M 6.5, R = 0 to 10 km, Rock Bin

For this example we selected the north (000) component of the Los Gatos Presentation Center (LGPC) site, which recorded the 1989 **M** 6.9 Loma Prieta earthquake. The site is located at a closest rupture distance of 6.1 km (Appendix A) and reflects WUS rock conditions. The north component acceleration and (processed) velocity and displacement time histories are shown in Figure 3-5, and the response spectra shown in Figure 3-6, for all three components. To scale this recording to CEUS hard rock conditions, the response spectrum is multiplied by the appropriate transfer function (Figure 3-4) to produce a CEUS hard rock target. The original WUS soft rock recording is then used as an input (basis) motion to a weak matching process (1 to 2 iterations). The resulting time history is shown in Figure 3-7, with the scaled CEUS hard rock response spectra shown in Figure 3-8, for all

three components. Comparing the WUS and CEUS time histories in Figures 3-5 and 3-7 respectively, the effects of scaling are mostly apparent in acceleration, dramatically increasing the frequency content and level of motion. The amplitudes and frequency contents of the velocity and displacement time series remain largely unaltered, as most of the amplification is at frequencies exceeding about 3 Hz (Figure 3-4). The scaled response spectra (Figure 3-8) reflect the shift in peaks from about 3 Hz for horizontal components and 10 Hz for the vertical component for WUS soft rock (Figure 3-6) to about 20 Hz and 30 Hz respectively, for CEUS hard rock site conditions. The frequency-to-frequency variation is largely unchanged. The low-frequency ($\leq$ 2 Hz) spectra are essentially unaltered in this process, preserving attributes of near-source records such as differences between fault normal and fault parallel components and the effects of rupture directivity on the average horizontal and vertical components.

Although the low-frequency response spectra remain largely unaffected by the scaling process, high-pass filtering of the scaled records at 0.1 Hz can affect the character of the velocity and displacement time histories. The filters applied to the scaled records consist of causal four-pole Butterworth filters, high-pass at 0.1 Hz and low-pass at 62.5 Hz. The filters are applied to each record and are intended to remove any spurious effects of the scaling and fitting process well outside the general frequency range of interest, 0.5 to 25 Hz. Causal filters are desirable because they minimize the potential effects of distortion due to wraparound of the filter transients. However, there may potentially be undesirable consequences of causal high-pass filters. The character of low-frequency time histories such as velocity and displacement may be altered as a result of the process. Comparing the velocity and displacement time histories for WUS soft rock and CEUS hard rock in Figures 3-5 and 3-7 respectively, differences in characteristics are apparent. Although the amplitudes are nearly the same, the initial peaks have sign reversals in the velocity records, and the largely single-sided WUS displacement time history near 8 sec has become a double sided pulse. While differences in the velocity records are not likely to result in significantly different structural demands at intermediate frequencies, the differences in displacements may be an issue in structural analyses. The double-sided pulse resulting from the causal filters may produce larger demands on long-period structures than the single-sided pulse, because there are more cycles and larger positive-to-negative excursions in displacement. This is only an issue for close-in (near source) short duration records and can be corrected by removing the causal filter and applying an appropriate acausal filter. Figure 3-9 illustrates the results of this process and shows both velocity and displacement time histories scaled to CEUS conditions. These records have very similar characteristics to those from the original processing (Figure 3-5). In this case the modulus of the Butterworth filter was applied in the frequency domain. Figure 3-10 compares the response spectra computed from the two time histories, filtered with a causal and with an acausal four-pole Butterworth high-pass filter, showing little difference between the two.

3.4 Matching WUS Time History to CEUS Spectrum

To demonstrate the process of closely matching a WUS motion to a CEUS spectral target, typical 10^{-4} rock UHS are used as targets, and the rock site Ferdows record from the 1978 **M** 7.4 Tabas earthquake is used as a WUS input motion (bin **M** 7+, distance 50 to 100 km rock; Table 3-3). The two target spectra are shown Figure 3-11. The spectra illustrate the large differences in WUS and

CEUS spectral amplitudes and shapes, reflecting differences in both hazard environment and in strong motion generation and wave propagation between the two regions.

Figure 3-12 shows the result of matching the WUS record to the WUS UHS, and Figure 3-13 shows the resulting time histories. The fit is acceptably close and the resulting time histories, as expected, are realistic in acceleration as well as integrations to velocity and displacement. Figure 3-14 shows the spectral match for the CEUS. Using the original sample internal of 0.02 sec, with a Nyquist frequency of 25 Hz, results in the low spectral values between 25 and 100 Hz (dashed line in Figure 3-14) and a low peak acceleration of 0.269g (target = 0.298g). Interpolating the record to 200 samples per second results in an improved match beyond 25 Hz and at peak acceleration. The resulting time histories are shown in Figures 3-15 and 3-16 for the two sample intervals (0.02 sec and 0.005 sec). The time histories are nearly identical and are comparable in overall shape to those resulting from the WUS match (Figure 3-13). The comparison of the corresponding Fourier amplitude spectra is shown in Figure 3-17. The result of matching to WUS and CEUS targets largely reflects a broad-band scale factor applied to the Fourier amplitude spectrum of the recorded motion. Decreasing the sample interval actually *lowers* the Fourier amplitude spectrum near 25 Hz as additional energy is available beyond 25 Hz for the higher frequency oscillators. The 25 Hz Fourier amplitude value for the 0.02 sec CEUS spectral match has the largest amplitude of all frequencies, suggesting an aliased record. Although this is not obvious in comparing Figures 3-15 and 3-16, the time history obtained using a higher Nyquist frequency (Figure 3-16) shows overall larger accelerations than the record with a sample interval of 0.02 sec. This may be a consequence of aliasing, however one would normally expect enhanced motions at frequencies below the Nyquist (25 Hz). Overall, these comparisons indicate that WUS motions can be used as inputs to matching CEUS spectra provided the sample interval reflects a Nyquist frequency ($f_N = [2\,\Delta t]^{-1}$) of at least 100 Hz. As a corollary, CEUS records could be used as input to matching WUS targets as well.

References

Arias, A. (1969). "A measure of earthquake intensity." in *Seismic Design for Nuclear Power Plants,* R. Hansen, Editor, Massachusetts Institute of Technology Press, Cambridge.

Atkinson, G.M. and Boore, D.M. (1998). "Evaluation of models for earthquake source spectra in Eastern North America." *Bull. Seism. Soc. Am.* 88(4), 917-934.

Atkinson, G.M. (1995). "Attenuation and source parameters of earthquakes in the Cascadia Region." *Bull. Seism. Soc. Am.,* 85(5), 1327-1342.

Carballo, J.E. and A. Cornell (1998). "Input to nonlinear structural analysis: modification of available accelerograms for different source and site characteristics." *Proceedings, 6th U.S. Nat'l Conference on Earthquake Engineering,* Seattle, Washington.

Dobry, I. M., I. M. Idriss and E. Ng. (1978). "Duration characteristics of horizontal components of strong motion earthquake records." *Bull. Seis. Soc. Amer.,* 68(5), 1487-1520.

Electric Power Research Institute (1993). "Guidelines for determining design basis ground motions." Electric Power Research Institute, Palo Alto, CA, Rept. TR-102293, vol. 1-5:
vol. 1: Methodology and guidelines for estimating earthquake ground motion in eastern North America.
vol. 2: Appendices for ground motion estimation.
vol. 3: Appendices for field investigations.
vol. 4: Appendices for laboratory investigations.
vol. 5: Quantification of seismic source effects.

Husid, R. L. (1969). "Analisis de terremotos." Analisis General, Revista del IDIEM, 8, 21-42, Santiago, Chile.

Kennedy, R.P., Short, S.A., Merz, K.L., Tokarz, F.J., Idriss, I.M., Power, M.S, and Sadigh, K. (1984). "Engineering characterization of ground motion, Task I: Effects of characteristics of free-field motion on structural response." U.S. Nuclear Regulatory Commission. NUREG/CR-3805, vol. 1.

Silva, W.J. (1997). "Characteristics of vertical Strong ground motions for applications to engineering design." Proc. Of the FHWA/NCEER Workshop on the Nat'l Representation of Seismic, I.M. Friedland, M.S Power and R. L. Mayes eds., Technical Report NCEER-97-0010.

Silva, W.J., N. Abrahamson, G. Toro, C. Costantino (1997). "Description and validation of the stochastic ground motion model." Report to Brookhaven National Laboratory, Associated Universities, Inc. Upton, New York, Contract 770573.

Silva, W.J. and R. Darragh (1995). "Engineering characterization of earthquake strong ground motion recorded at rock sites." Electric Power Research Institute, Palo Alto, CA, Rept. TR-102261.

Silva, W.J. (1991). "Global characteristies and site geometry." Proceedings: NSF/EPRI Workshop on Dynamic Soil Properties and Site Characterization. Electric Power Res. Inst., EPRI NP-7337.

Silva, W.J., Lee, K. (1987) *"WES RASCAL code for synthesizing earthquake ground motions"* State-of-the-Art for Assessing Earthquake Hazards in the United States, Report 24, U.S. Army Engineers Waterways Experiment Station, Misc. Paper S-73-1.

Table 3-1

GEOTECHNICAL SUBSURFACE CHARACTERISTICS

A = Rock. Instrument on rock (Vs > 600 mps) or < 5m of soil over rock.

B = Shallow (stiff) soil. Instrument on/in soil profile up to 20m thick overlying rock.

C = Deep narrow soil. Instrument on/in soil profile at least 20m thick overlying rock, in a narrow canyon or valley no more than several km wide.

D = Deep broad soil. Instrument on/in soil profile at least 20m thick overlying rock, in a broad valley.

E = Soft deep soil. Instrument on/in deep soil profile with average Vs < 150 mps.

Table 3-2
MAGNITUDE AND DISTANCE BINS AND DURATION CRITERIA

M	*R* (km)	Duration (sec)**	
		Rock	Soil
5.5 (5 - 6)	0 - 50*	1.1 - 3.6*	1.6 - 4.8*
	50 - 100	3.6 - 8.2	2.9 - 6.4
6.5 (6 - 7)	0 - 10	2.6 - 5.8	3.1 - 7.0
	10 - 50	3.1 - 7.0	3.6 - 8.2
	50 - 100	5.1 - 11.6	5.7 - 12.8
	100 - 200	8.1 - 18.3	8.7 - 19.5
	200 - 400***		
7.5 (7+)	0 - 10	6.1 - 13.8	6.6 - 15.0
	10 - 50	6.6 - 14.0	7.2 - 16.1
	50 - 100	8.7 - 19.5	12.2 - 27.5
	100 - 200	11.7 - 26.3	16.2 - 36.5
	200 - 400***		

*For **M** 5.5 bin, too few records were available for 0-10 km, so distance bins 0-10 km and 10-50 km were combined to 0-50 km

**5% - 75% total cumulative Arias Intensity

***CEUS only

Table 3-3 WUS TIME HISTORY BINS				
M	$\overline{M}$	R (km)	$\overline{R}$ (km)	Number of sets
5 - 6, rock	5.50	0 - 50	17.29	15
	6.00	50 - 100	64.88	15
5 - 6, soil	5.77	0 - 50	16.97	15
	5.75	50 - 100	64.38	15
6 - 7, rock	6.53	0 - 10	6.00	15
	6.39	10 - 50	31.29	30
	6.38	50 - 100	66.12	15
	6.66	100 - 200	89.03	15
6 - 7, soil	6.58	0 - 10	5.74	18
	6.41	10 - 50	27.83	15
	6.57	50 - 100	67.10	15
	6.64	100 - 200	131.53	15
7+, rock	7.25	0 - 10	5.83	15
	7.38	10 - 50	31.48	15
	7.49	50 - 100	76.88	15
	7.49	100 - 200	135.03	15
7+, soil	7.40	0 - 10	4.62	21
	7.47	10 - 50	29.60	15
	7.53	50 - 100	68.79	15
	7.44	100 - 200	134.73	15

Table 3-4
CEUS TIME HISTORY BINS

M	$\overline{M}$	R (km)	$\overline{R}$ (km)	Number of sets**
4.5* - 6, rock	5.50	0 - 50	17.29	0 (15)
	5.85	50 - 100	78.34	8 (7)
4.5* - 6, soil	5.69	0 - 50	18.81	1 (14)
	5.66	50 - 100	64.99	2 (13)
6 - 7, rock	6.53	0 - 10	6.18	2 (14)
	6.32	10 - 50	28.58	1 (14)
	6.38	50 - 100	66.12	0 (15)
	6.66	100 - 200	89.03	0 (15)
6 - 7, soil	6.58	0 - 10	5.74	0 (18)
	6.41	10 - 50	27.83	0 (15)
	6.57	50 - 100	67.10	0 (15)
	6.64	100 - 200	131.53	0 (15)
7+, rock	7.25	0 - 10	5.83	0 (15)
	7.38	10 - 50	31.48	0 (15)
	7.49	50 - 100	76.88	0 (15)
	7.49	100 - 200	135.03	0 (15)
7+, soil	7.40	0 - 10	4.62	0 (21)
	7.47	10 - 50	29.60	0 (15)
	7.53	50 - 100	68.79	0 (15)
	7.44	100 - 200	134.73	0 (15)

*M range extended to M 4.5

**Supplemented with WUS to CEUS scaled records, first number reflects number of actual CEUS recordings, parentheses show number of scaled WUS to CEUS three component sets.

Table 3-5

WUS ANALYSIS TIME HISTORY STATISTICS

Magnitude Bins (M)	
Range	Bin Center
5 - 6	5.5
6 - 7	6.5
7+	7.5

Distance bin (km)	$\overline{M}$	$\overline{R}$ (km)	Number of sets	PGA*(g), σ_{ln}	PGV*(cm/sec), σ_{ln}	PGD*(cm), σ_{ln}	$\frac{PGV^*}{PGA}$ ($\frac{cm/sec}{g}$), σ_{ln}	$\frac{PGA \cdot PGD^*}{PGV^2}$, σ_{ln}
0 - 10, rock	6.53	6.00	15	0.46, 0.64	36.63, 0.74	7.63, 0.89	79.35, 0.35	2.57, 0.41
	7.25	5.83	15	0.39, 0.73	53.74, 0.73	22.86, 0.65	138.42, 0.58	3.01, 0.52
0 - 10, soil	6.58	5.74	18	0.41, 0.46	54.65, 0.51	19.61, 0.65	132.40, 0.43	2.66, 0.40
	7.40	4.62	21	0.34, 0.50	69.89, 0.44	50.15, 0.70	205.72, 0.44	3.42, 0.42
10 - 50, rock	6.39	31.29	30	0.11, 0.70	7.40, 0.79	1.61, 1.22	68.62, 0.52	3.11, 0.53
	7.38	31.48	15	0.15, 0.90	17.88, 0.88	9.27, 1.37	115.67, 0.68	4.40, 0.58
10 - 50, soil	6.41	27.83	15	0.14, 0.64	10.37, 0.73	2.46, 1.20	71.79, 0.33	3.24, 0.50
	7.47	29.60	15	0.16, 0.58	27.48, 0.74	18.28, 0.78	172.30, 0.27	3.79, 0.51
50 - 100, rock	6.00	64.88	15	0.05, 0.38	2.27, 0.55	0.23, 0.83	42.01, 0.44	2.37, 0.58
	6.38	66.12	15	0.04, 0.54	2.75, 0.61	0.51, 1.02	69.38, 0.41	2.64, 0.51
	7.49	76.88	15	0.06, 0.37	7.18, 0.57	5.68, 0.96	119.02, 0.46	6.52, 0.36
50 - 100, soil	5.75	64.38	15	0.06, 0.78	3.22, 0.70	0.36, 0.87	50.33, 0.22	2.20, 0.40
	6.57	67.10	15	0.06, 0.57	5.72, 0.60	1.33, 0.75	93.72, 0.39	2.44, 0.62
	7.53	68.79	15	0.07, 0.53	12.15, 0.52	7.33, 0.88	178.14, 0.49	3.32, 0.46
100 - 200, rock	6.66	89.03	15	0.03, 0.87	2.86, 0.55	1.05, 0.63	101.82, 0.54	3.55, 0.38

*Median values

Table 3-5 (cont.)

WUS ANALYSIS TIME HISTORY STATISTICS

Magnitude Bins (M)

Range	Bin Center
5 - 6	5.5
6 - 7	6.5
7+	7.5

Distance bin (km)	$\overline{M}$	$\overline{R}$ (km)	Number of sets	PGA*(g), σ_{ln}	PGV*(cm/sec), σ_{ln}	PGD*(cm), σ_{ln}	$\frac{PGV^*}{PGA}$ ($\frac{cm/sec}{g}$), σ_{ln}	$\frac{PGA \cdot PGD^*}{PGV^2}$, σ_{ln}
100 - 200, rock	7.49	135.03	15	0.03, 0.34	5.78, 0.64	3.83, 1.05	177.22, 0.48	3.67, 0.61
100 - 200, soil	6.64	131.53	15	0.03, 0.78	3.22, 0.59	0.92, 0.94	97.91, 0.51	2.86, 0.41
	7.44	134.73	15	0.05, 0.39	7.75, 0.40	4.91, 0.55	166.48, 0.26	3.73, 0.61
0 - 50, rock	5.50	17.29	15	0.16, 0.92	7.52, 0.99	0.76, 1.28	45.92, 0.41	2.17, 0.33
0 - 50, soil	5.77	16.97	15	0.20, 0.43	10.83, 0.54	1.31, 0.79	53.32, 0.26	2.22, 0.25

*Median values

Table 3-6

CEUS ANALYSIS TIME HISTORY STATISTICS

Magnitude Bins (M)

Range	Bin Center
5 - 6	5.5
6 - 7	6.5
7+	7.5

Distance bin (km)	$\overline{M}$	$\overline{R}$ (km)	Number of sets	PGA*(g), σ_{ln}	PGV*(cm/sec), σ_{ln}	PGD*(cm), σ_{ln}	$\frac{PGV^*}{PGA}$ ($\frac{cm/sec}{g}$), σ_{ln}	$\frac{PGA \cdot PGD^*}{PGV^2}$, σ_{ln}
0 - 10, rock	6.53	6.18	2 (14)	1.16, 0.66	39.74, 0.66	7.84, 0.94	34.37, 0.42	5.63, 0.45
	7.25	5.83	0 (15)	0.89, 0.90	58.40, 0.40	22.33, 0.57	65.84, 0.67	5.70, 0.45
0 - 10, soil	6.58	5.74	0 (18)	0.61, 0.44	59.36, 0.49	18.56, 0.62	97.46, 0.36	3.15, 0.34
	7.40	4.62	0 (21)	0.38, 0.54	59.38, 0.42	31.90, 0.59	156.54, 0.39	3.36, 0.36
10 - 50, rock	6.32	28.58	1 (14)	0.25, 0.78	7.95, 0.62	1.70, 0.99	31.75, 0.51	6.58, 0.70
	7.38	31.48	0 (15)	0.34, 0.94	19.85, 0.83	9.17, 1.14	58.24, 0.72	7.78, 0.63
10 - 50, soil	6.41	27.83	0 (15)	0.30, 0.61	15.33, 0.74	2.83, 1.08	51.74, 0.35	3.49, 0.47
	7.47	29.60	0 (15)	0.23, 0.57	29.58, 0.72	13.86, 0.98	128.74, 0.27	3.57, 0.35
50 - 100, rock	5.85	78.34	8 (7)	0.06, 1.41	1.24, 1.40	0.10, 1.57	21.28, 0.36	3.61, 0.50
	6.38	66.12	0 (15)	0.09, 0.55	2.99, 0.53	0.46, 0.83	32.59, 0.33	4.66, 0.52
	7.49	76.88	0 (15)	0.15, 0.49	7.33, 0.50	3.98, 0.76	50.29, 0.56	10.60, 0.46
50 - 100, soil	5.66	64.99	2 (13)	0.13, 1.20	4.74, 0.85	0.31, 1.35	37.05, 0.52	1.72, 1.18
	6.57	67.10	0 (15)	0.15, 0.59	8.35, 0.58	1.43, 0.65	56.04, 0.36	3.01, 0.48

*Median values

Table 3-6 (cont.)

CEUS ANALYSIS TIME HISTORY STATISTICS

Magnitude Bins (M)

Range	Bin Center
5 - 6	5.5
6 - 7	6.5
7+	7.5

Distance bin (km)	$\overline{M}$	$\overline{R}$ (km)	Number of sets	PGA*(g), σ_{ln}	PGV*(cm/sec), σ_{ln}	PGD*(cm), σ_{ln}	$\frac{PGV^*}{PGA}$ ($\frac{cm/sec}{g}$), σ_{ln}	$\frac{PGA \cdot PGD^*}{PGV^2}$, σ_{ln}
50 - 100, soil	7.53	68.79	0 (15)	0.12, 0.55	14.41, 0.47	5.54, 0.72	124.27, 0.47	3.03, 0.42
100 - 200, rock	6.66	89.03	0 (15)	0.08, 0.95	3.23, 0.65	0.85, 0.44	41.14, 0.47	6.29, 0.49
	7.49	135.03	0 (15)	0.09, 0.32	6.85, 0.56	3.08, 0.86	72.50, 0.47	6.07, 0.39
100 - 200, soil	6.64	131.53	0 (15)	0.10, 0.80	5.56, 0.66	0.96, 0.70	56.53, 0.40	2.98, 0.45
	7.44	134.73	0 (15)	0.11, 0.43	9.60, 0.44	3.77, 0.42	91.20, 0.37	4.22, 0.56
0 - 50, rock	5.50	17.29	0 (15)	0.29, 0.96	7.24, 0.93	0.59, 1.16	24.86, 0.41	3.20, 0.27
0 - 50, soil	5.69	18.81	1 (14)	0.31, 1.09	11.12, 1.21	1.01, 1.37	36.31, 0.27	2.46, 0.34

*Median values

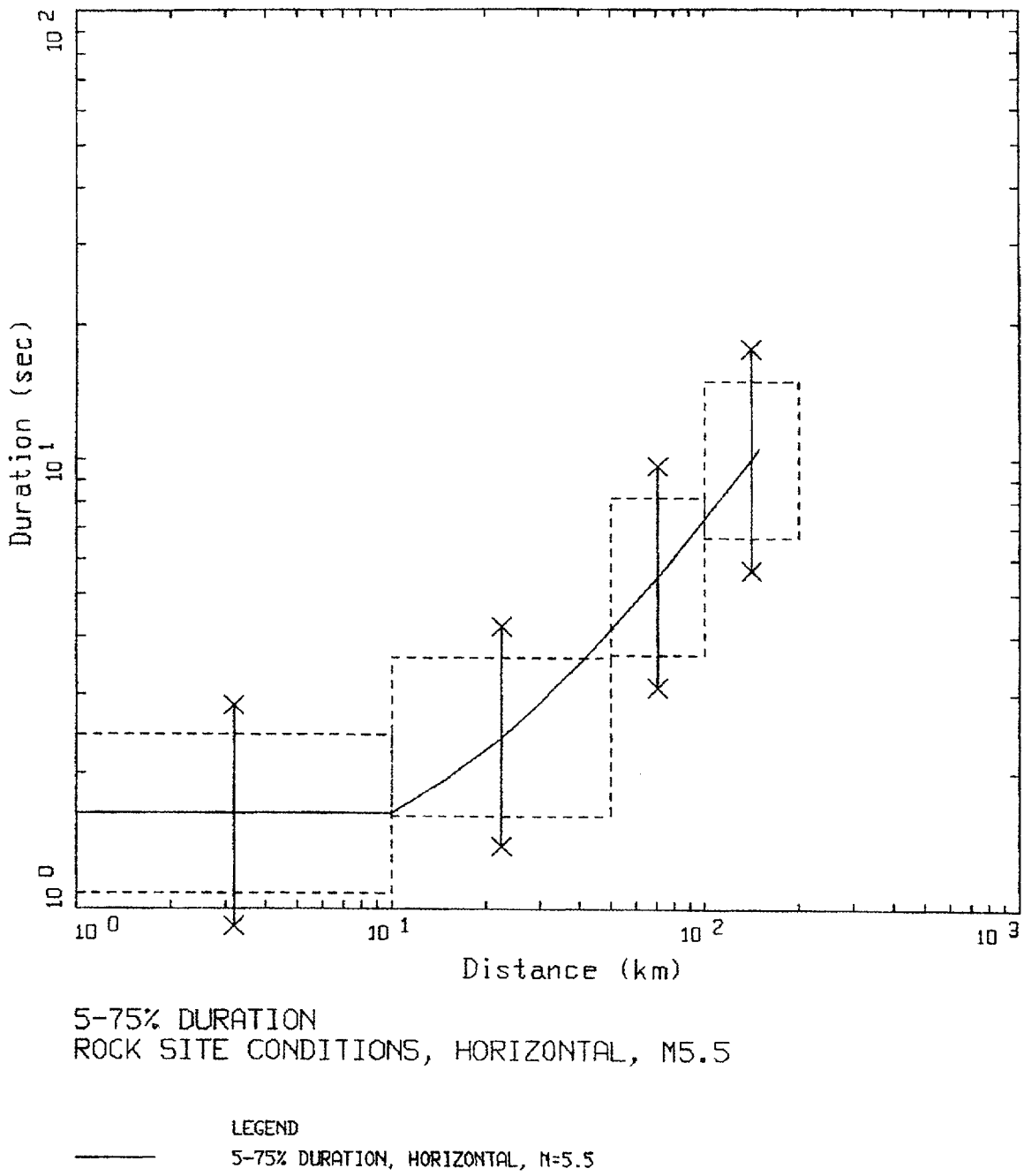

Figure 3-1. Example of duration bin criteria for **M** 5.5 bin and rock site conditions. Solid line is WUS empirical relation for 5 to 75% Arias Intensity (Appendix I) and X's reflect $\pm 1\sigma$ fractiles. Boxes represent $\pm 50\%$ duration bin (horizontal dashes) and distance bins: 0 to 10 km, 10 to 50 km, 50 to 100 km, 100 to 200 km (vertical dashes).

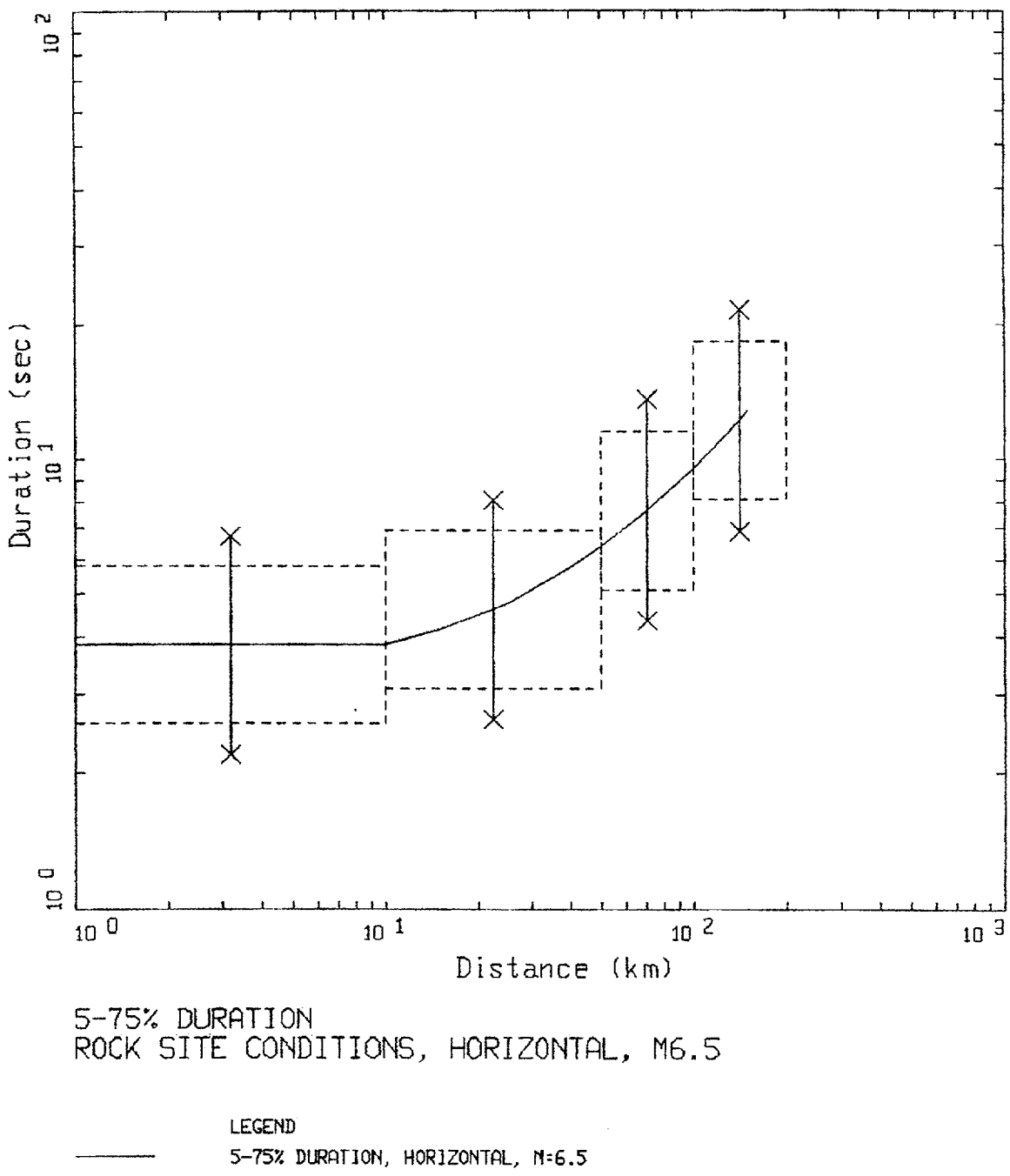

Figure 3-2. Example of duration bin criteria for **M** 6.5 bin and rock site conditions. Solid line is WUS empirical relation for 5 to 75% Arias Intensity (Appendix I) and X's reflect $\pm 1\sigma$ fractiles. Boxes represent $\pm 50\%$ duration bin (horizontal dashes) and distance bins: 0 to 10 km, 10 to 50 km, 50 to 100 km, 100 to 200 km, (vertical dashes).

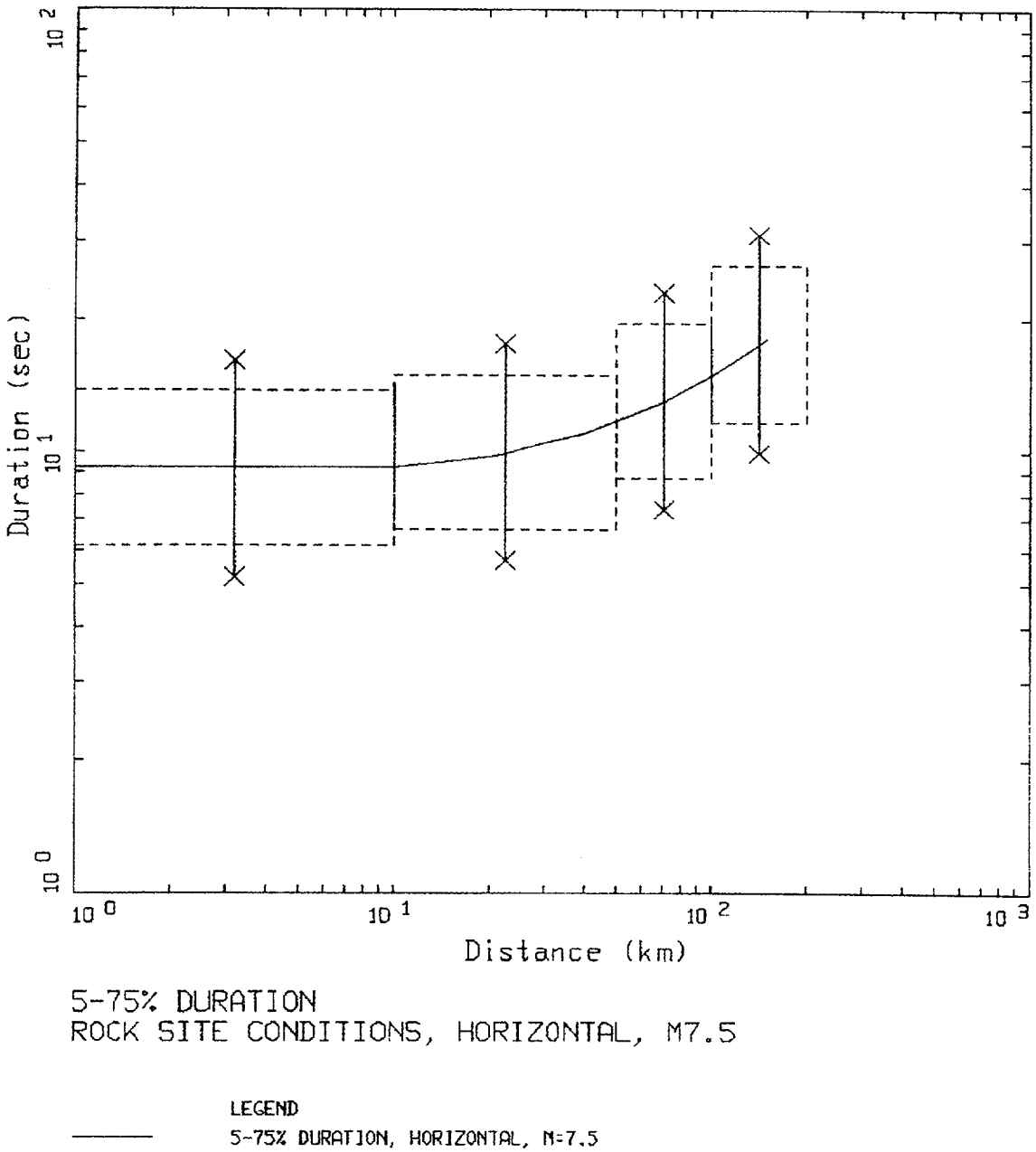

Figure 3-3. Example of duration bin criteria for **M** 7.5 bin and rock site conditions. Solid line is WUS empirical relation for 5 to 75% Arias Intensity (Appendix I) and X's reflect $\pm 1\sigma$ fractiles. Boxes represent $\pm 50\%$ duration bin (horizontal dashes) and distance bins: 0 to 10 km, 10 to 50 km, 50 to 100 km, 100 to 200 km (vertical dashes).

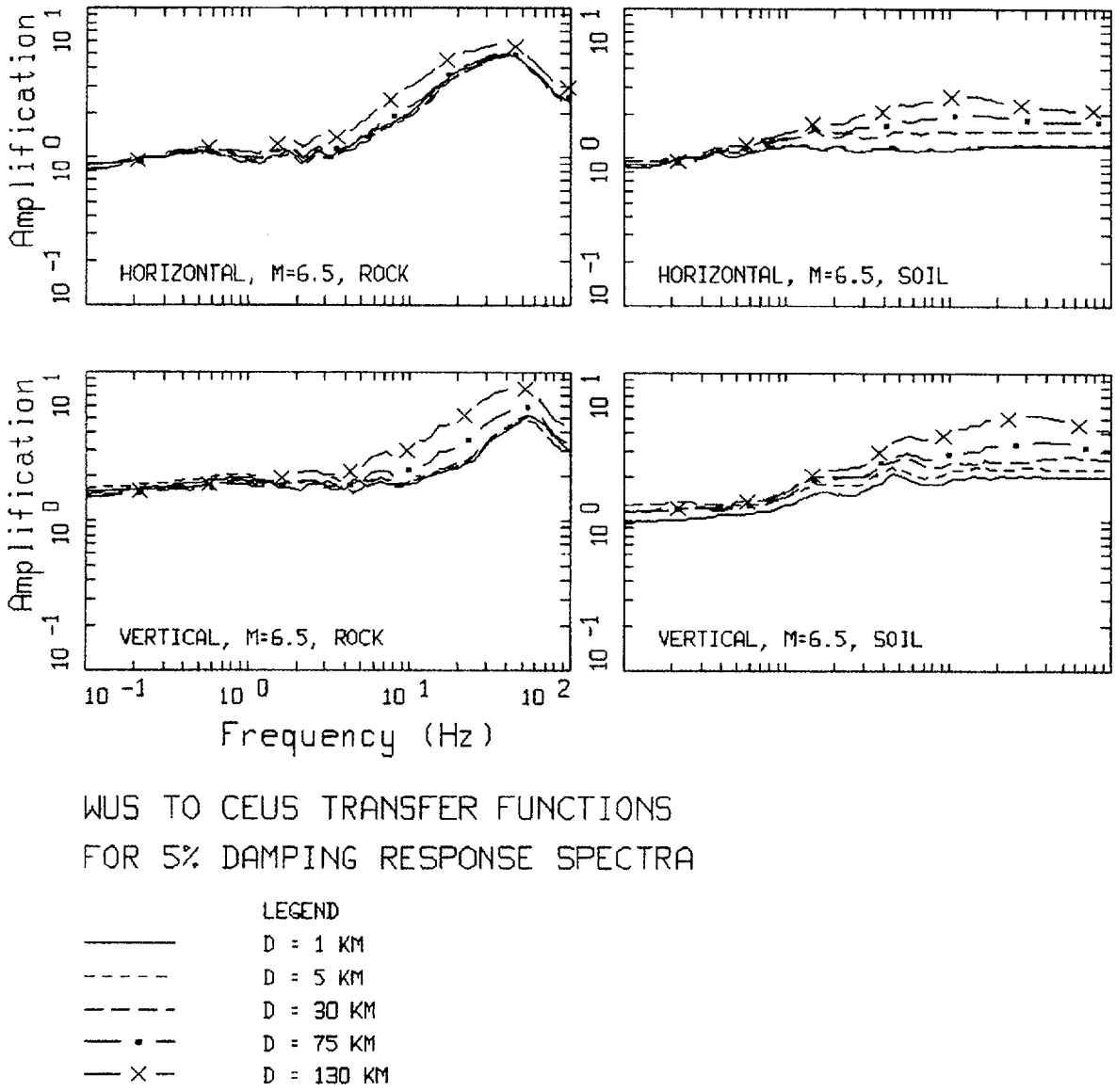

Figure 3-4. Example of rock and deep soil WUS-to-CEUS transfer functions (5% damped response spectra) computed for **M** = 6.5 and a suite of distances.

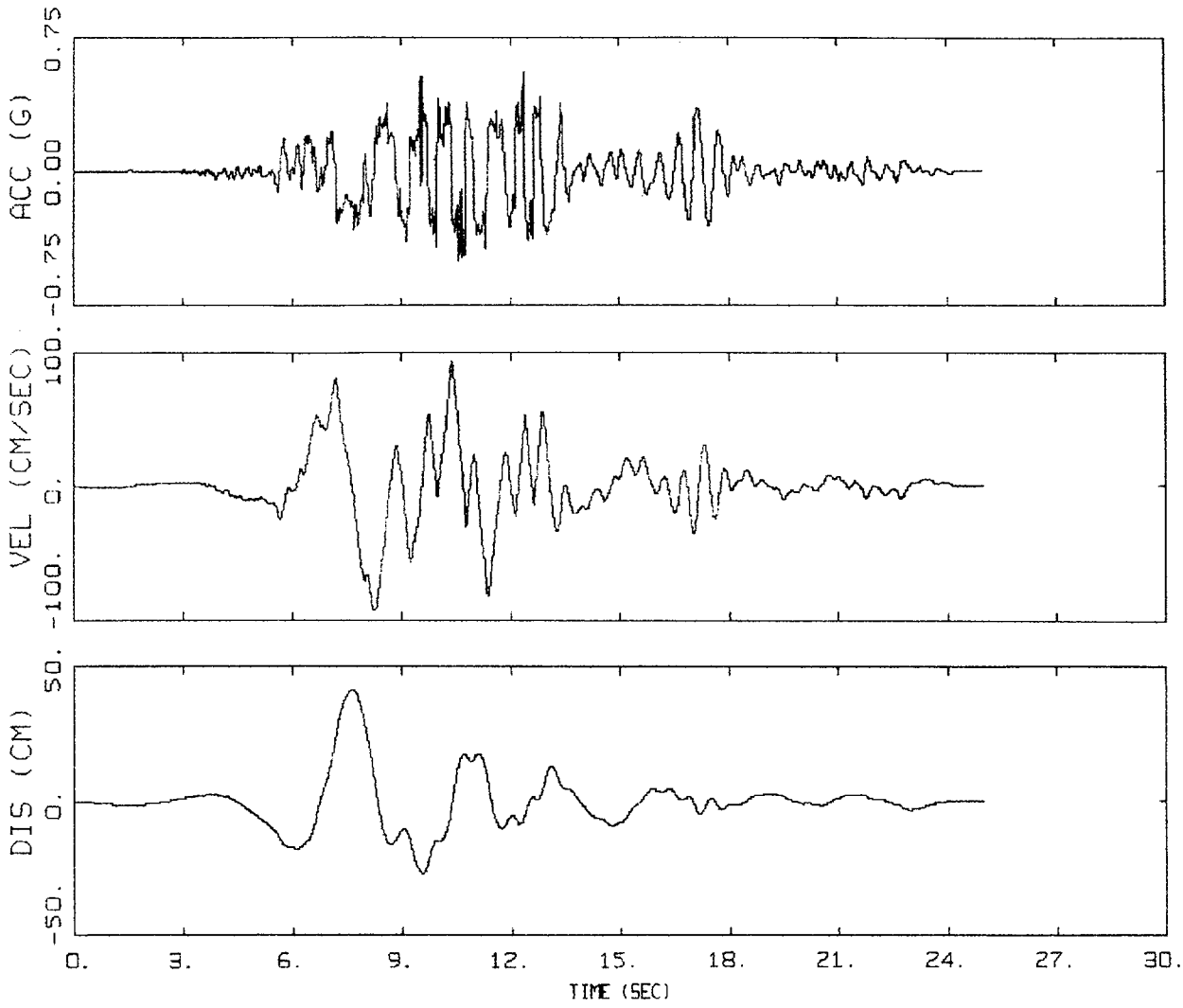

Figure 3-5. Acceleration, velocity, and displacement time histories from the 1989 **M** Loma Prieta earthquake recorded at the Los Gatos Presentation Center site (component 000), rupture distance of 6.1 km.

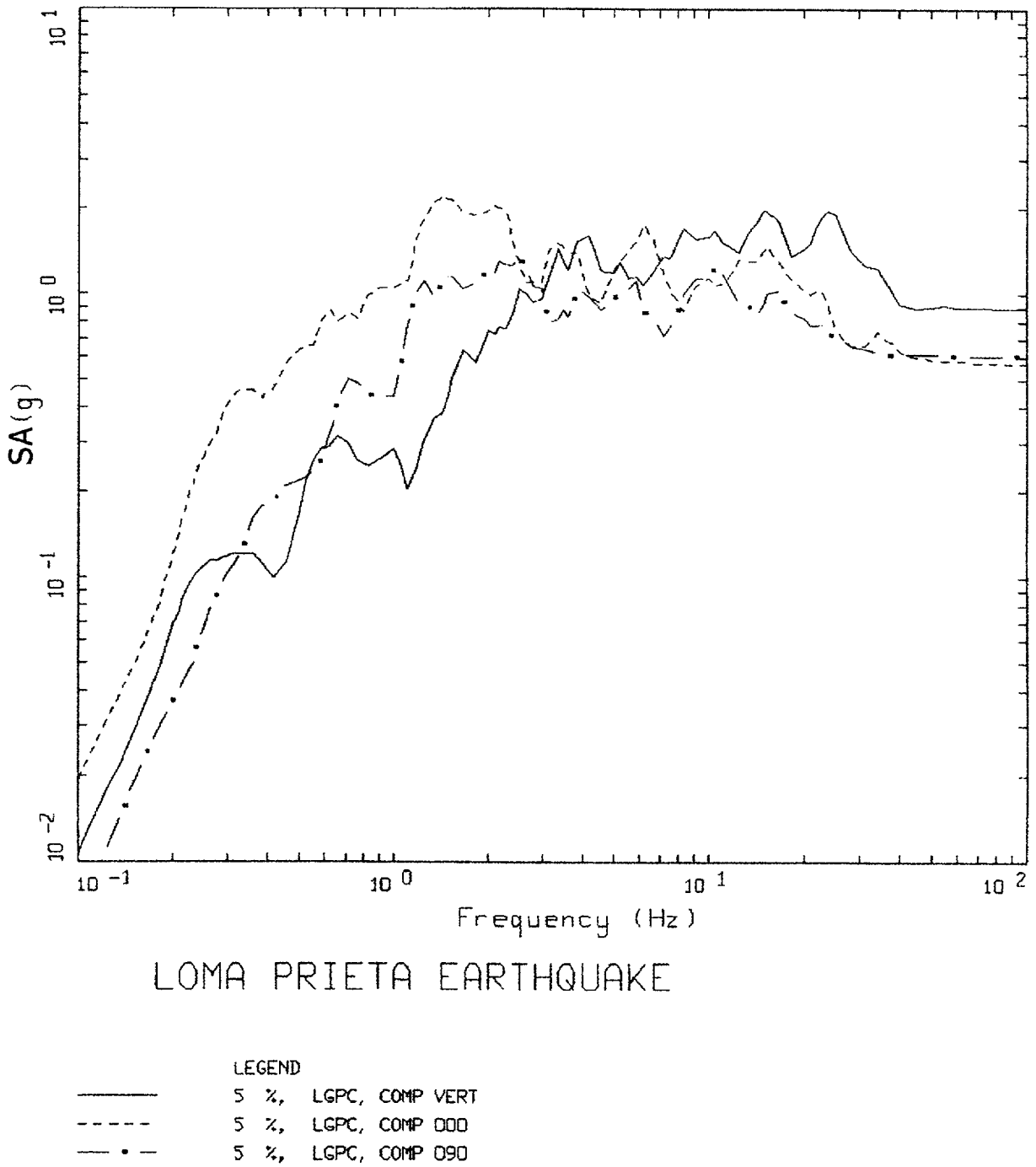

Figure 3-6. Response spectra (5% damping) for the motions recorded at site LGPC from the 1989 **M** 6.9 Loma Prieta earthquake.

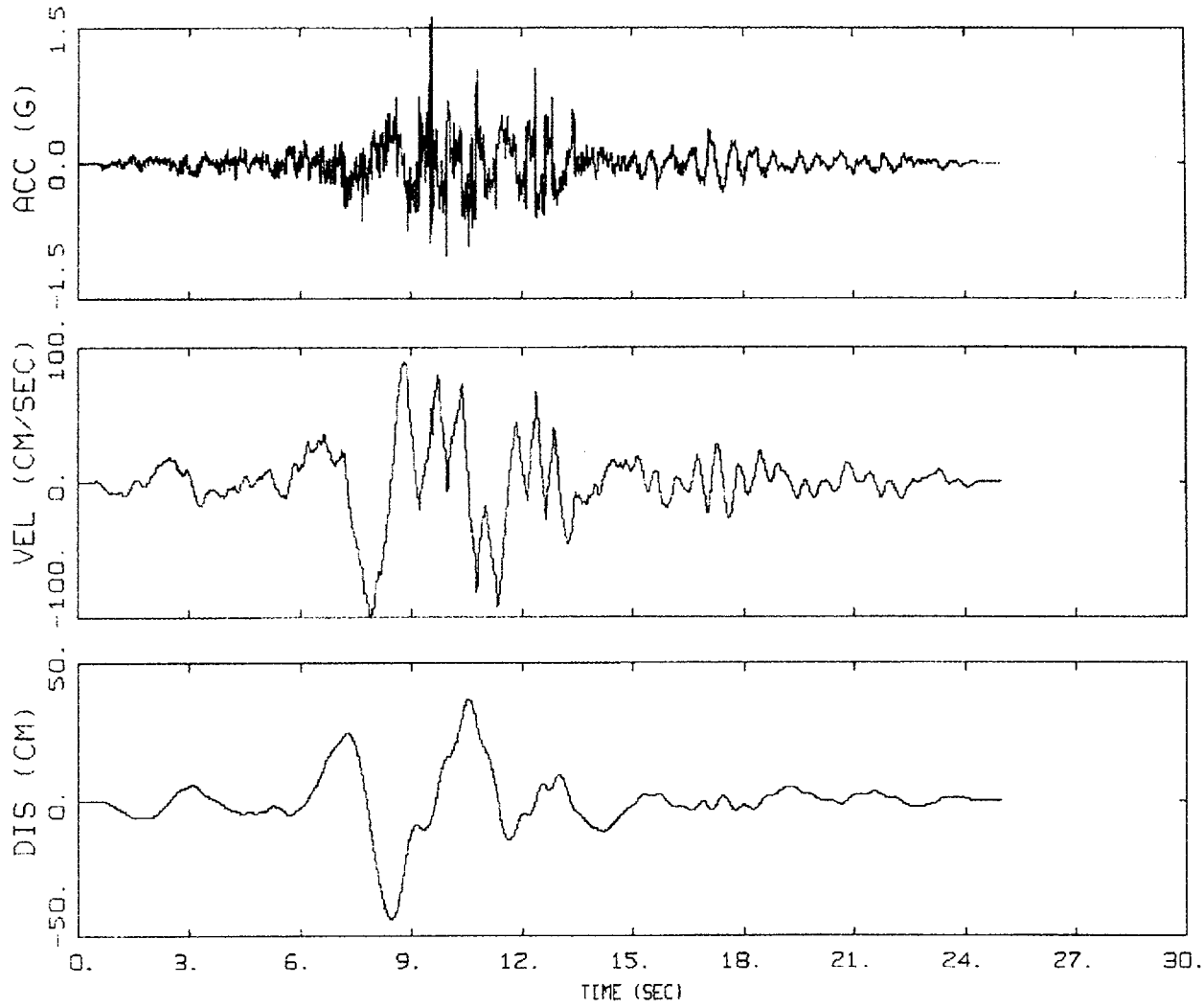

Figure 3-7. Acceleration, velocity, and displacement time histories from the 1989 **M** 6.9 Loma Prieta earthquake (Figure 3-5) scaled to CEUS hard rock site conditions.

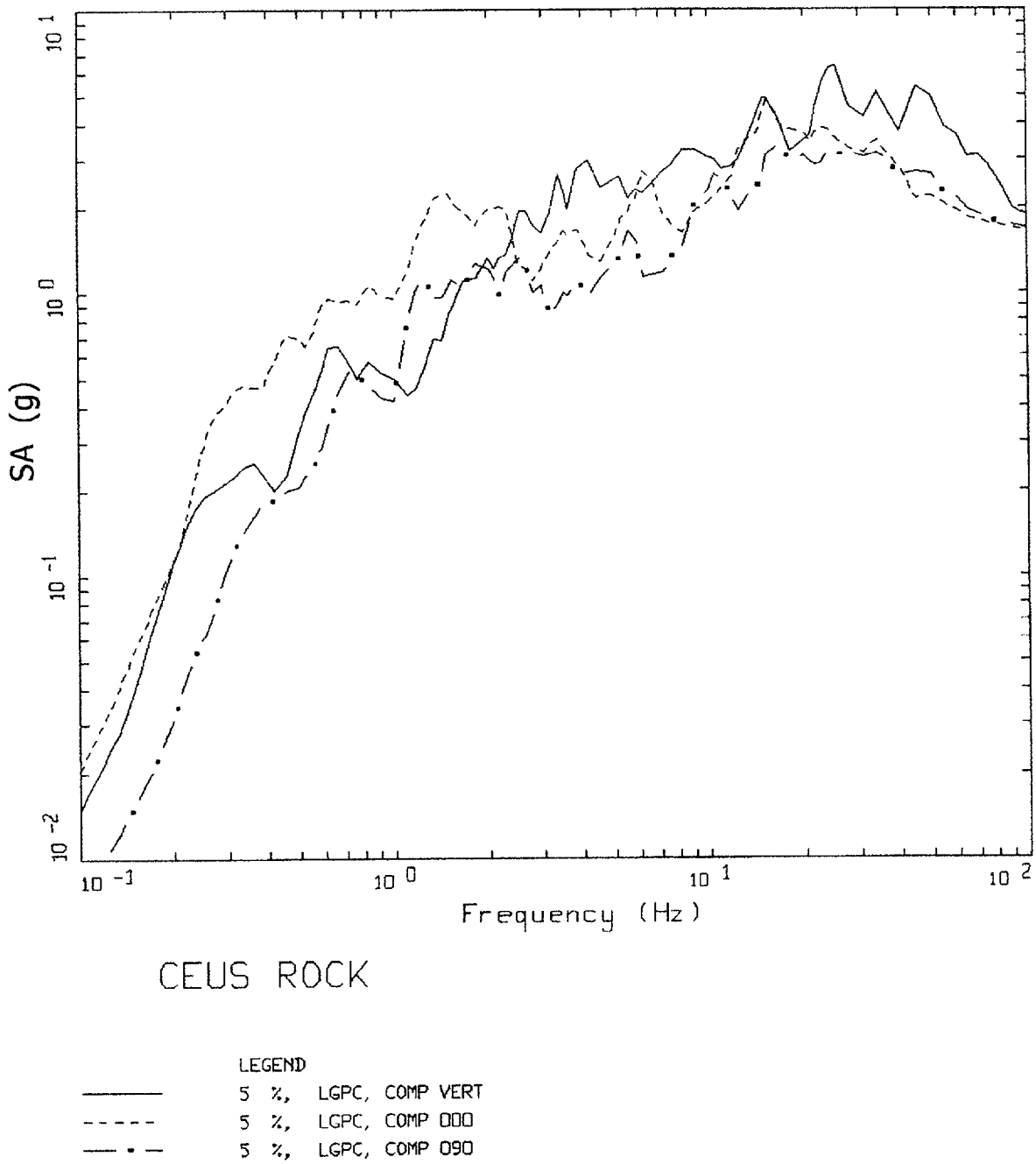

Figure 3-8. Response spectra (5% damping) for the recorded motions from the 1989 **M** 6.9 Loma Prieta earthquake (Figure 3-7) scaled to CEUS hard rock conditions.

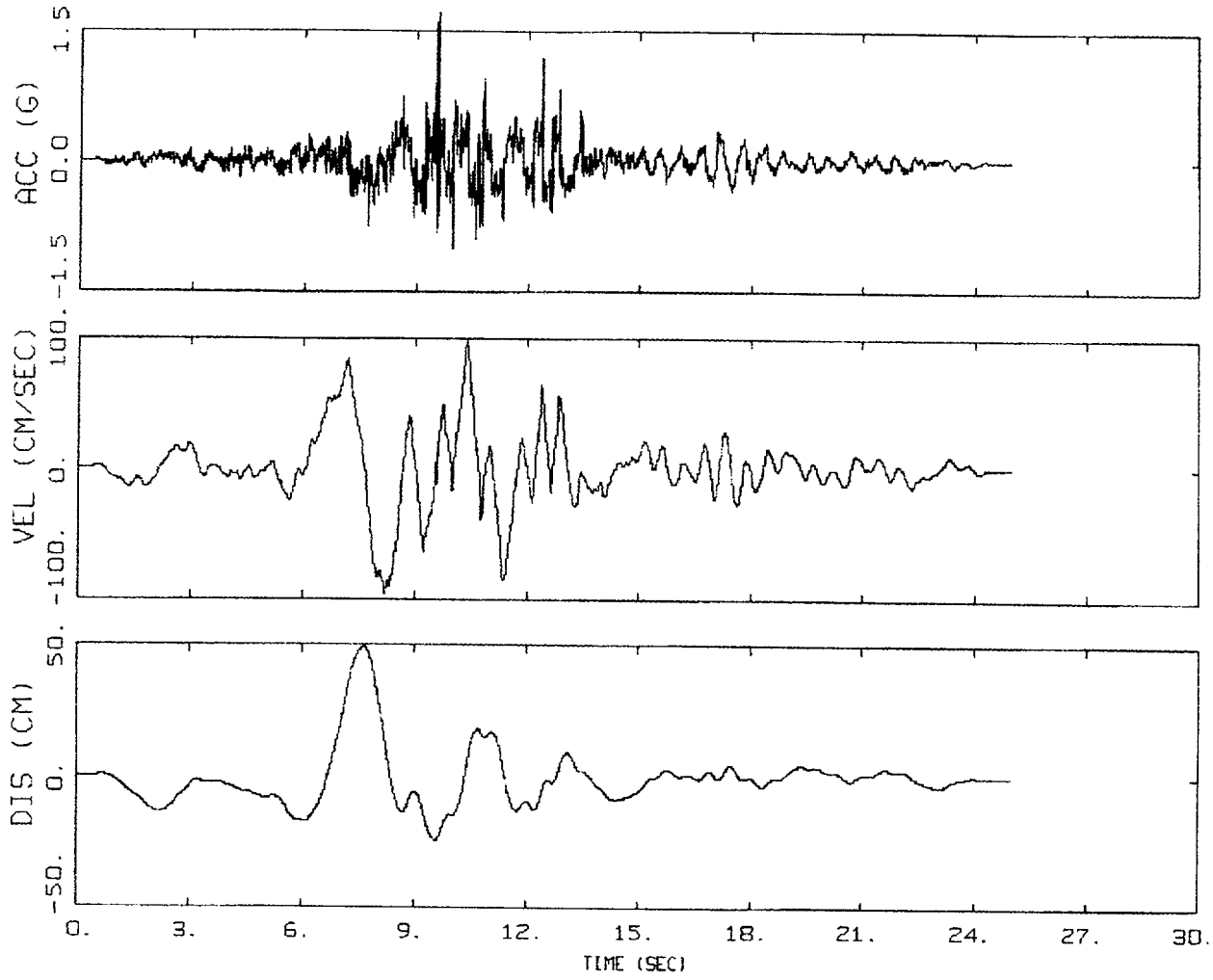

Figure 3-9. Acceleration, velocity, and displacement time histories from the 1989 **M** 6.9 Loma Prieta earthquake (Figure 3-5) scaled to CEUS hard rock site conditions, acausal high-pass filter.

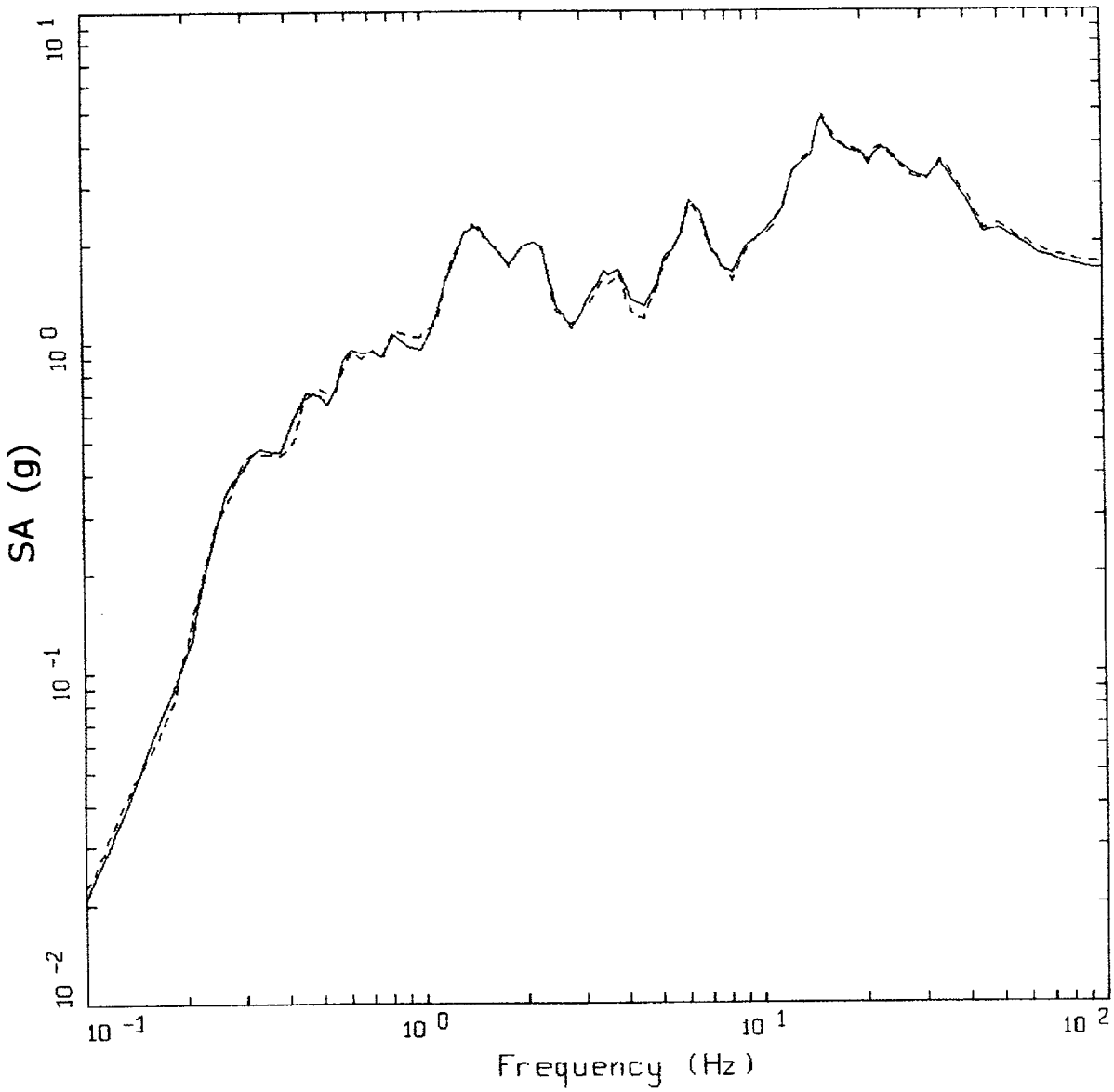

Figure 3-10. Comparison of 5% damped response spectra computed from scaled CEUS records to causal and acausal high-pass filters with 0.1 Hz corner frequencies. Corresponding time histories are shown in Figures 3-7 and 3-9 respectively.

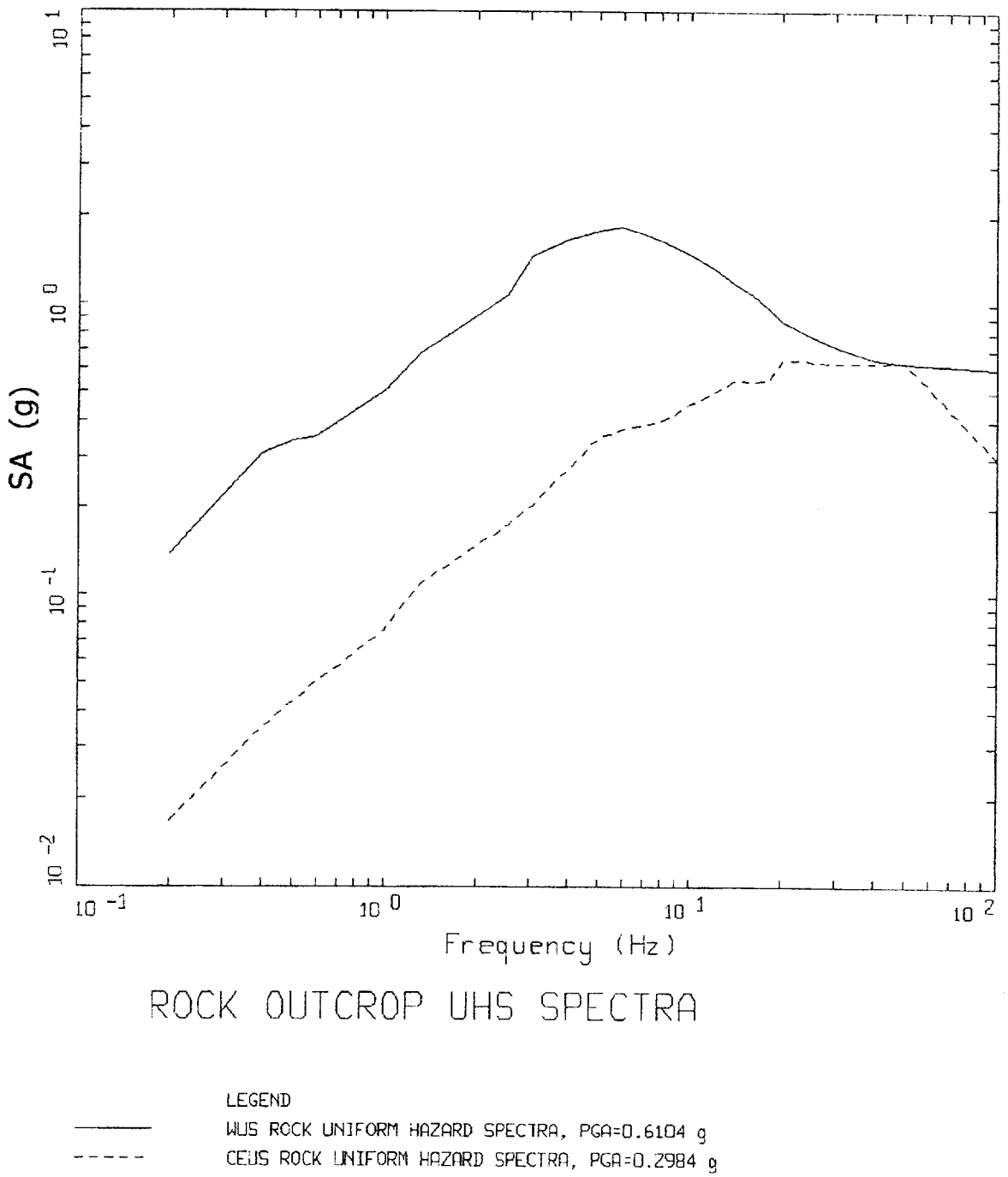

Figure 3-11. Comparison of 5% damped rock outcrop UHS spectra for CEUS and WUS conditions.

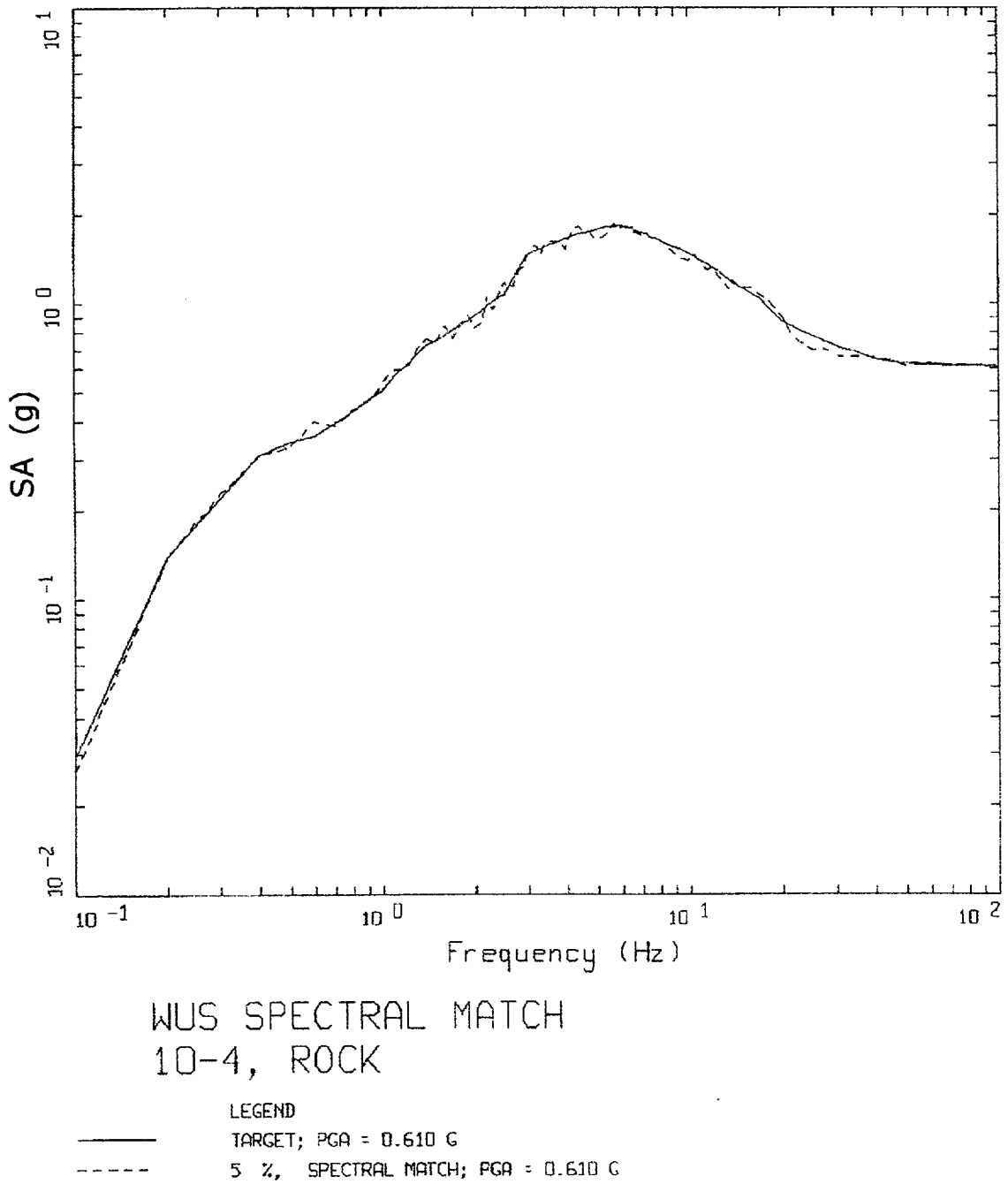

Figure 3-12. Spectral match of WUS record to WUS target: 10^{-4} rock UHS (Figure 3-11).

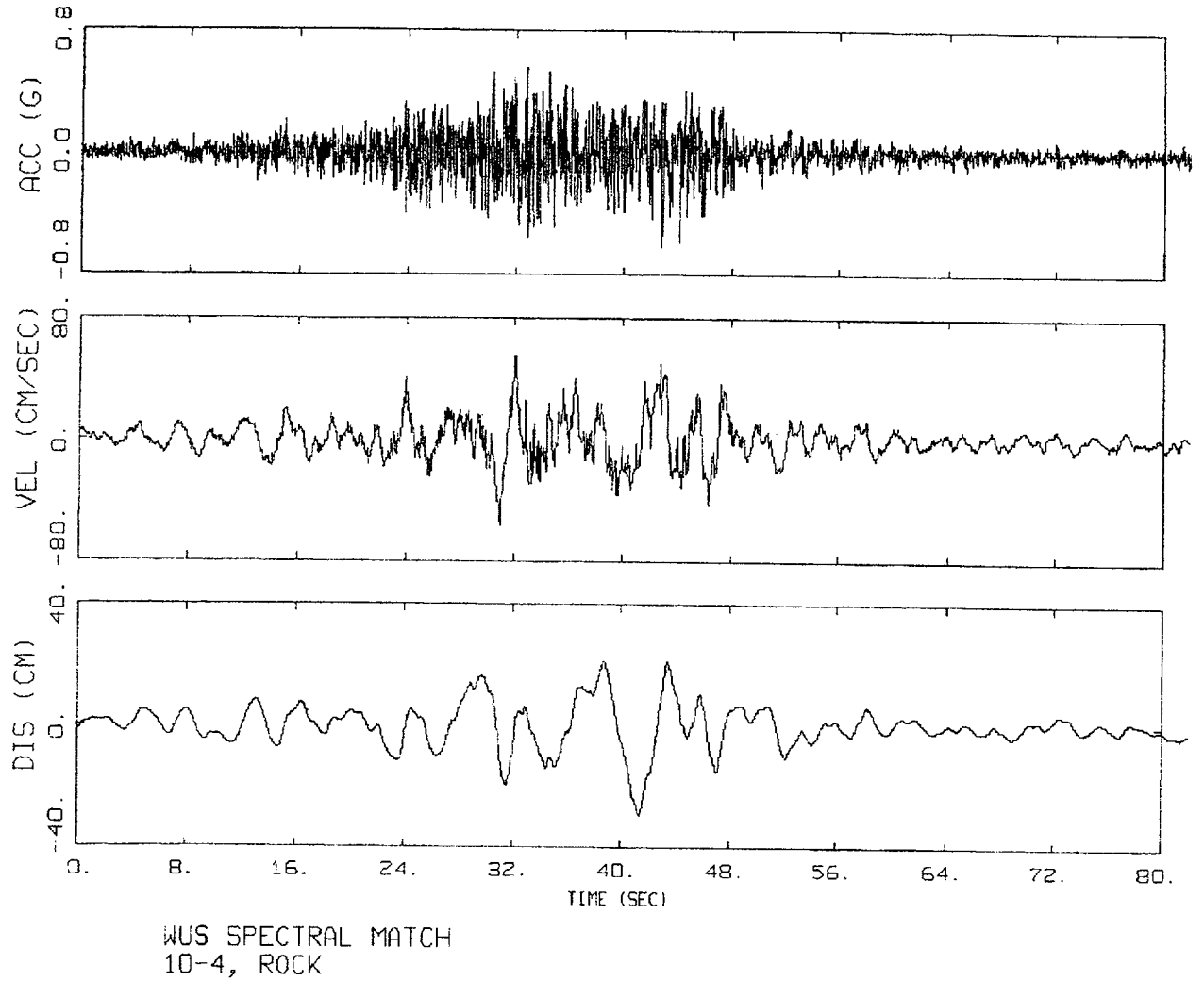

Figure 3-13. Acceleration, velocity, and displacement time histories resulting from match of WUS record to WUS target (Figure 3-11).

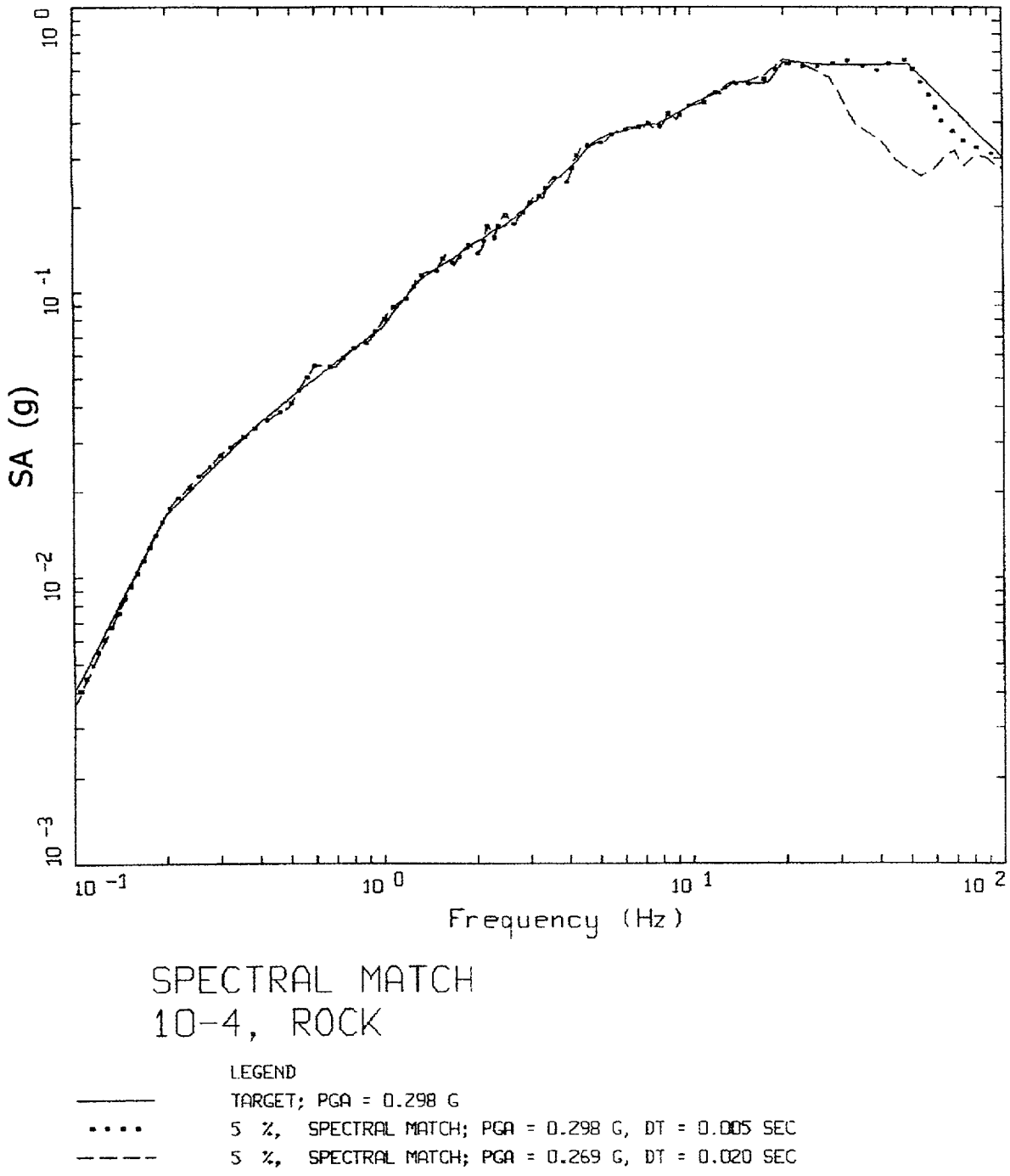

Figure 3-14. Spectral match of WUS record to CEUS target: 10^{-4} rock UHS using two sample intervals, 0.02 sec and 0.005 sec.

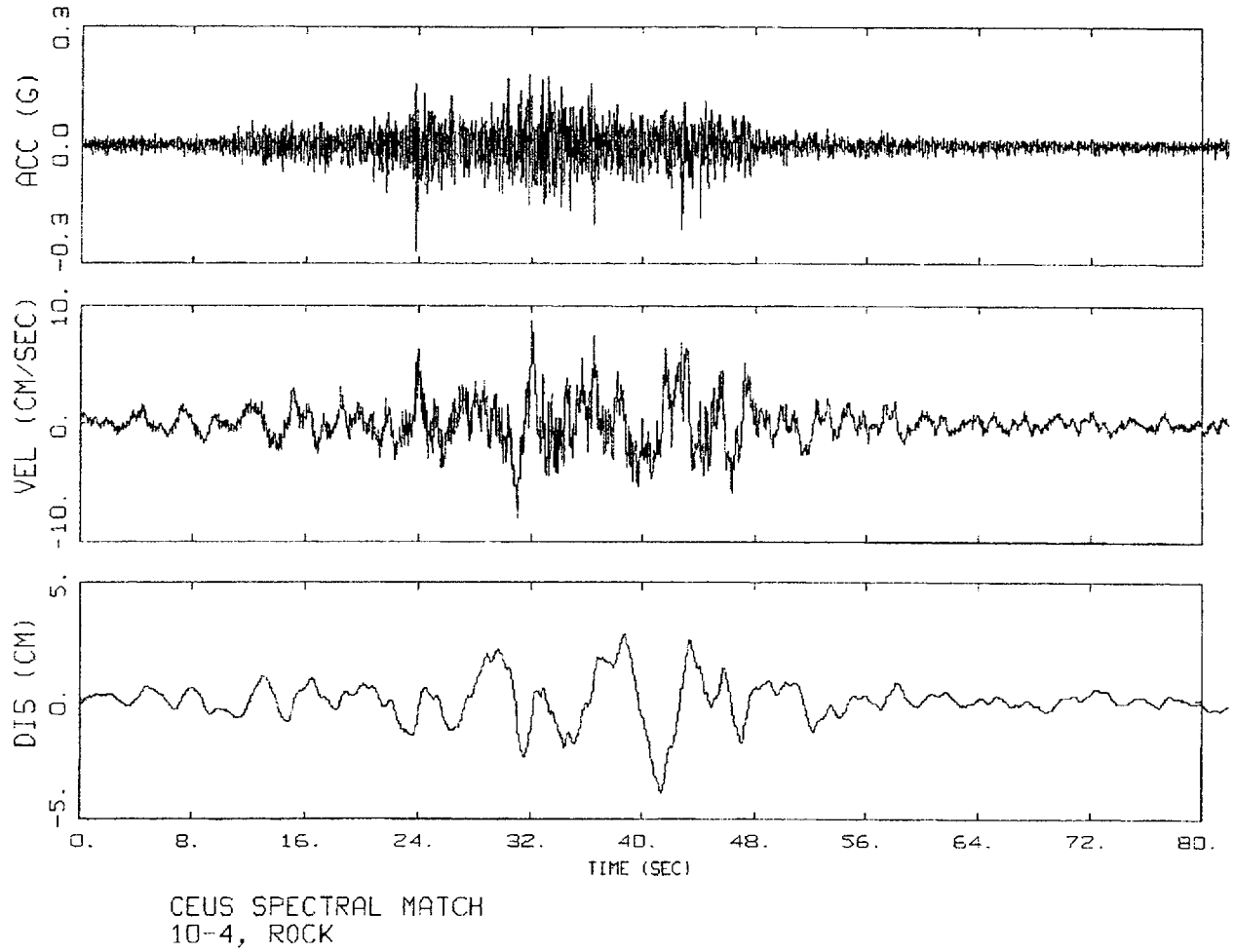

Figure 3-15. Acceleration, velocity, and displacement time histories resulting from match of WUS record to CEUS target, sample interval of 0.02 sec.

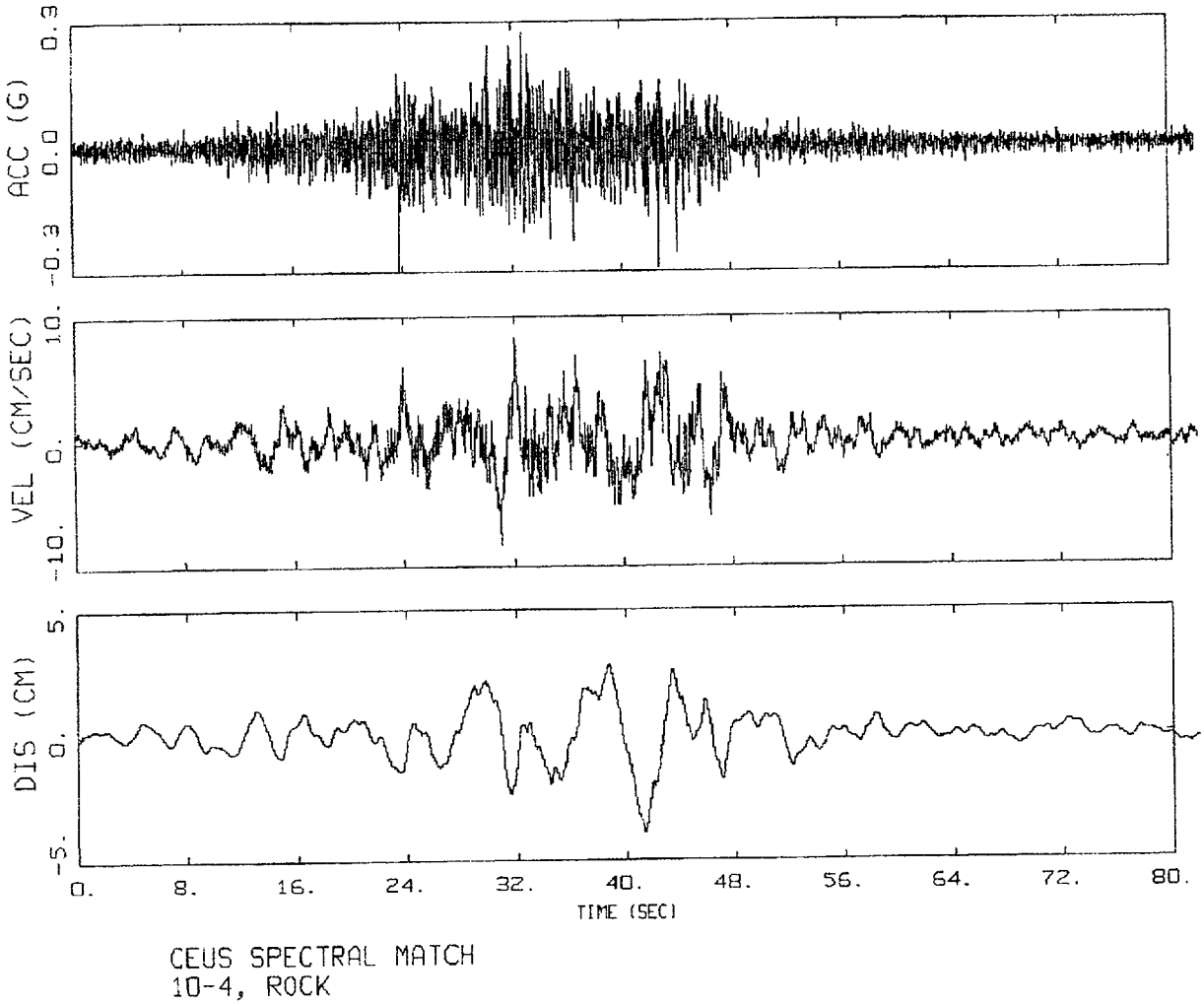

Figure 3-16. Acceleration, velocity, and displacement time histories resulting from match of WUS record to CEUS target, sample interval of 0.005 sec.

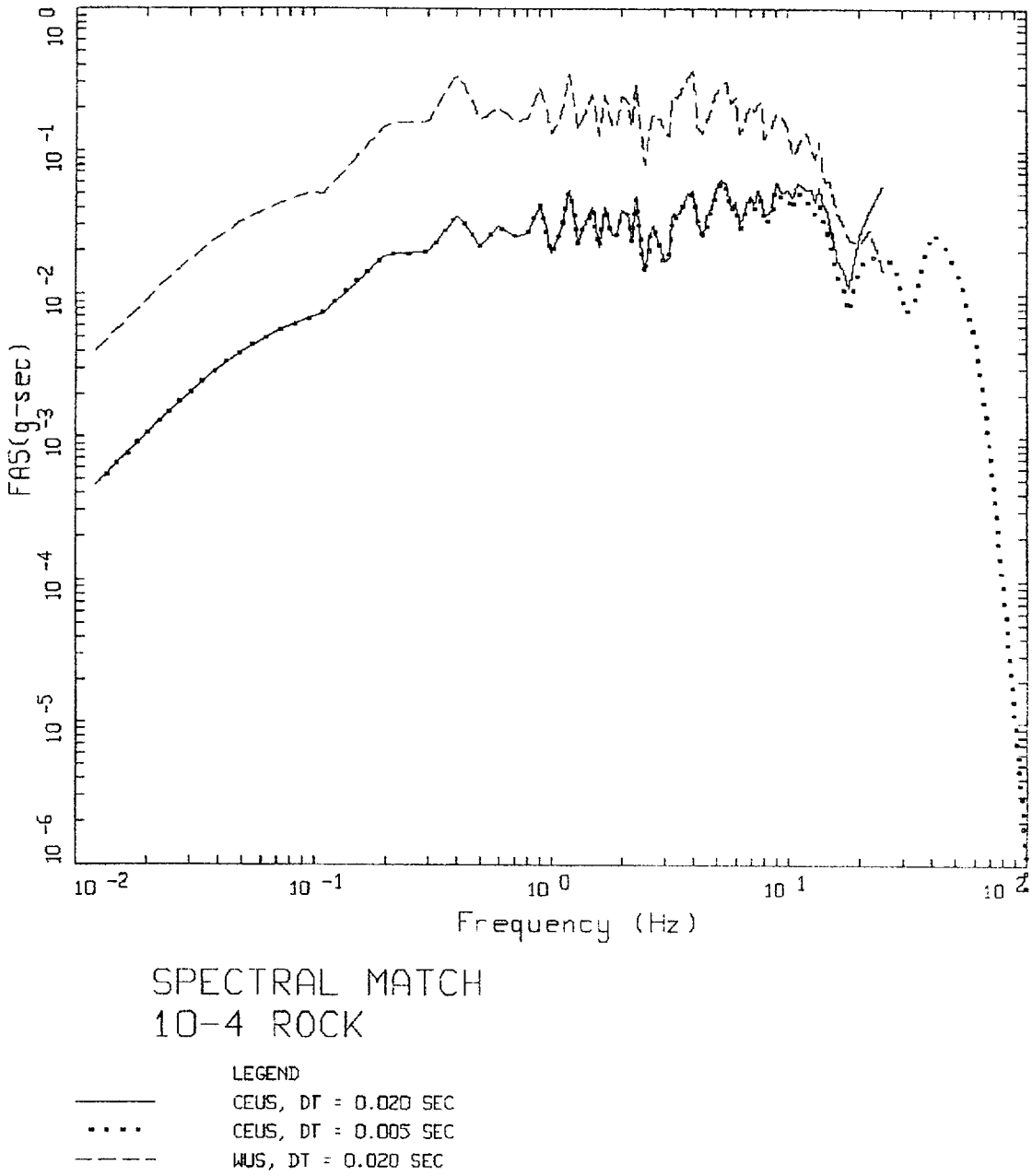

Figure 3-17. Fourier amplitude spectra resulting from fitting WUS record to WUS and CEUS targets (Figure 3-4). Fit to CEUS target used two sample intervals, 0.02 sec and 0.005 sec.

4 DEVELOPMENT OF DESIGN RESPONSE SPECTRAL SHAPES

In this section we document the recommended spectral shapes for both WUS (soft rock) and CEUS (hard rock) for 5% of critical damping. Recommendations for other damping levels are discussed in Section 4.8. For crustal earthquakes, the shapes are valid for moment magnitudes ranging from **M** 4 to **M** 8. For applications to subduction zone events (i.e. the Cascadia subduction zone) the shapes are valid up to **M** 9. The possible effects of mechanism and near-source conditions on the base shapes are discussed in Section 4.6.

In developing spectral shapes, three issues of particular significance arise: (1) selection of an appropriate normalization frequency and fractile level, (2) the paucity of data in the CEUS for **M** > 4.5, and (3) the likelihood that CEUS earthquake source processes for magnitudes larger than about **M** 6 produce significantly less intermediate frequency energy than corresponding WUS source processes (see Section 2 and Appendix D).

The first issue, selection of an appropriate normalization frequency and fractile level, is complicated somewhat by the desirability of having the fractile level uniform across frequency. This uniformity is highly desirable, as it is implicit in maintaining risk consistency (Section 7) or a constant level of conservatism in design analyses. Unfortunately, strong ground motions in the WUS (the tectonic regime with the most complete database in terms of magnitude and distance ranges) are characterized by a frequency-dependent, as well as magnitude-dependent, variability. Regression analyses on WUS strong ground motion data generally show empirical scatter (variation about the median) that decreases with increasing frequency (Abrahamson and Shedlock, 1997). This variability also decreases with increasing magnitude (Youngs et al., 1995) or ground motion amplitude (Campbell, 1993), particularly for **M** $\geq$ 6. These statistical properties are likely real and stable, not reflecting spurious trends due to a sparse sample size. They are probably related to fundamental physics of earthquake source, path, and site processes and can reasonably be expected to occur in the CEUS as well as the WUS.

The second issue relevant to developing response spectral shapes for the CEUS, the paucity of strong motion data, precludes a purely statistical approach to developing shapes. The direct effect of a small sample size is the necessity of using physical models, resulting in a significantly higher uncertainty in the shapes for applications to CEUS sites.

The third issue is driven largely by the lack of CEUS data for **M** $\geq$ 6 and contributes substantially to the larger uncertainty in CEUS shapes: the possibility that source processes in tectonically stable regions emit less intermediate frequency energy than corresponding sources in active regions (WUS). This difference in spectral content manifests itself seismologically in a second corner frequency (Section 2), which results in response spectral shapes that contain a well- developed spectral sag in a frequency range (near 1 Hz) that varies with magnitude. WUS sources do not show such a well-developed spectral sag, and it is not reflected in empirical attenuation relations. Recent studies, however, suggest that the sag may be present in a much more subtle form, being obscured (filled in) by amplification due to generally softer crustal rocks in the WUS as compared to CEUS crustal conditions. Theoretically this is appealing, suggesting an intrinsic commonality between WUS and CEUS source processes, although there is no compelling argument to prove this should be the case.

The possibility of commonality does not increase our confidence (lower the level of uncertainty) in CEUS shapes because the current state of knowledge does not reflect a high level of confidence in the physical process that produces a stable and predictable spectral sag for large magnitude ($M > 6$) earthquakes. As a result, until more CEUS data become available for $M > 6$ earthquakes, some uncertainty will exist as to the appropriateness and degree of sag in CEUS spectral shapes. The perspective taken in developing shapes for the CEUS is not to attempt resolution of this issue, but to produce spectral shapes using models that reflect both possibilities, i.e., with and without an intermediate-frequency spectral sag.

4.1 Approach

The overall approach taken to define response spectral shapes applicable to WUS and CEUS conditions is to rely as much as possible on recorded strong ground motions. These motions are supplemented, where necessary, by ground motion estimates from well-validated theoretical models. This approach will result both in confidence in the use of the spectral shapes as well as reasonable stability over time because the theoretical estimates will provide a guide where data are sparse, and will avoid fluctuations in empirical approaches caused by many data from one event.

To develop shapes appropriate for the WUS that incorporate magnitude and distance scaling, a suite of empirical attenuation relations were used and their estimates were averaged for a set of magnitude and distance bins. The empirical relations were weighted based on a goodness of fit evaluation (Section 4.4) with statistical shapes (Kimball, 1983). The statistical shapes are computed for the magnitude and distance bins from recorded motions listed in the strong motion catalog (Appendix A). The use of empirical relations rather than the statistical shapes directly (Mohraz et al., 1972; Newmark et al., 1973) provided a formalism for sampling expert opinion in smoothing, interpolation, and extrapolation within the poorly sampled bins and oscillator frequencies. Incorporating a robust weighting scheme based on how well each relation fits statistical shapes reduced bias in the selection of the empirical relations.

The spectral shapes from the weighted empirical relations were then fit to a functional form with magnitude and fault distance as independent variables. This process resulted in an attenuation relation for smooth WUS shapes that was largely driven by recordings and that incorporated the knowledge of a number of researchers of strong ground motions. The approach of producing an attenuation relation for shapes has the advantage of simplicity as well, being a continuous function of magnitude, distance, and frequency (Section 4.4).

For applications to the CEUS, insufficient data preclude a similar empirical approach, necessitating consideration of physical models. In general, reliance on model predictions for regions of sparse data results in increased uncertainty in the shapes. For the CEUS, this is further complicated by observations that strongly suggest the possibility that the spectral content in the intermediate frequency range for large magnitude CEUS sources is significantly different (lower) than corresponding WUS sources (Section 2). Because this issue is currently unresolved, consideration must be given to multiple CEUS spectral models.

To minimize the dependence on models in developing CEUS spectral shapes, we used model predictions in the form of ratios to produce transfer functions. The transfer functions, which are ratios of CEUS model shapes to WUS model shapes, were then applied to the empirical WUS shapes to produce shapes appropriate for CEUS conditions. We then fit an attenuation relation for the CEUS spectral shape.

The use of ratios of model predictions rather then model results directly minimizes the impact of potential model deficiencies. Another advantage of this approach is the emphasis placed on model validations for both WUS and CEUS conditions (Section 4.3).

4.2 WUS Statistical Spectral Shapes

Statistical response spectral shapes (Kimball, 1983) were developed for a suite of magnitude and distance bins by sampling the WUS strong motion data base (Appendix A). Shapes for 5% of critical damping were developed by normalizing each response spectrum by the spectral ordinate at the selected frequency and then averaging the scaled records within each bin. A lognormal distribution was assumed. The resulting suites of normalized spectra provided a basis for choosing the best normalization frequency and fractile level. This choice is illustrated in Section 4.2.2 below.

4.2.1 Magnitude and Distance Bins for WUS Spectral Shapes

Implicit in the selection of appropriate magnitude (**M**) and distance (fault distance, R) bins is the classic tradeoff of resolution and stability. In this context, resolution refers to the ability to clearly distinguish **M** and R dependencies in the spectral shapes (which is enhanced by more bins) while stability relates to low variability or statistical stability (which is enhanced by fewer bins, and more data in each bin). In terms of spectral shapes, high stability also results in the desirable feature of smoothness, or less variability from frequency to frequency.

The selection of bin widths and boundaries, in addition to achieving an acceptable compromise between resolution and stability based upon the distribution (in **M** and R) of data, was also conditioned by knowledge of shape sensitivity to **M** and R. In general, the distance dependency for WUS spectral shapes is small (less than about 30%) within about 30 to 50 km from the source. For CEUS spectral shapes the corresponding distance is about 50 to 100 km (Silva and Green, 1989). On the other hand, near-source effects are particularly strong for fault distances within about 10 to 15 km, particularly for vertical strike-slip mechanisms (Somerville et al., 1997). Additionally, seismic hazard is generally dominated by sources within about 100 km for WUS (about 200 km for Cascadia subduction zone sources), and within about 300 km for CEUS sources. For response spectral shapes, beyond about 50 km for WUS and 70 to 100 for CEUS, a factor of 2 change in distance results in about a 30% (factor of 1.3) change in spectral shape (Silva, 1991). With these considerations, distance bins of 0 to 10, 10 to 50, 50 to 100, 100 to 200 km for both WUS and CEUS shapes were considered appropriate with an additional bin of 200 to 400 km for CEUS shapes.

Magnitudes of about 5 to about 8 dominate the hazard for both the WUS and CEUS (except for sites affected by the Cascadia subduction zone sources). While a half magnitude change in **M** results in a 30 to 50% change in PGA normalized shapes (Silva and Green, 1989; Silva, 1991) depending upon

M and frequency, half **M** bins are too sparse at the larger **M** (**M** > 6.5). As a result, unit magnitude wide bins were selected centered on half magnitudes: **M** 5.5, 6.5, and 7.5 with ranges of 5 to 6, 6.01 to 7, and 7.01 and larger. Table 4-1 shows the bins along with summary statistics. For completeness, statistics for soil sites (Geomatrix classifications C and D, Appendix A) were included, in addition to a 0 to 50 km distance bin.

4.2.2 Development of WUS Statistical Spectral Shapes

The first issue to resolve in developing the set of shapes for applications to WUS and CEUS conditions was the appropriate normalization frequency and fractile level. To approach this issue, median bin shapes were computed for a suite of normalization frequencies to determine the degree of similarity between the shapes. Figure 4.1 shows an example for the **M** 6.5 and D = 10 to 50 km bin for normalization frequencies of 0.5, 1.0, 5.0, 10.0, 20.0, 34.0, and 100.0 Hz (the last value being equivalent to PGA). The shapes were computed down to frequencies that were 125% (factor of 1.25) of processing corner frequencies (Appendix A). This resulted in an increase in variability at lower frequencies as records dropped out due to noise contamination. For all seven normalization frequencies, the shapes were quite similar, and scaling each shape to unity at 100 Hz (PGA) presented a more convenient display (Figure 4.2). Similar results were obtained for the other bins suggesting a convenient resolution to the issue of selecting an appropriate normalization frequency. Since peak ground acceleration has the lowest variability among response spectral ordinates in the frequency range of 100.0 to 0.2 Hz (Abrahamson and Silva, 1997; Campbell, 1997, Boore et al., 1997; Sadigh et al., 1997), it is an attractive as well as conventional normalization parameter (Seed et al., 1976). Similar results would be obtained if normalization were done using spectral acceleration at any other frequency.

The selection of an appropriate fractile level for spectral shapes must consider the manner in which the shapes are to be used (Section 1). Current regulatory guidance (R.G. 1.165) recommends probabilistic seismic hazard evaluations for rock outcrop (or its equivalent), with coupling to deterministic evaluations using deaggregation of the uniform hazard spectrum (UHS), the deaggregation being done at several frequencies. Deterministic spectra are then scaled to the UHS at the deaggregation frequencies as a check on the suitability of the UHS and to provide control motions for site response evaluations. The deterministic spectra may be computed from the attenuation relations used in the UHS or may be based on the recommended spectral shapes. Additionally, the recommended spectral shapes may be used to evaluate existing design motions at the rock outcrop level. As a result, the development of median shapes is most consistent with intended uses, particularly in the context of UHS, where the desired hazard is appropriately set at the UHS exceedence level.

The bin statistical shapes (median $\pm$ 1 sigma) normalized by peak ground acceleration are shown in Figures 4.3 to 4.5 for rock and Figures 4.6 to 4.8 for soil.

4.3 Ground Motion Model for Spectral Shapes

The most desirable feature in a ground motion model for spectral ordinates is the ability to reliably and accurately capture magnitude, distance, and site dependencies with a minimum of parameters.

A necessary aspect of any ground motion model implemented in engineering design practice is a thorough validation with recorded motions. Since all models are mathematical approximations to complicated physical processes, rigorous validation exercises are necessary to assess model accuracy, reveal strengths and shortcomings, and constrain parameter values and their uncertainties (Roblee et al., 1996). Ideally, a ground motion model will be validated over the ranges of magnitudes, distances, site conditions, and tectonic environments for which it is implemented. In this sense, the model is more an interpolative tool that can be used with a confidence level reflected in quantified validation exercises (Abrahamson et al., 1990; EPRI, 1993; Silva et al., 1997). While this is becoming possible for WUS tectonic conditions, it is clearly not the case for the CEUS (Section 2). Because of the paucity of recording in CEUS conditions, thorough validation exercises to assess model accuracy and parameter distributions are not possible. This situation necessarily results in significantly higher uncertainty, which can be assessed only in a qualitative manner (Appendix D).

4.3.1 Point-Source Model

Since response spectral shapes are intended to reflect average horizontal motions at sites distributed at the same fault distance from the source, the effects of source finiteness are expected to be minimal (Silva and Darragh, 1995). The effects of rupture directivity and source mechanism on spectral shapes (Section 4.6) increase the variability associated with spectral shapes at close distances ($R \leq$ 15 km) and at low frequency ($\leq$ 1 Hz) but have little effect on the *average* shape. As a result, a point-source model with its attractive simplicity is appropriate. The stochastic point-source model, in the context of strong ground motion simulation, was originally developed by Hanks and McGuire (1981) and refined by Boore (1983; 1986). It has been validated in a comprehensive manner with 18 earthquakes at about 500 sites (Silva et al., 1997) and is described in detail in Appendix D. Table 4-2 lists the parameters used to develop the spectral shapes and transfer functions.

For applications to the CEUS, a single significant set of observations may fundamentally increase uncertainty in model predictions of spectral shapes. This phenomenon was illustrated with ground motions generated by the 1988 **M** 5.8 Saguenay, Ontario earthquake. Even prior to this earthquake, high frequency (> 5 Hz) motions at hard rock CEUS sites were known to be significantly greater than motions recorded on typical WUS soft rock conditions (Section 2). A number of small earthquake (**M** $\leq$ 5) CEUS data showed this increase in high-frequency content, and less damping in the shallow crust (1 to 2 km) of the CEUS was considered the likely cause for the difference (Silva and Darragh, 1995). This difference was observed for the Saguenay earthquake as well as the **M** 6.4 1985 Nahanni aftershock earthquakes. However, the Saguenay earthquake also showed anomalously low intermediate- frequency (0.5 to 2 Hz) energy (Boore and Atkinson, 1992; Atkinson, 1993; Silva and Darragh, 1995). This observation along with others (Choy and Boatwright, 1988; Boatwright and Choy, 1992; Atkinson, 1993; Boatwright, 1994) has led to the speculation that CEUS source processes may possess differences from WUS source processes that result in stable and significant differences in intermediate frequency content for earthquakes with magnitude (**M**) greater than about 5 (Atkinson and Boore, 1995; 1998). Seismologically this spectral sag may be interpreted as the presence of second corner frequency or change in slope of the earthquake source spectrum (Boatwright, 1994; Atkinson and Boore, 1998). Interestingly, recent observations have suggested this may be the case for WUS earthquake source as well (Silva et al., 1997; Atkinson and Silva, 1997), but manifested in a much more subtle effect on response spectra due to differences in crustal

conditions between WUS and CEUS (Appendix C). An example comparison of response spectra computed for **M** 6.5 at a distance of 25 km using both WUS and CEUS single-and double-corner frequency point-source models is shown in Figure 4.9 for shapes and Figure 4.10 for absolute spectral levels. The two single corner frequency shapes for the WUS and CEUS (solid lines) show large differences over the entire frequency range. The WUS shape exceeds the CEUS for frequencies less than about 10 Hz where the shapes cross. The WUS shape peaks near 5 Hz while the CEUS shape has a maximum amplification in the 30 to 50 Hz frequency range. These trends are very similar to the empirical WUS and CEUS rock site spectra shown in Section 2.

Comparing the single- and double-corner frequency spectra for WUS and CEUS, Figure 4.9 shows the spectral sag significantly more pronounced for the CEUS. At low frequencies (below about 1 Hz) the double corner CEUS spectrum is about a factor of 3 lower than the single corner CEUS spectrum. Over the same frequency range, the difference between single and double corner shapes for the WUS is only about 10 to 20%.

Comparing the absolute levels, Figure 4.10 shows that at low frequencies, the single-corner frequency model (solid lines) predicts similar motions for WUS and CEUS conditions. Peak accelerations for CEUS conditions are predicted to be larger than for WUS conditions, reversing the trends between spectral shapes (normalized by peak acceleration) and absolute spectral levels (Silva, 1991).

Though shifted in frequency, the differences between WUS and CEUS rock site shapes are not unlike the differences in the WUS statistical spectra between soft rock and deep soil shown in Figure 4.11. This is consistent with the explanation that CEUS spectral shapes are caused by the hard crustal conditions found there (Appendix C).

4.3.2 Comparison of Model Shapes to WUS Statistical Shapes

To provide a qualitative evaluation of model performance, Figure 4.12 compares model shapes to WUS statistical shapes in the distance range of 10 to 50 km and for magnitudes near 5.5, 6.5, and 7.5. Model shapes for both single and double corner source spectra are shown illustrating the generally small difference between the alternative source models for WUS conditions. In general, the model shapes reflect the statistical shapes very well for the **M** 5.5 and **M** 6.5 bins and over-predict for the **M** 7.5 statistical shape.

The well developed spectral sag in the **M** 7.5 R = 10 to 50 km statistical shape bin is also not matched by the empirical attenuation equations (Figure 4-14c). Since this magnitude bin is sparsely populated (Table 4-1), the statistical shapes may be biased by sampling only a few earthquakes and rock sites. It is intriguing nonetheless that the statistical shapes for **M** greater than 7 at rock sites show evidence of a well-developed second corner frequency source spectrum. The developers of the empirical attenuation relations used here have chosen to ignore this observation (Section 4.4), because of the few data on which it is based.

4.3.3 WUS to CEUS Transfer Functions

Using the point-source model, median spectral shapes were computed for single-corner WUS conditions and both double and single corner CEUS conditions using the parameters listed in Table 4-2. Ratios of the shapes, CEUS/WUS, for a dense grid in magnitude and distance were taken to provide transfer functions to apply to the weighted empirical shapes (Section 4.4). An example suite of the transfer functions is shown in Figure 4-13.

4.4 Design Response Spectra

4.4.1 Western US Spectral Shapes

The approach used to develop spectral shapes for rock site conditions appropriate for the WUS consisted of the following steps:

1. Use a number of empirical strong ground motion attenuation relationships to compute spectral amplification values, the ratio SA/PGA for the magnitude range ($5 \leq \mathbf{M} \leq 8$) and fault distance range ($0.1 \leq R^* \leq 200$ km) of interest.

2. Develop weights to apply to the relationships based on comparisons with a common set of recorded strong motion data.

3. Compute a weighted average of the empirical attenuation relationship spectral shapes for a dense grid of magnitude and distance pairs.

4. Develop a functional form to define spectral amplification over the magnitude and distance range of interest.

Five recently published empirical attenuation relationships were chosen to develop the spectral shapes for the WUS: Abrahamson and Silva (1997), Boore and others (1997), Campbell (1997), Idriss (1991), and Sadigh and others (1997). These relationships are henceforth referred to as A&S 97, Bao 97, C 97, I 91, and Sao 97, respectively. The spectral shapes predicted by these relationships are compared on Figure 4-14 to the statistical spectral shapes developed in Section 4.2. Note that the Bao 97 relationship is limited to $5.5 \leq \mathbf{M} \leq 7.5$ and $R \leq 80$ km and the C 97 relationship is limited to $R \leq 60$ km. The selected attenuation relationships have 14 spectral frequencies in common: 0.2, 0.25, 0.333, 0.5, 0.667, 1.0, 2.0, 3.33, 5.0, 6.67, 10.0, 13.33, 20, and 34 Hz. (Note that C 97 does not contain 0.2 Hz and Bao does not contain 0.2, 0.25, and 0.333 Hz. Also, the Bao 97 spectral accelerations for frequencies between 10 and 40 Hz were calculated here by linear interpolation in log-log space as recommended by D. Boore [personal communication, 1998]). Spectral amplifications were computed for each attenuation relationship by dividing the predicted spectral acceleration at each frequency by the predicted peak ground acceleration.

---

*For each empirical relation the appropriate distance definition is used.

4.4.2 Development of Weighted Empirical Spectral Shapes

The weights to be applied to the spectral shapes defined by the five empirical attenuation relationships were based on the relative ability of the relationships to predict the spectral shapes computed from the strong motion data base described in Section 4.2. To allow for the possibility that the relative prediction ability varies as a function of magnitude and distance, weights were computed for each of the 12 magnitude and distance bins defined in Section 4.2.

We defined the residual $(\varepsilon(f)_{ij})_k$ to be the difference between the log of the spectral amplification for frequency f of the j^{th} recorded motion from the i^{th} earthquake, $(SA(f)/PGA)_{ij}^r$ (the geometric mean of the two horizontal components) and the log of the spectral amplification predicted by the k^{th} attenuation relationship for magnitude $\mathbf{M}_i$ and source-to-site distance R_{ij}.

$$(\varepsilon(f)_{ij})_k = \ln\left[(SA(f)/PGA)_{ij}^r\right] - \ln\left[(SA(f)/PGA)^k\right] \tag{4-1}$$

These residuals are assumed to be normally distributed with a random effects variance structure (e.g. Brillinger and Preisler 1984, 1985; Youngs and others, 1995):

$$(\varepsilon(f)_{ij})_k = \varepsilon_1(f)_i + \varepsilon_2(f)_{ij} \tag{4-2}$$

where $\varepsilon_1(f)_i$ and $\varepsilon_2(f)_{ij}$ are independent, normal variates with variances $\tau_1^2(f)$ and $\tau_2^2(f)$, respectively.

Two approaches were used to assign weights to the five attenuation relationships for each spectral frequency within each magnitude and distance bin. The first approach was based on the relative bias of the relationships. For each frequency in each $\mathbf{M}$ and R bin, the mean residual for the k^{th} attenuation relationship, $(f)_k$, is found by maximizing the generalized normal distribution likelihood function:

$$L(\ (f)_k,\tau_1(f)_k,\tau_2(f)_k) = \frac{\exp\left[-\dfrac{[(\varepsilon(f)_{ij})_k - (f)_k]^T V(f)_k^{-1}[(\varepsilon(f)_{ij})_k - (f)]}{2}\right]}{2\pi|V(f)_k|^{1/2}} \tag{4-3}$$

where $V(f)_k$ is the block-diagonal variance matrix of $(\varepsilon(f)_{ij})_k - (f)_k$. Figure 4-15 shows the mean residuals and their 90% confidence intervals for the five attenuation relationships and 12 magnitude-distance bins.

The t statistic, $t_k = |\ (f)_k|/\sigma[\ (f)_k]$, together with the cumulative T distribution can be used to compute the probability a sample of size n from a population with zero mean would have a mean residual as large as $|\ (f)_k|$, $P(T \le t_k|n\text{-}1)$. If one considers that the relationships with the higher probability of producing the computed t statistic should be given higher weight, then the relative weight for the k^{th} attenuation relationship, $W(f)_k^T$ can be defined as:

$$W(f)_k^T = \frac{P(T \le t(f)_k|n-1)}{\sum_k P(T \le t(f)_k|n-1)} \tag{4-4}$$

These are referred to as "T" weights.

The second weighting approach uses relative likelihoods under the assumption that the mean residual is zero. The likelihood function is given by:

$$L(\ (f)_k=0,\tau_1(f)_k,\tau_2(f)_k) = \frac{\exp\left[-\frac{(\varepsilon(f)_{ij})_k^T V(f)_k^{-1} (\varepsilon(f)_{ij})_k}{2}\right]}{2\pi|V(f)_k|^{1/2}} \quad (4\text{-}5)$$

where $V(f)_k$ is the block-diagonal variance matrix of $(\varepsilon(f)_{ij})_k$. Equation (4-5) gives the probability of observing the sample set of residuals, given that the mean residual is zero. If one considers that the relationships with the higher likelihood should be given higher weight, then the relative weight for the k^{th} attenuation relationship, $W(f)_k^L$ can be defined as:

$$W(f)_k^L = \frac{L(f)_k}{\sum_k L(f)_k} \quad (4\text{-}6)$$

These are referred to as "L" weights.

The top plots in the two columns of Figure 4-16 show examples of the "T" and "L" weights for one of the 12 magnitude-distance bins. The weights display a highly irregular pattern, reflecting the variability in the mean residuals shown on Figure 4-15. The approach to developing the response spectral shapes outlined in Section 4.1 is based on the use of the empirical attenuation relationships to provide smoothly varying estimates of response spectral shapes over a magnitude and distance range that extends beyond the bulk of the recorded data. The use of the highly variable weights shown at the top of Figure 4-16, while providing a close match to the recorded data set, would rapidly switch from strongly favoring one attenuation relationship to favoring another over short frequency intervals, and thus tend to defeat the purpose of using the smooth empirical attenuation relationship spectra. In addition, limitations in the band-width of the processed data for the smaller recordings results in no weight estimates for some frequencies. These two issues were addressed by smoothing the weights across frequency with a Gaussian smoothing operator. The smoothed weights are defined by:

$$W(f_i)_k^* = \frac{\sum_{j=1}^{J} W(f_j)_k \cdot \exp(-\ln(f_j/f_i)^2/h^2)}{\sum_{j=1}^{J} \exp(-\ln(f_j/f_i)^2/h^2)} \quad (4\text{-}7)$$

where f_j, $j = 1$ to J are the 14 common spectral frequencies defined above and h determines the width of the smoothing operator. Larger values of h produce greater smoothing. The remaining plots on Figure 4-16 show smoothed weights for values of h of 0.25, 0.5, and 1.0.

Figure 4-17 shows examples of the weighted average empirical spectral shapes computed for the average magnitude and distance of two of the magnitude-distance bins using smoothed "L" and "T" weights. As indicated on the plot, variations in h have a very minor effect on the computed spectral shapes. Also, the "L" an "T" weights produce very similar spectral shapes. Therefore, the smoothed "L" and "T" weights were averaged to produce the final set of weights. A smoothing parameter of $h = 1.0$ was chosen for the final weights to produce a smoothly varying final set of weights. These are shown on Figure 4-18. Figure 4-19 shows examples of the weighted empirical response spectral shapes for magnitude of **M** 5 to 8 and distances of 1 to 200 km.

4.4.3 Magnitude and Distance Dependencies of Weighted Empirical Spectral Shapes

The response spectral shapes shown on Figure 4-19 vary with magnitude and distance. In order to provide relationships for specifying a response spectral shape for any magnitude and distance within the specified range of the attenuation relationships, a function form was fit to the weighted empirical spectral shapes. Figure 4-20 shows the statistical spectra for magnitude **M** 6 to 7 and R 10 to 50 km data. This spectral shape can be closely matched by the ad hoc relationship:

$$\ln[SA(f)/PGA] = \frac{C_1}{\cosh(C_2 f^{C_3})} + C_4 \left[\frac{\exp(C_5 f)}{f^{C_6}} \right] \qquad (4\text{-}8)$$

The form of Equation (4-8) is not based on a physical model, but is rather designed to fit the general characteristics of the spectral shapes. The first term fits the high frequency portion of the spectrum, decreasing exponentially to zero with increasing frequency. The second term models the low frequency portion of the spectrum. The factor $\exp(C_5 f)$ controls the transition of control from the low frequency to high frequency terms.

Coefficients C_1 through C_6 were defined as functions of magnitude and/or distance by creating a data set of 651 response spectral shapes (31 magnitudes times 21 distances) at 0.1 magnitude units from **M**5 to **M**8 and at fault distances (R) of 0.1, 1, 2, 3, 5, 10, 12, 15, 20, 25, 30, 40, 50, 60, 70, 85, 100, 125, 150, 175, and 200 km. Each response spectral shape contained spectral amplifications at the 14 frequencies common to the five empirical attenuation relationships. In addition, fitting time histories to the response spectral shapes requires specification of the spectral amplifications in the frequency range of 0.1 to 100 Hz. The solid diamonds shown on Figure 4-20 indicate the spectral amplifications predicted by an extrapolation of Equation (4-8), which was fit to the frequency range of 0.2 to 34 Hz. As indicated, the functional form provides a good fit in the extrapolated range both for $f > 34$ Hz and $f < 0.2$ Hz. The poorest fit is at 0.1 Hz, where the statistical spectra are becoming somewhat biased due to the exclusion of records with limited band-widths. The 651 weighted empirical spectral shapes were extended from the frequency range of 0.2 to 34 Hz to the frequency range of 0.1 to 100 Hz by fitting Equation (4-8) to each spectral shape and then using the parameters of that fit to predict spectral amplifications in the frequency range of 0.1 to 0.2 Hz and 34 to 100 Hz.

The entire extended data set was then used to obtain expressions for coefficients C_1 through C_6 by nonlinear least squares. The best fit was found by the parameter set listed in Table 4-3. Figure 4-21 shows examples of the response spectral shapes predicted using these relationships.

4.4.4 Model for Central and Eastern US Spectral Shapes

The approach used to develop spectral shapes for rock site conditions appropriate for the CEUS consisted of the following steps:

1. Use numerical modeling to develop scaling relationships between CEUS and WUS response spectral shapes.

2. Use the scaling relationships from step 1 to convert the weighted empirical WUS spectral shapes to CEUS spectral shapes.

3. Develop a functional form to define spectral amplification over the magnitude and distance range of interest.

These steps are discussed in the following subsections.

4.4.4.1 Scaling of WUS Weighted Empirical Spectral Shapes to CEUS Conditions

The scaling relationships for transferring WUS spectral shapes to CEUS spectral shapes are described in Section 4.3 and are shown on Figure 4-13. These scaling relationships were used to scale the extended (0.1 to 100 Hz) weighted empirical WUS response spectral shapes to produce CEUS spectral shapes. As discussed in Section 4.3, two sets of scaling relationships were defined, one based on single corner frequency CEUS earthquake source spectra and one based on double corner frequency CEUS earthquake source spectra. Both scaling relationships assume a single corner frequency WUS earthquake source spectra. Figure 4-22 shows examples of the CEUS response spectral shapes scaled from the weighted empirical WUS spectral shapes using the scaling relationships shown on Figure 4-13.

One problem that was encountered was an inconsistency or flat portion in CEUS spectral shapes around 10 Hz. Close comparison of the model and attenuation-based WUS spectral shapes indicated that the model shapes showed slightly higher spectral amplifications than the attenuation-based spectra around 10 Hz. This over-prediction or bias of WUS model spectral shapes caused an under-prediction of the CEUS/ WUS transfer function. As a result, the transfer function was slightly increased around 10 Hz. Figure 4-23 shows examples of the scaled (before adjustment) and adjusted spectral amplifications, for both the single- and double-corner CEUS spectral models.

4.4.4.2 Modeling the Effect of Magnitude and Distance on CEUS Spectral Shapes

Using the same approach as for WUS response spectral shapes, a functional form was fit to the scaled and adjusted empirical spectral shapes. A modified form of Equation (4-8) was used to model the CEUS shapes. The relationship is:

$$\ln[SA(f)/PGA] = \frac{C_1}{\cosh(C_2 f^{C_3})} + C_4 \left[\frac{\exp(C_5 f)}{f^{C_6}} + \frac{C_7 \exp(C_8 f)}{f^{C_9}} \right]^{1/2} \qquad (4\text{-}9)$$

A second term was added to the low-frequency portion of the model to provide more flexibility in the shape. Coefficients C_1 through C_9 were defined as functions of magnitude and/or distance using the data set of 651 CEUS response spectral shapes (31 magnitude values times 21 distances) by nonlinear least squares with the spectral amplifications in the frequency range of the adjustment down weighted to reduce their influence on the fitted parameters.

For the single and double corner frequency CEUS earthquake spectra, the resulting coefficients are listed in Table 4-3. Figures 4-24 and 4-25 shows examples of the response spectral shapes predicted using these relationships.

4.5 Comparison of Recommended Shapes to Current Regulatory Guidance

In this section we compare Newmark and Hall (1978) and Regulatory Guide 1.60 (1973) design spectra to both WUS and CEUS recommended design spectra for the most populated distance bin (0 to 50 km) and mean magnitudes of **M** 5.6, **M** 6.4, and **M** 7.3 (Table 4-1). Figure 4-26 shows comparisons to WUS recommended shapes and Figure 4-27 shows analogous comparisons to CEUS shapes. For Newmark and Hall design shapes, WUS bin median values for peak accelerations, velocities, and displacements are used for both WUS and CEUS conditions. Both median and 1-sigma amplification factors are used for the Newmark and Hall design spectra.

For the WUS motions, Figure 4-26 shows a reasonably good comparison between the Newmark and Hall spectra and the recommended shapes. The empirical PGV/PGA ratio is about 60 cm/sec/g for **M** 6.3 and 7.3. Increasing this ratio to the value recommended by Newmark and Hall (1978) of about 90 cm/sec/g would increase the low frequency levels but result in peak velocities not supported by the data. The dependence of the Newmark and Hall design shapes on peak parameters captures some of the effects of the empirical magnitude dependency and would presumably capture elements of the distance dependency as well. Conversely, the fixed R.G. 1.60 shape is quite conservative even for **M** 7.3, since it was based on **M**≅ 6.7, used a mixture of rock and soil data, and was derived with 1-sigma amplification factors (Figure 4-26).

For the CEUS, Figure 4-27 shows a similar suite of plots but with recommended shapes for both the single- and double-corner CEUS source models. The Newmark-Hall design shapes use the WUS bin parameters because comparable empirical CEUS data are not available. The expected peak accelerations for CEUS rock motions are larger than corresponding WUS rock motions, so the CEUS shapes (SA/PGA) appear to be lower than WUS shapes at low frequencies. In absolute levels however, single corner WUS and CEUS spectra have comparable spectral levels for frequencies below about 3 Hz (see Figure 4-10). Normalizing at around 1 to 5 Hz would be more indicative of absolute levels and would result in similar comparisons with WUS shapes (Figure 4-26) at frequencies $\leq$ 5 Hz while showing a larger difference between the R.G. 1.60 and recommended shapes at high frequencies (as illustrated in Figure 4-10).

4.6 Effects of Source Mechanism and Near-Fault Conditions on Response Spectral Shapes

Since both the WUS and CEUS shapes are intended to reflect an average horizontal component for a random source mechanism located at a fixed rupture distance (but at a random azimuth with respect

to a rupture surface), it is important to assess the effects implied by these limitations. Both source mechanism (reverse, oblique, strike-slip, normal) as well as hanging-wall vs. foot-wall site location for dipping faults have frequency-dependent effects (Abrahamson and Shedlock, 1997). Additionally, for potential sites located in the NW Pacific region of WUS, the tectonic environment may include the contribution of large (**M** 9) subduction zone earthquakes. Such sources may dominate the low frequency portion of the UHS requiring appropriate shapes for scaling.

For large magnitude (**M** $\geq$ 6.5) earthquakes, rupture directivity affects both low frequency spectral levels ($\leq$ 1 Hz) and time domain characteristics. Rupture towards a site enhances average spectral levels and reduces durations, while rupture away from a site reduces motions and increases durations, all of these changes being relative to average conditions (Somerville et al., 1997; Boatwright and Seekins, 1997). Differences in fault normal and fault parallel motions are also affected by rupture directivity and can be large at low frequencies (Somerville et al., 1997). Design decisions on whether to incorporate component differences in spectral levels and time domain characteristics should be made on a site-specific basis with consideration of uncertainties and the implications for analyses. Fault normal and fault parallel motions may not define principal directions for design purposes and these implications must be considered in two-dimensional analyses.

These source mechanism and near-fault issues become relevant when a high degree of certainty exists in the nature of the controlling sources as well as the source-site geometry. In calculating the hazard levels for a site, it is assumed that the appropriate degree of seismotectonic knowledge as well as epistemic uncertainty is incorporated in the attenuation relations used in the probabilistic hazard analysis. The UHS levels will then reflect appropriate contributions of source mechanism and site location. The recommended spectral shapes developed here, which are appropriate for average conditions, are scaled to the UHS at selected frequencies and do not reflect either conservatism or unconservatism in the frequency dependence of spectral levels based on source mechanism and site location.

4.6.1 Effects of Source Mechanism

Assessment of the effects of source mechanism, which is taken to include hanging wall vs. foot wall effects, relies on WUS empirical motions and is strictly appropriate for those conditions. Of the five empirical attenuation relations considered in the development of the WUS shapes (Section 4.4.1), two include frequency-dependent source mechanism effects (Abrahamson & Silva, 1997; Boore et al., 1997) and only one includes frequency-dependent hanging wall vs. foot wall effects (Abrahamson & Silva, 1997). To illustrate possible source mechanism effects on the revised WUS shapes, Figure 4-28 shows spectral shapes computed for the two relations for **M** 5.5 and **M** 6.5 earthquakes at a distance of 25 km. When normalizing by peak acceleration, the maximum effect of source mechanism is at low frequency (0.2 Hz) and shows a maximum expected range of about 50%. The shape for the strike-slip mechanism, the base case for the recommended shapes, is highest for frequencies below about 1 Hz, while normal faulting shapes are expected to be slightly higher than strike slip shapes for frequencies in the range of about 1 to 5 Hz. Since the normal faulting shape exceeds the strike-slip shape by less than 10%, use of the recommended shapes for normal faulting conditions is not considered to significantly underestimate design motions.

However, for large magnitude (**M** ≥ 6.4) earthquakes occurring on reverse faults, Figure 4-28 shows that the expected shape is lower than the strike-slip shape by about 10% in the 1 to 2 Hz frequency range. Scaling the reverse mechanism shape to a UHS in the 1 to 2 Hz range could then result in larger predicted motions for frequencies above the scaling frequency than scaling the recommended spectral shape. For sites controlled by reverse mechanism sources, care should be taken in evaluating the development of the low frequency design motions for frequencies in the range of the low frequency scaling frequency to the crossover frequency for the next deaggregation frequency (Section 5.5).

To examine the expected effects of site location for dipping faults, Figure 4-29 compares shapes computed for strike-slip mechanism to shapes computed for a dipping fault for both hanging-wall and foot-wall site locations. These site dependencies are strongest in the fault distance range of 8 to 18 km and are based on Somerville and Abrahamson (1995) and included in the Abrahamson and Silva, 1997 relationship. The Boore et al., 1997 relation includes an **M**, *R*, and frequency-independent hanging wall vs. foot wall effect implicitly in its distance definition. As a result their shapes are largely site location (hanging wall vs. foot wall) independent.

The hanging-wall vs. foot-wall frequency dependencies illustrated as amplification factors in Figure 4-29 are actually strongest for large magnitude (M ≥ 6.5) and at high frequency (PGA) and represent a maximum factor of about 1.4 for the horizontal component and about 1.9 for the vertical component (ratio of hanging-wall to "not-hanging-wall" PGA values). Since the hanging- wall shape is lower than the strike-slip shape (the basis mechanism for the recommended spectral shapes) by about 10% in the 1 to 2 Hz frequency range, scaling the hanging-wall shape instead of the strike-slip shape to the UHS in the 1 to 2 Hz frequency range will result in higher spectral levels for frequencies above the scaling frequency. Modifications to the recommended spectral shapes should be made on a site-specific basis, using all relevant records applicable to the site and the fault generating the hazard.

4.6.2 Subduction Zone Spectral Shapes

The possible occurrence of Cascadia subduction zone earthquakes with magnitudes up to **M** 9.0 can be significant contributors to the low frequency UHS for sites located in the Pacific Northwest (including Northern California), particularly near the Pacific coast. As a result, comparisons of empirical (Youngs et al., 1997) **M** 9.0 shapes at a suite of distances were made to the recommended shape for **M** 8.0 (the largest magnitude for which the empirical WUS relations are considered valid). The recommended shape is computed for a distance of 25 km since the dependence on distance is small within about 50 km. The comparisons are shown in Figure 4-30. Interestingly, for the same peak accelerations, the crustal earthquakes for **M** 8.0 are expected to have larger low frequency (≤ 2 Hz) motions than **M** 9.0 subduction zone earthquakes. The maximum difference in the 1 to 2 Hz range is about 10% and would be larger for smaller magnitude Cascadia sources. As with the source mechanism comparisons, if large magnitude (**M** > 8) subduction zone earthquakes contribute substantially to the low frequency hazard, appropriate spectral shapes should be developed on a site-specific basis.

4.7 Vertical Motions

Current regulatory guidance for vertical (V) ground motions specifies spectral levels that are equal to the horizontal (H) at frequencies > 3.5 Hz and that are 2/3 the horizontal for frequencies < 0.25 Hz, with the ratio varying between 1 and 2/3 between 3.5 Hz and 0.25 Hz (R.G. 1.60). As with the horizontal spectral shape, the implied V/H ratio is independent of magnitude, distance, and site condition and is shown in Figure 4-31. For the Newmark-Hall design motions, the V/H ratio is taken as independent of frequency as well as magnitude, distance, and site condition, having a constant value of 2/3 (Figure 4-31). With the dramatic increase in strong motion data since the development of these design specifications in the 1970's, the conclusion that the vertical and average horizontal ground motions vary in stable and predictable ways with magnitude, distance, and site condition has become increasingly compelling. In general, vertical motions exceed horizontal (average of both component) motions at high frequency and at close fault distances (within about 10 to 15 km). The amount and frequency range of the exceedence depends on magnitude, distance, and site conditions. For different site conditions, time domain characteristics of vertical motions can be quite different at close distances and may be a consideration in selecting input motions for spectral matching or scaling procedures. Appendix K illustrates the expected differences in vertical and horizontal motions based on magnitude, distance, and site conditions and forms a background for the procedures recommended to develop vertical component spectra that are consistent with the WUS and CEUS revised rock horizontal component shapes.

Because structures, systems, and components have limited capacities for dynamic vertical demands, it is important to accommodate stable and predictable differences in vertical loads based on significant contributors (**M** and R) to the seismic hazard at a site. Since there are fewer attenuation relations for vertical motions in the WUS and currently none available for the CEUS, the general approach to developing vertical component design spectra is to use a frequency- dependent V/H ratio. It is difficult to capture the appropriate degree of uncertainty in the V/H ratio as well as the corresponding hazard level of the vertical component design spectrum after scaling the horizontal UHS spectrum by the V/H ratio. Thus, the usual assumption is that the derived vertical motions reflect a hazard level consistent with the horizontal UHS. To maintain consistency with the horizontal median shapes developed earlier in this Section, median V/H ratios are developed.

4.7.1 V/H Ratios for WUS Rock Site Conditions

Of the five empirical WUS attenuation relations used in developing the horizontal spectral shapes (Section 4.4.1), three include vertical motions: Abrahamson and Silva, 1997; Campbell, 1997; and Sadigh et al., 1997 (verticals from Sadigh et al., 1993). To develop V/H ratios for WUS rock site conditions, median V/median H ratios for strike slip mechanisms were produced for each relation and averaged assuming equal weights. The resulting V/H dependencies on magnitude and distance are illustrated in Figures 4-32 and 4-33. Figure 4-32 shows expected ratios for **M** 5.5, **M** 6.5, and **M** 7.5 earthquakes for a suite of distances ranging from 1 to 50 km. The ratios are magnitude-dependent, decreasing with decreasing magnitude and with the sensitivity to magnitude decreasing with increasing distance.

These effects are likely driven by the differences in magnitude scaling (change in spectral levels with magnitude) between the horizontal and vertical components. The dependence of the V/H ratios on magnitude decreases with distance (Figure 4-32) as the difference in magnitude scaling between the vertical and horizontal components decreases.

The effects of source mechanism on the V/H ratios (included only in the Abrahamson and Silva, 1997 relation) is small, with strike slip ratios generally exceeding the ratios for oblique, reverse, and normal faulting mechanisms. For hanging wall sites and for fault distances in the 4 to 24 km range, V/H ratios are higher at high frequencies by a maximum of about 30% for **M** greater than about 6 (Abrahamson and Somerville, 1996; Abrahamson and Silva, 1997). These effects should be considered in developing vertical component spectra for both WUS and CEUS sites, when the geometry of a site with respect to a dominant fault is known.

Figure 4-33 illustrates the distance dependencies for each magnitude, showing a stronger distance effect with increasing magnitude. The peaks in the V/H ratios near 15 Hz are stable with magnitude and distance, and are controlled by the frequency of maximum spectral amplification for the vertical motions. The slight troughs in the ratios in the 1-3 Hz frequency range vary with magnitude (see Figure 4-32) and are controlled by the peaks (maximum spectral amplifications) in the horizontal component spectra. These features, as well as the differences in magnitude scaling between horizontal and vertical spectra, are illustrated in Figures 4-34 and 4-35. These figures show expected median spectra (5% damped) for horizontal and vertical components from the Abrahamson and Silva, 1997 empirical relations for a suite of magnitudes. For the horizontal component spectra, Figure 4-34 shows the strong shift in peak values with increasing magnitude while the vertical spectra (Figure 4-35) show peaks at a constant frequency in the 10-20 Hz range.

The location of peaks in V/H ratios results from peaks in the vertical spectra and are likely controlled by the shallow damping (Figure 2-4 and Appendix K). As a result, these peaks are expected to occur at a higher frequency for CEUS hard rock conditions, which have lower damping values (Appendix K). Additionally, for WUS empirical relations, smaller V/H ratios occur at low frequency ($\leq$ 2 Hz) with soil sites (Appendix K) where the effects of nonlinearity in the horizontal component is small. This suggests that for linear response conditions, the V/H ratio increases with profile stiffness. As a result, V/H ratios for hard rock conditions in the CEUS would be expected to be somewhat higher overall than WUS soft rock conditions.

These trends suggest that magnitude and distance dependencies may be largely captured by the expected peak acceleration of the horizontal motions, with larger V/H ratios associated with higher expected horizontal peak accelerations. The trends in Figures 4-32 and 4-33 clearly show V/H ratios exceeding unity at high frequencies for distances out to about 20 km for **M** 7.5 earthquakes. The average expected horizontal peak acceleration for **M** 7.5 at 20 km is about 0.3g suggesting that the current R.G. 1.60 ratio may be appropriate for conditions where the design peak accelerations are less than about 0.3g. The conventional assumption of vertical spectra taken as a constant 2/3 the horizontal is unconservative in the 10 to 30 Hz frequency range even out to 50 km.

To provide for a reasonable accommodation of magnitude and distance dependency in the revised vertical motions for WUS rock site conditions, Figure 4-36 shows recommended V/H ratios for

ranges of expected horizontal peak accelerations. These ratios are simply the averages of the empirical relations. The values are listed in Table 4-4. The ranges in horizontal peak accelerations are intended to capture important **M** and *R* dependencies, maintain reasonable conservatism, and result in a procedure that is simple to implement. Direct multiplication of the revised horizontal shapes by these smooth V/H ratios is intended to result in smooth vertical spectra appropriate for design and analyses.

4.7.2 V/H Ratios For CEUS Rock Site Conditions

For applications to CEUS hard rock site conditions, the only numerous empirical V/H ratios available are for small magnitude (**M** ≤ 5) earthquakes recorded at distances beyond about 20 km at hard rock sites (Atkinson, 1993). This empirical ratio, computed for Fourier amplitude spectra, is defined only from 1 Hz to 10 Hz and decreases from a value of 0.9 at 1 Hz to 0.7 at 10 Hz. The ratio is independent of distance and is based on recordings at sites in the distance range of about 20 to 1,000 km. This trend of decreasing V/H ratio in the 1 to 10 Hz frequency range, although weak, is opposite to the trend shown in the WUS V/H ratios. This difference may reflect differences in Fourier amplitude and response spectra but the average value of about 0.8 suggests higher V/H ratios at large distance for CEUS rock sites than WUS rock sites. For linear response conditions, this trend is consistent with increasing V/H ratios as profile stiffness increases. This results from less shear-wave (SV) energy being converted from the vertical component to the horizontal component due to wave refraction, for stiffer profiles.

A few V/H ratios are available from recordings at CEUS rock sites (and other intraplate sites) for earthquakes with magnitudes greater than **M** 5. Figure 4-37 shows results from the **M** 5.9 Saguenay and **M** 6.8 Nahanni and Gazli earthquakes. For the Saguenay earthquake, the V/H ratio varies between about 0.7 and 1 suggesting a higher ratio in the CEUS than the WUS at large distances (average distance is 111 km). While the ratio was computed from a large number of sites, it is still a single earthquake that is both deep, with a hypocentral depth of about 30 km, and considered anomalous in its high frequency spectral levels (Boore and Atkinson, 1992). For the larger magnitude data (Gazli and Nahanni earthquakes) only three sites are available for V/H ratios. Sites Karakyr and S1, for the Gazli and Nahanni earthquakes respectively, are located very close to the rupture surfaces at an average distance of about 4.5 km. Site Karakyr is not considered a hard rock site, having about 1.4 km of sedimentary rock (with some clays) overlying a hard schist basement rock (Hartzell, 1980). This geology, with an estimated kappa value of 0.015 sec, may be considered a CEUS soft rock site (Silva and Darragh, 1995). The V/H ratio for the most distant Nahanni site at 16 km (S3, Figure 4-37), shows ratios consistent with those of the Saguenay earthquake, ranging from about 0.6 to about 1 for frequencies above 1 Hz. Interestingly, for frequencies ≤ 0.6 Hz, the V/H ratio is near 2. These V/H ratios from Nahanni are for only a single earthquake, as with Saguenay, and at only a single site but they do suggest the possibility of higher ratios for CEUS sites as well as a high degree of uncertainty in the ratios.

For the near source V/H ratios (distance of 4.5 km), Figure 4-37 shows ratios near unity up to about 5 Hz and values near 2 for frequencies above 10 Hz. These trends are consistent at the two sites for the two earthquakes. Both sites (Karakyr and Site 1) have vertical peak accelerations exceeding 1g (1.3g for Gazli and 2.1g for Nahanni, Appendix A), about double the average horizontal peak

accelerations. These results, reflecting few data for poorly understood earthquakes and largely unknown site conditions, indicate that very large V/H ratios may be likely at very close rupture distances to CEUS earthquakes. Larger than average high frequency ($\geq$ 3 Hz) ratios likely result from both S1 and Karakyr being located on the hanging wall of the fault. As with the more distant Nahanni site, S3, these results suggest higher V/H ratios for CEUS rock sites than WUS sites and show that ratios at near-fault sites can be quite large at high frequencies.

To develop recommended V/H values for applications to CEUS rock sites, the simple point source model (Section 4.3) was extended to consider P-SV waves and was used to estimate vertical component spectra (Appendix K; EPRI, 1993). The model predicts the general trends in the WUS V/H ratios and has been validated at rock sites that recorded the 1989 **M** 6.9 Loma Prieta earthquake (EPRI, 1993), so V/H ratios computed for the generic CEUS rock site conditions (Figure 2-2) may be used with reasonable confidence to develop guidelines. The V/H ratios predicted by the model for CEUS conditions are illustrated in Figure 4-38. The low frequency peaks (1 to 30 Hz) result from resonances associated with compressional- and shear-wave velocity profiles and would be smoothed out if the velocities were randomized. The peak in the ratios near 60 Hz is associated with the vertical spectra and corresponds to the peak in the WUS ratios (Figures 4-35 and 4-36) but shifted from about 15 to 20 Hz to about 60 Hz because of the lower kappa values for the CEUS vertical motions (κ = 0.003 sec). The magnitude dependencies in the CEUS ratios are smaller than for the WUS probably because the WUS model currently does not include magnitude saturation, apart from a stress drop that decreases with increasing magnitude (Section 6; Atkinson and Silva, 1997). Since this stress drop scaling affects both vertical and horizontal components equally, the simple model does not show the same trends as the empirical V/H ratios (Figure 4-32). However, the model does show higher ratios at low frequencies (< 3 Hz) than the WUS ratios, consistent with available observations. Based on the trends shown in the model predictions as well as the CEUS recordings, a reasonable approach to defining recommended ratios is to shift the WUS ratios to higher frequencies, so that the peaks correspond to about 60 Hz. Also the low frequency WUS levels should be scaled up by about 50% (factor of 1.5), a proportion reflected in comparing the CEUS and WUS model estimates of the V/H ratios (Appendix K). The recommended ratios are shown in Figure 4-39 and are listed in Table 4-5. Maintaining the same peak acceleration ranges in the horizontal component for the CEUS V/H ratios adds conservatism necessitated by the large uncertainties. For cases where the site is located on the hanging wall of a dipping fault within a rupture distance of about 20 km, the V/H ratio could be significantly larger ($\approx$ 30%) for large magnitude earthquakes, warranting careful site-specific studies.

To illustrate the vertical spectra resulting from the process of scaling the horizontal spectra, Figure 4-40 shows WUS vertical motions while Figures 4-41 and 4-42 show corresponding CEUS vertical motions. Both WUS and CEUS verticals are based on the **M** 6.4 bin shapes shown in Figures 4-26 and 4-27 and reflect vertical motions relative to 1g horizontal motions. For the WUS verticals, the vertical peak acceleration exceeds the horizontal for horizontal peak accelerations exceeding 0.5g. For peak horizontal accelerations in the 0.2 to 0.5g range, the vertical spectra exceed the horizontal spectra in the frequency range of about 10 to 30 Hz, but the vertical peak accelerations are lower than the horizontal. At low frequency, below about 3 Hz, the verticals spectra are about one half the horizontal. For the CEUS verticals shown in Figures 4-41 and 4-42, both the single and double

corner vertical spectra show trends relative to the horizontals that are similar to the WUS but shifted to higher frequencies, as expected.

In general, both WUS and CEUS V/H ratios provide smooth and reasonable vertical motions when applied to the recommended spectral shapes for horizontal components.

4.8 Intermediate Rock Site Conditions

For rock site conditions intermediate to the CEUS and WUS (which have kappa values of 0.006 sec and 0.04 sec respectively), an appropriate mix of the WUS and CEUS shapes should be based on a site specific kappa value. Weights for the WUS and CEUS rock shapes can easily be determined using the following equations:

$$\kappa_s = \kappa_W W_W + \kappa_E W_E \tag{4-10}$$

$$W_W + W_E = 1 \tag{4-11}$$

where κ_S is the site specific kappa value, W_W and W_E are the WUS and CEUS shape weights, and κ_W and κ_E are the WUS and CEUS rock kappa values. For κ_s values outside κ_W and κ_E, the shape for the closest kappa value should be used.

If a site specific kappa value is not available, a reasonable approach would be to use the inverse of the average shear-wave velocity over the top 30m in Equation 4.10 in lieu of the kappa values (see Equation D5, Appendix D). Appropriate average shear-wave velocity values for the WUS and CEUS rock sites are 520m/sec and 2,800m/sec respectively. The weights used for the CEUS and WUS shapes should also be used for a weighted V/H ratio.

4.9 Estimation of Spectra For Other Dampings

Several methods are available to estimate design response spectra for dampings other than 5%. All are based on scaling the 5% damped spectrum higher or lower. The scaling factors are a function of natural frequency.

4.9.1 Random Vibration Methods

The most theoretically consistent method of accounting for damping is through random vibration theory. The recommended procedure is as follows.

For frequencies $1 \leq f < 5$ Hz, the procedure of Rosenblueth (1980) should be used. This scales the spectral acceleration SA at any frequency f and damping ξ by spectral acceleration at $\xi = 0.05$ by:

$$SA\ (f, \xi) = SA\ (f, 0.05) \left[\frac{1 + 4.9\ \xi\ f\ D}{1 + 4.9\ x\ 0.05\ f\ D} \right]^{-0.41} \tag{4.12}$$

where D is strong motion duration. For frequencies of 5 Hz and above, the recommended procedure is based on the concept of Vanmarcke (1976) that the response is controlled by a static portion (governed by PGA) and a dynamic portion (governed by equation 4.10). This procedure provides a transition to the peak ground acceleration (PGA)-controlled portion of the spectrum in a realistic way as follows:

$$SA\ (f,\xi) = \left\{ PGA^2 + \left[SA\ (f,\ 0.05)^2 - PGA^2\right]\left[\frac{1 + 4.9\ \xi f D}{1 + 4.9\ x\ 0.05\ f D}\right]^{-0.82}\right\}^{1/2} \qquad (4.13)$$

where the second term on the right-hand-side (involving a subtraction) should not be less than 0.

The strong-motion duration D is distance dependent. For the WUS, D can be estimated from Abrahamson and Silva (1997). For the CEUS, D can be estimated from Atkinson and Boore (1997).

The two equations above allow estimation of dampings in the range of 0.5% to 20% from a design spectrum that is developed for 5% damping. These equations are applicable to both horizontal and vertical motion.

For frequencies below 1 Hz, equation (4.10) can be used as an approximation, but at very low frequencies (0.2 to 0.1 sec) it should be checked to ensure that spectral displacements are approaching the peak ground displacement for all dampings.

4.9.2 Empirical Methods

Several empirical methods have been developed based on recorded motions in California and these can be used to produce spectra at dampings other than 5%.

Abrahamson and Silva (1996) developed a model of the effects of damping based on statistical analyses of strong motion records. Their scaling factor is as follows:

$$\ln\left[\frac{SA\ (f,\ \xi)}{SA\ (f,\ 5\%)}\right] = \begin{cases} c_1(f,\ \xi) & \text{for } f > 1.43\text{Hz} \\ c_1(f,\ \xi) + g_2(f,\ \xi)(M-6) + g_3\ (f,\ \xi)(8.5-M)^2 & \text{for } f < 1.43\text{Hz} \end{cases} \qquad (4.14)$$

Coefficients for equation 4.12 are listed in Tables 4-6 through 4-8. Separate coefficients are given for horizontal and vertical motions, and scaling factors are reported for periods of 5 sec to 0.02 sec (0.2 Hz to 50 Hz). They are applicable to damping values between 0.5% and 20%.

Idriss (1993) also developed empirical scale factors for damping based on ground motions during the 1971 San Fernando and 1979 Imperial Valley earthquakes. His scale factor is defined as:

$$\frac{SA\ (f,\ \xi)}{SA\ (f,\ 5\%)} = \begin{cases} a_1 - b_1\ \ln(\xi) & \text{for } \xi \le 5\% \\ a_2 - b_2\ \ln(\xi) & \text{for } \xi > 5\% \end{cases} \qquad (4.15)$$

The coefficients a_1, a_2, b_1 and b_2, are listed in Table 4-9 for a range of natural periods from 0.03 sec to 5 sec (33 Hz to 0.2 Hz). These scaling factors are applicable to horizontal motions and to damping values between 1% and 15% (Idriss, personal communication, 1999).

Newmark and Hall (1978) recommended scale factors for different damping values, but these were for different parts of the spectrum controlled by peak acceleration, velocity, and displacement. That is, separate scaling factors were not developed frequency-by-frequency, but were developed for the high-frequency range (3 to 8 Hz), the mid-frequency range (.3 to 3 Hz) and the low-frequency range (below 0.3 Hz). This worked well when scaling spectra from peak values but would leave discontinuities if applied to uniform hazard spectra. For this reason the Newmark and Hall damping factors are not recommended.

References

Abrahamson, N.A. and W.J. Silva (1996). *Empirical ground motion models*, Rept submitted to Brookhaven Nat'l Lab., May 6.

Abrahamson, N.A. and W.J. Silva (1997). "Empirical response spectral attenuation relations for shallow crustal earthquakes." *Seism. Soc. Am.*, 68(1), 94-127.

Abrahamson, N.A and K.M. Shedlock (1997). "Overview." *Seism. Research Lett.*, 68(1), 9-23.

Abrahamson, N.A. and P.G. Somerville (1996). "Effects of hanging wall and foot wall on ground motions and recorded during the Northridge earthquake." *Bull. Seism. Soc. Am.* 86(1B), S93-S99.

Abrahamson, N.A. and P.G. Somerville (1997). "Empirical response spectral attenuation relations for shallow crustal earthquakes." *Seism. Soc. Am.*, 68(1), 94-127.

Abrahamson, N.A., P.G. Somerville, C.A. Cornell (1990). "Uncertainty in numerical strong motion predictions" *Proc. Fourth U.S. Nat. Conf. Earth. Engin.*, Palm Springs, CA., 1, 407-416.

Atkinson, G.M. and D.M. Boore (1998). "Evaluation of models for earthquake source spectra in Eastern North America." *Bull. Seism. Soc. Am.* 88(4), 917-934.

Atkinson, G.M. and D.M. Boore (1997). "Some comparisons between recent ground-motion relations." *Seism. Res. Lett.* 68(1), 24-40.

Atkinson, G.M. and D.M. Boore (1995). "Ground motion relations for eastern North America." *Bull. Seism. Soc. Am.*, 85(1), 17-30.

Atkinson, G.M and W.J. Silva (1997). "An empirical study of earthquake source spectra for California earthquakes." *Bull. Seism. Soc. Am.* 87(1), 97-113.

Atkinson, G.M. (1993). "Source spectra for earthquakes in eastern North America." *Bull. Seism. Soc. Am.*, 83(6), 1778-1798.

Boatwright, J. (1994). "Regional propagation characteristics and source parameters of earthquakes in Northeastern North America." *Bull. Seism. Soc. Am.*, 84(1), 1-15.

Boatwright, J and G. Choy (1992). "Acceleration source spectra anticipated for large earthquakes in Northeastern North America." *Bull. Seism. Soc. Am.*, 82(2), 660-682.

Boatwright, J. and L. Seekins (1997). "Response spectra from the 1989 Loma Prieta, California, earthquake regressed for site amplification, attenuation, and directivity." USGS Open-File Report 97-858.

Boore, D.M., W.B. Joyner, and T.E. Fumal (1997). "Equations for estimating horizontal response spectra and peak acceleration from Western North American earthquakes: A summary of recent work." *Seism. Res. Lett.* 68(1), 128-153.

Boore, D.M., G.M. Atkinson (1992). "Source spectra for the 1988 Saguenay, Quebec, earthquakes." *Bull. Seism. Soc. Am.*, 82(2), 683-719.

Boore, D.M. (1983). "Stochastic simulation of high-frequency ground motions based on seismological models of the radiated spectra." *Bull. Seism. Soc. Am.*, 73(6), 1865-1894.

Boore, D.M. (1986). "The effect of finite bandwidth on seismic scaling relationships." in *Earthquake Source Mechanics, Maurice Ewing Ser.*, S.Das, ed., Amer. Geophys. Union, Wash. D.C. vol.6.

Brillinger, D.R., and H.K. Preisler (1984). An exploratory analysis of the Joyner-Boore attenuation data, *Bull. Seism. Soc. Am.*, **74**, 1441-1450.

Brillinger, D.R., and H.K. Preisler (1985). Further analysis of the Joyner-Boore attenuation data, *Bull. Seism. Soc. Am.*, **75**, 611-614.

Campbell, K W. (1997). "Empirical near-source attenuation relationships for horizontal and vertical components of peak ground acceleration, peak ground velocity, and pseudo-absolute acceleration response spectra." *Bull. Seism. Soc. Am.*, 68(1), 154-176.

Campbell, K.W. (1993) "Empirical prediction of near-source ground motion from large earthquakes." in V.K. Gaur, ed., *Proceedings, Intern'l Workshop on Earthquake Hazard and Large Dams in the Himalya.* INTACH, New Delhi, p. 93-103.

Choy, G.L. and J. Boatwright (1988). "Teleseismic and near-field analysis of the Nahanni earthquakes in the Northwest Territories, Canada." *Bull. Seism. Soc. Am.*, 78(5), 1627-1652.

EPRI (1993). "Guidelines for determining design basis ground motions." Electric Power Research Institute, Palo Alto, CA, Rept. TR-102293, vol 1-5:
vol. 1: Methodology and guidelines for estimating earthquake ground motion in eastern North America.
vol. 2: Appendices for ground motion estimation.
vol. 3: Appendices for field investigations.
vol. 4: Appendices for laboratory investigations.
vol. 5: Quantification of seismic source effects.

Hanks, T.C., and R.K. McGuire (1981). "The character of high-frequency strong ground motion." *Bull. Seism. Soc. Am.*, 71(6), 2071-2095.

Hartzell, S. (1980). "Faulting Process of the May 17, 1976, Gazli, USSR Earthquake." *Bull. Seism. Soc. Am.*, 70(5), 1715-1736.

Idriss, I.M. (1991). "Earthquake ground motions at soft soil sites." *Proceedings: 2nd Int'l Confer. on Recent Advances in Geotechnical Earthquake Engineering and Soil Dynamics,* Saint Louis, Missouri, Invited Paper LP01, 2265-2272.

Idriss, I.M. (1993). "Procedures for selecting earthquake ground motions at rock sites," Nat. Inst. of Stan. And Tech., Rept. NIST GCR 93-625.

Kimball, J.K. (1983). "The use of site dependent spectra." *Proc. Workshop on Site-Specific Effects of Soil and Rock on Ground Motion and the Importance for Earthquake-Resistant Design,* Santa Fe, New Mexico, USGS Open-File Rept. 83-845, 410-422.

Mohraz, B., W.J. Hall and N.M. Newmark (1972). "A study of vertical and horizontal earthquake spectra." Nathan M. Newmark Consulting Engineering Services, Urbana, Illinois: *AEC Report* No. WASH-1255.

Newmark, N.M. and W.J. Hall (1978). "Development of criteria for seismic review of selected nuclear power plants." US Nuc. Reg. Comm., NUREG/CR-0098, May.

Newmark, N.M., W.J. Hall, and B. Mohraz (1973). *A Study of Vertical and Horizontal Earthquake Spectra.* Directorate of Licensing, U.S. Atomic Energy Commission, Rept. WASH-1255.

Newmark, N.M., J.A. Blume and K.K. Kapur (1973). "Seismic design criteria for nuclear power plants." *Journal of the Power Division,* ASCE 99, 287-303.

Regulatory Guide 1.60 (1973). *"Design response spectra for seismic design of nuclear power plants."* U.S. Atomic Energy Commission, Directorate of Regulatory Standards.

Roblee, C.J., W.J. Silva, G.R. Toro, and N. Abrahamson (1996). "Variability in Site-Specific Seismic Ground-Motion Predictions." Uncertainty in the Geologic Environment: From Theory to Practice, *Proceedings* Uncertainty '96 *ASCE* Specialty Conference, Edited by C.D. Shackelford, P.P. Nelson, and M.J.S. Roth, Madison, WI, Aug. 1-3, pp. 1113-1133.

Rosenblueth, E. (1980) Characteristics of Earthquakes, In E. Rosenblueth, editor, *Design of Earthquake Resistant Structures*, Ch. 1, Wiley.

Sadigh, K., C.-Y. Chang, J.A. Egan, F. Makdisi, and R.R. Youngs (1997). "Attenuation relationships for shallow crustal earthquakes based on California strong motion data." *Bull. Seism. Soc. Am.*, 68(1), 180-189.

Sadigh, K., C.-Y. Chang, N.A. Abrahamson, S.J. Chiou, and M.S. Power (1993). "Specification of long-period ground motions: Updated attenuation relationships for rock site conditions and adjustment factors for near-fault effects." in *Proc. ATC-17-1, Seminar on Seismic Isolation, Passive Energy Dissipation, and Active Control, March 11-12, San Francisco, California, 59-70.*

Silva, W.J., N.A. Abrahamson, G.R. Toro, C.J. Costantino (1997). "Description and validation of the stochastic ground motion model." Report to Brookhaven National Laboratory, Associated Universities, Inc. Upton, New York, Contract 770573.

Silva, W.J. and R. Darragh (1995). "Engineering characterization of earthquake strong ground motion recorded at rock sites." EPRI, Palo Alto, CA, Rept. TR-102261.

Silva, W.J. (1991). "Global characteristics and site geometry." Chapter 6 in *Proceedings: NSF/ EPRI Workshop on Dynamic Soil Properties and Site Characterization.* Electric Power Research Institute, Palo Alto, CA, Rept. NP-7337.

Silva, W.J., and R.K. Green (1989). "Magnitude and distance scaling of response spectral shapes for rock sites with applications to North American tectonic environment." *Earthquake Spectra,* 5(3), 591-624.

Seed, H.B., C. Ugas and J. Lysmer. (1976). "Site-dependent spectra for earthquake resistant design." *Bull. Seism. Soc. Am.*, 66(1), 221-243.

Somerville, P.G., N.F. Smith, R.W. Graves, and N.A. Abrahamson, (1997). "Modification of empirical strong ground motion attenuation relations to include the amplitude and duration effects of rupture directivity." *Seism. Res. Lett.*, 68(1), 199-222.

Somerville, P.G. and N.A. Abrahamson (1995). "Ground motion prediction for thrust earth-quakes." *Proc. of the SMIP95 Seminar on Seismological and Engineering Implications of Recent Strong Motion Data*, San Francisco, California.

Vanmarcke, E.H. (1976). Structural response to earthquakes, in *Seismic Risk and Engineering Decisions*, edited by C. Lomnitz and E. Rosenblueth, Elsevier Publishing Co., Amsterdam, London, New York.

Youngs, R.R., S.J. Chiou, W.J. Silva, and J.R. Humphrey (1997), "Strong ground motion attenuation relationships for subduction zone earthquakes." *Seism. Res. Lett.*, 68(1), 58-73.

Youngs, R.R., N.A. Abrahamson, F. Makdisi, and K. Sadigh (1995). "Magnitude dependent dispersion in peak ground acceleration." *Bull. Seism. Soc. Am.*, 85(1), 1161-1176.

Table 4-1
WUS STATISTICAL SHAPE BINS

Magnitude Bins (**M**)

Range	Bin Center
5 - 6	5.5
6 - 7	6.5
7+	7.5

Distance Bin (km)	$\overline{M}$	$\overline{R}$ (km)	Number of Spectra	PGA*(g), σ_{ln}	PGV*(cm/sec), σ_{ln}	PGD*(cm), σ_{ln}	$\frac{PGV^*}{PGA}$ ($\frac{cm/sec}{g}$), σ_{ln}	$\frac{PGA \cdot PGD^*}{PGV^2}$, σ_{ln}
0 - 10, rock	5.54	7.91	30	0.18, 0.91	8.14, 1.14	0.80, 1.60	44.50, 0.58	2.17, 0.28
	6.53	5.75	32	0.44, 0.76	32.65, 0.93	06.22, 1.26	73.51, 0.40	2.54, 0.42
	7.27	4.20	6	0.93, 0.26	81.73, 0.25	47.42, 0.66	87.94, 0.39	6.47, 0.60
0 - 10, soil	5.76	7.80	24	0.26, 0.65	18.57, 0.56	3.11, 0.46	70.72, 0.33	2.32, 0.35
	6.46	6.00	77	0.38, 0.43	46.88, 0.59	14.79, 0.89	122.00, 0.44	2.54, 0.41
	7.05	8.90	4	0.40, 0.62	44.46, 0.56	21.27, 0.25	110.42, 0.07	4.25, 0.24
10 - 50, rock	5.57	21.80	180	0.11, 0.87	5.08, 0.85	0.54, 1.04	46.96, 0.37	2.24, 0.38
	6.43	30.28	238	0.13, 0.73	8.81, 0.76	1.96, 1.01	70.41, 0.49	3.09, 0.54
	7.27	31.00	6	0.17, 0.85	8.80, 0.88	2.50, 1.56	50.59, 0.37	5.51, 0.90
10 - 50, soil	5.69	21.82	378	0.11, 0.73	6.63, 0.77	0.87, 0.94	59.88, 0.34	2.16, 0.33
	6.35	28.27	542	0.14, 0.63	10.77, 0.74	2.25, 1.04	78.77, 0.41	2.57, 0.41

* median values

Table 4-1 (cont.)
WUS STATISTICAL SHAPE BINS

Magnitude Bins (M)

Range	Bin Center
5 - 6	5.5
6 - 7	6.5
7+	7.5

Distance Bin (km)	$\overline{M}$	$\overline{R}$ (km)	Number of Spectra	PGA*(g), σ_{ln}	PGV*(cm/sec), σ_{ln}	PGD*(cm), σ_{ln}	$\frac{PGV^*}{PGA}$ ($\frac{cm/sec}{g}$), σ_{ln}	$\frac{PGA \cdot PGD^*}{PGV^2}$, σ_{ln}
10 - 50, soil	7.29	33.46	56	0.16, 0.35	22.38, 0.38	10.46, 0.39	141.17, 0.36	3.25, 0.56
50 - 100, rock	5.91	64.27	34	0.05, 0.40	2.22, 0.53	0.21, 0.83	41.16, 0.43	2.24, 0.57
	6.51	70.35	102	0.06, 0.51	3.87, 0.82	0.79, 1.23	69.89, 0.56	2.88, 0.56
	7.32	81.46	10	0.06, 0.52	5.16, 0.87	2.64, 1.17	80.63, 0.45	6.23, 0.50
50 - 100, soil	5.80	67.22	42	0.06, 0.80	3.12, 0.78	0.38, 0.92	53.20, 0.23	2.28, 0.49
	6.49	67.34	158	0.07, 0.67	6.23, 0.78	1.26, 0.99	88.00, 0.42	2.26, 0.44
	7.31	76.57	14	0.10, 0.12	11.24, 0.34	5.42, 0.60	111.37, 0.35	4.24, 0.50
100 - 200, rock	5.4	107.80	2	0.02, ----	1.16, ----	0.10, ----	49.72, ----	1.74, ----
	6.64	114.57	14	0.02, 0.86	2.03, 0.38	1.09, 0.68	132.54, 0.59	3.98, 0.27
	7.30	152.01	14	0.03, 0.47	5.55, 0.66	2.43, 1.06	184.16, 0.35	2.34, 0.31
100 - 200, soil	6.0	105.00	2	0.03, ----	1.50, ----	0.11, ----	42.92, ----	1.74, ----

* median values

Table 4-1 (cont.)
WUS STATISTICAL SHAPE BINS

Magnitude Bins (M)

Range	Bin Center
5 - 6	5.5
6 - 7	6.5
7+	7.5

Distance Bin (km)	$\overline{M}$	$\overline{R}$ (km)	Number of Spectra	PGA**(g), σ_{ln}	PGV*(cm/sec), σ_{ln}	PGD*(cm), σ_{ln}	$\frac{PGV^*}{PGA}$ ($\frac{cm/\sec}{g}$), σ_{ln}	$\frac{PGA \cdot PGD^*}{PGV^2}$, σ_{ln}
100 - 200, soil	6.64	132.97	28	0.03, 0.78	3.05, 0.58	0.89, 0.97	98.24, 0.53	2.90, 0.42
	7.31	147.07	88	0.04, 0.25	8.09, 0.39	3.50, 0.76	188.64, 0.36	2.25, 0.29
0 - 50, rock	5.57	19.91	208	0.12, 0.89	5.39, 0.91	0.57, 1.14	46.73, 0.40	2.22, 0.37
	6.44	27.39	270	0.15, 0.84	10.27, 0.89	2.24, 1.10	70.77, 0.48	3.02, 0.53
	7.27	17.60	12	0.40, 1.07	26.82, 1.35	10.89, 1.94	66.70, 0.46	5.97, 0.69
0 - 50, soil	5.69	21.10	398	0.12, 0.75	7.02, 0.79	0.93, 0.97	60.48, 0.34	2.16, 0.33
	6.37	25.50	619	0.16, 0.70	12.93, 0.87	2.85, 1.20	83.17, 0.44	2.57, 0.41
	7.27	31.82	60	0.17, 0.42	23.43, 0.42	10.97, 0.42	138.87, 0.36	3.30, 0.55

**Median values

Table 4-2 POINT-SOURCE PARAMETERS*		
	WUS	CEUS
$\Delta\sigma$ (bars)	65	120
kappa (sec)	0.040	0.006
Q_o	220	351
η	0.60	0.84
β (km/sec)	3.50	3.52
ρ (g/cc)	2.70	2.60
Amplification	soft rock (Figure 2-3)	hard rock (Figure 2-3)
Double Corner	Atkinson and Silva (1997)	Atkinson (1993)

* based on Silva et al. (1997)

Table 4-3
RESPONSE SPECTRAL SHAPE COEFFICIENTS FOR 5% DAMPING

	WUS	CEUS (1C)*	CEUS (2C)*
C_1	1.8197	0.88657	0.97697
C_2	0.30163	exp(-10.411)	exp(-9.4827)
C_3	0.47498+0.034356**M**+0.0057204ln(R+1)	2.5099	2.3006
C_4	-12.650+**M**·[2.4796-0.14732**M** +0.034605ln(0.040762R+1)]	-7.4408+**M**[1.5220-0.088588**M** +0.0073069ln(0.12639R+1)]	-12.665+**M**[2.4869-0.14562**M** +0.024477ln(0.041807R+1)]
C_5	-0.25746	-0.34965	-0.21002
C_6	0.29784+0.010723**M**-0.0000133R	-0.31162+0.0019646R	0.74361+0.0000671R
C_7	n.a.	3.7841	exp[-13.476+**M**(4.4007-0.31651**M** +0.000235R)]
C_8	n.a.	-0.89019	0.95259+**M**(-0.58275+0.000166R)
C_9	n.a.	0.39806+0.058832**M**	-3.3534+0.44094**M**

Note: Equation (4-8) is used for the WUS; equation (4-9) is used for the CEUS.

M = moment magnitude
R = fault distance
*1C = single corner frequency model
2 C = double corner frequency model

Table 4-4 RECOMMENDED V/H RATIOS FOR WUS ROCK SITE CONDITIONS			
Frequency (Hz)	≤ 0.2g*	0.2 - 0.5g*	> 0.5g*
.100+00	.503E+00	.558E+00	.696E+00
.333E+00	.503E+00	.558E+00	.696E+00
.500E+00	.461E+00	.508E+00	.651E+00
.667E+00	.458E+00	.495E+00	.645E+00
.100E+01	.440E+00	.461E+00	.608E+00
.118E+01	.434E+00	.454E+00	.597E+00
.133E+01	.431E+00	.451E+00	.592E+00
.167E+01	.420E+00	.447E+00	.585E+00
.200E+01	.416E+00	.447E+00	.583E+00
.217E+01	.417E+00	.452E+00	.592E+00
.250E+01	.426E+00	.467E+00	.616E+00
.278E+01	.436E+00	.482E+00	.638E+00
.333E+01	.456E+00	.511E+00	.681E+00
.417E+01	.495E+00	.571E+00	.758E+00
.500E+01	.536E+00	.628E+00	.836E+00
.588E+01	.581E+00	.691E+00	.918E+00
.666E+01	.625E+00	.751E+00	.997E+00
.833E+01	.715E+00	.888E+00	.119E+01
.100E+02	.796E+00	.101E+01	.137E+01
.111E+02	.840E+00	.107E+01	.144E+01
.125E+02	.885E+00	.112E+01	.150E+01
.167E+02	.904E+00	.114E+01	.152E+01
.200E+02	.888E+00	.112E+01	.148E+01
.250E+02	.810E+00	.102E+01	.133E+01
.333E+02	.744E+00	.912E+00	.117E+01
.500E+02	.704E+00	.848E+00	.107E+01
.100E+03	.704E+00	.848E+00	.107E+01

*Range in rock outcrop horizontal component peak acceleration

Table 4-5
RECOMMENDED V/H RATIOS FOR CEUS ROCK SITE CONDITIONS

Frequency (Hz)	≤ 0.2g*	0.2 - 0.5g*	> 0.5g*
0.10	0.67	0.75	0.90
10.00	0.67	0.75	0.90
18.75	0.70	0.81	1.01
22.06	0.73	0.85	1.08
25.00	0.75	0.88	1.12
31.25	0.77	0.95	1.25
37.50	0.81	1.00	1.37
41.67	0.84	1.07	1.44
46.88	0.85	1.12	1.50
62.50	0.90	1.14	1.52
75.00	0.89	1.12	1.48
93.75	0.81	1.02	1.33
100.0	0.78	1.00	1.30

*Range in rock outcrop horizontal component peak acceleration

Table 4-6a
Horizontal c_1 values for separate damping levels
for equation (4.12), Abrahamson and Silva (1996)

Period (sec)	c1 (0.5%)	c1 (1.0%)	c1 (2.0%)	c1 (3.0%)	c1 (7.0%)	c1 (10.0%)	c1 (15.0%)	c1 (20.0%)
5.00	0.3698	0.2891	0.1830	0.1084	-0.0812	-0.1763	-0.2964	-0.3899
4.00	0.3955	0.3092	0.1957	0.1159	-0.0869	-0.1886	-0.3171	-0.4170
3.00	0.4233	0.3310	0.2095	0.1241	-0.0930	-0.2018	-0.3393	-0.4463
2.00	0.4526	0.3538	0.2239	0.1326	-0.0994	-0.2157	-0.3628	-0.4471
1.50	0.4667	0.3648	0.2309	0.1368	-0.1025	-0.2225	-0.3741	-0.4920
1.00	0.4780	0.3737	0.2365	0.1401	-0.1050	-0.2279	-0.3832	-0.5040
0.85	0.4801	0.3753	0.2375	0.1407	-0.1054	-0.2289	-0.3848	-0.5061
0.75	0.4808	0.3759	0.2379	0.1409	-0.1056	-0.2292	-0.3854	-0.5069
0.60	0.4808	0.3759	0.2379	0.1409	-0.1056	-0.2292	-0.3854	-0.5069
0.50	0.4808	0.3759	0.2379	0.1409	-0.1056	-0.2292	-0.3854	-0.5069
0.46	0.4808	0.3759	0.2379	0.1409	-0.1056	-0.2292	-0.3854	-0.5069
0.40	0.4808	0.3759	0.2379	0.1409	-0.1056	-0.2292	-0.3854	-0.5069
0.36	0.4808	0.3759	0.2379	0.1409	-0.1056	-0.2292	-0.3854	-0.5069
0.30	0.4808	0.3759	0.2379	0.1409	-0.1056	-0.2292	-0.3854	-0.5069
0.24	0.4808	0.3759	0.2379	0.1409	-0.1056	-0.2292	-0.3854	-0.5069
0.20	0.4808	0.3759	0.2379	0.1409	-0.1056	-0.2292	-0.3854	-0.5069
0.17	0.4808	0.3759	0.2379	0.1409	-0.1056	-0.2292	-0.3854	-0.5069
0.15	0.4616	0.3609	0.2284	0.1353	-0.1014	-0.2200	-0.3700	-0.4866
0.12	0.4327	0.3383	0.2141	0.1268	-0.0950	-0.2063	-0.3469	-0.4562
0.10	0.3885	0.3037	0.1922	0.1138	-0.0853	-0.1852	-0.3114	-0.4096
0.09	0.3630	0.2838	0.1796	0.1064	-0.0797	-0.1730	-0.2910	-0.3827
0.07	0.3193	0.2496	0.1580	0.0936	-0.0701	-0.1522	-0.2559	-0.3366
0.06	0.2654	0.2075	0.1313	0.0778	-0.0583	-0.1265	-0.2127	-0.2798
0.05	0.2212	0.1729	0.1094	0.0648	-0.0486	-0.1054	-0.1773	-0.2332
0.04	0.1673	0.1308	0.0828	0.0490	-0.0367	-0.0798	-0.1341	-0.1764
0.03	0.0933	0.0729	0.0462	0.0273	-0.0205	-0.0445	-0.0748	-0.0983
0.02	0.0000	0.0000	0.0000	0.0000	0.0000	0.0000	0.0000	0.0000

Table 4-6b
Vertical c_1 values for separate damping levels
for equation (4.12), Abrahamson and Silva (1996)

Period (sec)	c1 (0.5%)	c1 (1.0%)	c1 (2.0%)	c1 (3.0%)	c1 (7.0%)	c1 (10.0%)	c1 (15.0%)	c1 (20.0%)
5.00	0.4135	0.3230	0.2033	0.1196	-0.0871	-0.1872	-0.3114	-0.4065
4.00	0.4462	0.3485	0.2193	0.1291	-0.0940	-0.2020	-0.3359	-0.4385
3.00	0.4814	0.3760	0.2366	0.1393	-0.1014	-0.2180	-0.3625	-0.4372
2.00	0.5186	0.4050	0.2549	0.1500	-0.1093	-0.2348	-0.3904	-0.5097
1.50	0.5365	0.4190	0.2637	0.1552	-0.1131	-0.2429	-0.4039	-0.5273
1.00	0.5511	0.4304	0.2709	0.1594	-0.1161	-0.2495	-0.4149	-0.5417
0.85	0.5538	0.4325	0.2722	0.1602	-0.1167	-0.2507	-0.4169	-0.5443
0.75	0.5548	0.4333	0.2727	0.1605	-0.1169	-0.2512	-0.4177	-0.5453
0.60	0.5548	0.4333	0.2727	0.1605	-0.1169	-0.2512	-0.4177	-0.5453
0.50	0.5548	0.4333	0.2727	0.1605	-0.1169	-0.2512	-0.4177	-0.5453
0.46	0.5548	0.4333	0.2727	0.1605	-0.1169	-0.2512	-0.4177	-0.5453
0.40	0.5548	0.4333	0.2727	0.1605	-0.1169	-0.2512	-0.4177	-0.5453
0.36	0.5548	0.4333	0.2727	0.1605	-0.1169	-0.2512	-0.4177	-0.5453
0.30	0.5548	0.4333	0.2727	0.1605	-0.1169	-0.2512	-0.4177	-0.5453
0.24	0.5647	0.4411	0.2776	0.1634	-0.1190	-0.2557	-0.4252	-0.5551
0.20	0.5776	0.4511	0.2839	0.1671	-0.1217	-0.2615	-0.4348	-0.5677
0.17	0.5920	0.4623	0.2910	0.1713	-0.1247	-0.2680	-0.4457	-0.5818
0.15	0.5965	0.4658	0.2932	0.1726	-0.1257	-0.2701	-0.4491	--0.5862
0.12	0.5880	0.4593	0.2890	0.1701	-0.1239	-0.2662	-0.4427	-0.5780
0.10	0.5732	0.4477	0.2818	0.1658	-0.1208	-0.2595	-0.4316	-0.5634
0.09	0.5471	0.4273	0.2689	0.1583	-0.1153	-0.2477	-0.4119	-0.5378
0.07	0.5062	0.3954	0.2488	0.1464	-0.1067	-0.2292	-0.3811	-0.4976
0.06	0.4615	0.3604	0.2268	0.1335	-0.0972	-0.2090	-0.3475	-0.4536
0.05	0.4216	0.3293	0.2072	0.1220	-0.0888	-0.1909	-0.3174	-0.4144
0.04	0.3751	0.2930	0.1844	0.1085	-0.0790	-0.1698	-0.2824	-0.3687
0.03	0.2507	0.1958	0.1232	0.0725	-0.0528	-0.1135	-0.1887	-0.2464
0.02	0.0000	0.0000	0.0000	0.0000	0.0000	0.0000	0.0000	0.0000

Table 4-7a
Horizontal g_2 values for separate damping levels
for equation (4.12), Abrahamson and Silva (1996)

Period (sec)	g2 (0.5%)	g2 (1.0%)	g2 (2.0%)	g2 (3.0%)	g2 (7.0%)	g2 (10.0%)	g2 (15.0%)	g2 (20.0%)
5.00	0.0214	0.0168	0.0106	0.0063	-0.0047	-0.0102	-0.0172	-0.0226
4.00	0.0189	0.0148	0.0094	0.0055	-0.0042	-0.0090	-0.0152	-0.0199
3.00	0.0157	0.0122	0.0078	0.0046	-0.0034	-0.0075	-0.0126	-0.0165
2.00	0.0111	0.0087	0.0055	0.0032	-0.0024	-0.0053	-0.0089	-0.0117
1.50	0.0078	0.0061	0.0039	0.0023	-0.0017	-0.0037	-0.0063	-0.0083
1.00	0.0033	0.0025	0.0016	0.0010	-0.0007	-0.0016	-0.0026	-0.0034
0.85	0.0014	0.0011	0.0007	0.0004	-0.0003	-0.0007	-0.0011	-0.0015
0.75	0.0	0.0	0.0	0.0	0.0	0.0	0.0	0.0
0.60	0.0	0.0	0.0	0.0	0.0	0.0	0.0	0.0
0.50	0.0	0.0	0.0	0.0	0.0	0.0	0.0	0.0
0.46	0.0	0.0	0.0	0.0	0.0	0.0	0.0	0.0
0.40	0.0	0.0	0.0	0.0	0.0	0.0	0.0	0.0
0.36	0.0	0.0	0.0	0.0	0.0	0.0	0.0	0.0
0.30	0.0	0.0	0.0	0.0	0.0	0.0	0.0	0.0
0.24	0.0	0.0	0.0	0.0	0.0	0.0	0.0	0.0
0.20	0.0	0.0	0.0	0.0	0.0	0.0	0.0	0.0
0.17	0.0	0.0	0.0	0.0	0.0	0.0	0.0	0.0
0.15	0.0	0.0	0.0	0.0	0.0	0.0	0.0	0.0
0.12	0.0	0.0	0.0	0.0	0.0	0.0	0.0	0.0
0.10	0.0	0.0	0.0	0.0	0.0	0.0	0.0	0.0
0.09	0.0	0.0	0.0	0.0	0.0	0.0	0.0	0.0
0.07	0.0	0.0	0.0	0.0	0.0	0.0	0.0	0.0
0.06	0.0	0.0	0.0	0.0	0.0	0.0	0.0	0.0
0.05	0.0	0.0	0.0	0.0	0.0	0.0	0.0	0.0
0.04	0.0	0.0	0.0	0.0	0.0	0.0	0.0	0.0
0.03	0.0	0.0	0.0	0.0	0.0	0.0	0.0	0.0
0.02	0.0	0.0	0.0	0.0	0.0	0.0	0.0	0.0

Table 4-7b
Vertical g_2 values for separate damping levels
for equation (4.12), Abrahamson and Silva (1996)

Period (sec)	g2 (0.5%)	g2 (1.0%)	g2 (2.0%)	g2 (3.0%)	g2 (7.0%)	g2 (10.0%)	g2 (15.0%)	g2 (20.0%)
5.00	0.0247	0.0193	0.0122	0.0072	-0.0052	-0.0112	-0.0186	-0.0243
4.00	0.0218	0.0170	0.0107	0.0063	-0.0046	-0.0099	-0.0164	-0.0215
3.00	0.0181	0.0141	0.0089	0.0052	-0.0038	-0.0082	-0.0136	-0.0178
2.00	0.0128	0.0100	0.0063	0.0037	-0.0027	-0.0058	-0.0096	-0.0126
1.50	0.0090	0.0071	0.0044	0.0026	-0.0019	-0.0041	-0.0068	-0.0089
1.00	0.0038	0.0029	0.0018	0.0011	-0.0008	-0.0017	-0.0028	-0.0037
0.85	0.0016	0.0013	0.0008	0.0005	-0.0003	-0.0007	-0.0012	-0.0016
0.75	0.0	0.0	0.0	0.0	0.0	0.0	0.0	0.0
0.60	0.0	0.0	0.0	0.0	0.0	0.0	0.0	0.0
0.50	0.0	0.0	0.0	0.0	0.0	0.0	0.0	0.0
0.46	0.0	0.0	0.0	0.0	0.0	0.0	0.0	0.0
0.40	0.0	0.0	0.0	0.0	0.0	0.0	0.0	0.0
0.36	0.0	0.0	0.0	0.0	0.0	0.0	0.0	0.0
0.30	0.0	0.0	0.0	0.0	0.0	0.0	0.0	0.0
0.24	0.0	0.0	0.0	0.0	0.0	0.0	0.0	0.0
0.20	0.0	0.0	0.0	0.0	0.0	0.0	0.0	0.0
0.17	0.0	0.0	0.0	0.0	0.0	0.0	0.0	0.0
0.15	0.0	0.0	0.0	0.0	0.0	0.0	0.0	0.0
0.12	0.0	0.0	0.0	0.0	0.0	0.0	0.0	0.0
0.10	0.0	0.0	0.0	0.0	0.0	0.0	0.0	0.0
0.09	0.0	0.0	0.0	0.0	0.0	0.0	0.0	0.0
0.07	0.0	0.0	0.0	0.0	0.0	0.0	0.0	0.0
0.06	0.0	0.0	0.0	0.0	0.0	0.0	0.0	0.0
0.05	0.0	0.0	0.0	0.0	0.0	0.0	0.0	0.0
0.04	0.0	0.0	0.0	0.0	0.0	0.0	0.0	0.0
0.03	0.0	0.0	0.0	0.0	0.0	0.0	0.0	0.0
0.02	0.0	0.0	0.0	0.0	0.0	0.0	0.0	0.0

Table 4-8a
Horizontal g_3 values for separate damping levels
for equation (4.12), Abrahamson and Silva (1996)

Period (sec)	g3 (0.5%)	g3 (1.0%)	g3 (2.0%)	g3 (3.0%)	g3 (7.0%)	g3 (10.0%)	g3 (15.0%)	g3 (20.0%)
5.00	-0.0166	-0.0130	-0.0082	-0.0049	0.0036	0.0079	0.0133	0.0175
4.00	-0.0146	-0.0114	-0.0072	-0.0043	0.0032	0.0070	0.0117	0.0154
3.00	-0.0121	-0.0095	-0.0060	-0.0036	0.0027	0.0058	0.0097	0.0128
2.00	-0.0086	-0.0067	-0.0042	-0.0025	0.0019	0.0041	0.0069	0.0090
1.50	-0.0061	-0.0047	-0.0030	-0.0018	0.0013	0.0029	0.0049	0.0064
1.00	-0.0025	-0.0020	-0.0012	-0.0007	0.0006	0.0012	0.0020	0.0027
0.85	-0.0011	-0.0009	-0.0005	-0.0003	0.0002	0.0005	0.0009	0.0012
0.75	0.0	0.0	0.0	0.0	0.0	0.0	0.0	0.0
0.60	0.0	0.0	0.0	0.0	0.0	0.0	0.0	0.0
0.50	0.0	0.0	0.0	0.0	0.0	0.0	0.0	0.0
0.46	0.0	0.0	0.0	0.0	0.0	0.0	0.0	0.0
0.40	0.0	0.0	0.0	0.0	0.0	0.0	0.0	0.0
0.36	0.0	0.0	0.0	0.0	0.0	0.0	0.0	0.0
0.30	0.0	0.0	0.0	0.0	0.0	0.0	0.0	0.0
0.24	0.0	0.0	0.0	0.0	0.0	0.0	0.0	0.0
0.20	0.0	0.0	0.0	0.0	0.0	0.0	0.0	0.0
0.17	0.0	0.0	0.0	0.0	0.0	0.0	0.0	0.0
0.15	0.0	0.0	0.0	0.0	0.0	0.0	0.0	0.0
0.12	0.0	0.0	0.0	0.0	0.0	0.0	0.0	0.0
0.10	0.0	0.0	0.0	0.0	0.0	0.0	0.0	0.0
0.09	0.0	0.0	0.0	0.0	0.0	0.0	0.0	0.0
0.07	0.0	0.0	0.0	0.0	0.0	0.0	0.0	0.0
0.06	0.0	0.0	0.0	0.0	0.0	0.0	0.0	0.0
0.05	0.0	0.0	0.0	0.0	0.0	0.0	0.0	0.0
0.04	0.0	0.0	0.0	0.0	0.0	0.0	0.0	0.0
0.03	0.0	0.0	0.0	0.0	0.0	0.0	0.0	0.0
0.02	0.0	0.0	0.0	0.0	0.0	0.0	0.0	0.0

Table 4-8b
Vertical g_3 values for separate damping levels
for equation (4.12), Abrahamson and Silva (1996)

Period (sec)	g3 (0.5%)	g3 (1.0%)	g3 (2.0%)	g3 (3.0%)	g3 (7.0%)	g3 (10.0%)	g3 (15.0%)	g3 (20.0%)
5.00	-0.0191	-0.0150	-0.0094	-0.0055	0.0040	0.0087	0.0144	0.0188
4.00	-0.0169	-0.0132	-0.0083	-0.0049	0.0036	0.0076	0.0127	0.0166
3.00	-0.0140	-0.0109	-0.0069	-0.0040	0.0029	0.0063	0.0105	0.0138
2.00	-0.0099	-0.0077	-0.0049	-0.0029	0.0021	0.0045	0.0075	0.0097
1.50	-0.0070	-0.0055	-0.0034	-0.0020	0.0015	0.0032	0.0053	0.0069
1.00	-0.0029	-0.0023	-0.0014	-0.0008	0.0006	0.0013	0.0022	0.0029
0.85	-0.0013	-0.0010	-0.0006	-0.0004	0.0003	0.0006	0.0010	0.0012
0.75	0.0	0.0	0.0	0.0	0.0	0.0	0.0	0.0
0.60	0.0	0.0	0.0	0.0	0.0	0.0	0.0	0.0
0.50	0.0	0.0	0.0	0.0	0.0	0.0	0.0	0.0
0.46	0.0	0.0	0.0	0.0	0.0	0.0	0.0	0.0
0.40	0.0	0.0	0.0	0.0	0.0	0.0	0.0	0.0
0.36	0.0	0.0	0.0	0.0	0.0	0.0	0.0	0.0
0.30	0.0	0.0	0.0	0.0	0.0	0.0	0.0	0.0
0.24	0.0	0.0	0.0	0.0	0.0	0.0	0.0	0.0
0.20	0.0	0.0	0.0	0.0	0.0	0.0	0.0	0.0
0.17	0.0	0.0	0.0	0.0	0.0	0.0	0.0	0.0
0.15	0.0	0.0	0.0	0.0	0.0	0.0	0.0	0.0
0.12	0.0	0.0	0.0	0.0	0.0	0.0	0.0	0.0
0.10	0.0	0.0	0.0	0.0	0.0	0.0	0.0	0.0
0.09	0.0	0.0	0.0	0.0	0.0	0.0	0.0	0.0
0.07	0.0	0.0	0.0	0.0	0.0	0.0	0.0	0.0
0.06	0.0	0.0	0.0	0.0	0.0	0.0	0.0	0.0
0.05	0.0	0.0	0.0	0.0	0.0	0.0	0.0	0.0
0.04	0.0	0.0	0.0	0.0	0.0	0.0	0.0	0.0
0.03	0.0	0.0	0.0	0.0	0.0	0.0	0.0	0.0
0.02	0.0	0.0	0.0	0.0	0.0	0.0	0.0	0.0

Table 4-9
Coefficients for Equation (4.13), Idriss (1993)

Period - sec	a_1	b_1	a_2	b_2
0.03	1	0	1	0
0.05	1.1142	0.0709	1.0830	0.0505
0.075	1.3513	0.2183	1.2902	0.1803
0.1	1.4918	0.3056	1.4179	0.2597
0.15	1.5796	0.3601	1.4992	0.3102
0.2	1.6148	0.3820	1.5340	0.3318
0.25	1.6148	0.3820	1.5340	0.3318
0.3	1.6148	0.3820	1.5340	0.3318
0.35	1.6060	0.3765	1.5224	0.3246
0.4	1.5972	0.3711	1.5108	.03174
0.5	1.5796	0.3605	1.4992	0.3102
0.6	1.5445	0.3383	1.4876	0.303
0.7	1.5269	0.3274	1.4876	0.303
0.8	1.5094	0.3165	1.4760	0.2958
0.9	1.4918	0.3056	1.4690	0.2914
1	1.4742	0.2947	1.4644	0.2885
1.5	1.4391	0.2728	1.4644	0.2885
2	1.4216	0.2619	1.4644	0.2885
3	1.4040	0.2510	1.4644	0.2885
4	1.4040	0.2510	1.4644	02885
5	1.4040	0.2510	1.4644	0.2885

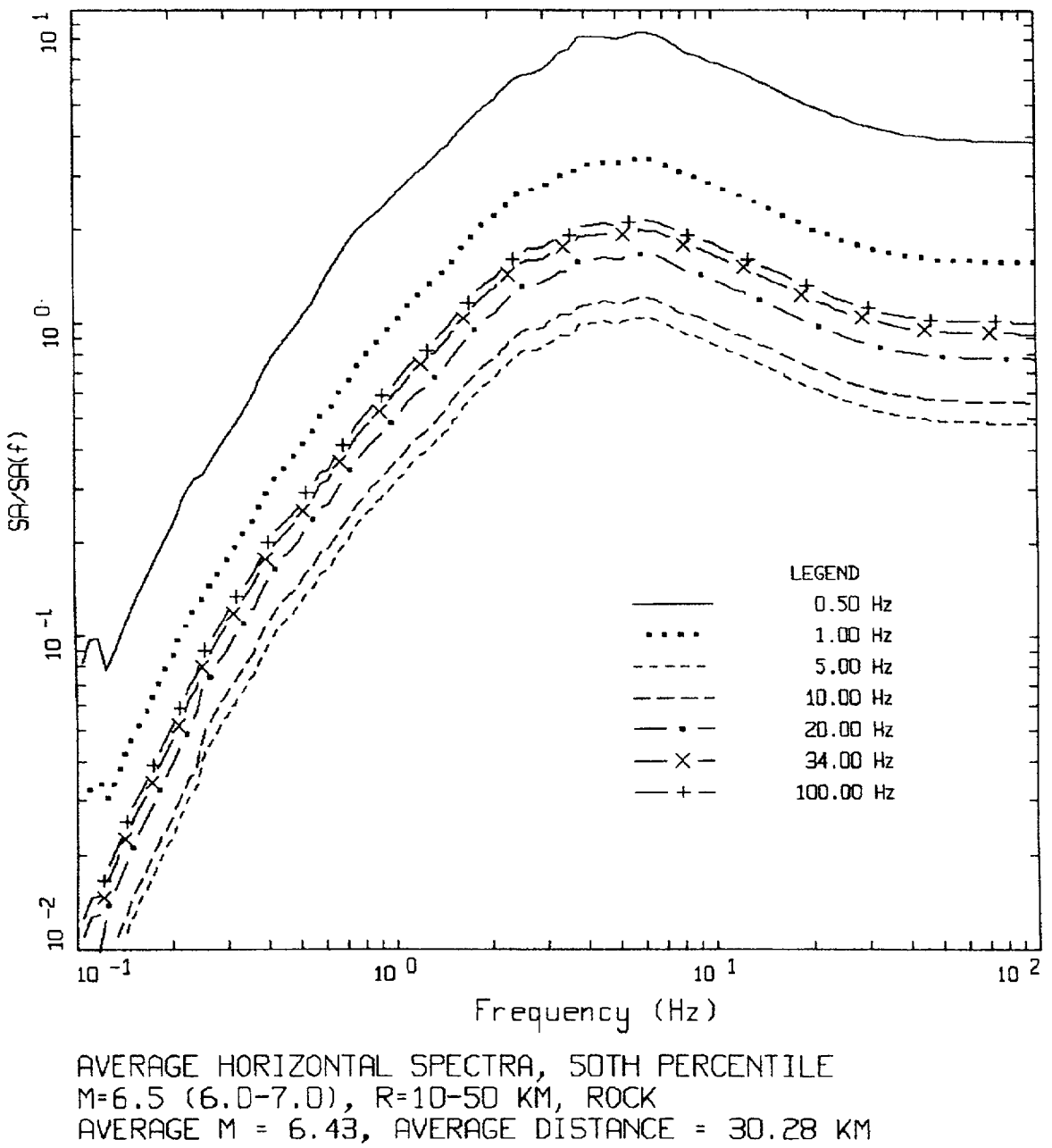

Figure 4-1. Response spectral shapes (5% damping) for the **M** 6.5, R = 10 to 50 km bins normalized by spectral ordinates at a suite of frequencies (0.5 to 100.0 Hz)

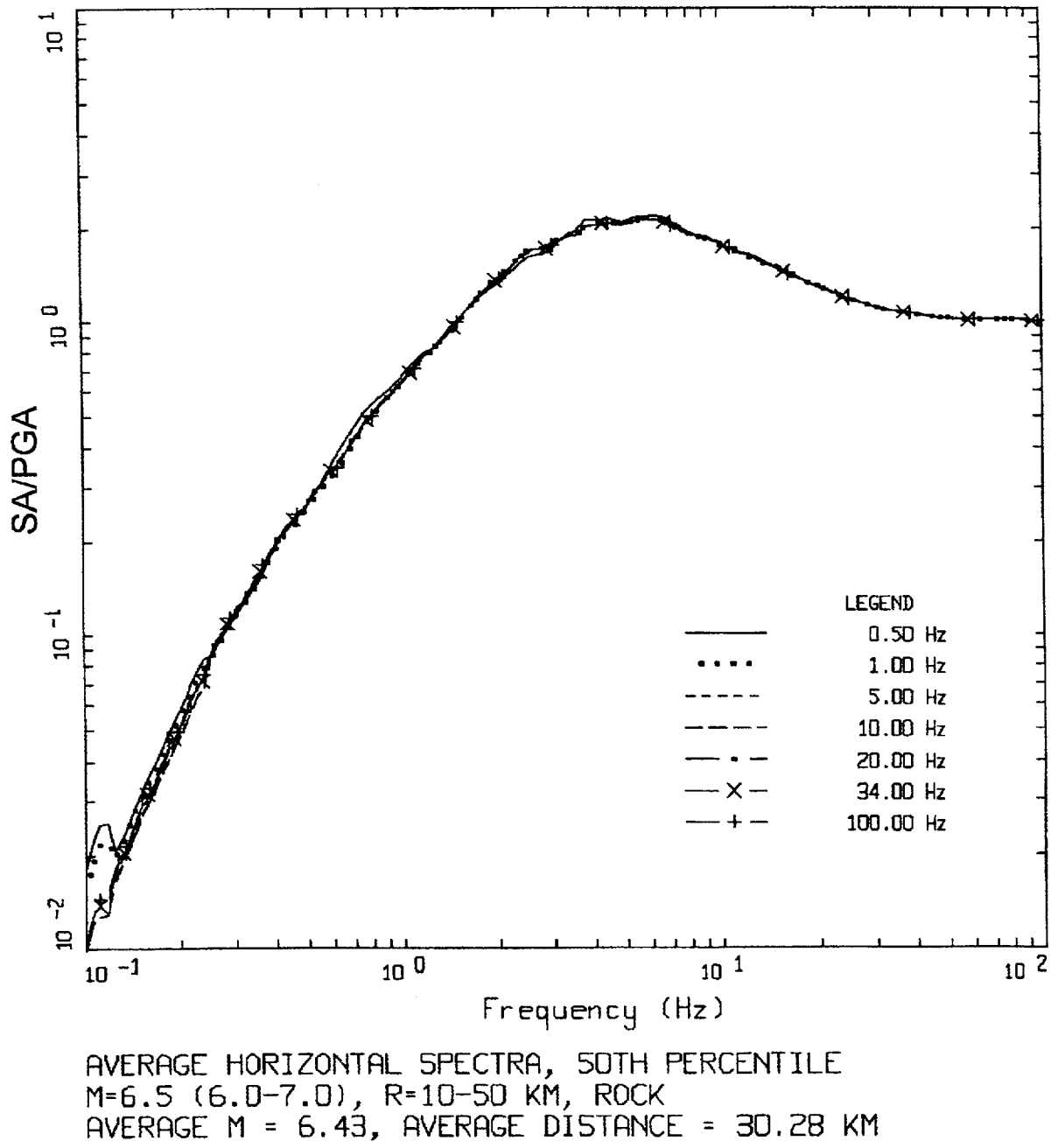

Figure 4-2. Response spectral shapes (5% damping) for the **M** 6.5, R = 10 to 50 km bins from Figure 1 renormalized by their respective 100 Hz values.

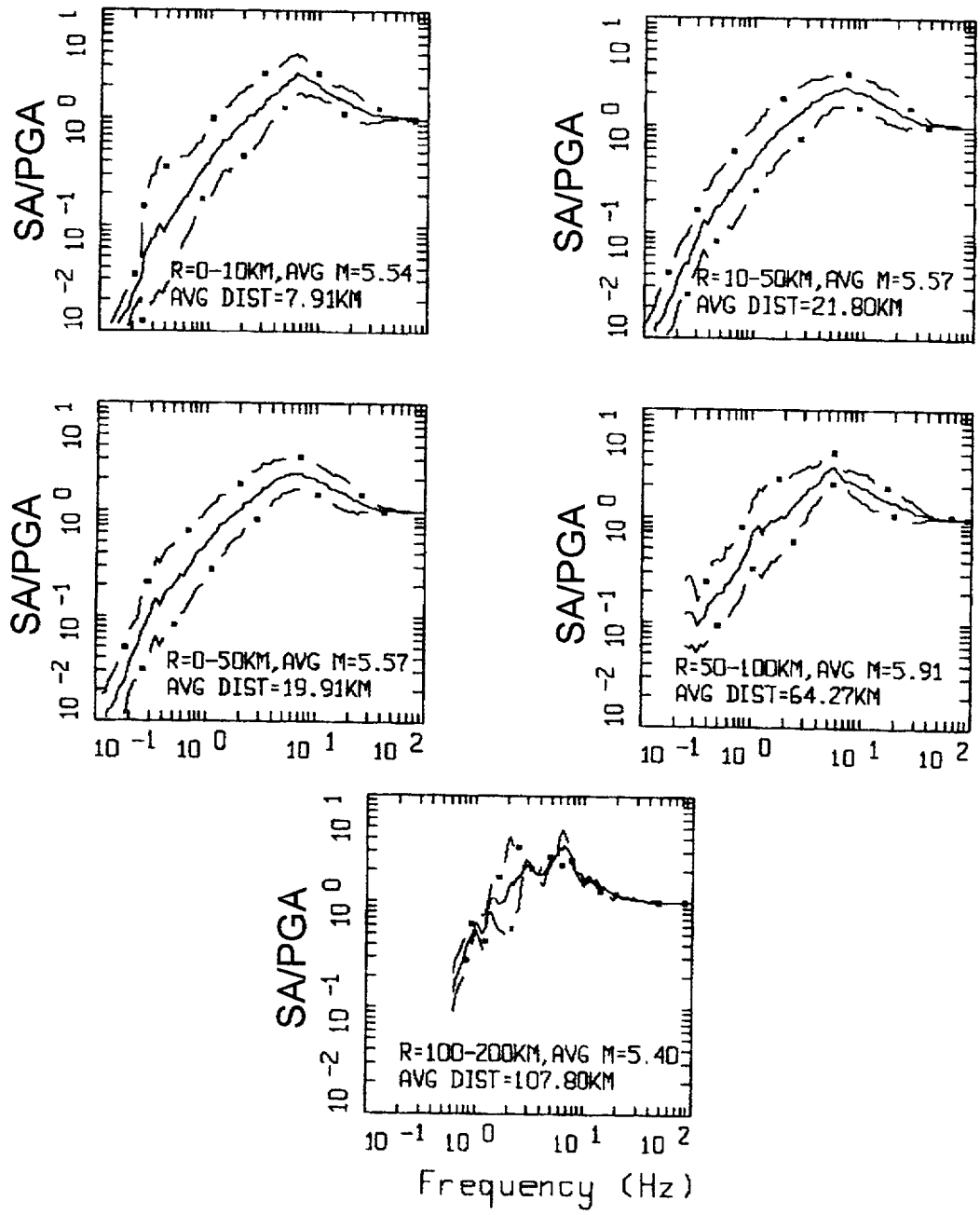

Figure 4-3. Response spectral shapes (5% damping) computed for the **M** = 5.5 magnitude bin for WUS soft rock site conditions.

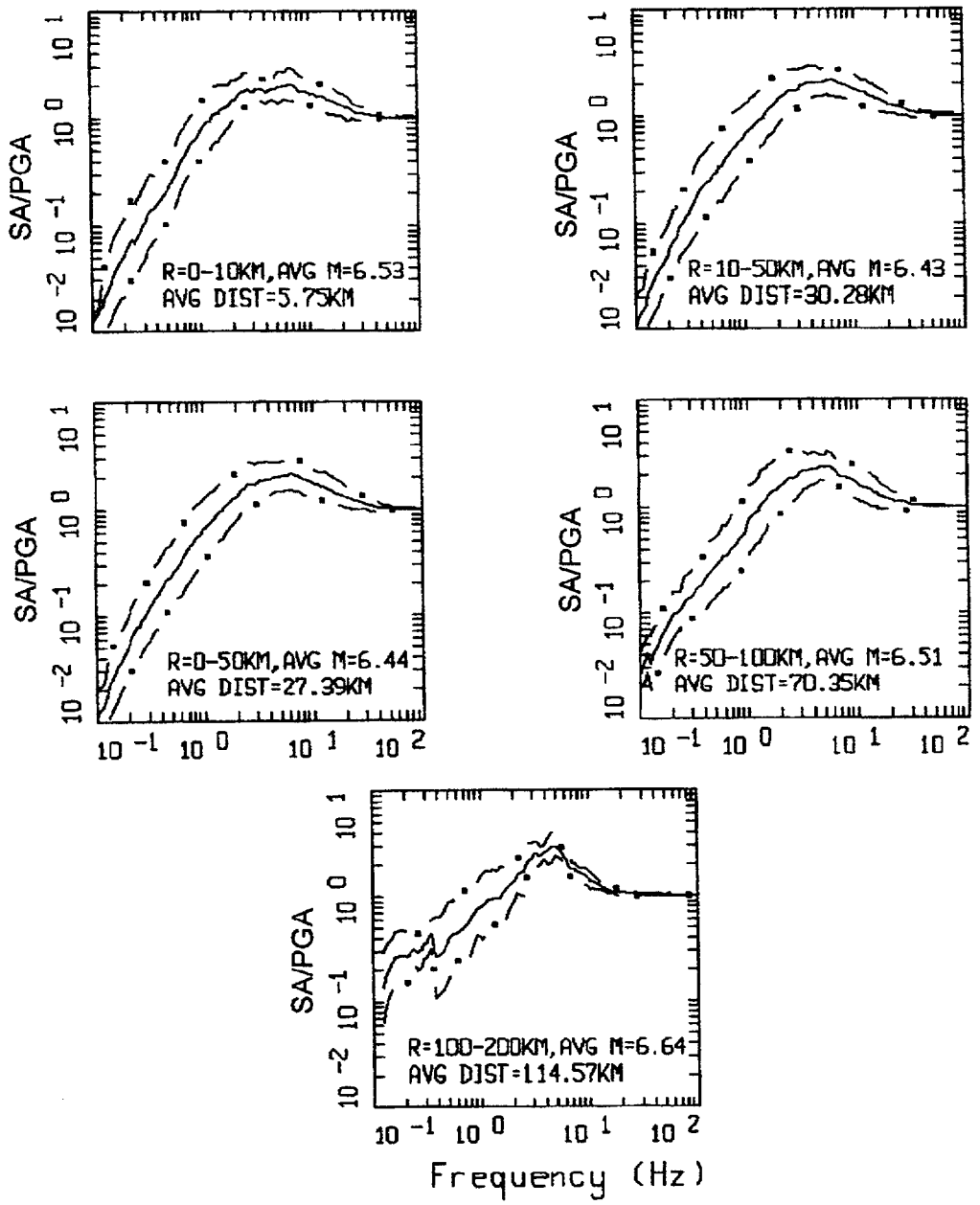

Figure 4-4. Response spectral shapes (5% damping) computed for the **M** = 6.5 magnitude bin for WUS soft rock site conditions.

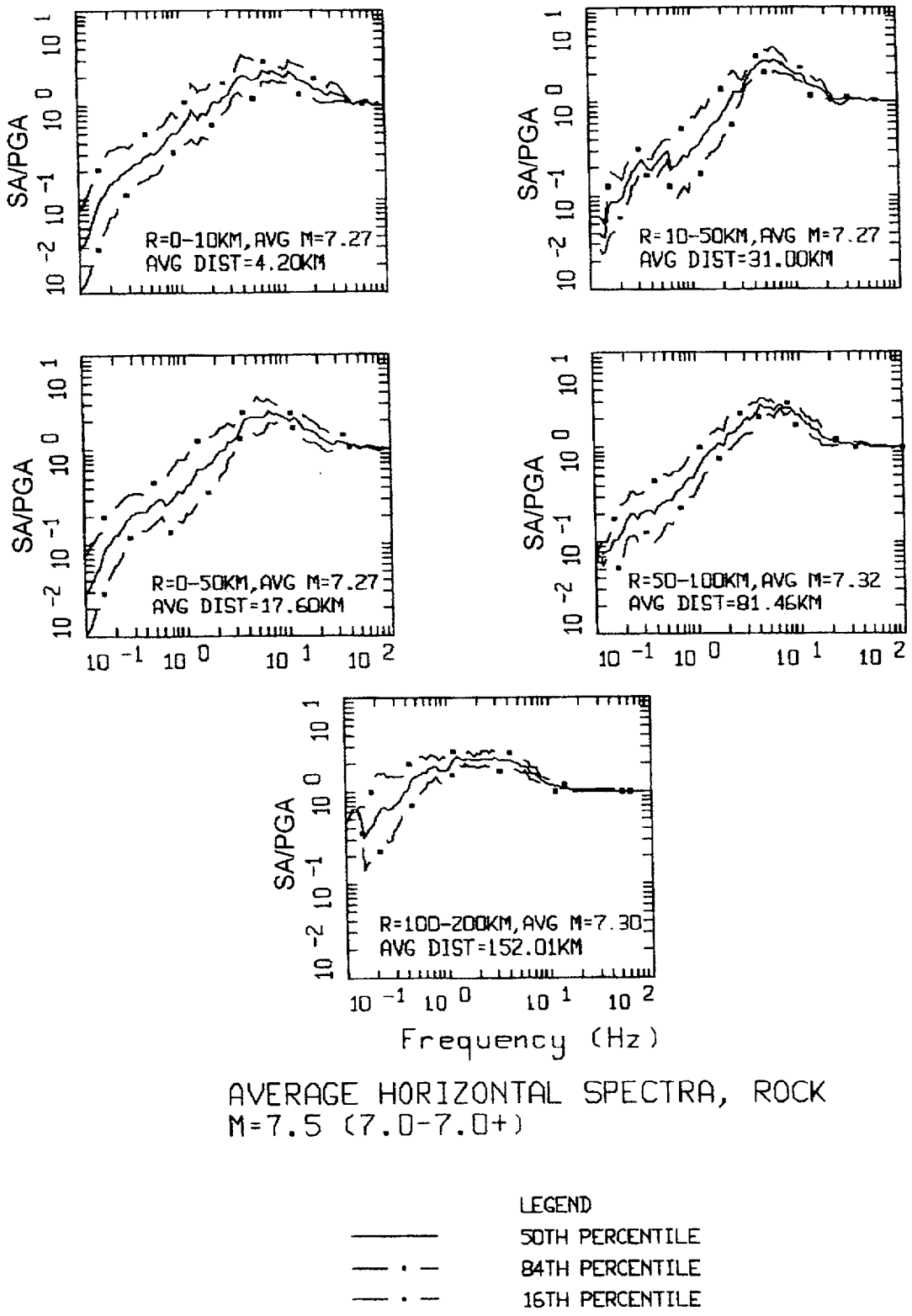

Figure 4-5. Response spectral shapes (5% damping) computed for the **M** = 7.5 magnitude bins for WUS soft rock site conditions.

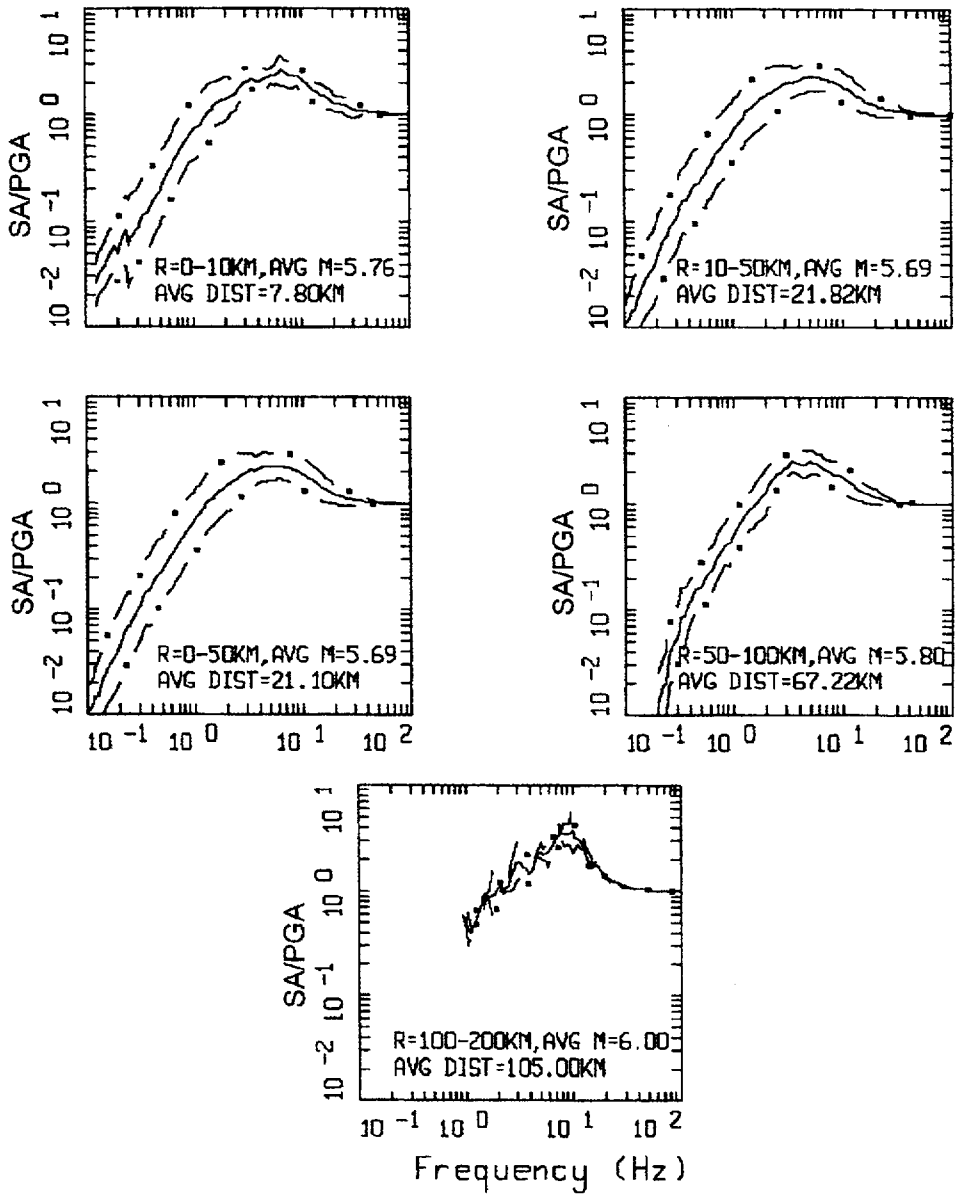

Figure 4-6. Response to spectral shapes (5% damping) computed for the **M** = 5.5 magnitude bins for WUS deep soil site conditions.

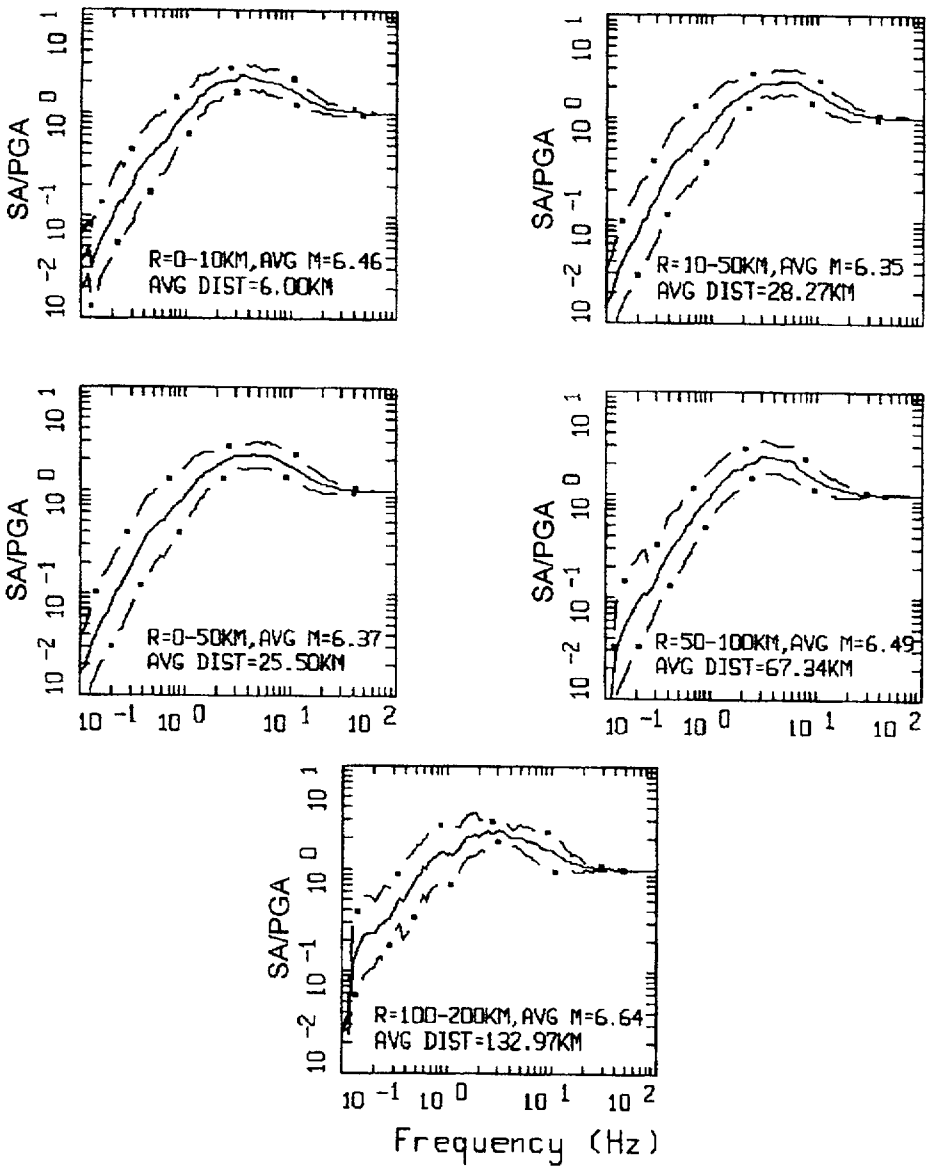

Figure 4-7. Response spectral shapes (5% damping) computed for the **M** = 6.5 magnitude bin for WUS deep soil conditions.

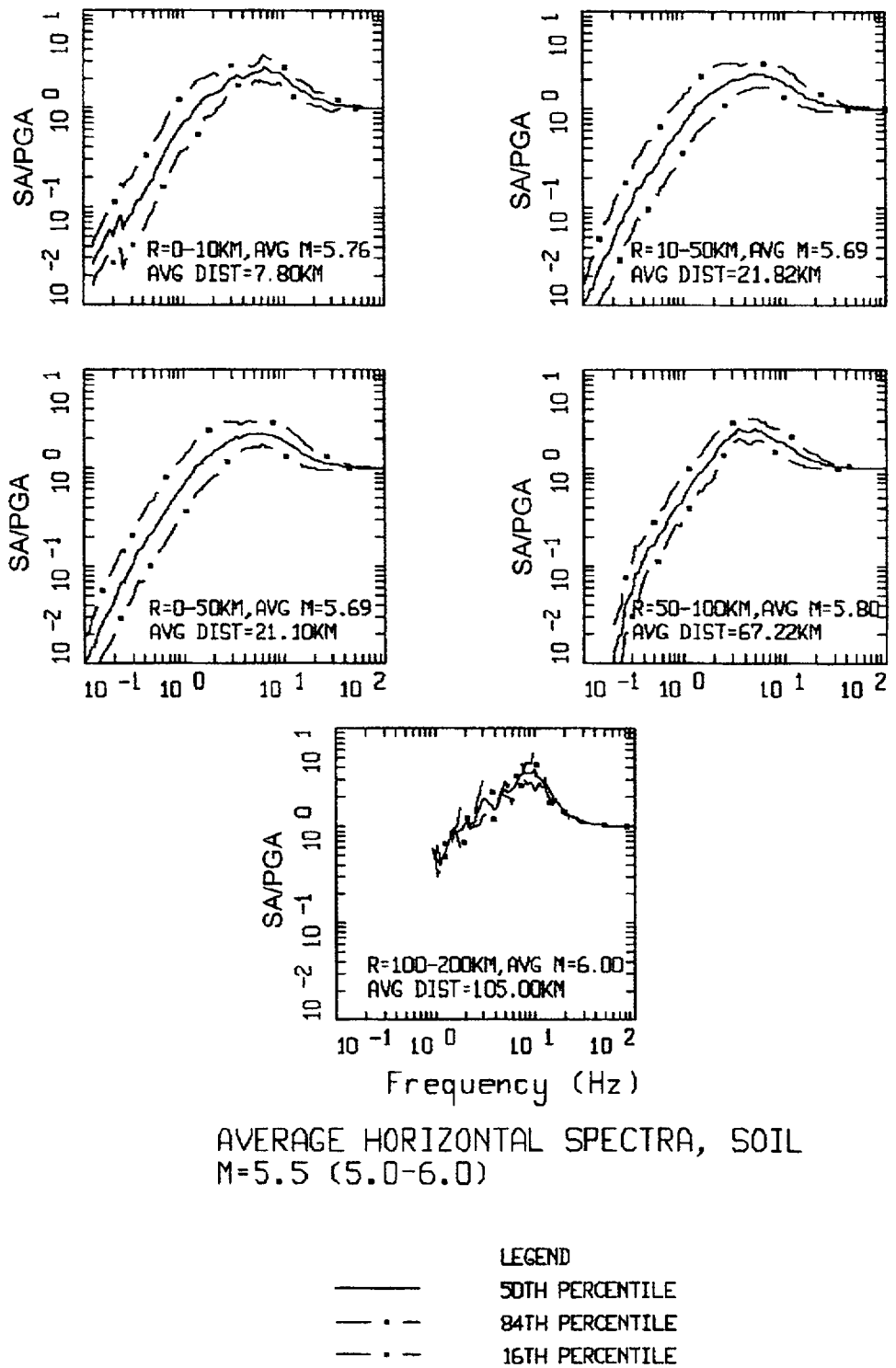

Figure 4-8. Response spectral shapes (5% damping) computed for the **M** = 7.5 magnitude bin for WUS deep soil conditions.

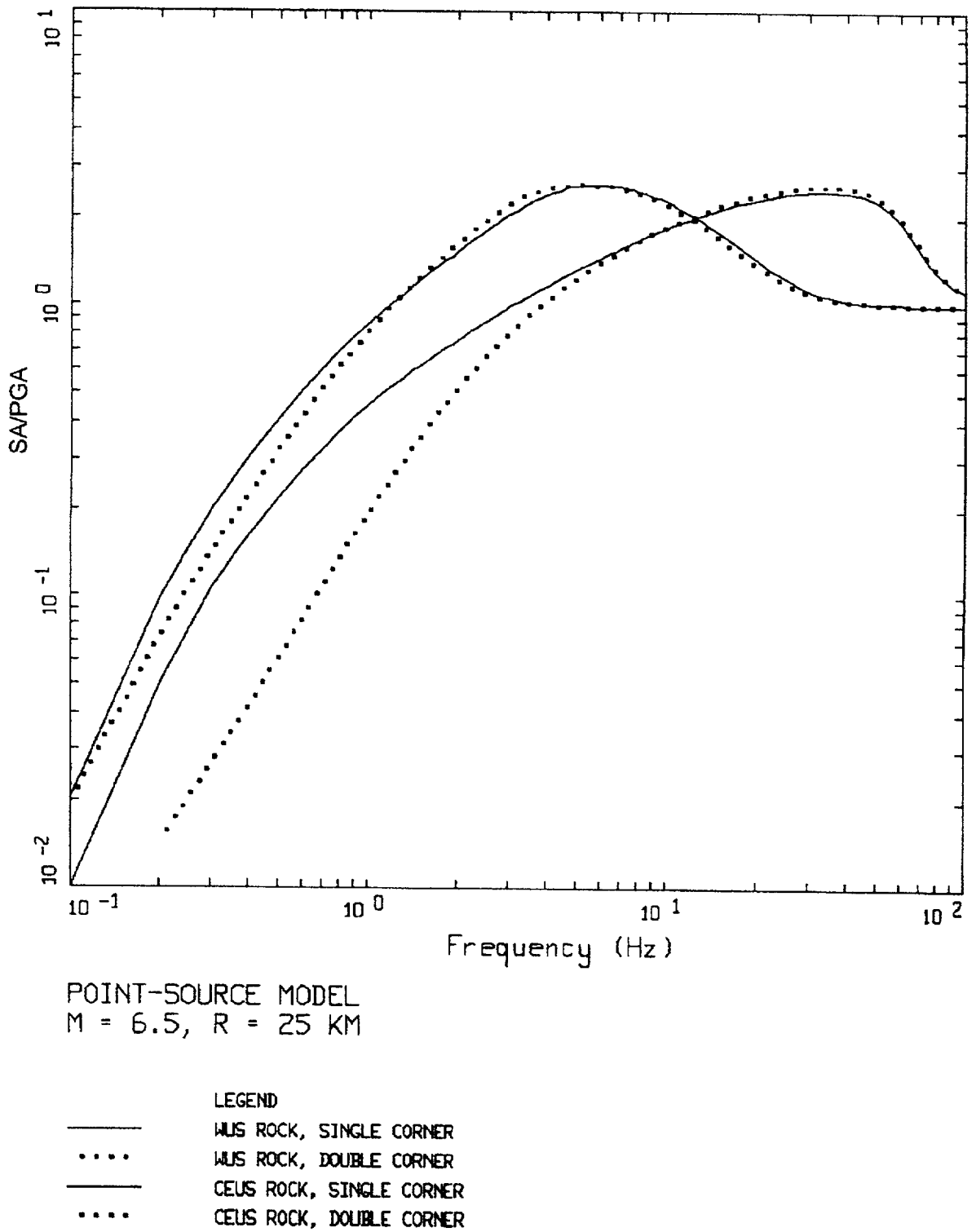

Figure 4-9. Response spectral shapes (5% damping) computed for **M** = 6.5 at R = 25 km using both single and double corner frequency source spectra for WUS and CEUS conditions.

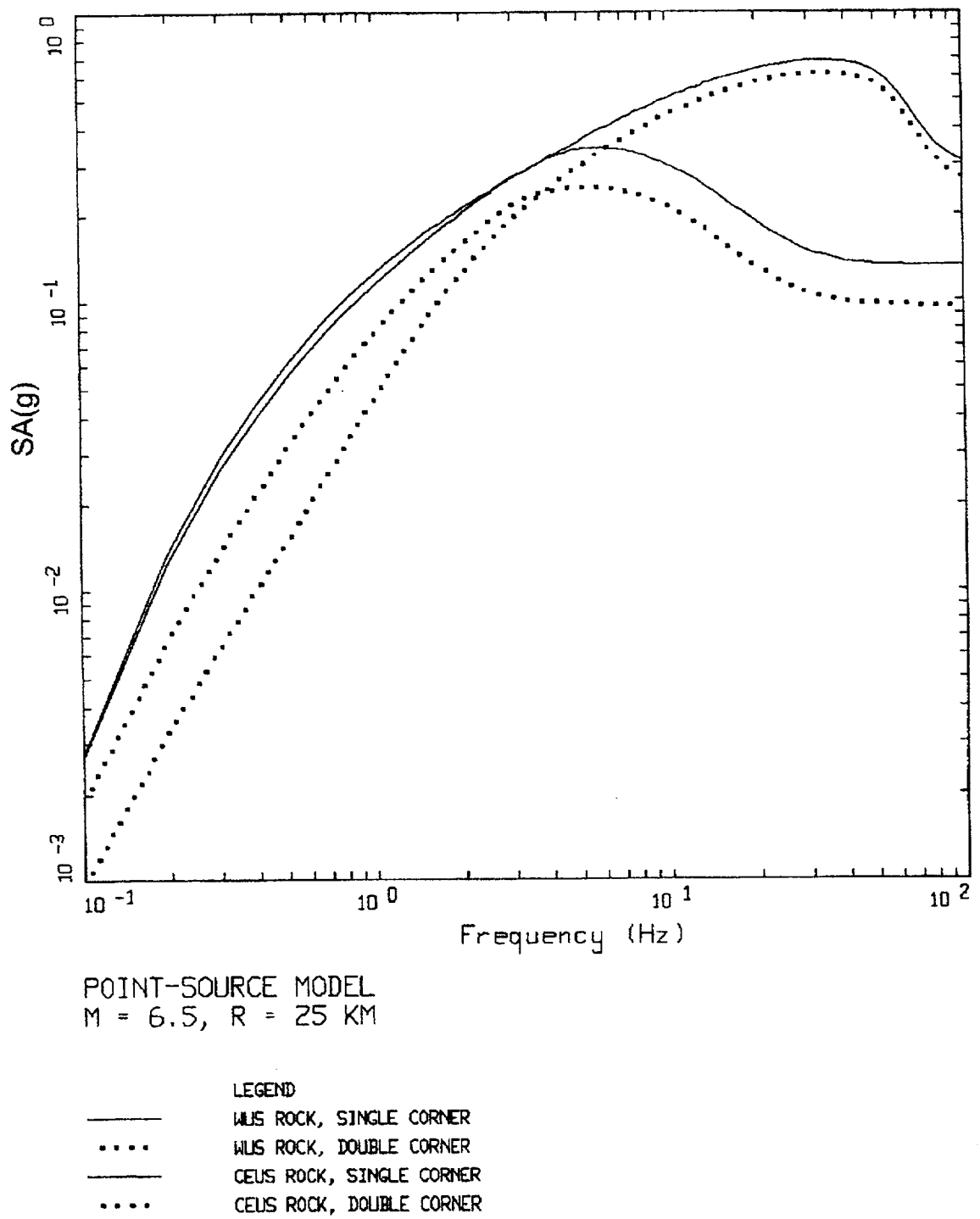

Figure 4-10. Absolute response spectra (5% damping) computed for **M** = 6.5 at R = 25 km using both single and double corner frequency source spectra for WUS and CEUS conditions.

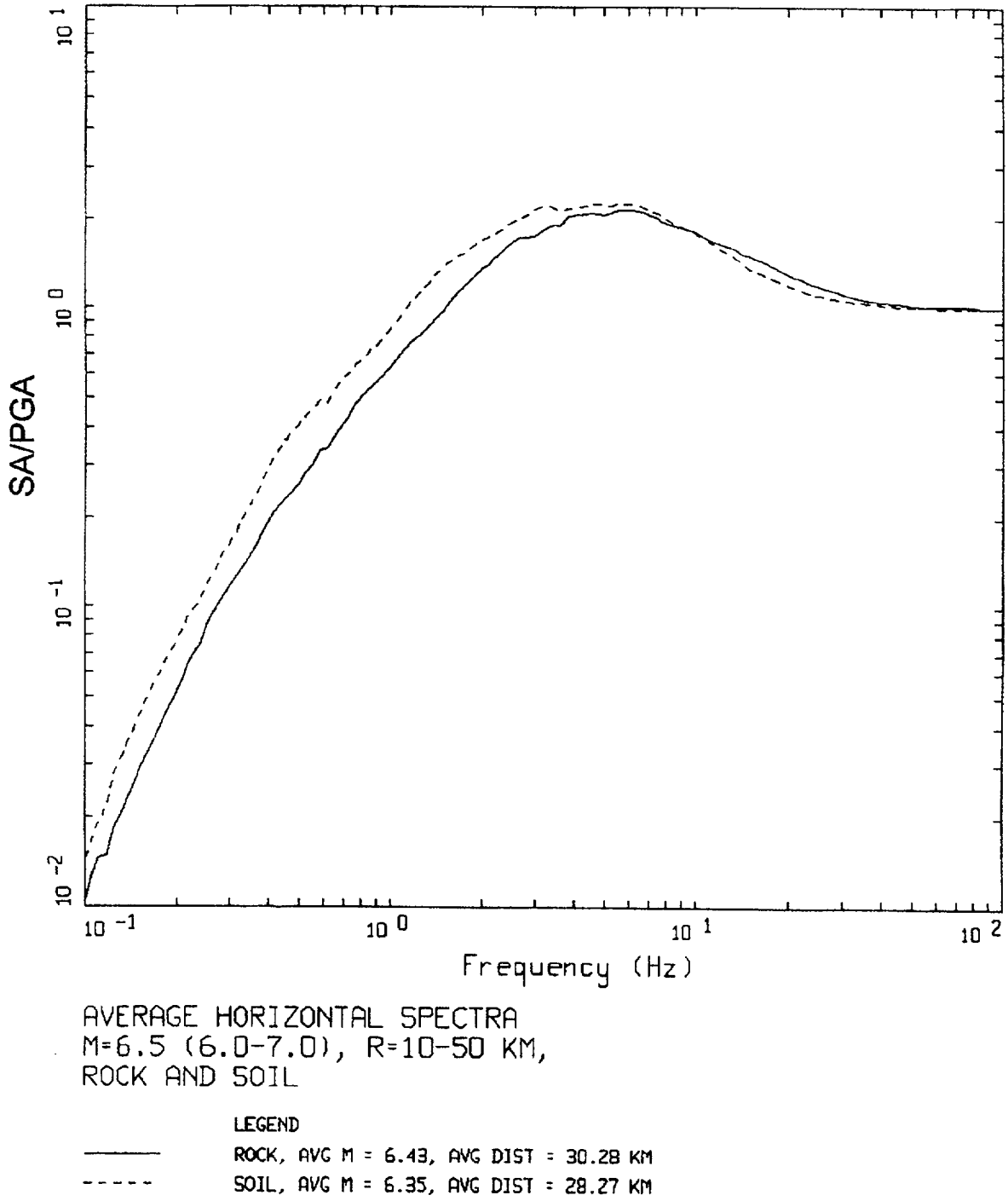

Figure 4-11. Comparison of WUS statistical response spectral shapes (5% damping) for the **M** 6.5, R = 10 to 50 km bins for rock and deep soil site conditions.

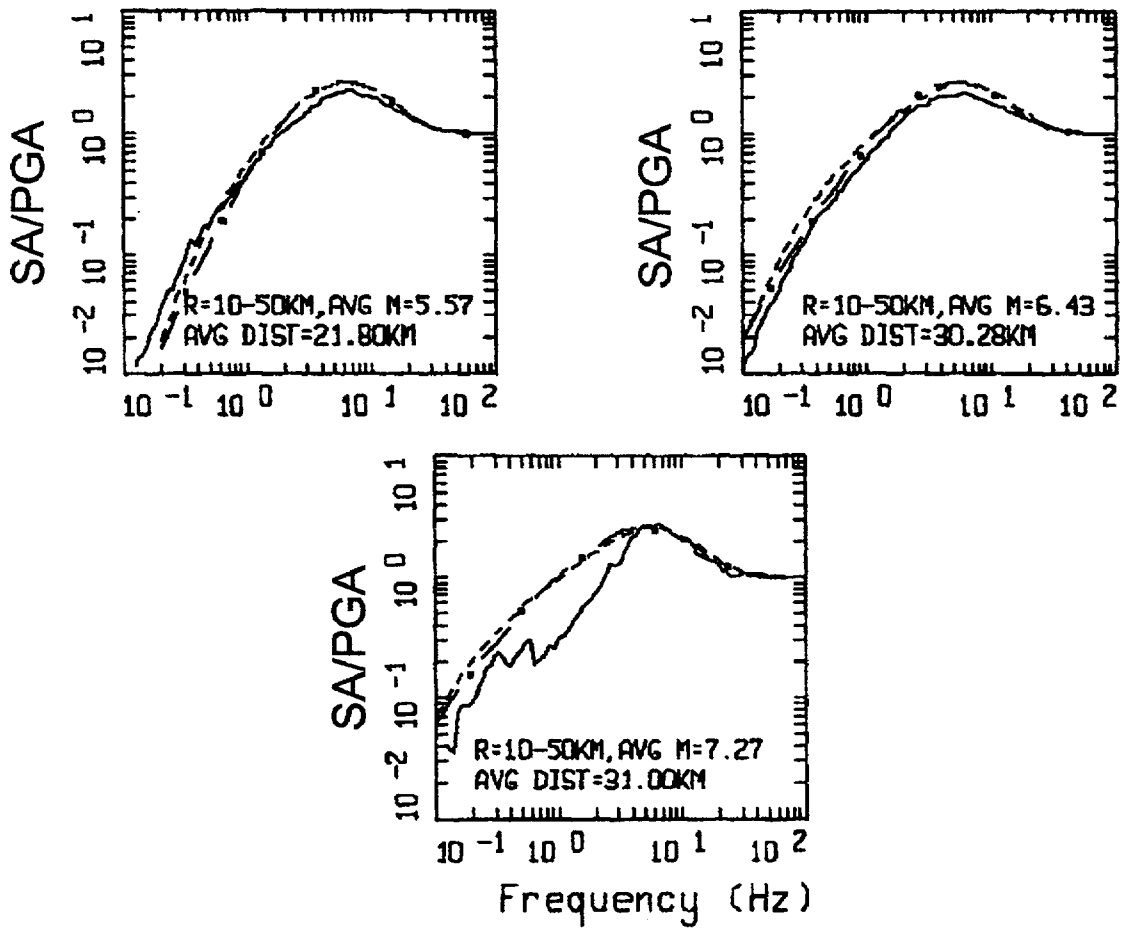

Figure 4-12. Response spectral shapes (5% damping) computed for the **M** = 5.5 to 7.5, R = 10 to 50 km bins for WUS rock site conditions.

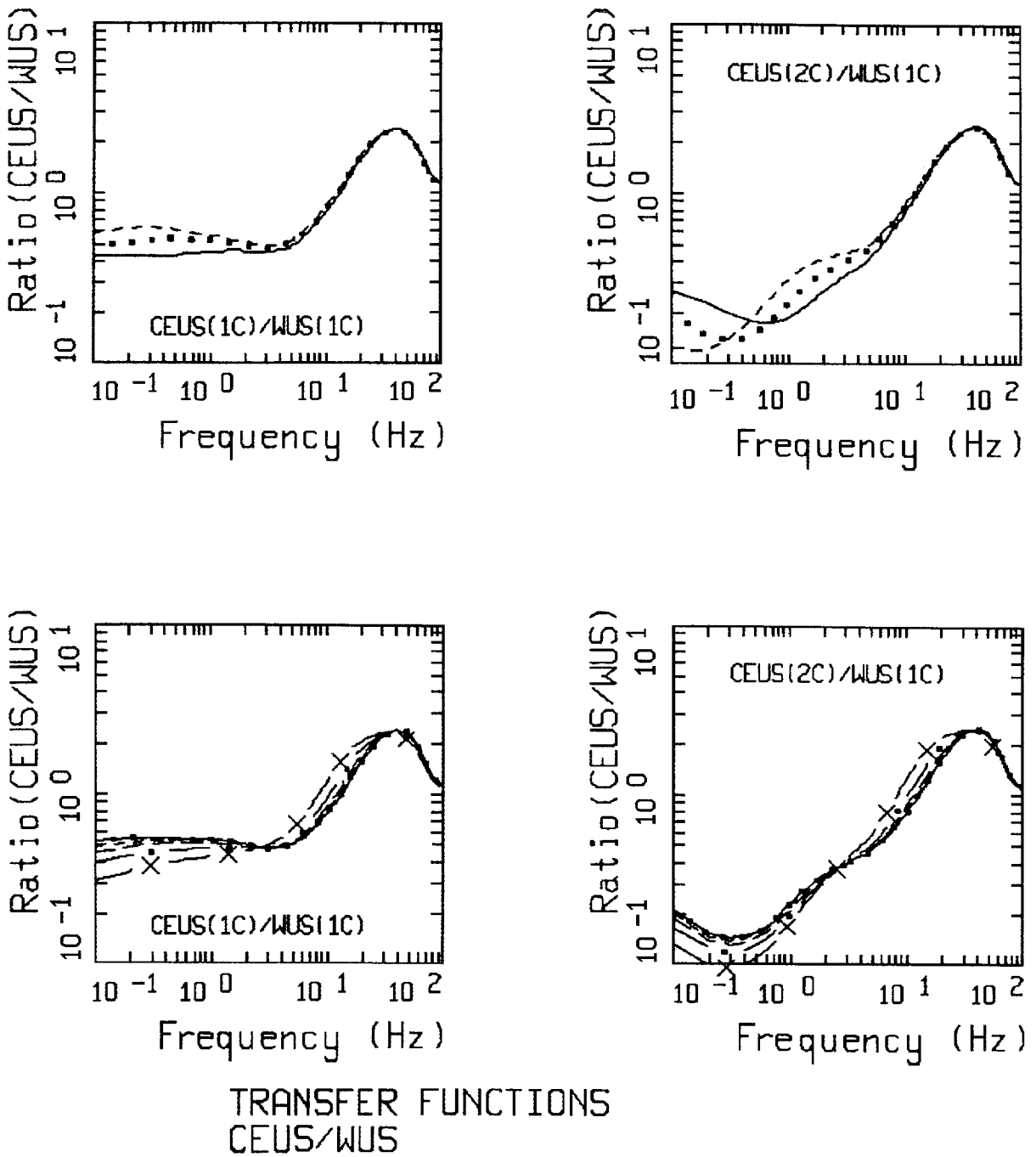

Figure 4-13. WUS to CEUS transfer functions. Top, magnitude dependencies at a distance of 25 km; bottom, distance dependencies for **M** 6.5.

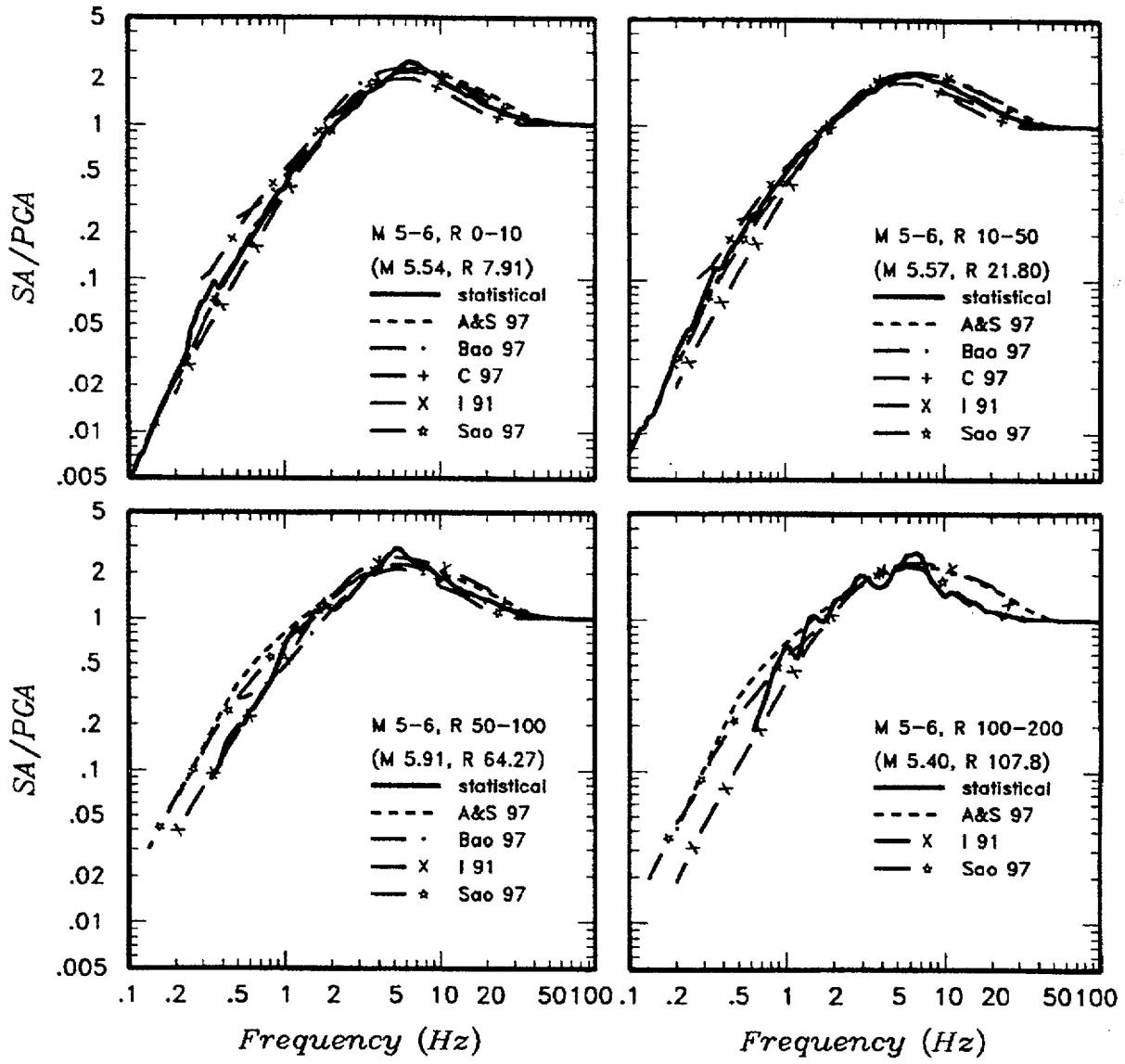

Figure 4-14. Comparison of the statistical shapes from Figures 3 to 5 with spectral shapes predicted by the attenuation relationships of Abrahamson and Silva (1997) [A&S 97], Boore and others (1997) [Bao 97], Campbell (1997) [C 97], Idriss (1991) [I 91], and Sadigh and others (1997) [Sao 97].

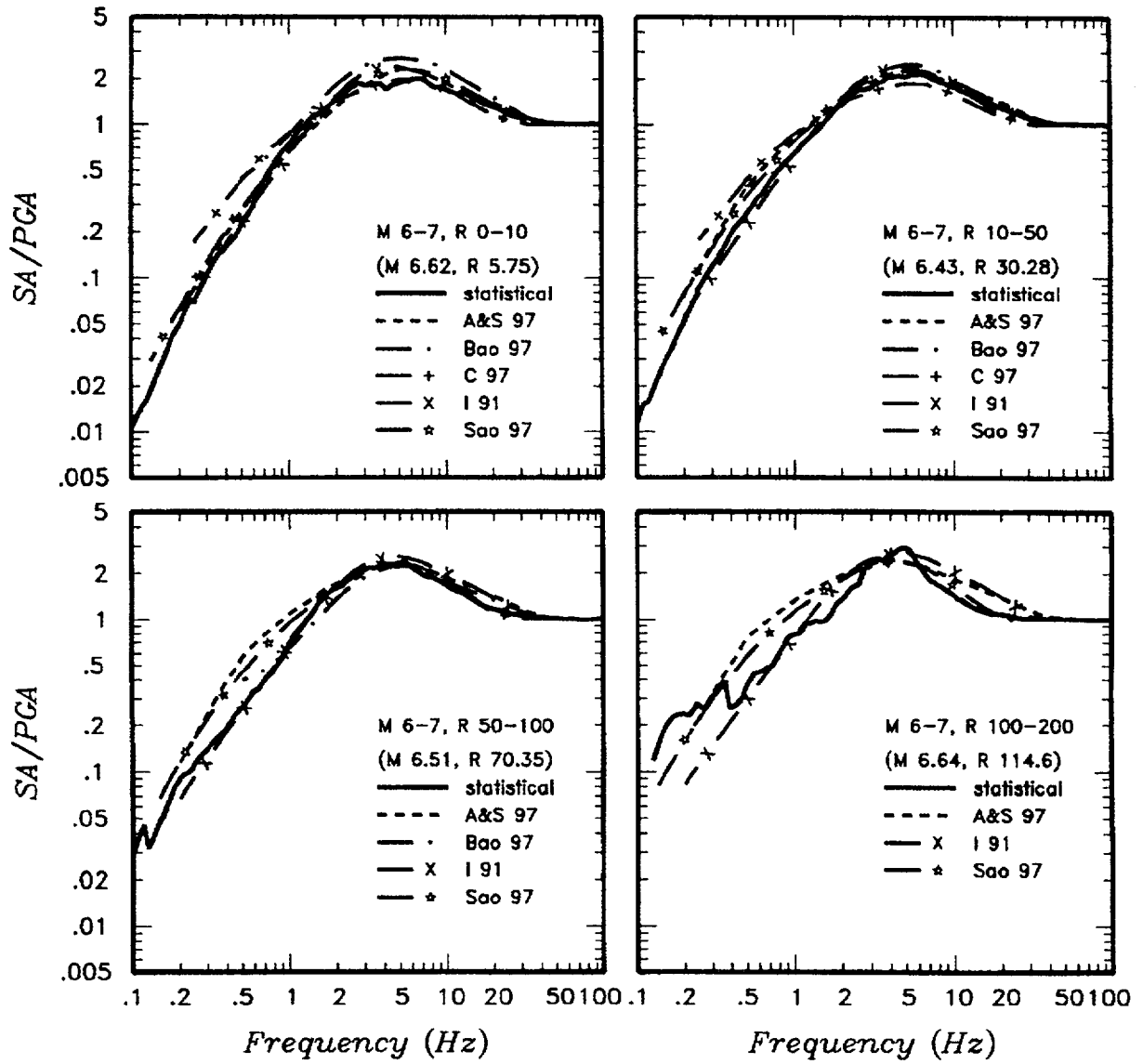

Figure 4-14b. (Continued)

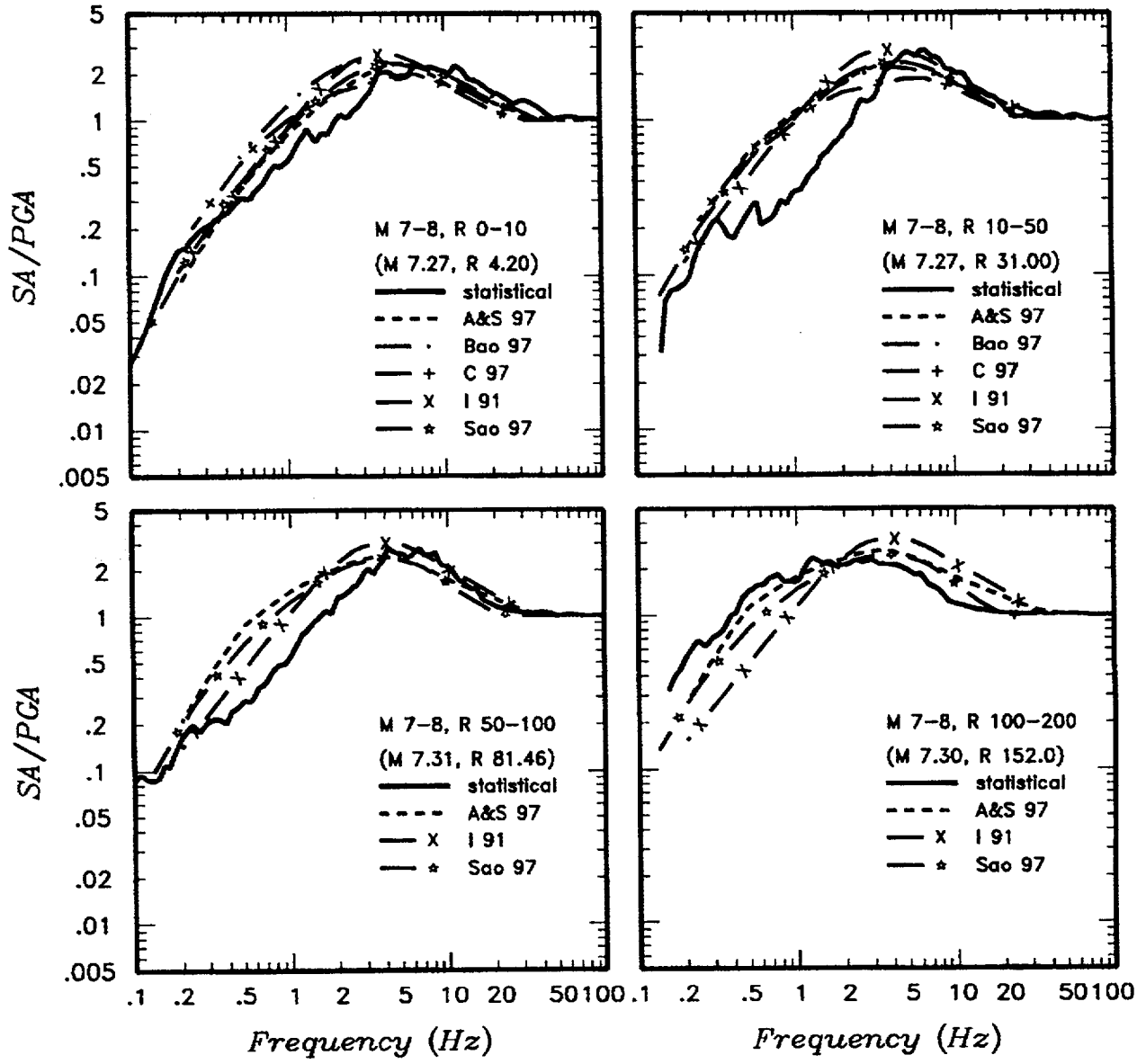

Figure 4-14c. (Continued)

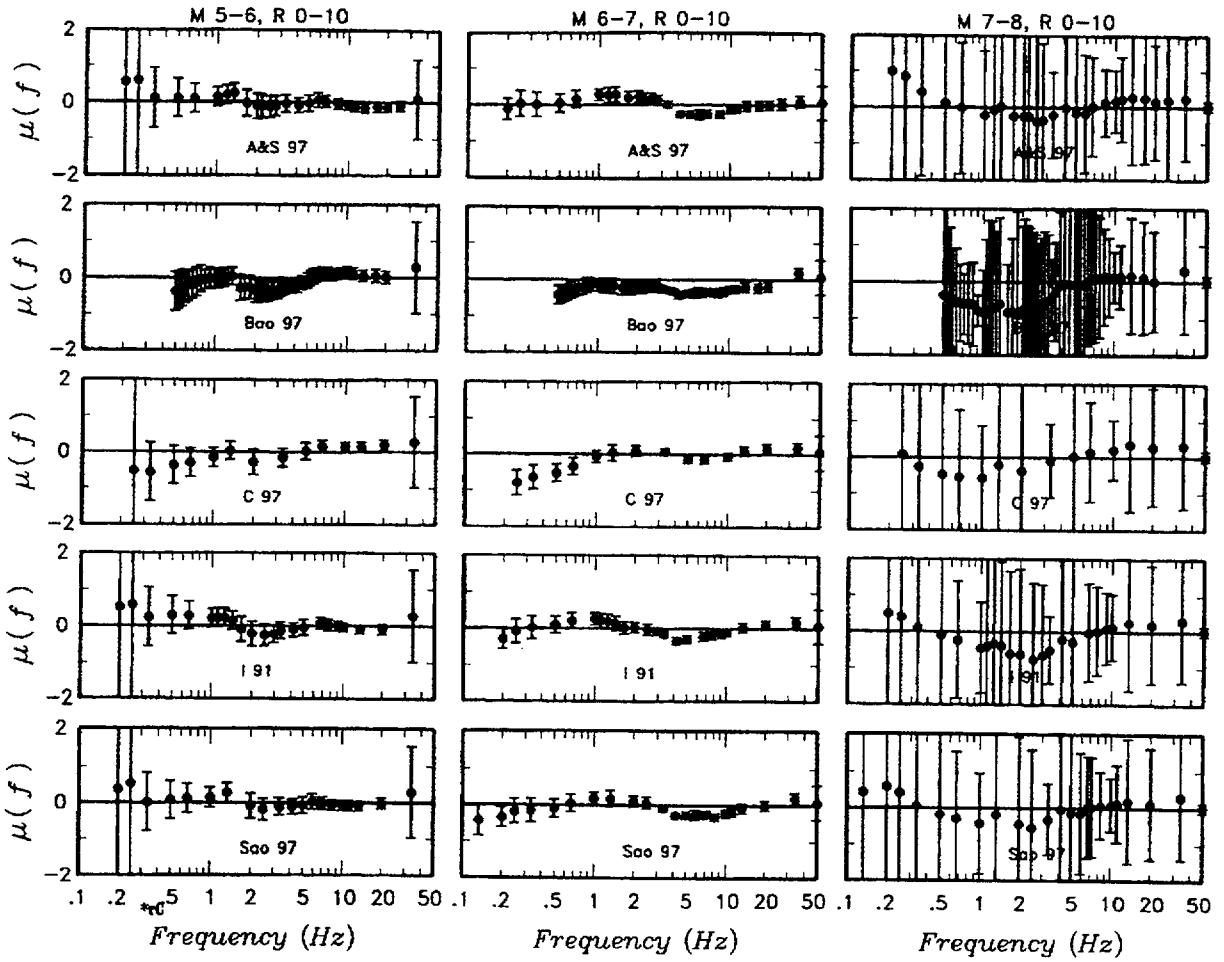

Figure 4-15. Mean residuals and their 90% confidence intervals for the five attenuation relationships.

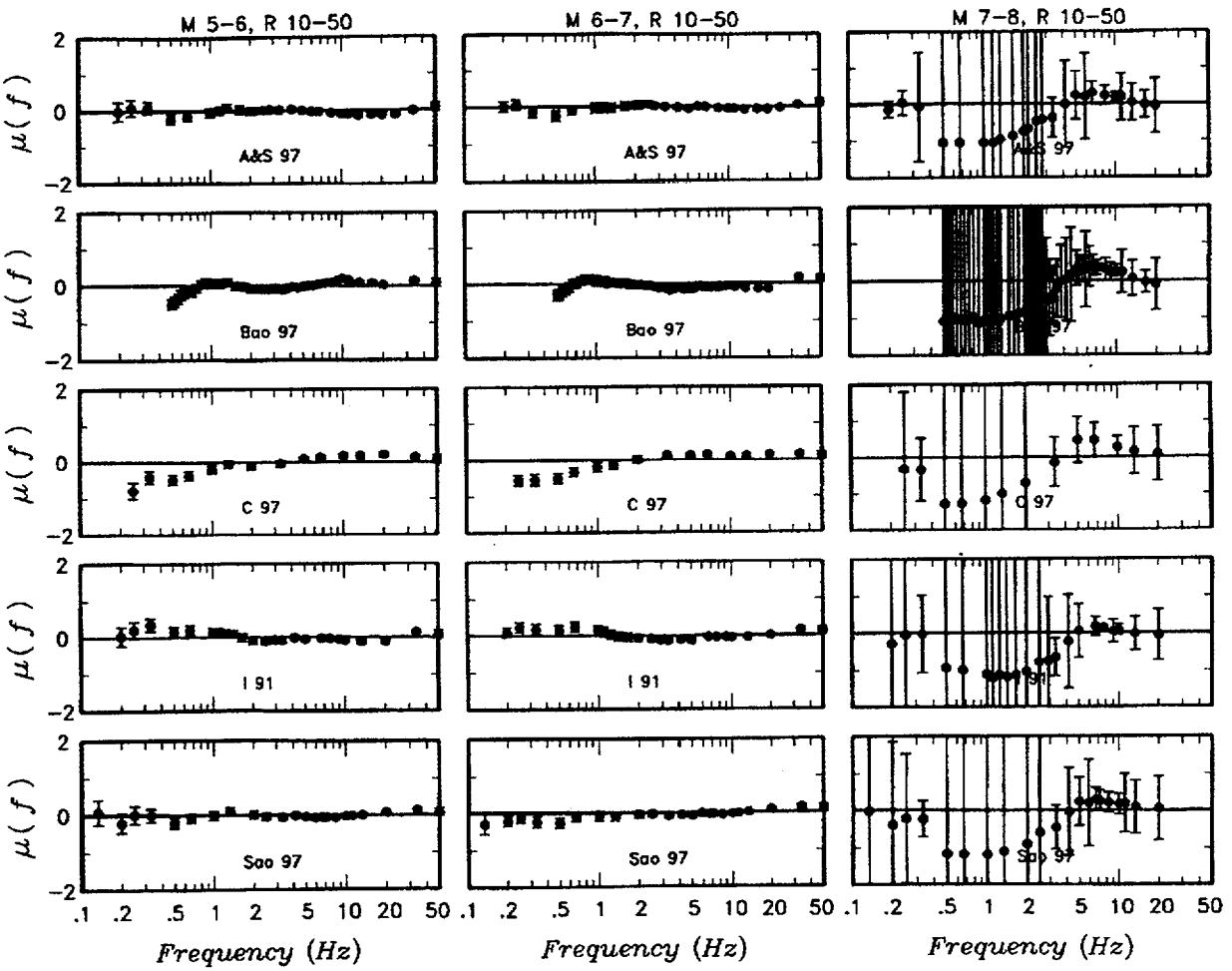

Figure 4-15b. (Continued)

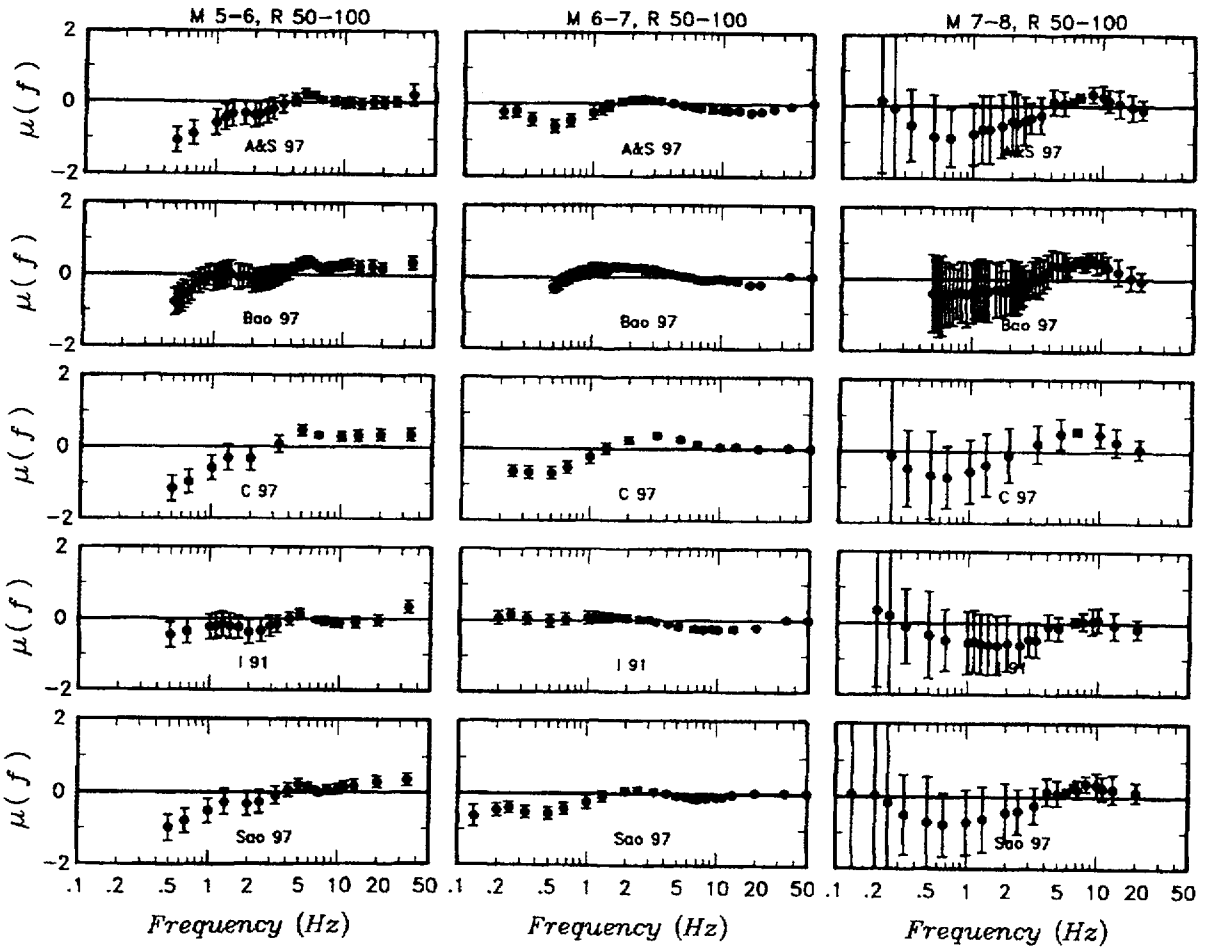

Figure 4-15c. (Continued)

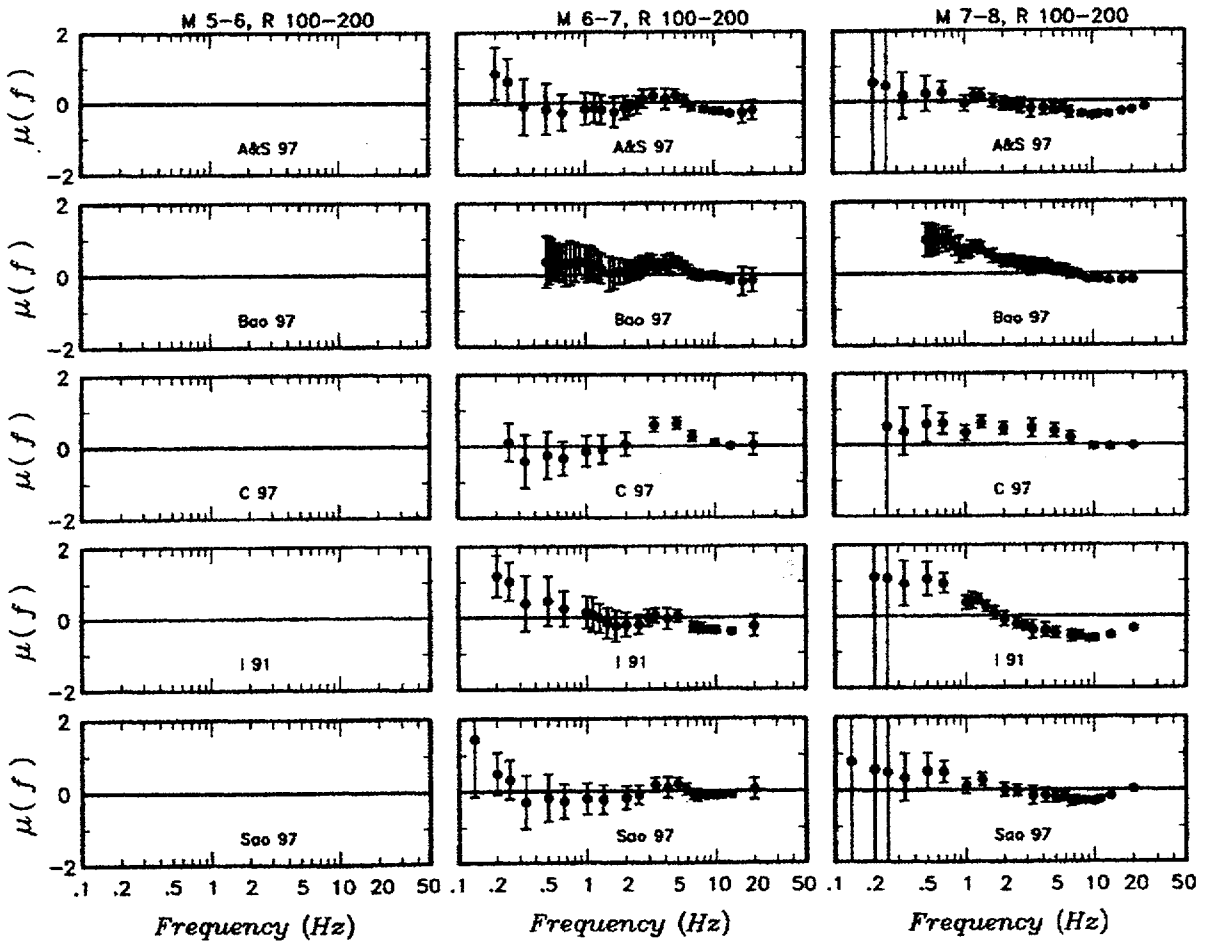

Figure 4-15d. (Continued)

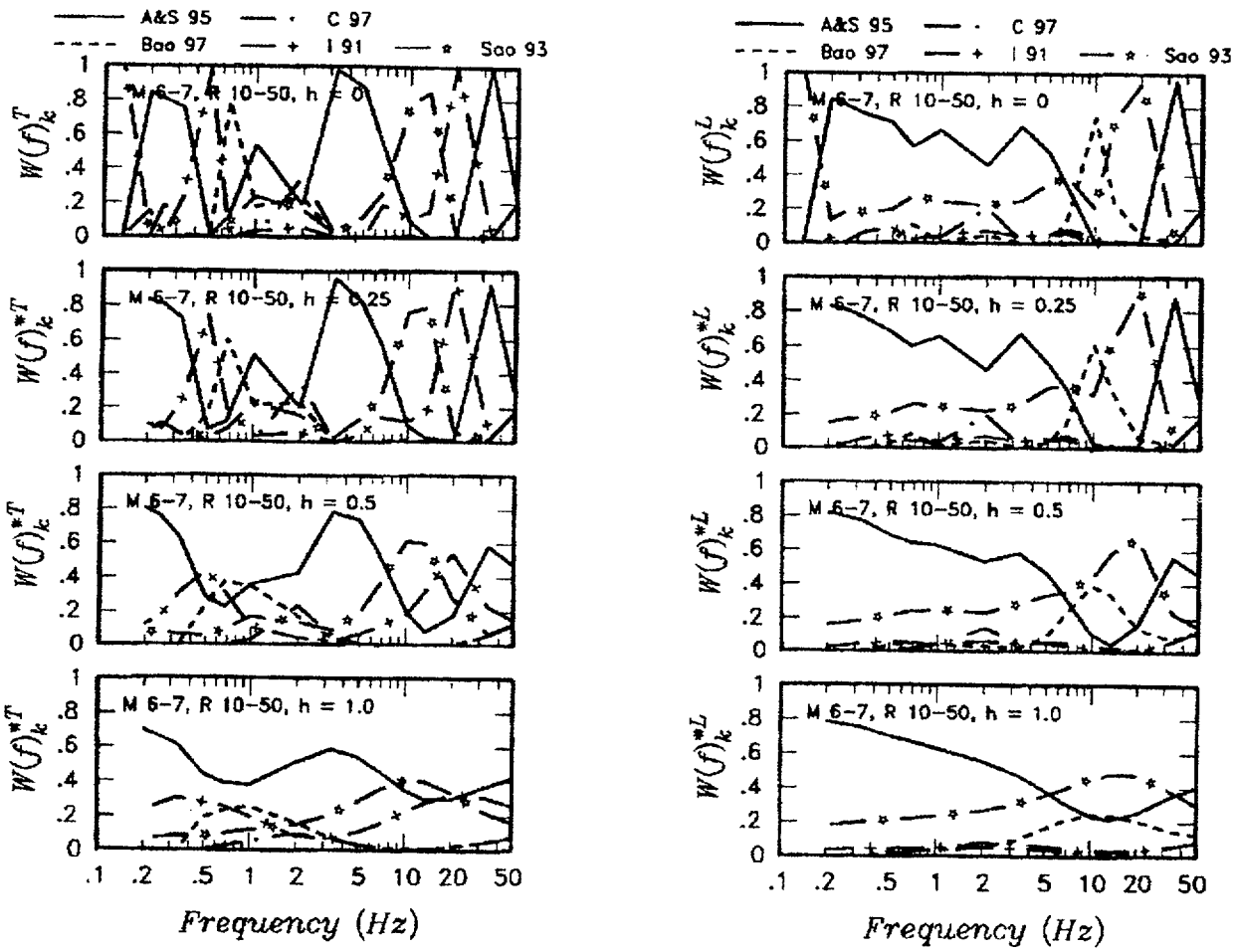

Figure 4-16. Relative bias ("*T*") weights (left column) and relative likelihood ("*L*") weights (right column) for **M** 6-7 and *R* 10-50 km magnitude distance bins. Top plot in each column shows weights computed using Equations (4-4) and (4-6). The remaining plots show the smoothed weights obtained using Equation (4-7) with values of *h* from 0.25 to 1.0.

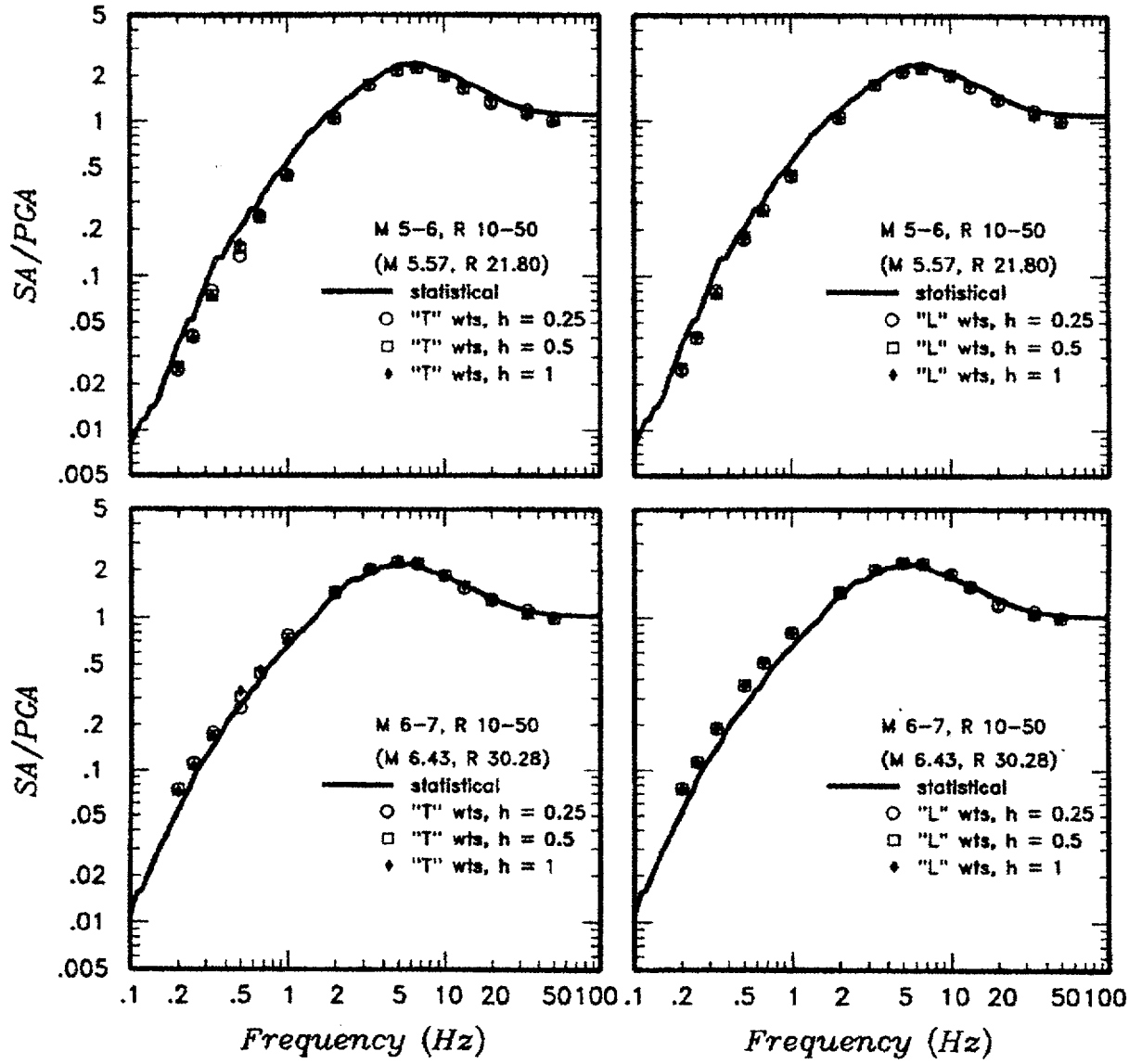

Figure 4-17. Example comparisons of the statistical spectral shapes from Figure 4-5 with spectral shapes predicted by the weighted combination of the five attenuation relationships. Weighted empirical spectral shapes are shown for smoothed "*T*" and "*L*" weights and values of *h* from 0.25 to 1.0.

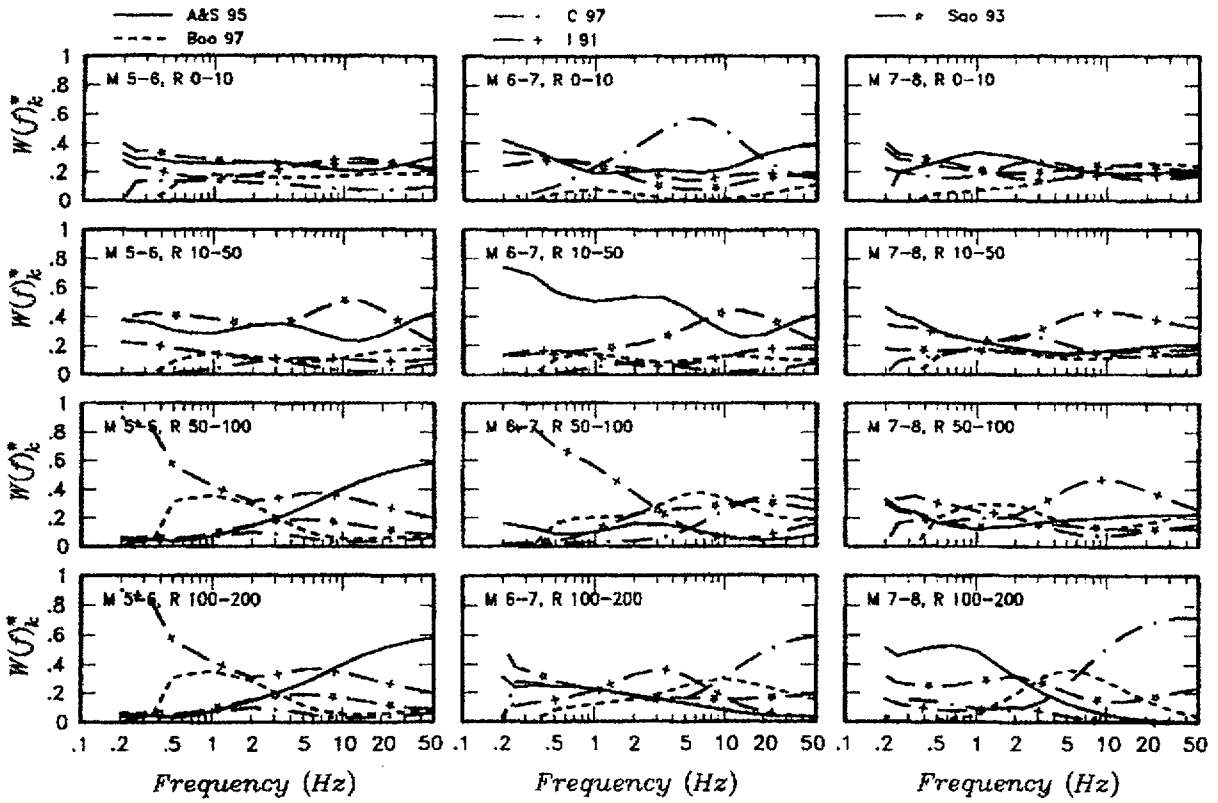

Figure 4-18. Relative weights used to obtain weighted empirical attenuation spectral shapes. The weights are the average of the smoothed "T" and "L" weights with $h = 1.0$.

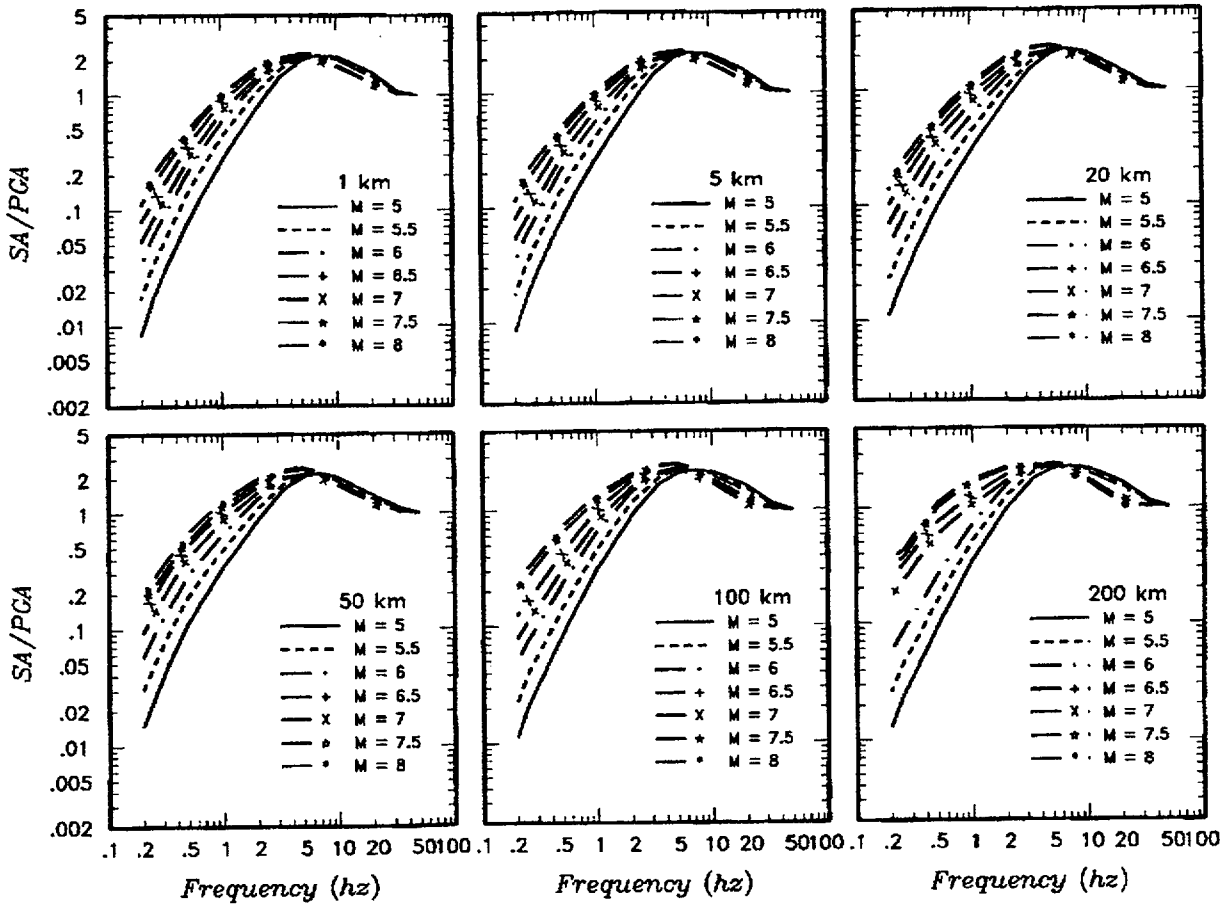

Figure 4-19. Weighted empirical attenuation response spectral shapes obtained using the relative weights shown on Figure 4-18.

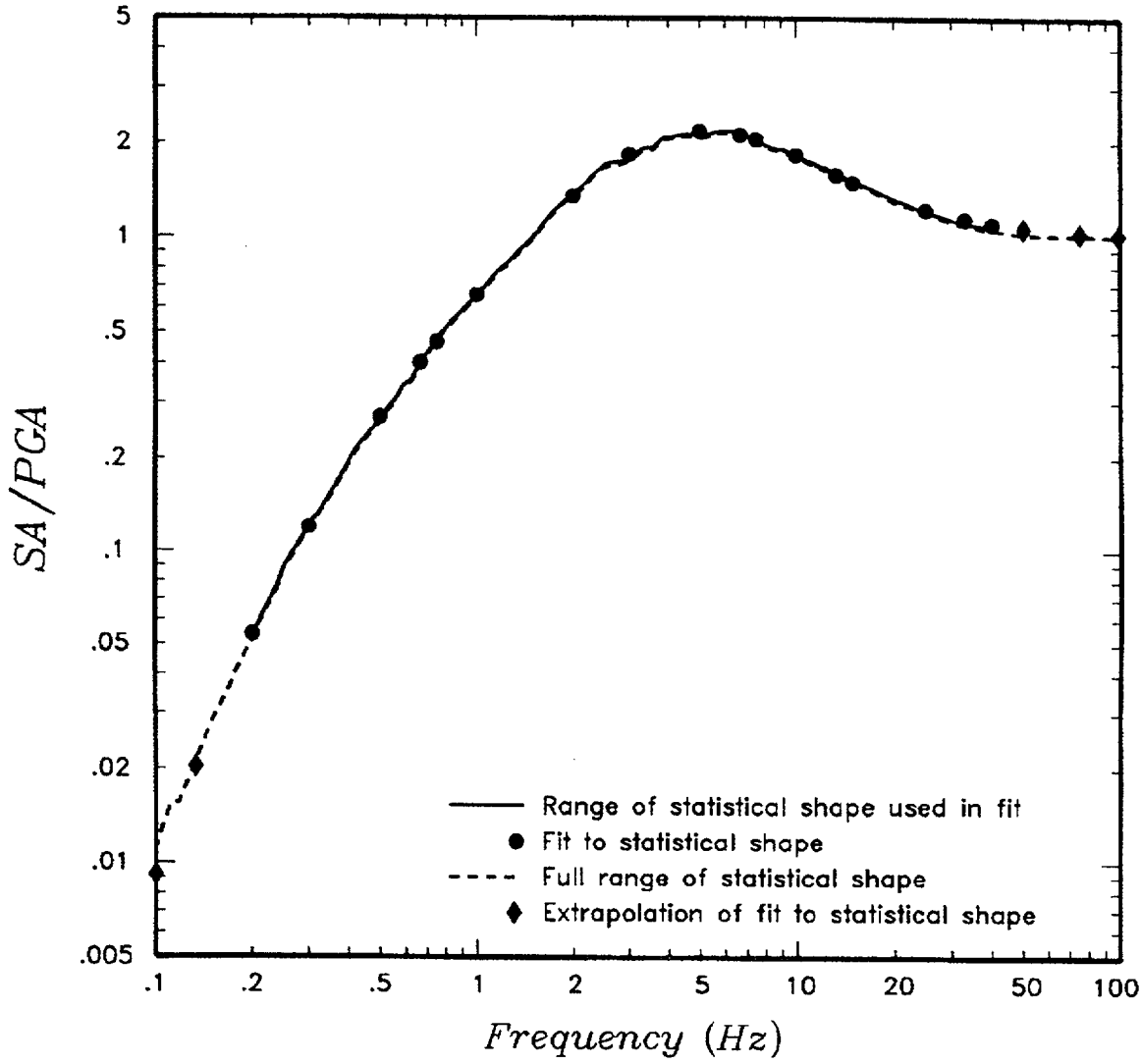

Figure 4-20. Example of a fit of Equation (4-8) to an individual spectral shape.

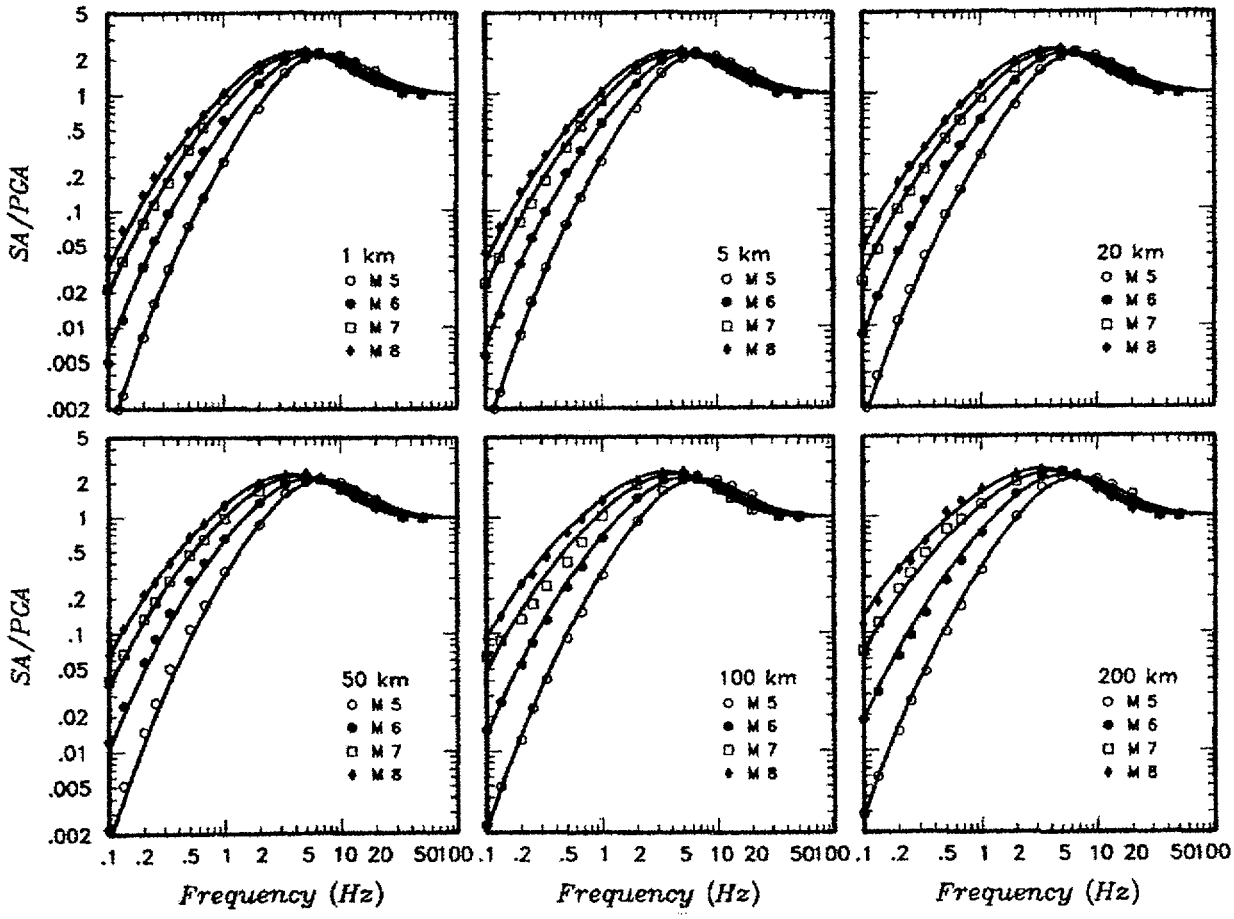

Figure 4-21. Example WUS response spectral shapes predicted by Equation (4-8) with parameters listed in Table 4-3 compared to the weighted empirical spectral shape data used in the fit.

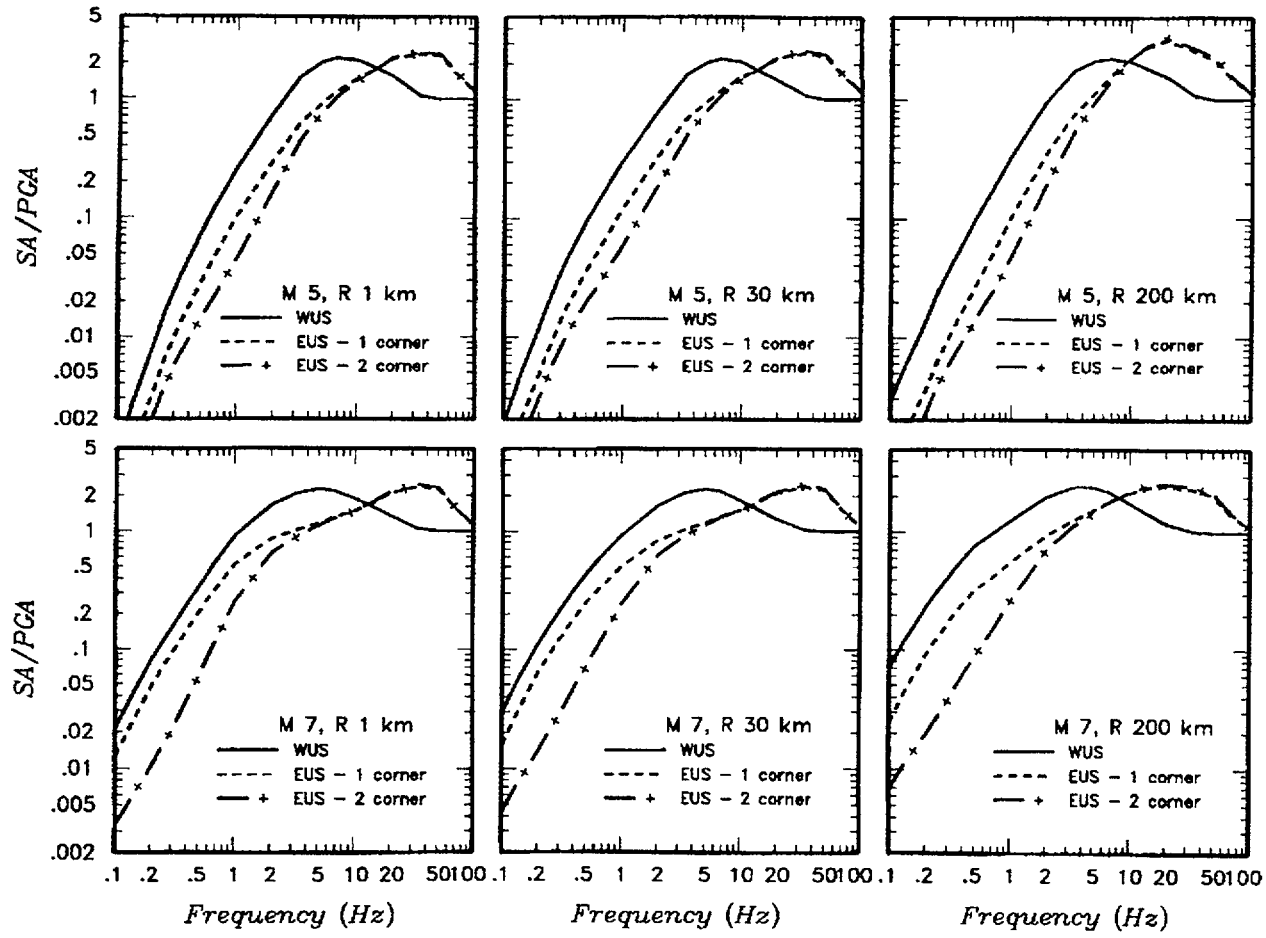

Figure 4-22. Example EUS response spectral shapes obtained by scaling weighted empirical WUS response spectral shapes.

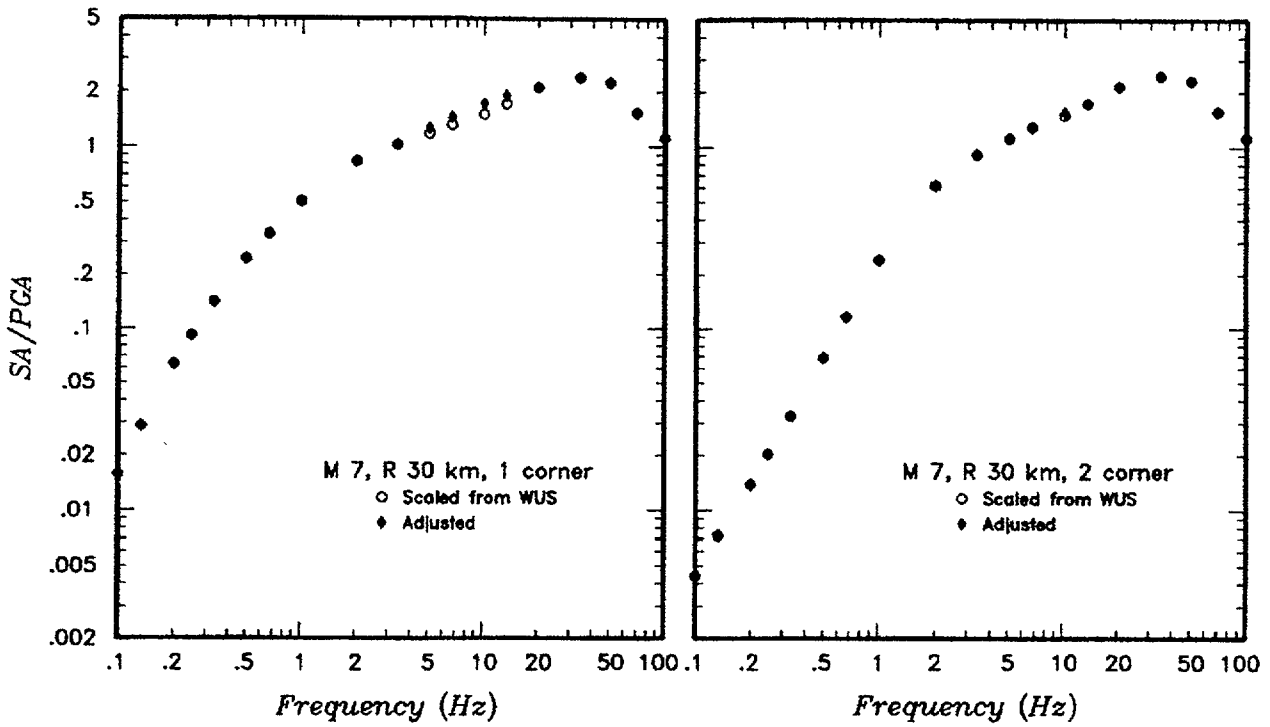

Figure 4-23. Examples of adjustments to scaled EUS response spectral shapes to remove valley near 10 Hz.

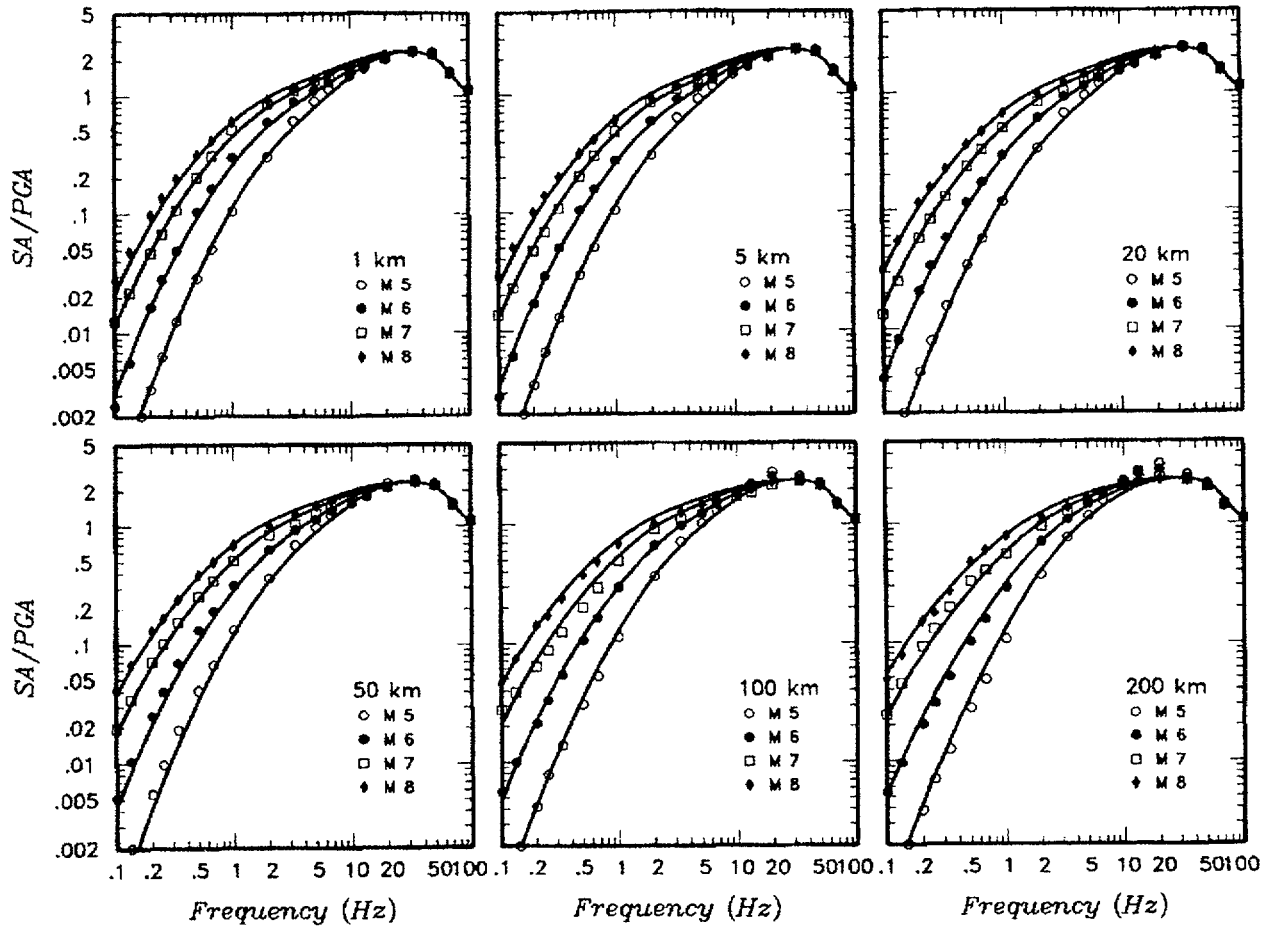

Figure 4-24. Example EUS single-corner response spectral shapes predicted by Equation (4-9) with parameters listed in Table 4-3 compared to the scaled and adjusted EUS spectral shape data used in the fit.

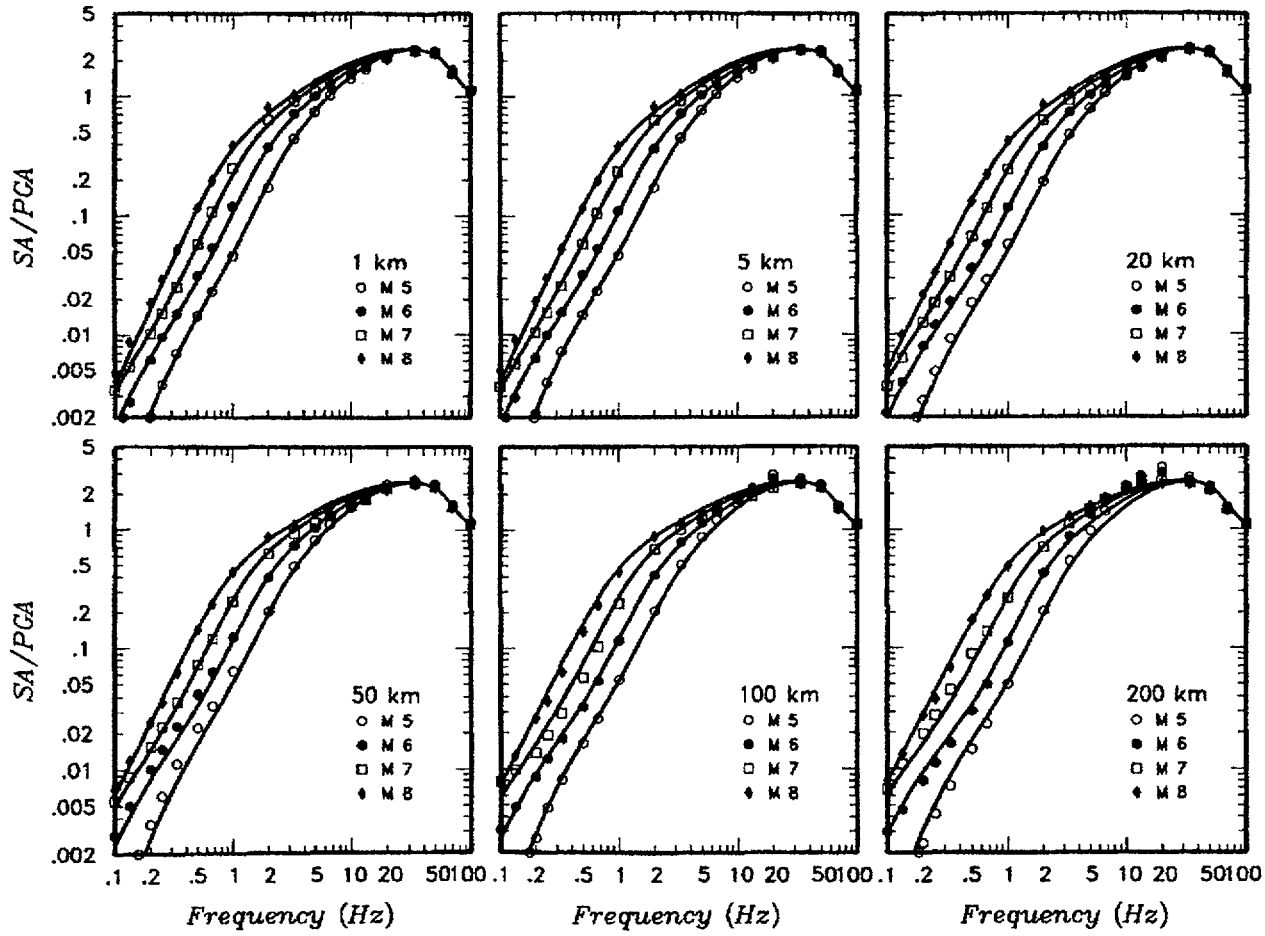

Figure 4-25. Example EUS double-corner response spectral shapes predicted by Equation (4-9) with parameters listed in Table 4-3 compared to the scaled and adjusted EUS spectral shape data used in the fit.

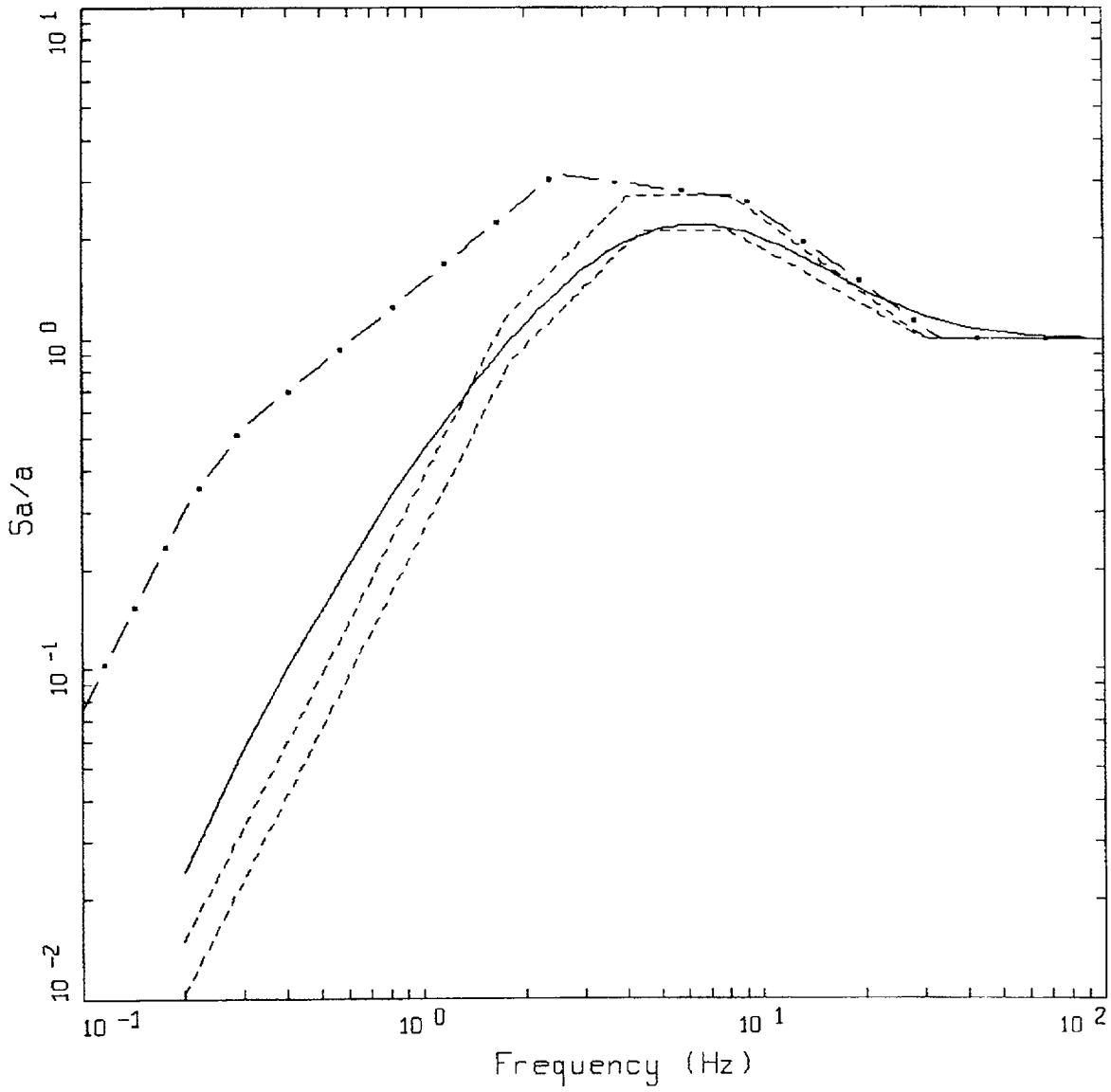

Figure Set 4-26. Comparison of recommended WUS shapes (solid line) to current regulatory guidance R.G. 1.60 and Newmark-Hall shapes for the distance bin 0 to 50 km and for mean magnitudes 5.6, 4.4, and 7.3. Peak parameters are taken from Table 4-1 for the Newmark-Hall shapes.

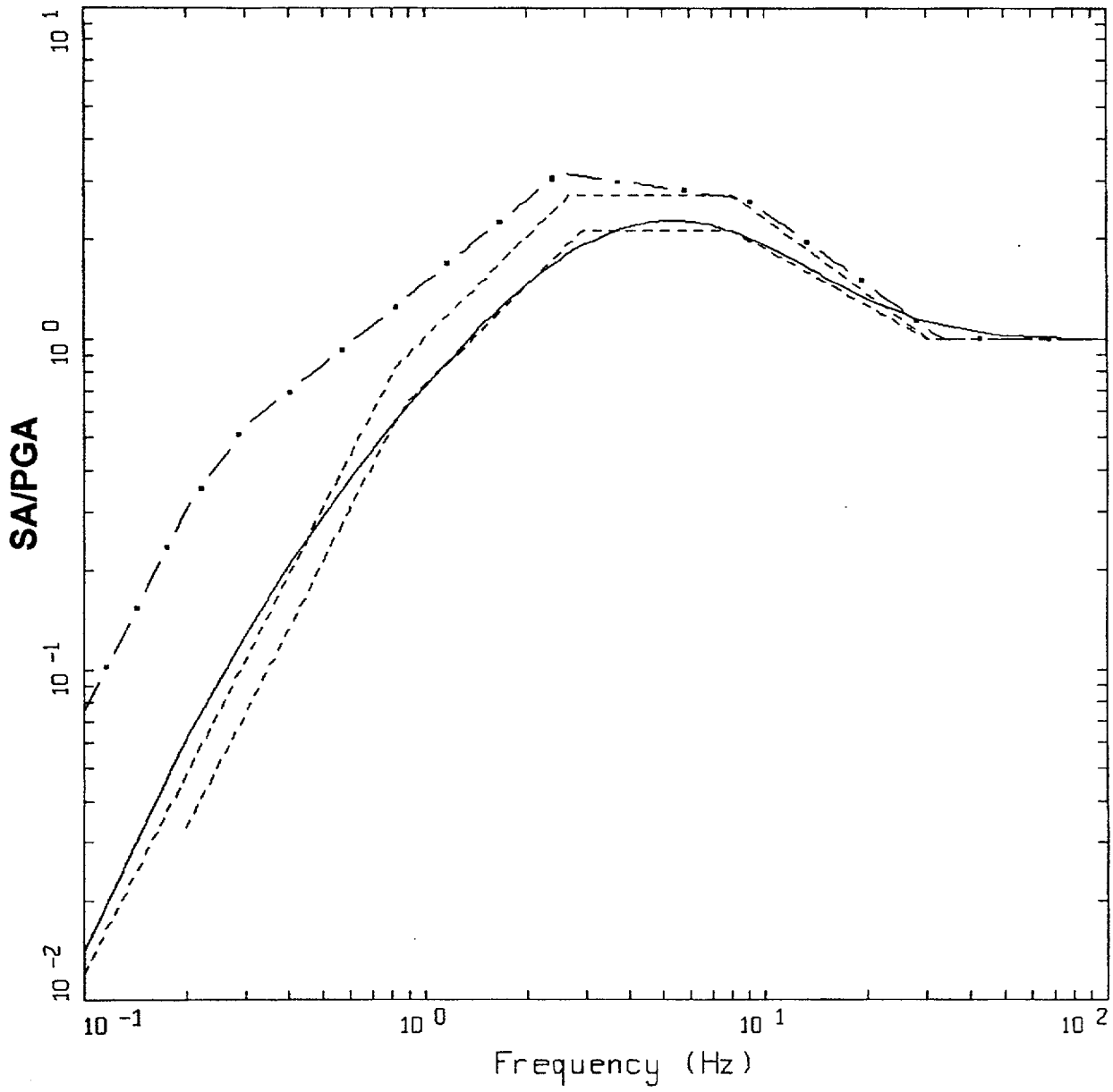

M=6.4, R=27.4 KM, ROCK
PGA=0.15 G, PGV=10.27 CM/S, PGD=2.24 CM

LEGEND

——— 5% DAMPED, RECOMMENDED NRC SPECTRA, 50th percentile

- - - - - 5% DAMPED, NEWMARK&HALL SPECTRA WUS, 50th percentile

- - - - - 5% DAMPED, NEWMARK&HALL SPECTRA, 84th percentile

— • — 5% DAMPED, REG GUIDE 1.60

Figure Set 4-26 (Cont'd)

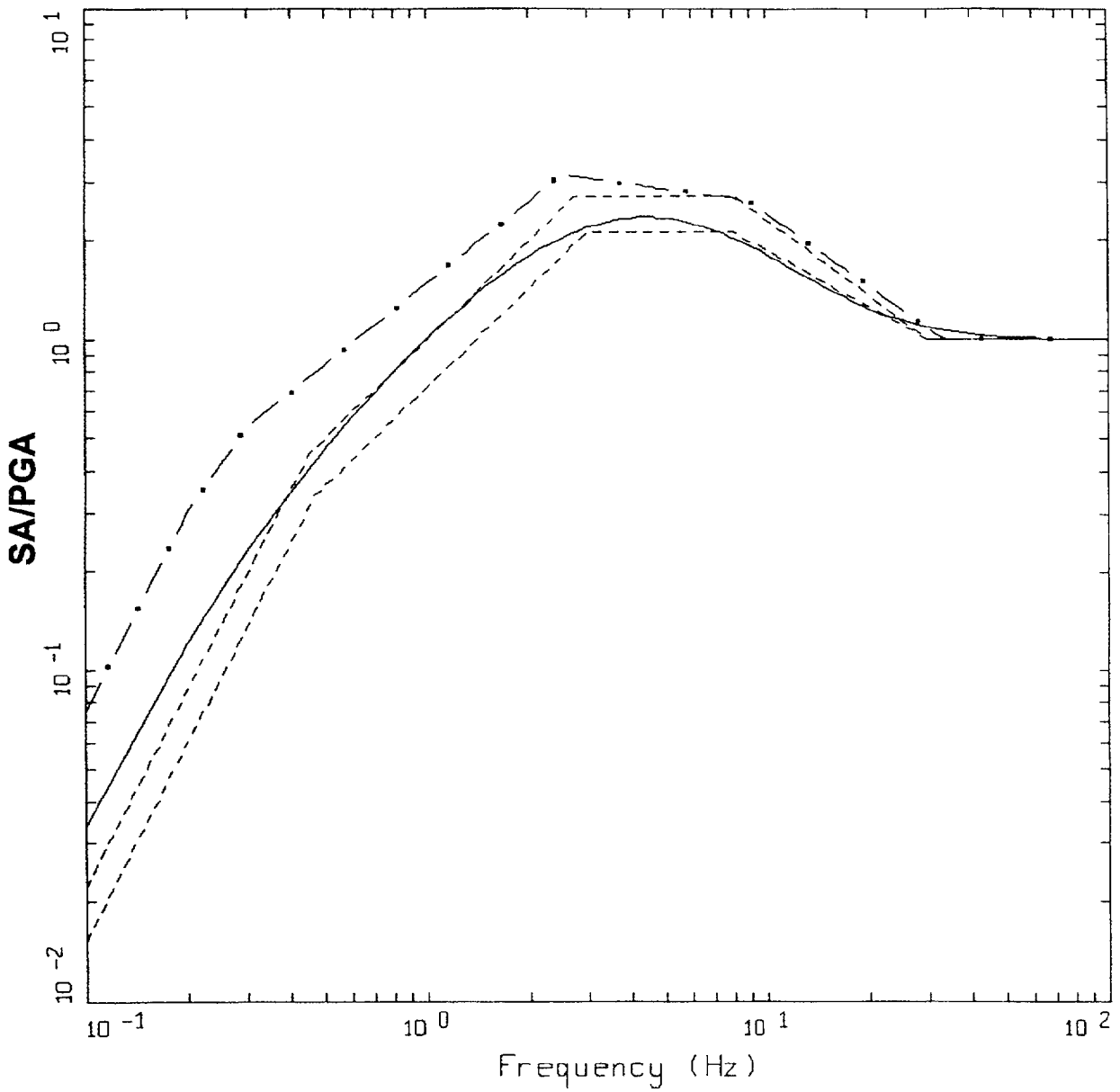

M=7.3, R=17.6 KM, ROCK
PGA=0.40 G, PGV=26.82 CM/S, PGD=10.89 CM

LEGEND

——— 5% DAMPED, RECOMMENDED NRC SPECTRA, 50th percentile

- - - - - 5% DAMPED, NEWMARK&HALL SPECTRA WUS, 50th percentile

- - - - - 5% DAMPED, NEWMARK&HALL SPECTRA, 84th percentile

—•— 5% DAMPED, REG GUIDE 1.60

Figure Set 4-26. (Cont'd)

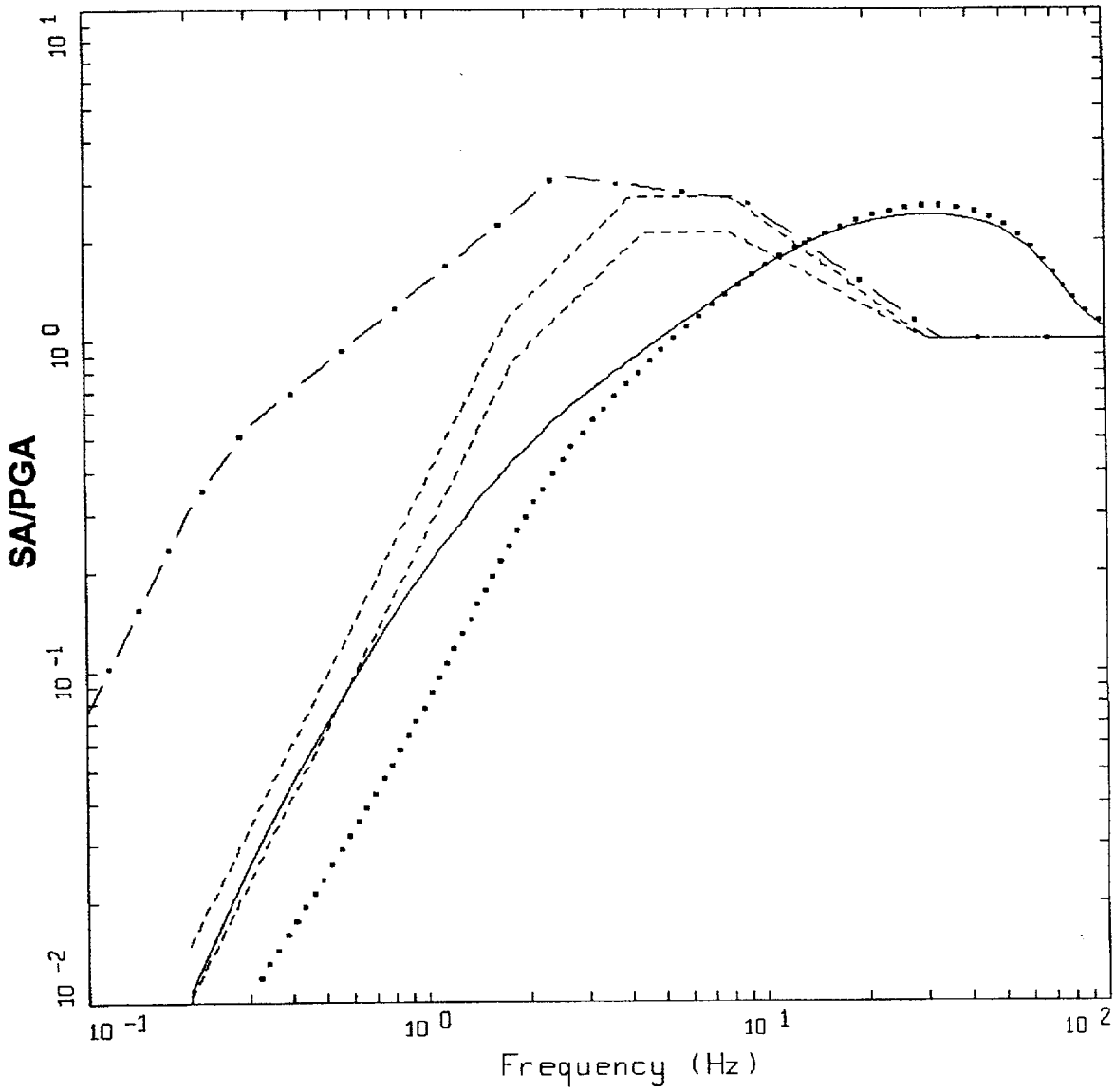

Figure Set 4-27. Comparison of recommended CEUS shapes (solid line) to current regulatory guidance R.G. 1.60 and Newmark-Hall shapes for the distance bin 0 to 50 km and for mean magnitudes 5.6, 6.4, and 7.3. Peak parameters are taken from Table 4-1 for the Newmark-Hall shapes.

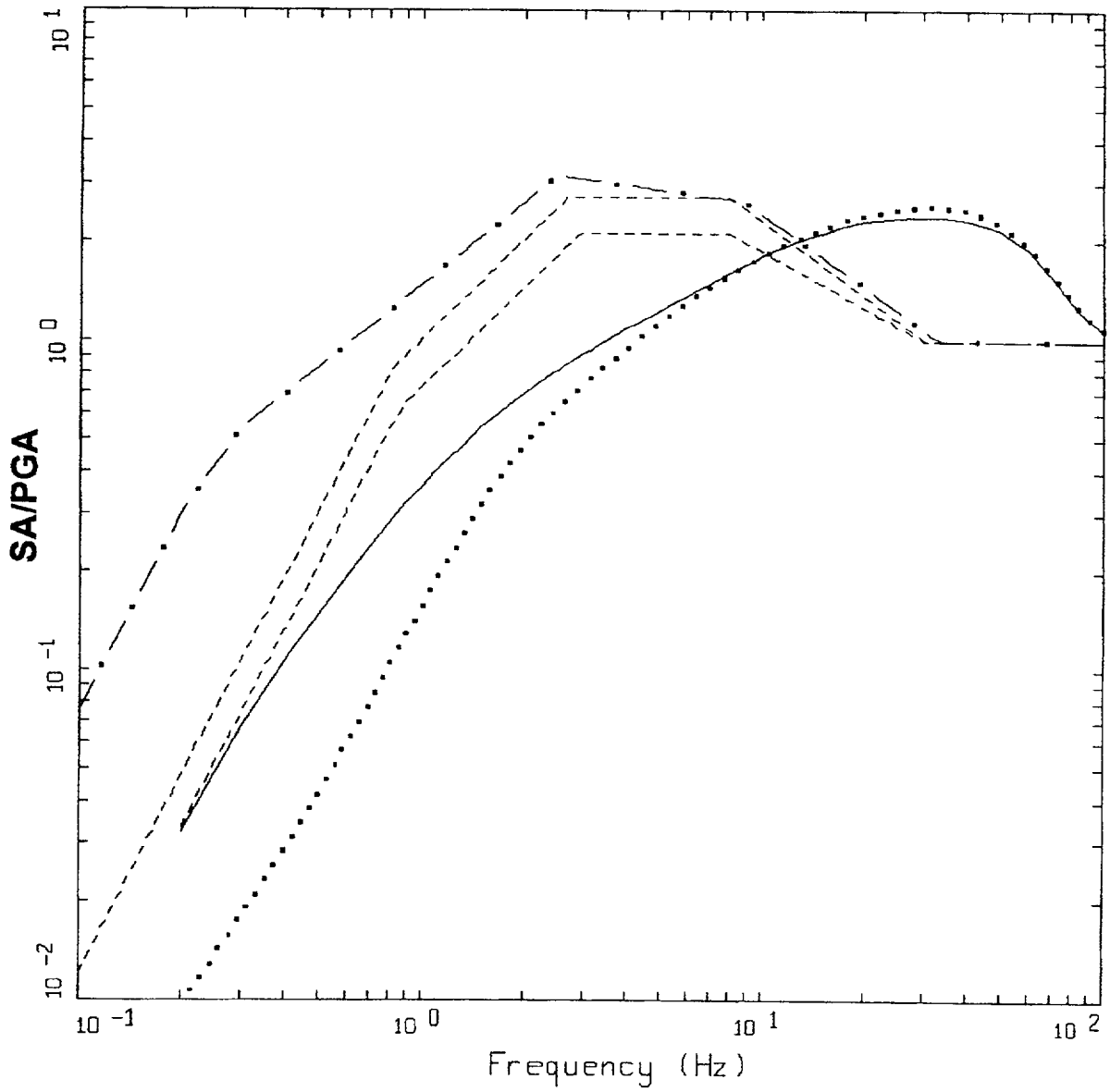

M=6.4, R=27.4 KM, ROCK
PGA=0.15 G, PGV=10.27 CM/S, PGD=2.24 CM

LEGEND

———	5% DAMPED, RECOMMENDED NRC SPECTRA CEUS 1 CORNER, 50th percentile
• • • •	5% DAMPED, RECOMMENDED NRC SPECTRA CEUS 2 CORNER, 50th percentile
- - - - -	5% DAMPED, NEWMARK&HALL SPECTRA, 50th percentile
- - - - -	5% DAMPED, NEWMARK&HALL SPECTRA, 84th percentile
— • —	5% DAMPED, REG GUIDE 1.60

Figure Set 4-27. (Cont'd)

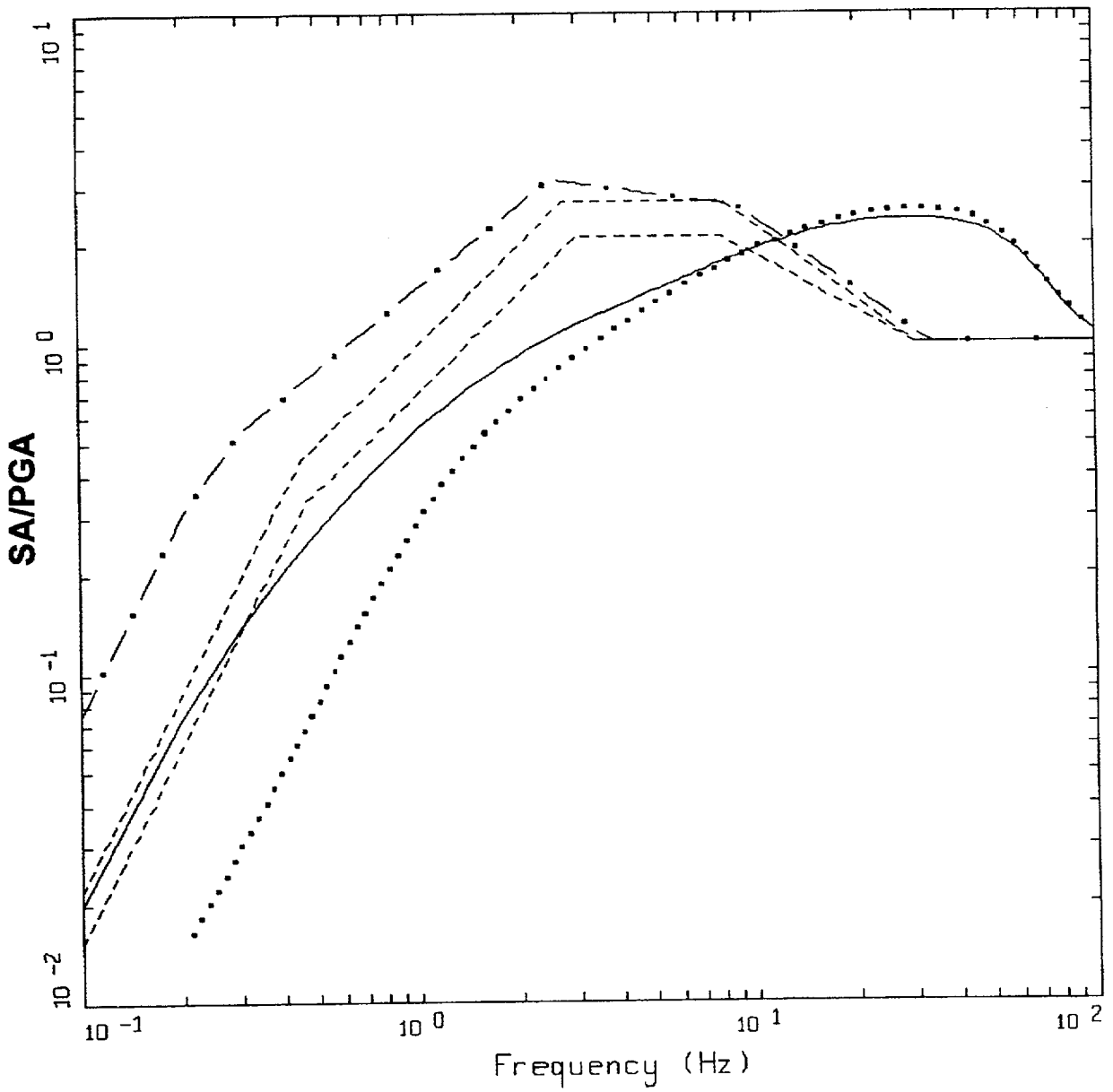

M=7.3, R=17.6 KM, ROCK
PGA=0.40 G, PGV=26.82 CM/S, PGD=10.89 CM

LEGEND

———	5% DAMPED, RECOMMENDED NRC SPECTRA CEUS 1 CORNER, 50th percentile
• • • •	5% DAMPED, RECOMMENDED NRC SPECTRA CEUS 2 CORNER, 50th percentile
- - - - -	5% DAMPED, NEWMARK&HALL SPECTRA, 50th percentile
- - - - -	5% DAMPED, NEWMARK&HALL SPECTRA, 84th percentile
— • —	5% DAMPED, REG GUIDE 1.60

Figure Set 4-27. (Cont'd)

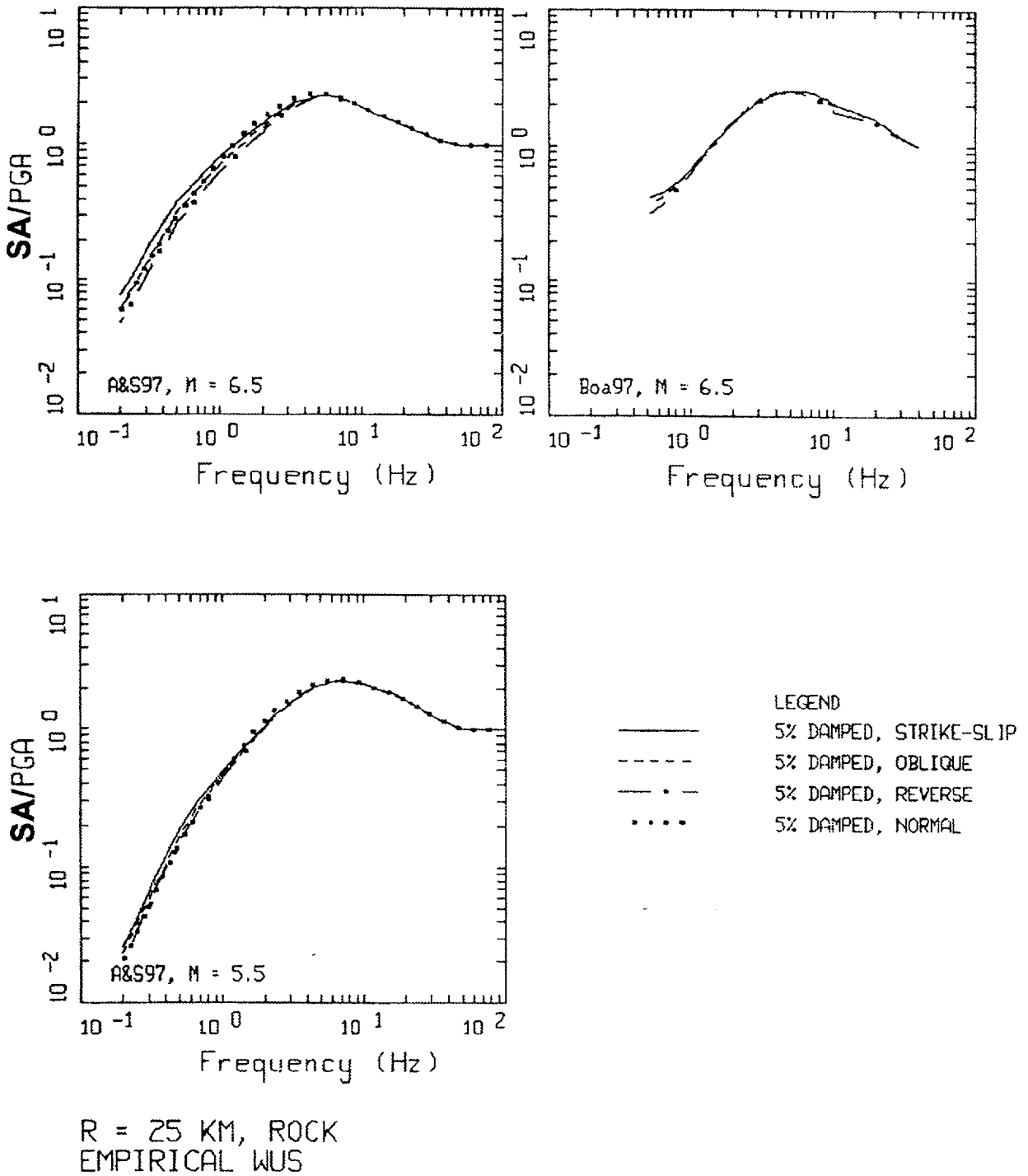

Figure 4-28. Predicted effects of source mechanism on spectral shapes for empirical WUS attenuation relations. For the Abrahamson and Silva, 1997 empirical relation, the frequency dependence differs for small and large magnitudes.

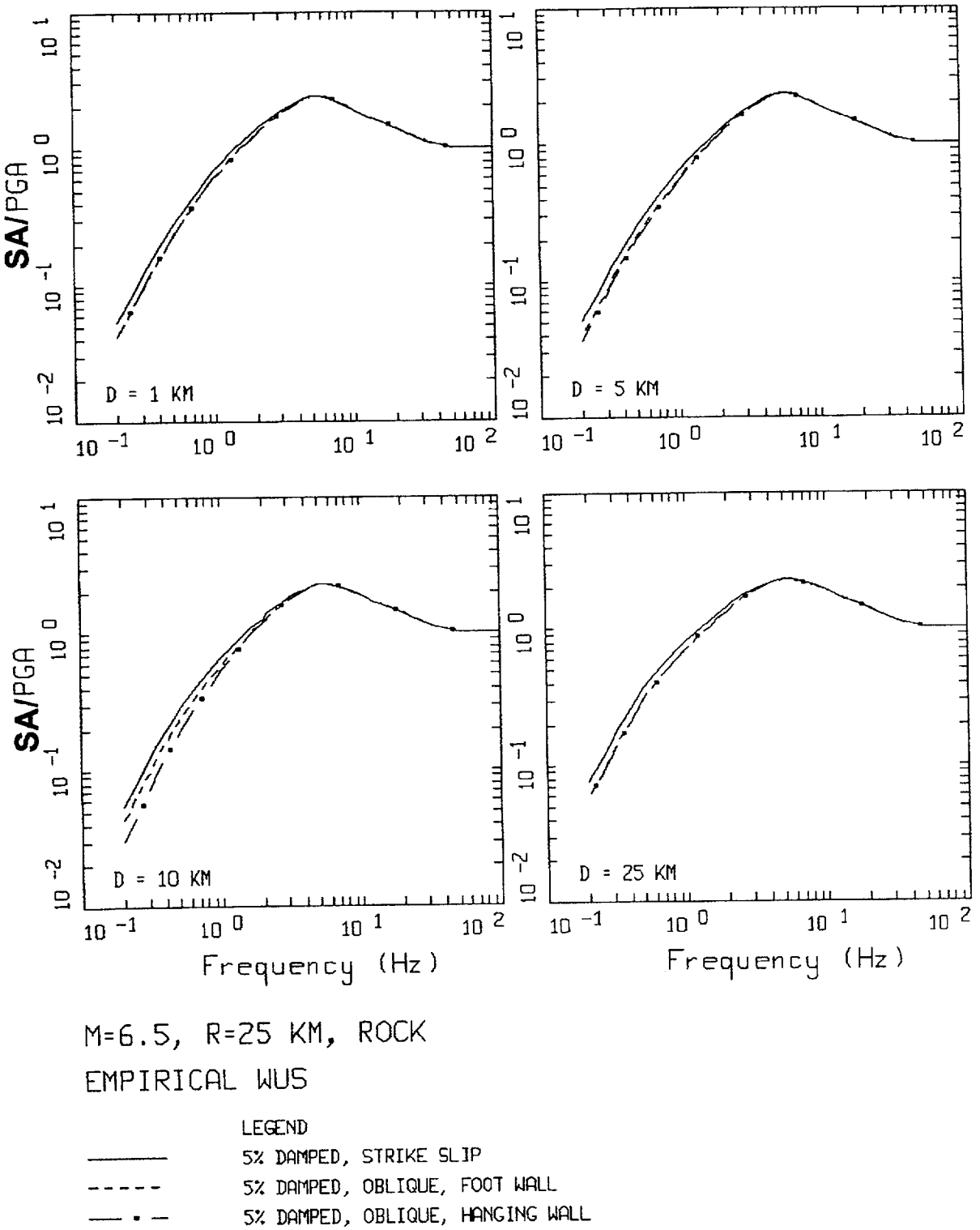

Figure 4-29. Predicted effects of site location (hanging wall vs. foot wall) for oblique-slip source mechanisms on spectral shapes compared to strike-slip spectral shapes for an empirical WUS attenuation relation (Abrahamson and Silva, 1997).

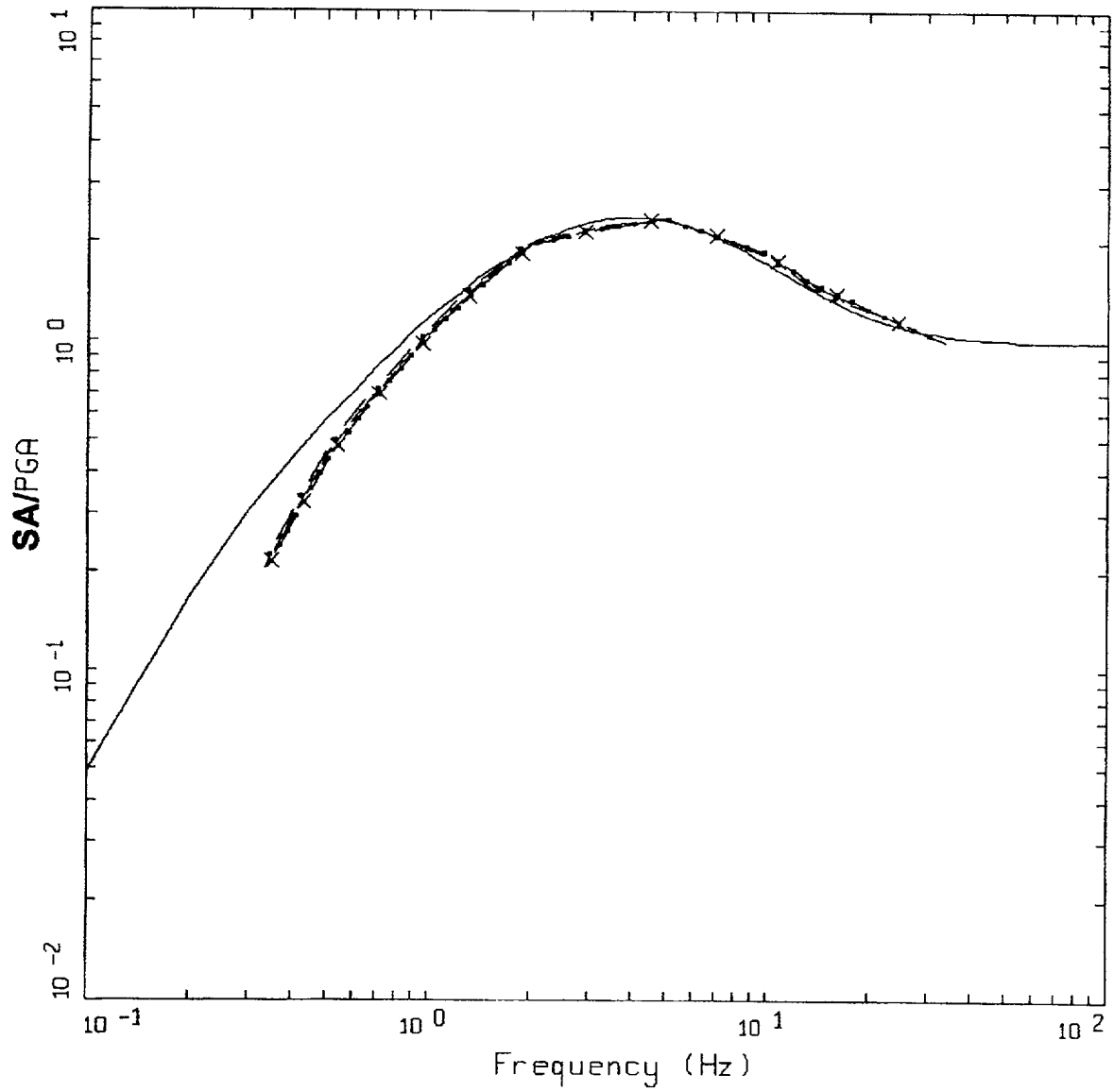

Figure 4-30. Comparison of recommended shapes for **M** 8.0 at $R = 25$ km to empirical subduction zone shapes for **M** 9.0 at a suite of distances (Youngs et al., 1997).

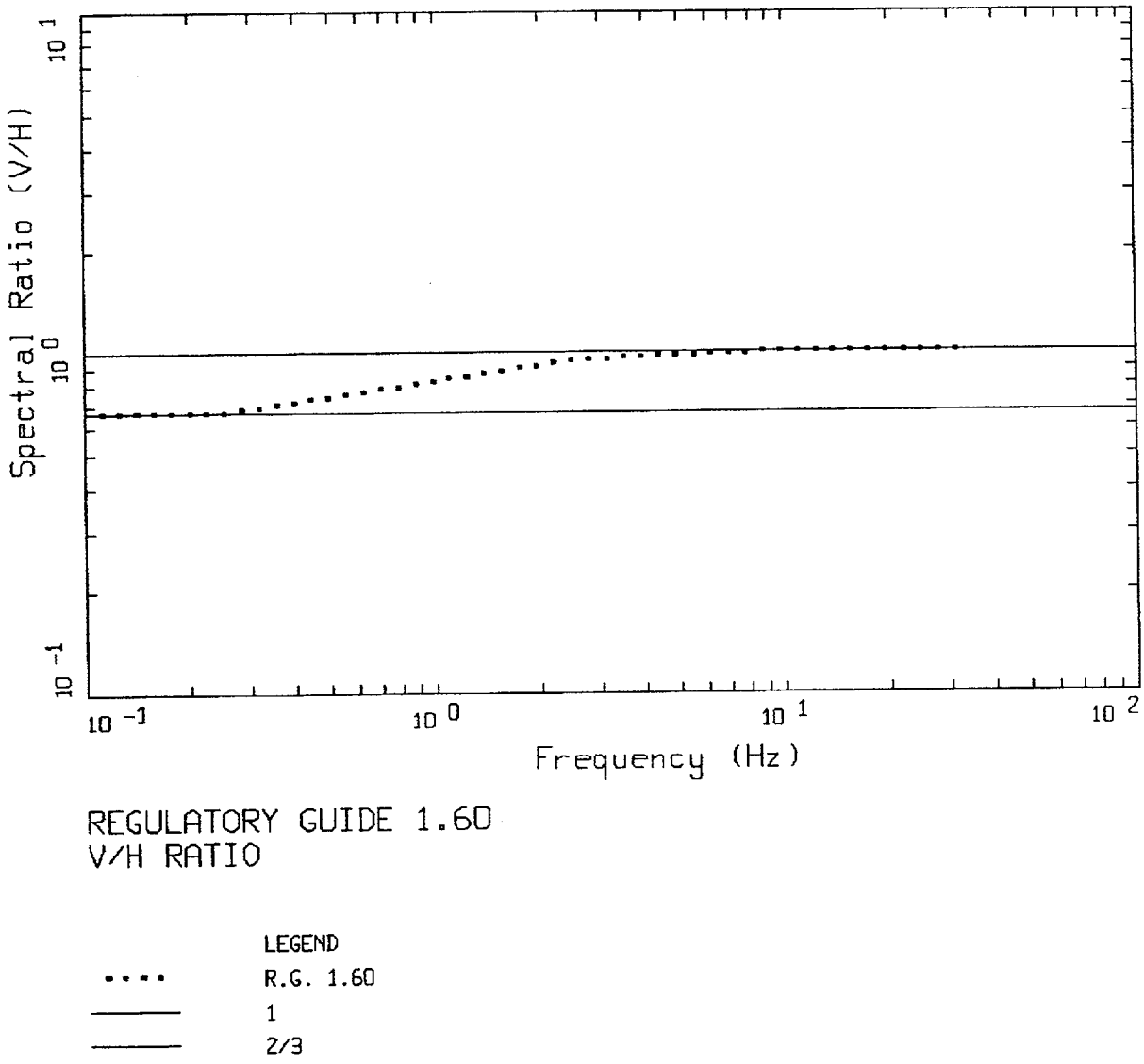

Figure 4-31. V/H ratio for 5% damped response spectra implied by the R.G. 1.60 design motions.

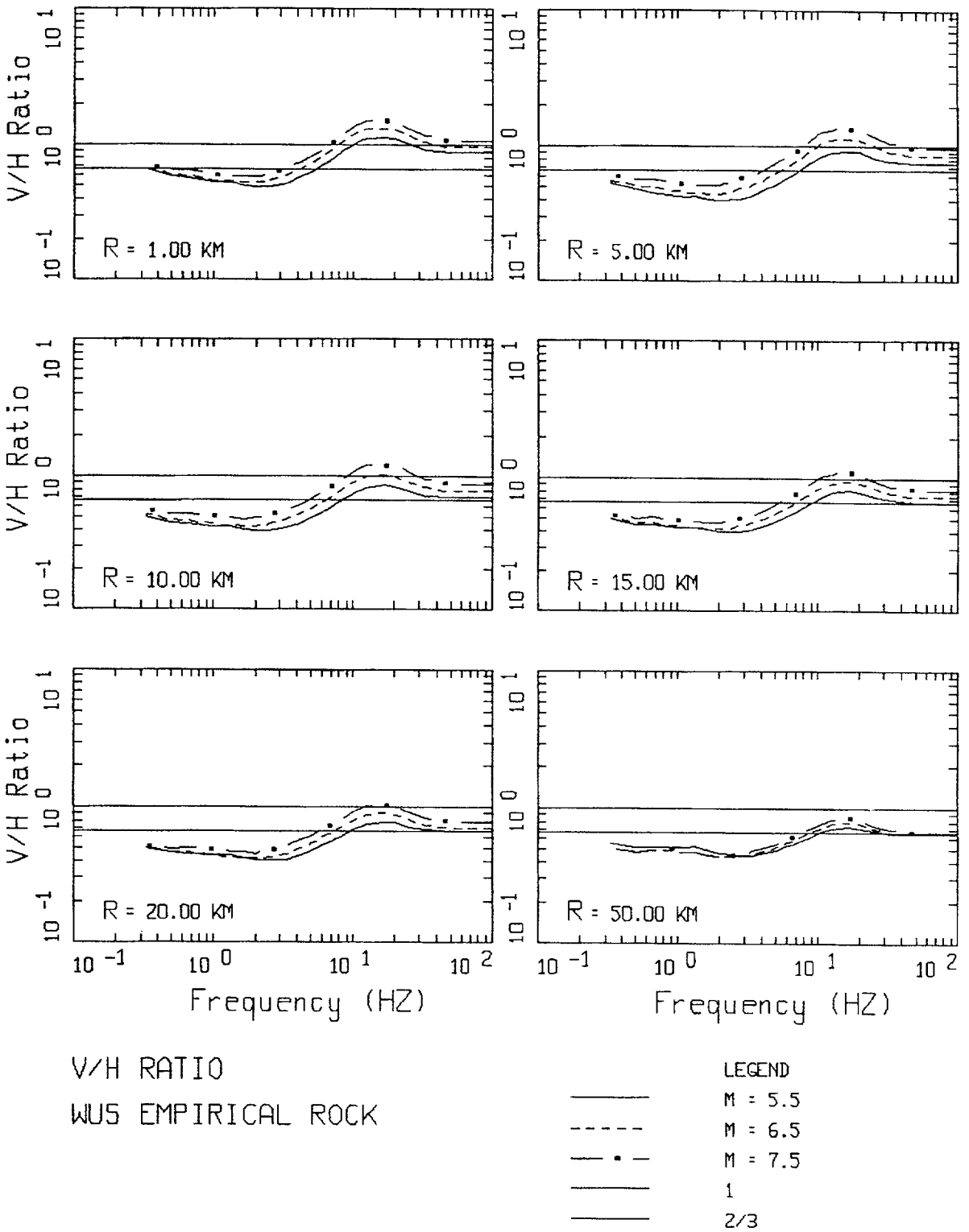

Figure 4-32. Average V/H ratio (5% damped) magnitude dependencies based on the Abrahamson and Silva, 1997; Campbell, 1997; and Sadigh et al., 1997 empirical WUS rock attenuation relations for a suite of magnitudes.

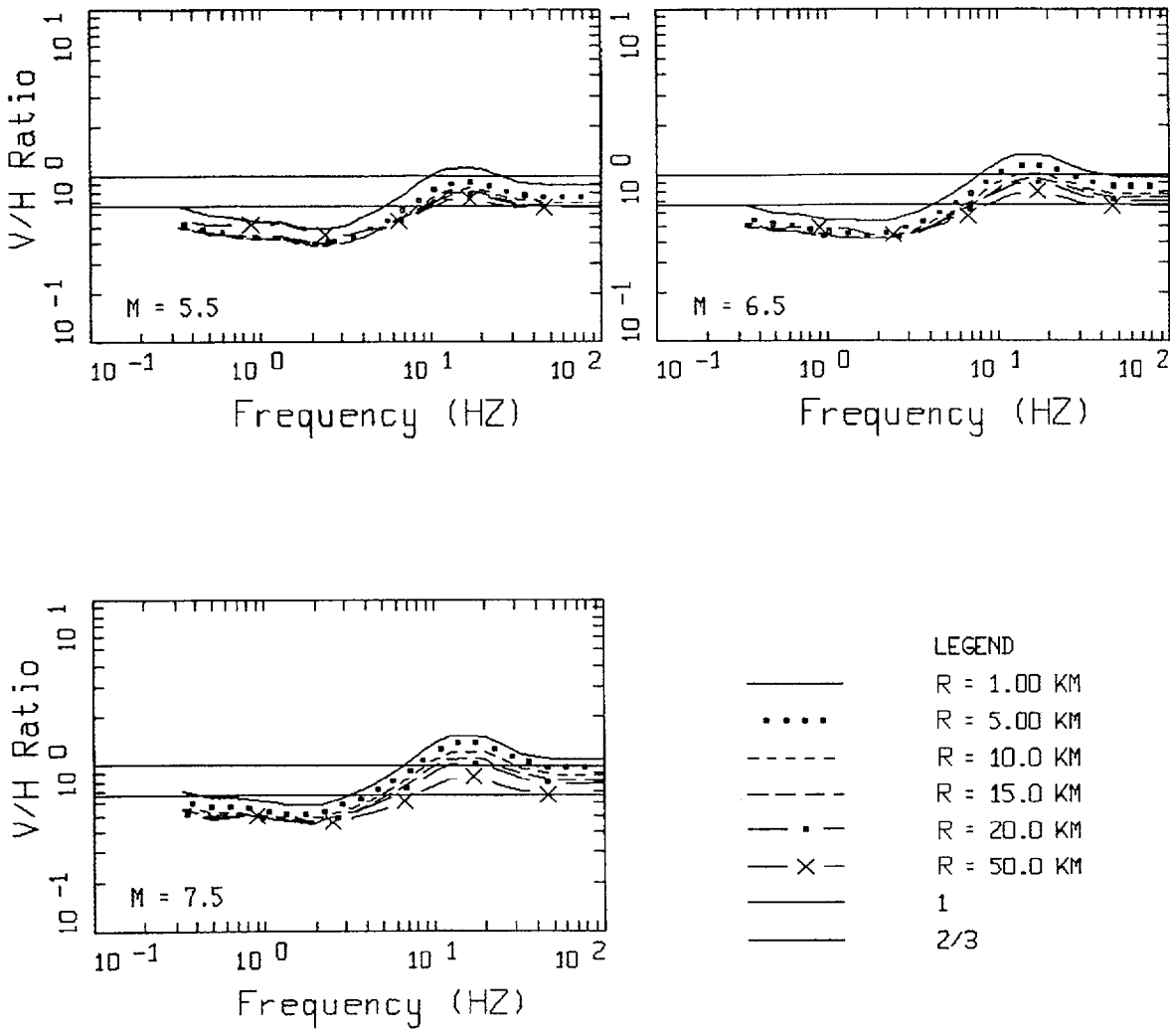

Figure 4-33. Average V/H ratio (5% damped) distance dependencies based on Abrahamson and Silva, 1997; Campbell, 1997; and Sadigh et al., 1997 empirical WUS rock attenuation relations for a suite of magnitudes.

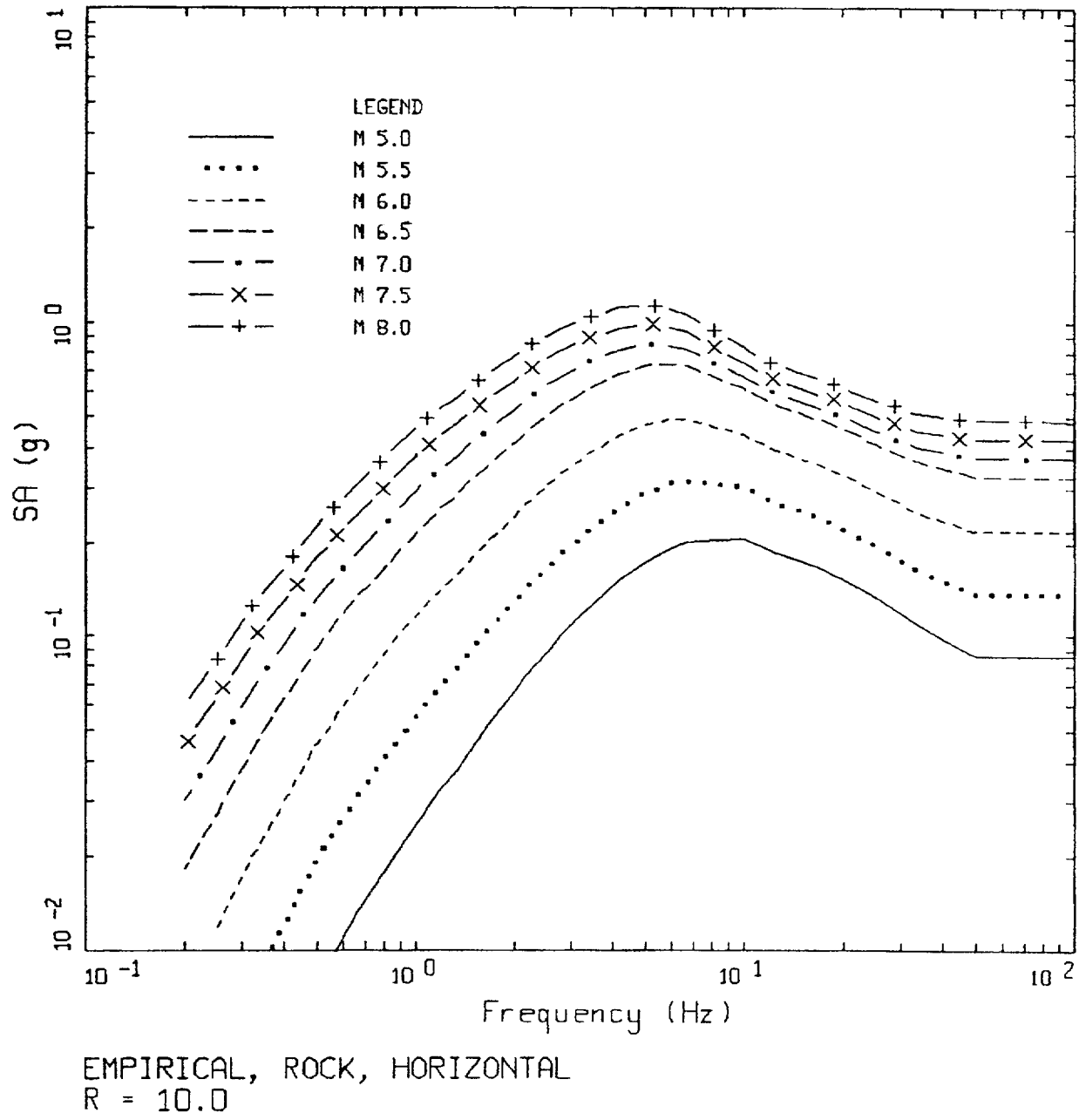

Figure 4-34. Magnitude dependence of 5% damped horizontal component response spectral acceleration at a rupture distance of 10 km for a WUS rock empirical attenuation relation (Abrahamson and Silva, 1997).

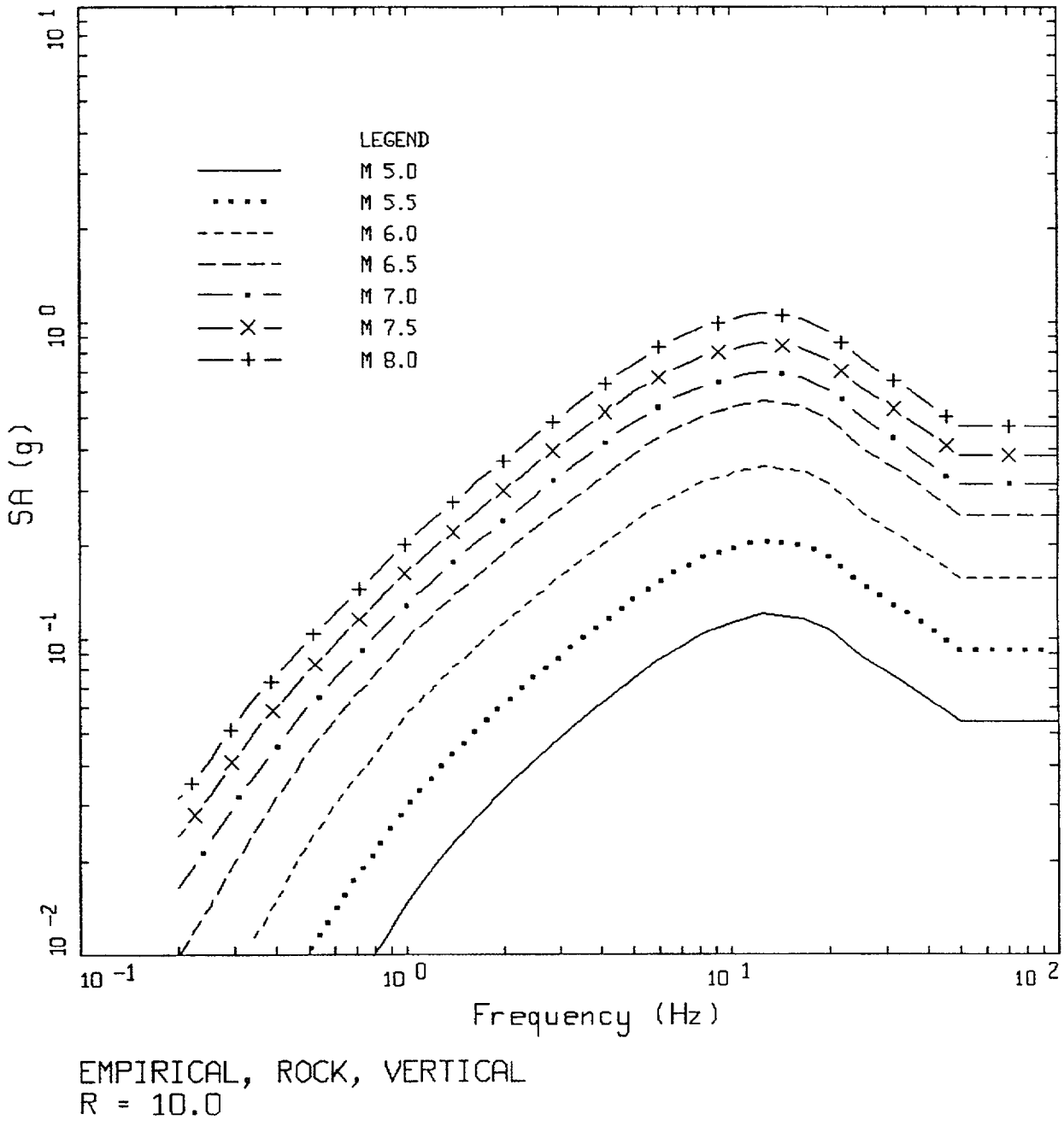

Figure 4-35. Magnitude dependence of 5% damped vertical component response spectral acceleration at a rupture distance of 10 km for a WUS rock empirical attenuation relation (Abrahamson and Silva, 1997).

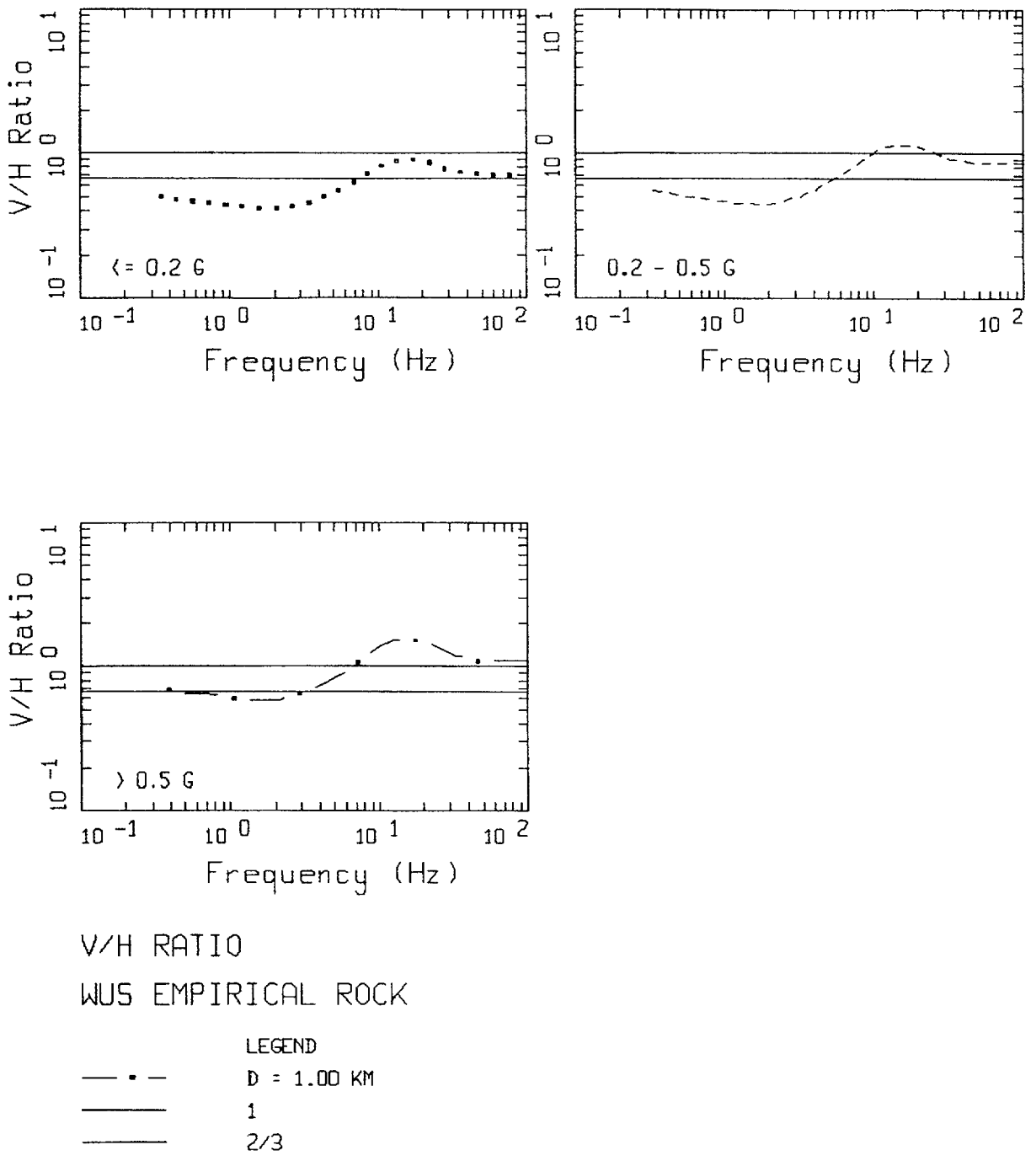

Figure 4-36. Recommended V/H ratios (5% damped) for WUS soft rock site conditions for ranges in horizontal component peak accelerations.

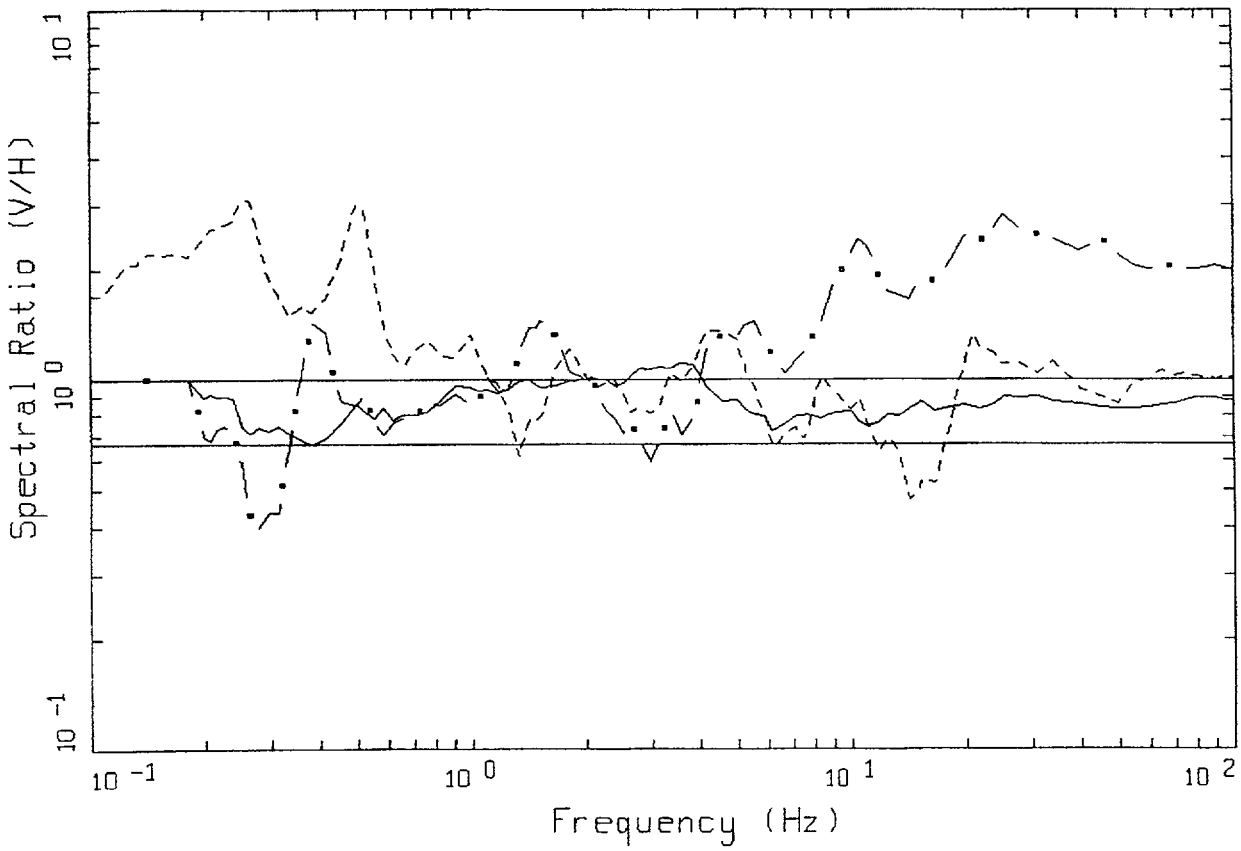

Figure 4-37. V/H ratios (5% damped) computed from recordings of the **M** 5.9 1988 Saguenay, and **M** 6.8 1976 Gazlie, and 1985 Nahanni earthquakes. The Gazli and Nahanni earthquakes are considered to represent CEUS source, path, and site conditions.

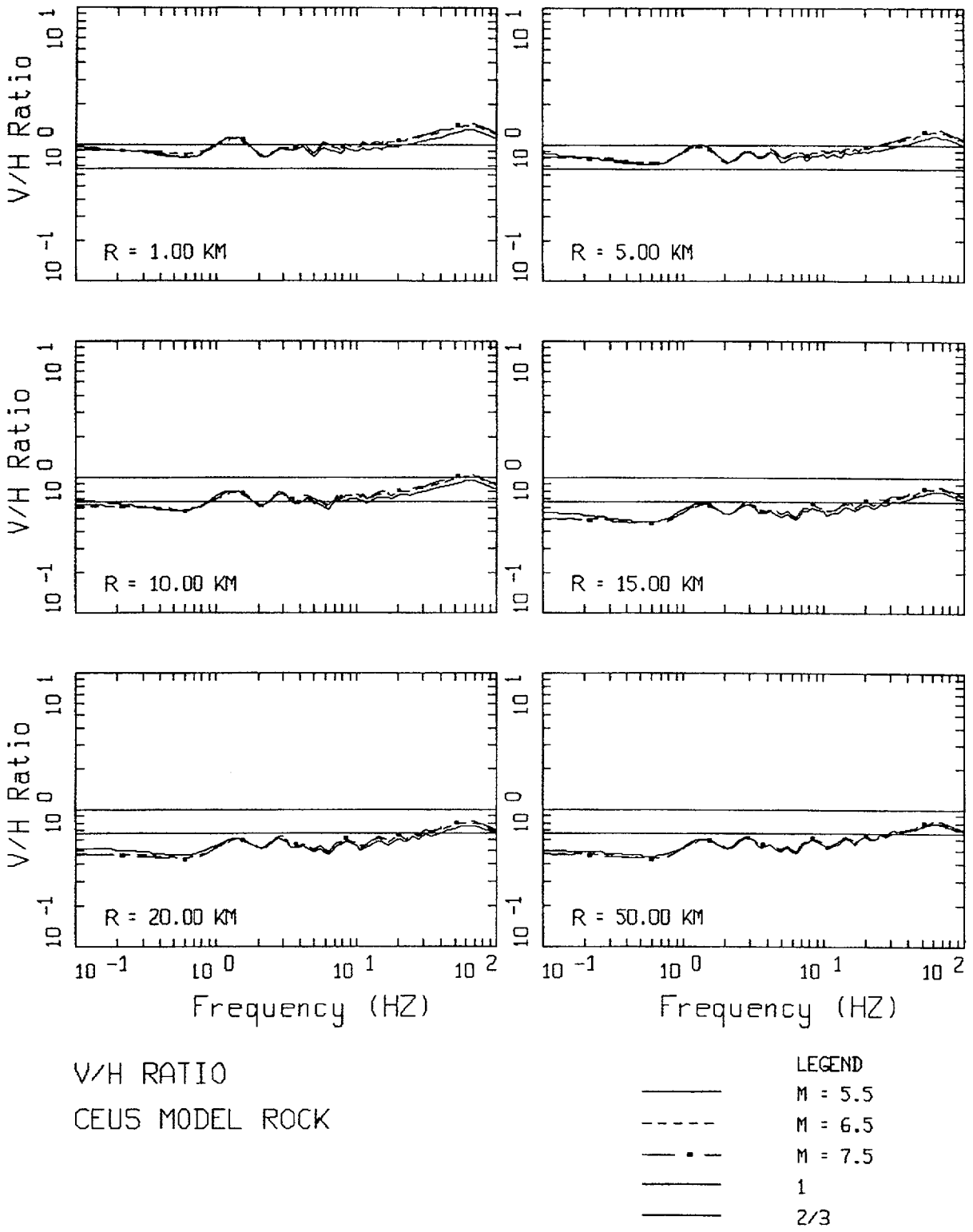

Figure 4-38. V/H ratios (5% damped) for CEUS rock site conditions computed with the simple point-source model.

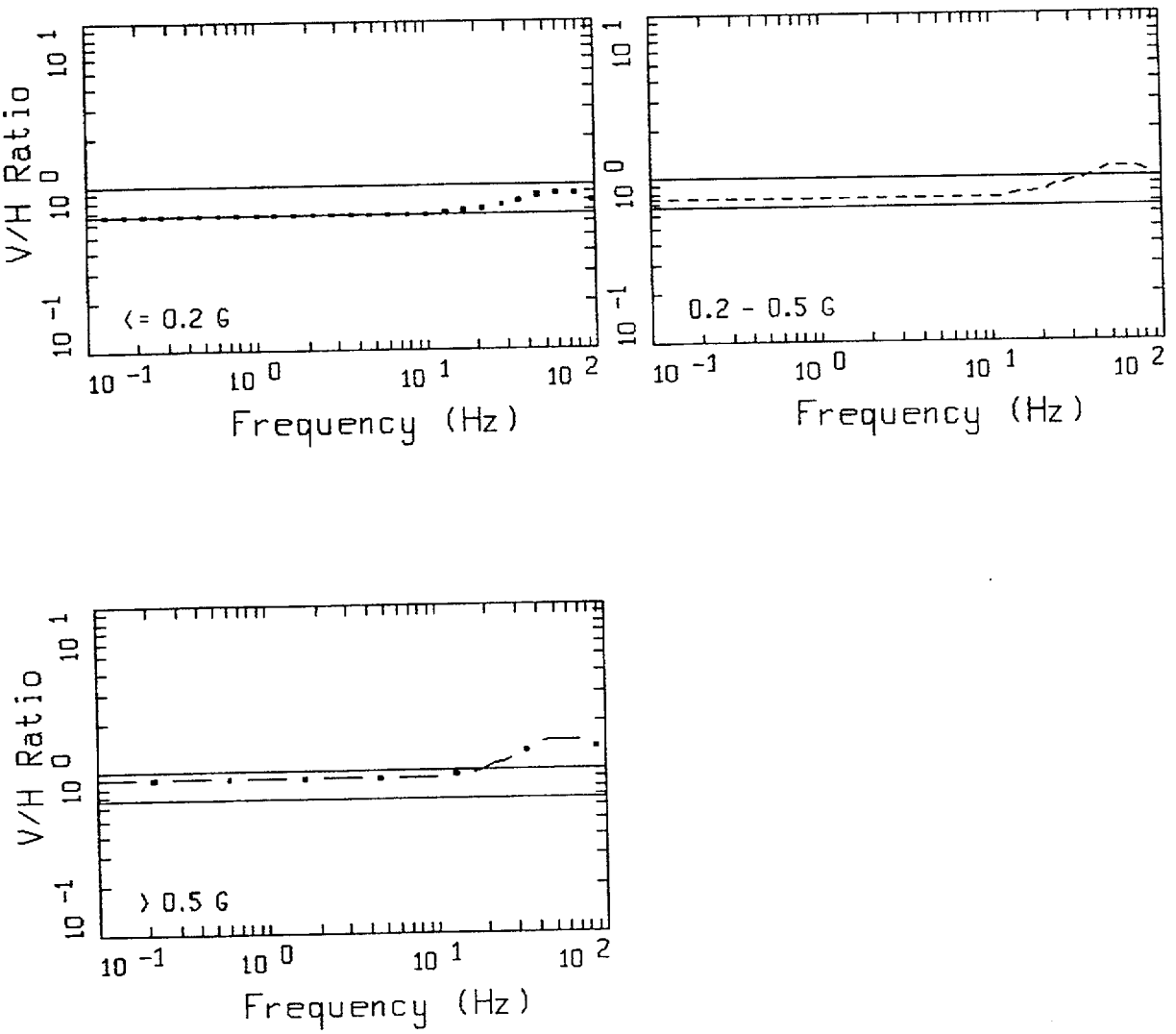

Figure 4-39. Recommended V/H ratios (5% damped) for CEUS hard rock site conditions for ranges in horizontal component peak accelerations.

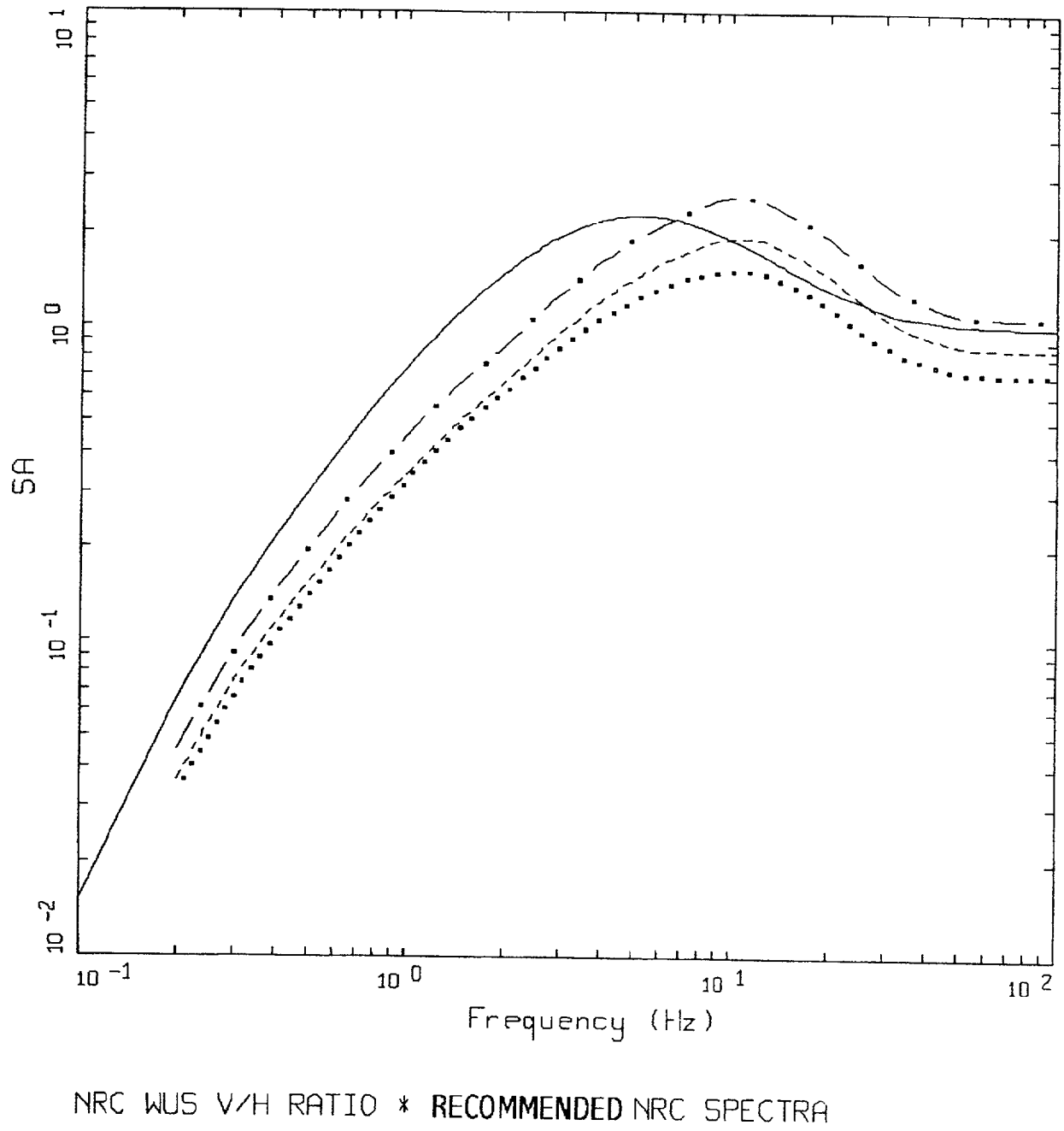

Figure 4-40. WUS vertical component response spectra (5% damped) based on the **M** 6.4, R = 27.4 km horizontal shape (Figure Set 4-26) and recommended V/H ratios (Table 4-4).

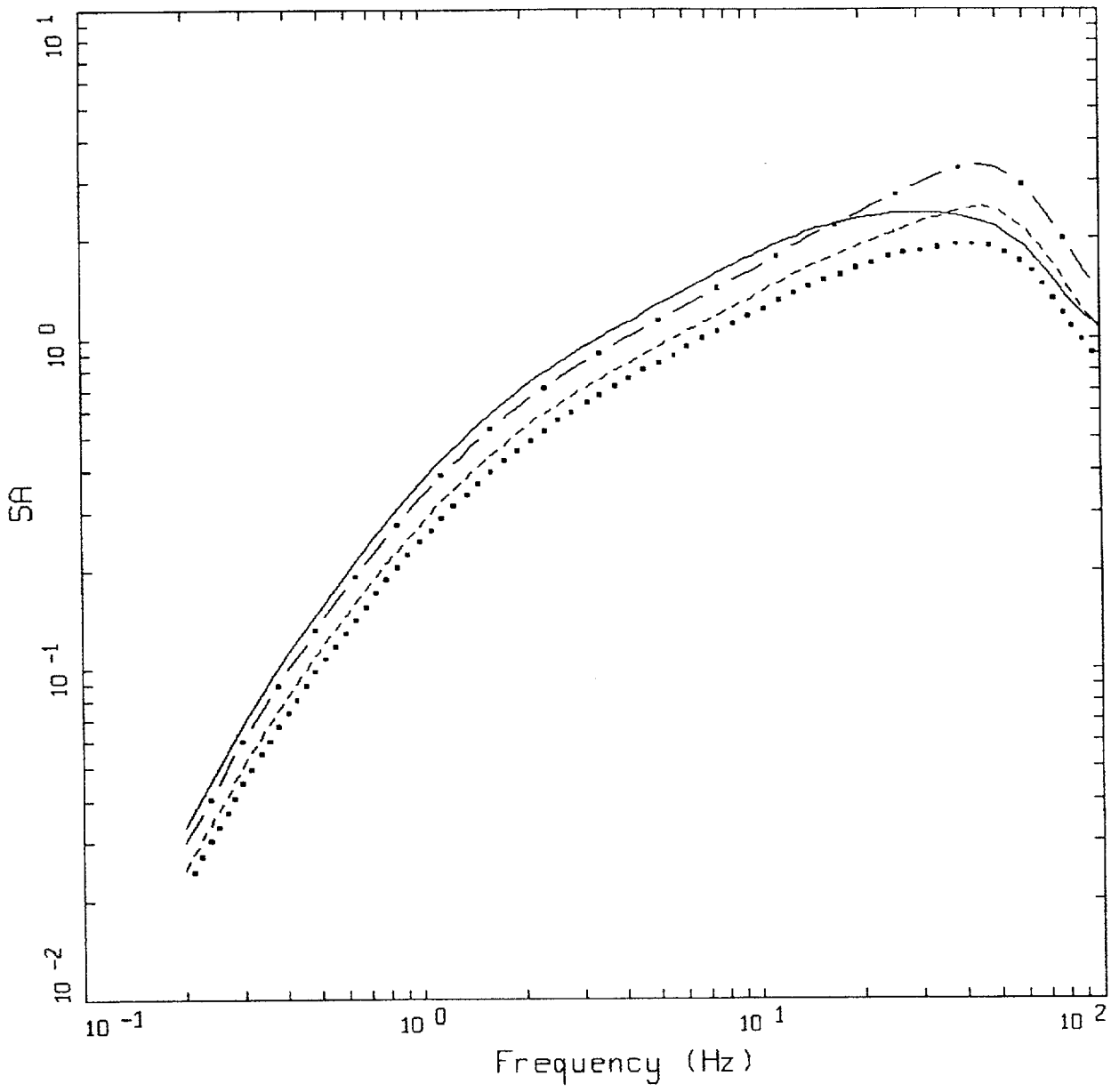

Figure 4-41. CEUS vertical component response spectra (5% damped) based on the **M** 6.4, R = 27.4 km single corner horizontal shape (Figure Set 4-27) and recommended V/H ratios (Table 4-5).

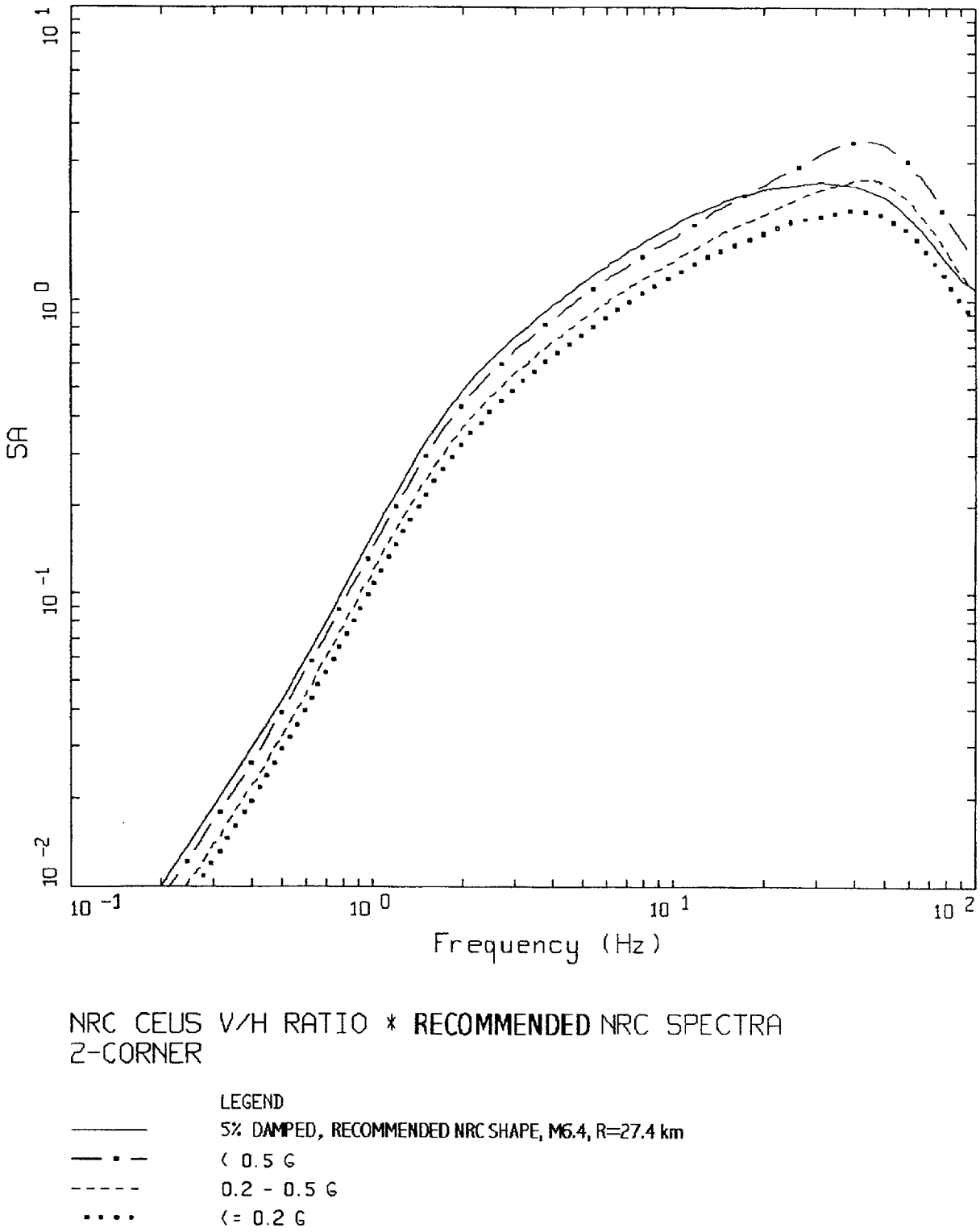

Figure 4-42. CEUS vertical component response spectra based on the **M** 6.4, R = 27.4 km double corner horizontal shape (Figure Set 4-26) and recommended V/H ratios (Table 4-5).